Technische Universität München
Department of Electrical and Computer Engineering
Institute for Renewable and Sustainable Energy Systems

Charging infrastructure optimisation for electric taxis

Reinhard Sellmair

Vollständiger Abdruck der von der Fakultät für Elektrotechnik und Informationstechnik der Technischen Universität München zur Erlangung des akademischen Grades eines

Doktor-Ingenieurs (Dr.-Ing.)

genehmigte Dissertation.

Vorsitzender: Prof. Dr.-Ing. Ulf Schlichtmann

Prüfende der Dissertation:

1. Prof. Dr. rer. nat. Thomas Hamacher
2. Prof. Dr.-Ing. Fritz Busch

Die Dissertation wurde am 29.11.2017 bei der Technischen Universität München eingereicht und durch die Fakultät der Elektrotechnik und Informationstechnik am 24.07.2018 angenommen.

Acknowledgement

I entirely carried out this thesis as Research Associate of TUMCREATE in Singapore. This work was financially supported by the Singapore National Research Foundation under its Campus for Research Excellence And Technological Enterprise (CREATE) programme. I want to express my gratitude for giving me the chance of being part of this project and supporting me in my research.

I want to thank Prof. Dr. Thomas Hamacher for giving me the opportunity to write this thesis under his supervision. I sincerely appreciated his support, feedback and the freedom he gave me throughout the years to elaborate on this topic. Furthermore, I want to thank Prof. Dr. Fritz Busch for our discussions and taking over the role of co-supervisor.

Especially I want to thank Tony Heng, Shaun Lee, Angela Khew, and Bernard Tan from SMRT Taxis. It would not have been possible to carry out this thesis without their support and the data they gave me access to. Our numerous discussions gave me invaluable insights into the perspective of a taxi operator.

Furthermore, I'm thanking Robert Kochhan for his excellent support throughout our collaboration with SMRT. Without his expertise in economics I would not have been able to elaborate on this topic in the same depth.

Among the many colleagues and friends at TUMCREATE from whom I got the chance to learn from I want to highlight Tom Schelo, David Ciechanowicz, Marc Gallet, and Sascha Moecker. Sharing their knowledge with me broadened my expertise and as a consequence improved the quality of this thesis.

Most of all I want to thank my wife Yün Yün and my parents for their everlasting encouragement and support throughout my journey.

Abstract

Replacing conventional taxis with electric vehicles would be an efficient measure to reduce CO_2 emissions in the transportation sector. The high daily mileage of taxis offers the chance to compensate the higher purchasing price of electric vehicles by lower energy costs. However, due to their limited range and long charging times, covering high mileage still poses a challenge on today's electric vehicles. To tackle this challenge and at the same time, to offer a convenient solution to the drivers, a customised charging infrastructure is vital to make electric taxis an attractive alternative.

This thesis proposes a method to optimise a charging infrastructure for electric taxis and applies this method in the context of Singapore. Therefore, a detailed driving profile analysis of almost 3,000 taxis was conducted. Furthermore, vehicle energy models were developed to simulate the energy consumption and charging process of electric vehicles. The aim of the infrastructure optimisation is to maximise the economic profit of both, the taxi drivers and a charging infrastructure provider while taking today's taxi drivers' activity patterns and break location choices into account. Therefore, a bi-level simulation-optimisation approach was chosen.

For this purpose, an agent-based taxi driving profile simulation was developed which is capable of reproducing today's taxis' driving patterns while respecting electric vehicle restrictions regarding range and charging time. This simulation model was validated with respect to the recorded driving profiles.

To quantify the economic potential of electric taxis, Total Cost of Ownership (TCO) models were applied to assess electric vehicles and charging stations. In order to take economic considerations into account for the charging infrastructure optimisation, the objective function's parameters were derived from the TCO models.

The objective of the optimisation is to minimise the opportunity cost from detours and waiting times as well as charging infrastructure costs. These costs are minimised by selecting locations where charging stations shall be placed and assigning the ideal number of charging stations to each location. This problem is described as the multiple server location problem.

The optimisation results showed that today's electric vehicles can reach almost the same mileage as conventional taxis. Thereby, electric taxi drivers would not have to adjust their activity patterns by changing the time of their breaks or even work longer.

Lower energy costs of electric vehicles compensate for the lower achievable revenue so that the economic potential of electric and conventional taxis is almost identical. Upcoming electric vehicles with longer range and shorter charging times are expected to exceed the economic potential of today's conventional taxis.

Kurzfassung

Das Ersetzen von konventionellen Taxis durch Elektroautos wäre eine effiziente Maßnahme um CO_2 Emissionen im Verkehrssektor einzusparen. Die hohe tägliche Laufleistung von Taxis bietet die Möglichkeit höhere Kaufpreise von Elektroautos durch geringere Energiekosten zu kompensieren. Aufgrund der begrenzten Reichweite und langen Ladezeiten stellt das Erreichen einer hohen täglichen Laufleistung nach wie vor eine Herausforderung für heutige Elektroautos dar. Um diese Herausforderung zu bewältigen und gleichzeitig Taxifahrern eine komfortable Lösung anbieten zu können ist eine speziell für diesen Anwendungsfall ausgelegte Ladeinfrastruktur essentiell. Nur unter dieser Bedingung können Elektrotaxis eine attraktive Alternative zu konventionellen Taxis darstellen.

Diese Arbeit schlägt eine Methodik vor um eine Ladeinfrastruktur für Elektrotaxis zu optimieren und wendet diese Methodik für Taxis in Singapur an. Dafür wurde eine detaillierte Analyse der Fahrprofile von nahezu 3.000 Taxis durchgeführt. Außerdem wurden Energiemodelle entwickelt um den Energieverbrauch und den Ladevorgang von Elektroautos zu simulieren. Das Ziel der Infrastrukturoptimierung ist es den wirtschaftlichen Gewinn von sowohl Taxifahrern als auch einem Ladeinfrastrukturbetreiber zu maximieren. Gleichzeitig werden hierbei die Bewegungsprofile und die Auswahl an Orten um Pause zu machen von Taxifahrern berücksichtigt. Hierfür wurde ein zweistufiger Simulation-Optimierungsansatz gewählt.

Für diesen Zweck wurde eine agentenbasierte Fahrprofilsimulation für Taxis entwickelt die sowohl Fahrprofile heutiger Taxis reproduziert und gleichzeitig Einschränkungen von Elektroautos bezüglich Reichweite und Ladezeiten berücksichtigt. Dieses Modell wurde anhand der aufgezeichneten Fahrprofile validiert.

Des Weiteren, wurden Gesamtwirtschaftlichkeitsmodelle angewandt um das wirtschaftliche Potenzial von Elektrofahrzeugen und Ladestationen zu quantifizieren. Um wirtschaftliche Faktoren in der Ladeinfrastrukturoptimierung zu berücksichtigen wurden Parameter von den Wirtschaftlichkeitsmodellen abgeleitet und in die Zielfunktion der Optimierung integriert.

Das Ziel der Optimierung ist es Opportunitätskosten von Umwegen um Ladestationen zu erreichen, Wartezeiten auf eine verfügbare Ladestation und Ladeinfrastrukturkosten zu minimieren. Hierfür werden sowohl optimale Orte für das Aufstellen von Ladestationen ausgewählt als auch die optimale Anzahl an Ladestationen an jedem dieser Orte identifiziert. Dieses Optimierungsproblem ist beschrieben als ein multiple server location problem.

Die Optimierungsergebnisse zeigten, dass Fahrer von heutigen Elektroautos annähernd die gleiche Laufleistung und Einnahmen von Fahrern mit konventionellen Taxis erreichen könnten. Dabei müssten Elektrotaxifahrer weder länger arbeiten noch ihre gewöhnlichen Pausenzeiten anpassen.

Die geringeren Energiekosten von Elektroautos gleichen die etwas geringeren Einnahmen aus, sodass das wirtschaftliche Potenzial von konventionellen und Elektrotaxis nahezu identisch ist. Es ist zu erwarten, dass in naher Zukunft Elektrofahrzeuge mit höheren Reichweiten und geringeren Ladezeiten das wirtschaftliche Potenzial konventioneller Taxis übertreffen werden.

Contents

1 Introduction **1**
- 1.1 Motivation . . . 1
- 1.2 Aim . . . 2
- 1.3 Approach and structure . . . 2
- 1.4 Contribution . . . 5

2 Context and data background **6**
- 2.1 Taxis in Singapore . . . 6
- 2.2 Electric vehicles . . . 7
- 2.3 Charging infrastructure . . . 9
- 2.4 Driving profile data . . . 11
  - 2.4.1 Logger data . . . 11
  - 2.4.2 Status data . . . 12
  - 2.4.3 Revenue data . . . 13
- 2.5 Street network . . . 13

3 Driving profile analysis **17**
- 3.1 Pre-processing and merging of data sets . . . 17
- 3.2 Standstill periods . . . 19
  - 3.2.1 Detection . . . 19
  - 3.2.2 Classification . . . 19
  - 3.2.3 Location clustering . . . 23
  - 3.2.4 Shift schedules . . . 24
- 3.3 Trips . . . 25
  - 3.3.1 Status and classification . . . 25
  - 3.3.2 Mileage and revenue estimation . . . 27
  - 3.3.3 Map-matching . . . 29
- 3.4 Traffic statistics . . . 30
  - 3.4.1 Choice of street types . . . 31
  - 3.4.2 Speed profiles . . . 31
  - 3.4.3 Acceleration . . . 34
  - 3.4.4 Driving shares . . . 35

4 Vehicle energy model **37**
- 4.1 Energy consumption model . . . 37
  - 4.1.1 Model and parameter . . . 38
  - 4.1.2 Speed-based approach . . . 41

4.1.3 Route-based approach . . . 43
4.2 Charging model . . . 45
4.2.1 Charging curve . . . 46
4.2.2 Model and parameter . . . 46
4.2.3 Charging process . . . 48

5 Driving profile simulation 51
5.1 Literature review . . . 51
5.2 Approach and model design . . . 53
5.3 Actions . . . 55
5.4 Shift schedule pool . . . 57
5.5 Trip generator . . . 61
5.5.1 Trip synthetisation . . . 61
5.5.2 Trip sampling . . . 63
5.6 Agent memory . . . 66
5.7 Behaviour models . . . 68
5.7.1 Standstill behaviour . . . 68
5.7.2 Charging behaviour . . . 71
5.8 Validation . . . 74
5.9 Case studies . . . 76

6 Economic model 81
6.1 TCO of taxis . . . 81
6.1.1 Acquisition costs . . . 81
6.1.2 Operation costs . . . 82
6.1.3 End-of-life value . . . 83
6.1.4 Cost comparison of vehicle types . . . 84
6.2 TCO of charging stations . . . 85
6.3 Cost factors and profit . . . 88

7 Infrastructure Optimisation 90
7.1 Infrastructure concept . . . 90
7.2 Optimisation criteria . . . 91
7.3 Literature review . . . 92
7.3.1 Flow-capturing model . . . 92
7.3.2 P-median problem . . . 93
7.3.3 Maximum covering problem . . . 93
7.3.4 Analytical model . . . 93
7.3.5 Simulation-based heuristic . . . 94
7.3.6 Multiple server location problem . . . 94
7.3.7 Matching of optimisation criteria . . . 95
7.4 Approach . . . 97
7.5 Waiting time estimation . . . 99
7.6 Optimisation problem . . . 102
7.6.1 Charging location optimisation . . . 103
7.6.2 Charging station optimisation . . . 106
7.6.3 Charging demand reallocation . . . 107

8 Results **110**
8.1 Scenario definition 110
8.2 Infrastructure design 111
8.3 Driving profile analysis 115
8.4 Economic analysis 120

9 Summary and discussion **124**
9.1 Summary 124
9.2 Main Uncertainties 127
9.3 Future Work 129
9.4 Conclusion 130

Bibliography **132**

Glossary **144**

Acronyms **149**

List of Figures **151**

List of Tables **154**

A OSM street type description **156**

B Speed clusters **158**

C Fit parameter **159**

D Database design **173**

E Simulation model classes **177**

F Functional design of actions **182**

G Infrastructure optimisation approaches **189**

Chapter 1

Introduction

This chapter gives the introduction to this thesis. First, the motivation for optimising a charging infrastructure for electric taxis in Singapore is explained in Chapter 1.1. Subsequently, the aim of this work is described in Chapter 1.2. Next, the overall approach and structure of this work is presented in Chapter 1.3. Finally, a brief summary of some highlights of this thesis is given in Chapter 1.4.

1.1 Motivation

Combating climate change is one of the United Nations' sustainable development goals, joining the likes of no poverty, zero hunger, good health and well-being (United Nations, 2015). In 2009, transport contributed about one quarter of energy-related global greenhouse gas emissions and consumed one fifth of the total energy use. According to the Climate Summit 2014, one of the options to reduce the carbon footprint is to accelerate the introduction of urban electric transport (United Nations, 2014). This can be achieved by substituting internal combustion engine vehicles with battery electric vehicles. Battery electric vehicles[1] are vehicles whose energy source comes exclusively from battery and are typically recharged at charging stations.

Apart from reducing CO_2 emissions, local air pollution and noise, electric vehicles also require lower maintenance and energy costs (Thomas, 2009; Verheijen and Jabben, 2010; Egbue and Long, 2012). However, in contrast to these advantages, electric vehicles still have the problem of higher investment costs, limited range, and long recharging times (Kochhan and Sellmair, 2016). Hence, the key is finding the context in which the benefits of electric vehicles use outweigh its disadvantages.

High vehicle mileage and consequently, low operational cost are necessary to compensate for the higher investment costs. Due to the range limitation of electric vehicles, it would be ideal to split the mileage into many short trips with the possibility of postponing subsequent trips in order to charge the battery. The driving patterns of taxis are matching these characteristics very well. Since taxis are operated in one or two shifts which are about eight to twelve hours long, high mileage is reached. Furthermore, trips with passengers on board are on average around 10 km long and taxi drivers are free to decide after each trip whether they serve the next customer or have a break to recharge the battery. Another advantage of electric taxis would be that many people would have

[1] in the remainder of this thesis this type of vehicles is referred as "electric vehicles"

the chance to get in touch with this technology and may consider to buy an electric vehicle of their own in the future. Having a substantial amount of electric vehicles would also reflect positively on a city's sustainable and innovative image.

Electric taxis can only be economically competitive if the amount of time they use for driving to charging stations, waiting for an available charging station, and recharging the battery is low. Thus, it is of utmost importance to provide a well-designed charging infrastructure in order to ensure their economic competitiveness.

The developed methodology in this thesis is applied in the context of taxis in Singapore. Singapore is an island city-state with a total area of 719 km^2 (Department of Statistics Singapore, 2016b) and a population of 5,607,000 people (Department of Statistics Singapore, 2016a). Due to its spatial constraints, the use of private vehicles is limited by high taxes. As a result, the contribution of taxis to Singapore's transportation system is significantly higher than in most other cities. Thus, substituting conventional vehicle taxis by electric taxis would have a disproportional high impact on emission savings.

Furthermore, Singapore is seen as a role model for many cities in the Asian region. A successful launch of electric taxis there could spearhead the adoption of electric vehicles in the whole region.

1.2 Aim

The aim of this thesis is to present a methodology to optimise a charging infrastructure for electric taxis for different electric vehicle types and charging stations. Thereby, individual driving patterns of taxi drivers have to be taken into account in order to ensure that drivers can combine their usual breaks with recharging the battery at their preferred location and time of the day. The optimisation algorithm has to decide how many charging stations shall be placed at a suitable set of candidate locations.

The optimisation objective is to maximise the economic benefit of the whole system consisting of taxi drivers, the taxi operators which rent the vehicles to drivers and the charging infrastructure providers. Thereby, the costs of detours to reach charging stations, waiting times at charging stations, and additional stop durations caused by charging the battery have to be considered.

Based on the optimised charging infrastructures, the economic potential of different electric vehicle types shall be assessed. Furthermore, roadmaps are to be developed which describe the set up and extension of charging infrastructures beginning with a small test fleet and ultimately extending to an entirely electrified taxi fleet. Apart from that, an economically ideal configuration regarding the taxi's battery capacity and charging power shall be derived.

1.3 Approach and structure

The approach presented in this thesis requires driving profile data of taxis, the city's street network, and electric vehicle and charging station characteristics as inputs to derive the objectives defined in the previous section. Provided that this information is available, this approach is applicable for any city. Figure 1.1 illustrates the required input, processing steps and output of this approach. The structure of this thesis is derived from this scheme.

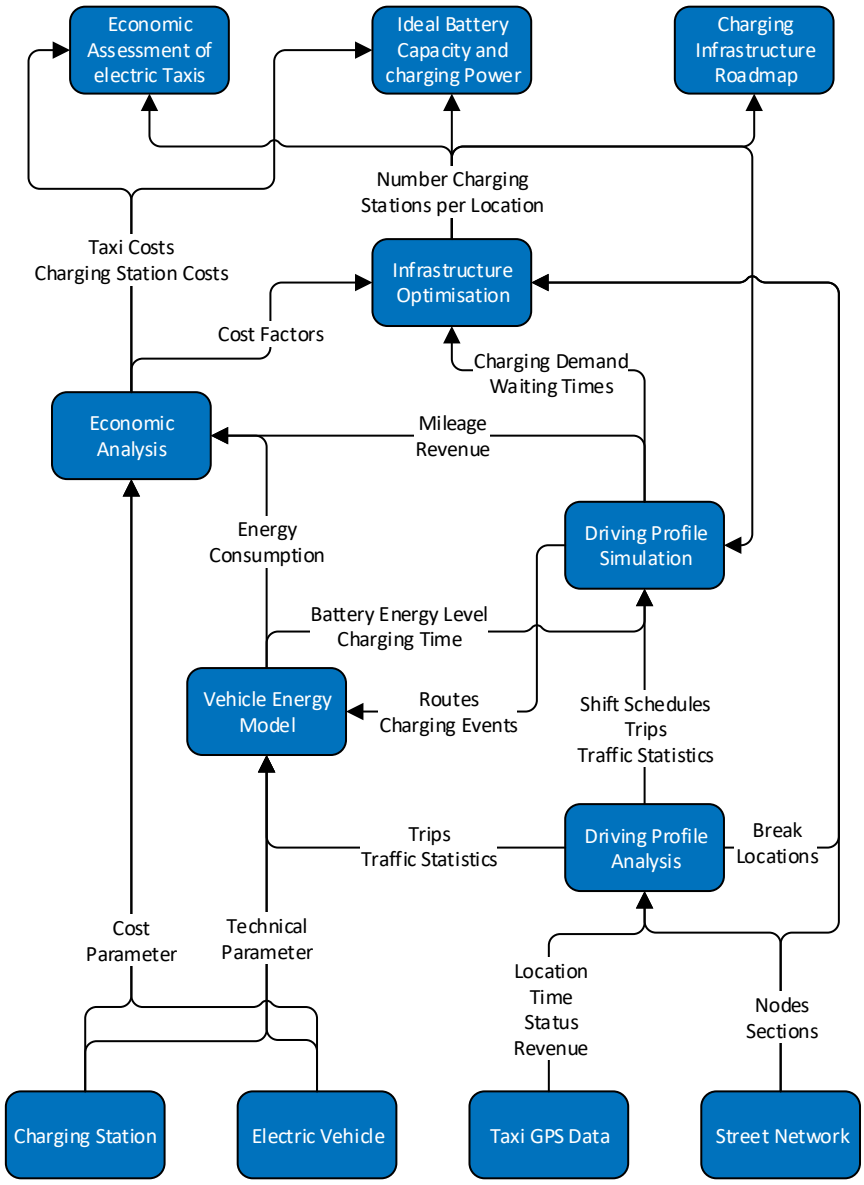

Figure 1.1: Approach of thesis

The context and data background of this thesis is described in Chapter 2. It explains the selection of electric vehicles and charging stations which are considered in this work. Furthermore, the taxi driving profile data sets are introduced as well. These data sets contain information about the taxis' location, status, and revenue. Apart from that, Singapore's Open Street Map (OSM) data set is described at the end of this chapter.

Subsequently, the driving profile data sets are analysed in combination with the street network in Chapter 3. Thereby, trips and *shift schedules* which describe the drivers' activity patterns are extracted from the data. Moreover, traffic statistics are derived from the trips' speed profiles and a clustering algorithm is applied to extract the drivers' most frequently chosen break location.

Chapter 4 introduces the vehicle energy model which is applied to simulate the vehicles' energy consumption and charging process. The energy consumption can be estimated with respect to a speed profiles extracted from recorded trips or with respect to a given route. The route-based approach utilises the traffic statistics derived in the previous chapter.

The vehicle energy model is integrated into the driving profile simulation model which is presented in Chapter 5. The driving profile simulation is not only capable of reproducing driving profiles of conventional taxis but is also applicable to simulate driving profiles of electric taxis with respect to the vehicle type and the charging infrastructure. The simulation results allow to extract mileage, revenue, waiting times, and the charging demand of electric taxis. Thereby, the derived trips and *shift schedules* in Chapter 3 constitute the statistical background of this model.

A Total Cost of Ownership (TCO) analysis regarding electric vehicles (Kochhan, 2017) and charging stations is made in Chapter 6. The applied economic models are used to evaluate the economic potential of electric taxis with respect to the vehicle type, charging infrastructure, and driving profile simulation results. Furthermore, cost factors are derived to parametrise the infrastructure optimisation objective function.

The developed methodology to optimise a charging infrastructure for electric taxis is presented in Chapter 7. The optimisation problem is formulated as a bi-level simulation-optimisation multiple server location problem (Berman and Drezner, 2007). Thereby, the driving profile simulation model is applied to generate the charging demand of an electric taxi fleet and an optimisation algorithm decides to which charging locations this demand shall be allocated to and how many charging stations are required at each location. The optimisation's objective is to minimise detour, waiting time, and charging infrastructure costs.

The optimised placement of charging stations is presented in Chapter 8. Several optimisations for different numbers of electric taxis were executed so that a roadmap regarding how to set up and extend a charging infrastructure can be derived from the results. Furthermore, driving profiles were simulated on the basis of the optimised charging infrastructures, so that the economic potential of different electric vehicle types could be compared with conventional taxis. Moreover, different combinations of battery capacity and charging power were analysed in order to derive an ideal configuration for electric taxis.

Finally, Chapter 9 summarises and concludes this thesis.

This thesis contains a number of custom-defined terms. To help the reader with keeping track of those terms, all custom-defined terms are written in italic font and described in the glossary.

1.4 Contribution

This section summarises some highlights of this work which surpass the current state of the art.

This work is based on a broad data basis including status and revenue information of a taxi fleet of almost 3,000 taxis. The implemented driving profile simulation model utilises this data basis and is therefore capable of reproducing individual driving patterns of almost 3,000 taxis. Hence, the simulated share of active taxis with respect to time complies with the activity patterns extracted from the recorded data. Furthermore, the simulated agents have breaks at the same time and location as real taxi drivers.

These characteristics are very important as it is assumed that the drivers would predominantly utilise their usual break times and locations to recharge the vehicle's battery. The charging demand extracted from the simulation results reflects these habits. Moreover, as the simulated charging demand is given as input to the charging infrastructure optimisation, individual taxi driver profiles are also considered in the resulting optimised charging infrastructure.

Regarding the optimisation, a trade-off between infrastructure costs and the availability of charging stations has to be found. On the one hand, a lack of charging stations would cause long detours and waiting times for taxi drivers which would ultimately affect their revenue. On the other hand, if too many charging stations were available, their utilisation would be too low to justify the related investment costs.

Therefore, in order to balance these two aspects, this work presents an holistic approach to maximise the economic profit of both the electric taxi drivers and a charging infrastructure provider. Thus, in contrast to most other approaches, the presented methodology returns the ideal number of charging stations for a given taxi fleet instead of requiring this number as constraint.

The ideal number of charging stations can only be derived by balancing waiting time and charging station costs. Thus, it is essential to estimate the taxis' waiting times with respect to the charging demand and the number of charging stations at a specific location. In the literature, this estimation was either made by a non-linear function or vastly simplified. Using a non-linear function makes the solving of the optimisation problem significantly more difficult and does not ensure that the global optimum could be found, while over-simplified estimations affect the quality of the solution. This thesis presents an approach of accurately respecting waiting times while formulating a linear optimisation problem to identify ideal charging locations.

Chapter 2

Context and data background

This chapter introduces the context to which the developed methodology is applied to and describes the main data sources. Therefore, Chapter 2.1 provides an introduction to Singapore and its taxi business. Subsequently, Chapter 2.2 and 2.3 describe the chosen vehicle types and charging concept. The analysed taxi driving profile data sets are explained in Chapter 2.4. Finally, Singapore's street network data set is introduced in Chapter 2.5.

2.1 Taxis in Singapore

As this work was carried out in the context of taxis in Singapore, this section gives a brief introduction to Singapore and its taxi business.

Figure 2.1: Map of Singapore (Open Street Map, 2017a)

Singapore is an island city-state with a total area of 719 km^2 (Department of Statistics Singapore, 2016b) and a population of 5,607,000 people (Department of Statistics

Singapore, 2016a). A map of Singapore is depicted in Figure 2.1. Singapore's Central Business District (CBD) is in the south (where the word "SINGAPORE" is written). There are two big nature reserves in the middle and the west of the island, it's main public airport is located in the very east of the island. The map also shows the expressways as grey lines and major roads as red lines. Singapore is connected by two bridges in the north and west with the main land of Malaysia.

Due to Singapore's limited size and high population, roads account for 12% of the land area (LTA, 2013b). Hence, in order to limit the number of vehicles on the road, the Land Transport Authority (LTA) imposes very high taxes on vehicles. The most expensive taxes is the Additional Registration Fee (ARF), which ranges between 100 and 180% of the vehicle's Open Market Value (OMV) (LTA, 2017c) and the Certificate Of Entitlement (COE) which is obtained by a bidding system and had an average value of 62,195 SGD[1] in 2015 (Kochhan, 2017). As a result, only 536,882 private vehicles were registered in 2014 (LTA, 2015b), which translates into a proportion of 9.6% of the inhabitants owning a car.

Therefore, taxis are a very popular mode of transport in Singapore. In 2015, there were 27,534 taxis registered and 100,411 citizens holding a taxi driver's vocational license (LTA, 2016b). The average daily ridership by taxi was 1,020,000 (LTA, 2015b) which translates to a daily ridership per inhabitant of 0.19. That's clearly higher than other megacities like New York (0.07), London (0.04), or Tokyo (0.10) (Commission Taxi & Limousine, 2014; Sustrans, 2014; Association Tokyo Hire-Taxi, 2015), which can be explained by the low fares of taxis in Singapore. The 2017 Taxi Price Index ranked Singapore's taxi prices as the 20th cheapest among 80 surveyed cities (Carspring, 2017), ahead of other Asian cities such as Hong Kong (ranked 31st) and Seoul (ranked 30th). This might come as a surprise, given that Singapore was recently ranked the most expensive city in the world according to the 2017 Economist Intelligence Unit's annual worldwide cost of living survey (The Economist, 2017).

Taxi drivers in Singapore are self-employed, meaning that they rent a car from a taxi operator, pay for the fuel, and keep the generated revenue (Kochhan and Sellmair, 2016). Many drivers operate their taxi in two shifts and share the rental fees with the relieve driver. Due to these conditions driving profiles of taxis are very heterogeneous, e.g. the average daily mileage of taxis ranges from 150 km to up to 650 km.

In 2016, the first all-electric taxi operator HDT Singapore Taxi started operating as part of the government's electric vehicle test bed. In early 2017, it has reached a fleet size of 50 BYD e6 taxis and targeted to reach a size of 100 taxis by mid 2017. These taxis were supplied by 57 charging stations in total, which were distributed across seven charging locations. In contrast to all other taxi operators, drivers are hired by HDT and get a fixed salary plus bonus if they manage to exceed a monthly revenue target (Lim, 2016; Ying, 2017).

2.2 Electric vehicles

The criteria for selecting electric vehicles for this work were that these vehicles must be on the market already, otherwise an economic assessment would not be possible. Furthermore, these vehicles must be operable as taxis, therefore each vehicle must already

[1] the average exchange rate from 2006 to 2015 of 1 Singapore Dollar (SGD) was 0.7332 to USD and 0.5558 to EUR (Kochhan, 2017)

been used as a taxi in at least one city. Based on these requirements, the chosen vehicles were:

- BYD e6 (BYD, 2017)
- Kia Soul EV (Kia, 2017)
- Nissan Leaf (Nissan, 2017a)
- Tesla Model S (Tesla, 2017b)

Table 2.1: Cities with electric taxis

Vehicle	City
BYD e6	Singapore (Lim, 2016), Brussels (BYD, 2015), Shenzhen (Huifeng, 2015), Beijing (Vetter, 2016), London (Vetter, 2016), Bogota (Vetter, 2016)
Kia Soul EV	Sofia (Hadzhistoykov, 2015), Montreal (Hanley, 2015)
Nissan Leaf	New York (Ross, 2013), Rio de Janeiro (Crowe, 2013a), Zurich (Edelstein, 2013), Amsterdam (Vetter, 2016), Mexico City (Crowe, 2013b), Madrid (Crowe, 2014), Barcelona (Crowe, 2014), Montreal (Hanley, 2015), Budapest (Vetter, 2016)
Tesla Model S	Montreal (Hanley, 2015), Amsterdam (Vetter, 2016), Oslo (Wolfram, 2015), Sydney (Parkinson, 2015), Vienna (Ungureanu, 2014)

Table 2.1 gives an overview of the cities and the distribution of electric vehicles that are operated as taxis. With over 230,000 units sold between year 2011 and 2016, the Nissan Leaf is not only the most sold electric vehicle worldwide (Ranarison et al., 2017), but also the vehicle which is most commonly operated as electric taxi. In contrast, the Kia Soul EV is operated in the smallest number of cities, which may be due to its latest start of production compared to the other vehicles.

The listed vehicles were compared with EVA (Bender et al., 2014), an electric vehicle prototype developed by TUMCREATE. EVA was specially designed to be used as a taxi in tropical megacities. Therefore, in order to minimise the loss of time due to charging, which is a critical factor for this purpose, it was designed for a charging power of 160 kW. Although EVA is not on the market and consequently there is no official price, a detailed economic evaluation was carried out in (Kochhan and Sellmair, 2016) so that it could be compared with the other vehicles.

The most important technical parameter of the chosen vehicles are listed in Table 2.2. The weights of the BYD e6, Kia Soul EV, Nissan Leaf SV, and Tesla Model S 70D were taken from (EPA, 2016). These values include not only the vehicle's curb weight but also additional weight of 136 kg in total. In order to make EVA comparable, the same weight was added to its curb weight of 1,500 kg. Despite having the lowest weight, EVA's battery capacity is considerably higher than those of the Kia Soul EV and Nissan Leaf. The reduction of EVA's weight comes mainly from its carbon fibre reinforced polymer (CFRP) body, which is 150 kg lighter than a comparable steel body (TUM CREATE, 2013). Whereby the BYD e6 has the highest weight due to its battery size and steel

Table 2.2: Technical parameter of electric vehicles

Vehicle	Weight [kg]	Battery capacity [kWh]	Charging power [kW]
BYD e6	2,495	61.4	40
EVA	1,636	50	160
Kia Soul EV	1,644	27	100
Nissan Leaf SV	1,701	30	50
Tesla Model S 70D	2,286	70	60

body (BYD, 2014). The weight is an especially important factor for electric vehicles as it affects the energy consumption which in turn affects the vehicle's range and energy costs.

The charging power of BYD e6 vehicles was estimated to be 40 kW as HDT claims that one and a half hours are required to fully charge the battery (Lim, 2016). Although, the Tesla Model S is capable of using Tesla's Superchargers which deliver a charging power of 120 kW, the power output of privately-owned Superchargers is restricted to 60 kW per vehicle (Lambert, 2016). Therefore, the later is used as charging power estimate for these vehicles. Although the disparity between Tesla- versus private-owned charging capacity was not made clear, a plausible explanation could be that Tesla limits the charging power to avoid extensive fast charging in order to limit battery degradation. The charging power of the remaining vehicles was set to their designed maximum charging power limit. Chapter 6.1 contains an economic assessment of these electric vehicles for the use case of taxis.

Electric taxis with an energy consumption of 170 Wh/km and a charging station efficiency of 92.6% (Genovese et al., 2015) could with respect to Singapore's electricity emission grid factor of 0.4313 $kgCO_2$/kWh (Energy Market Authority, 2016) save 72% CO_2 emissions compared to diesel taxis and 35% compared to hybrid taxis. Meaning that in total 694,000 respectively 150,000 tons of CO_2 emissions could be saved compared to a pure taxi fleet of diesel respectively hybrid vehicles. Thereby, the used vehicle energy consumptions were 0.104 l/km for diesel vehicles (Chevrolet Epica) and 0.053 l/km for hybrid vehicles (Toyota Prius) (Kochhan, 2017). The applied fuel emission factors are 2.31 $kgCO_2$/l for gasoline (used by hybrid vehicles) and 2.68 $kgCO_2$/l for diesel (Ogden and Anderson, 2011).

2.3 Charging infrastructure

There are three main approaches to recharge a vehicle's battery: conductive charging, inductive charging, and battery swapping.

Conductive charging means that the electric vehicle is connected by a cable to a charging station which supplies electrical energy to recharge the battery. All of today's electric vehicles have this option. Unfortunately, there are different charging standards which prevent the ubiquitous use of all charging stations by any vehicle type. An overview of all charging standards can be found in (Falvo et al., 2014).

There are two types of conductive charging: AC and DC charging. AC charging means that the vehicle is supplied with AC voltage and the vehicle's on-board charger inverts the voltage to DC to charge the battery. This charging type can not only be used

to recharge via charging stations but also to use normal household sockets. However, the charging power is limited by the design of the on-board charger which has an efficiency of 97.1% (Genovese et al., 2015). EVA's on-board charger is designed for the lowest charging power of 3.3 kW (Bender et al., 2014), whereby the BYD e6 can be charged with the highest AC charging power of 40 kW.

DC charging is necessary to recharge the battery with higher power. In this case, a transformer in the charging station inverts AC voltage to the DC voltage required by the battery management system. This voltage is directly applied to recharge the battery. Due to the cost of the transformer, DC charging stations are significantly more expensive than AC charging stations. The efficiency of a DC charging station is 92.6% (Genovese et al., 2015). A cost analysis of charging stations follows in Chapter 6.2.

A more convenient option is inductive charging, which does not require a physical connection of the vehicle with the charging equipment. The recharging power is transmitted by an electromagnetic field which is generated by primary coils in the ground and received by one or more secondary coils installed at the bottom of the vehicle. The vehicle can be inductively charged while it is stationary (static) as well as while it is moving (dynamic). A review on the state of the art technology in the field of inductive charging can be found in (Bi et al., 2016). A static inductive charging concept with 5 kW power and an overall efficiency from the AC grid to the battery pack of 90% was presented in (Wu et al., 2012). As dynamic inductive charging is technically more challenging, (Choi et al., 2015) measured a lower efficiency of 72 - 83% for a charging power between 3 and 25 kW. The estimated costs for a 3.3 kW static inductive charger range between 1,940 and 2,440 USD (2,646 to 3,328 SGD) (Plugless Power, 2015) while the hardware and deployment costs of an one mile long dynamic charging lane were estimated to 2.8 million USD (3.8 million SGD) (Jones and Onar, 2014). As only EVA is eligible for static inductive charging among the vehicles included in the thesis, this charging concept is not further explored.

Battery swapping is an alternative to the options above. In this case, the driver has to come to a swapping station where the vehicle's discharged battery is automatically replaced by another fully charged battery within minutes. This concept was pioneered and implemented by the company Better Place which declared bankruptcy in 2013. In the same year, Tesla presented a battery swapping prototype which was only applicable to Tesla vehicles and was never brought into series production. The main drawbacks of this concept are that batteries have to be standardised and that customers may not accept to replace the battery they bought by an older one (Kerns, 2016). To date, there is no battery swapping applicable electric vehicle model on the market. Therefore, battery swapping will not be discussed further.

Apart from charging concepts, research was also conducted in the field of smart charging algorithms. Thereby, the scheduling to recharge the battery is optimised with respect to electricity prices (Glanzer et al., 2011), grid constraints (Sundstrom and Binding, 2012), battery degradation (Trippe et al., 2014) and other considerations. These techniques are most efficient, the more time is available to schedule the charging procedure, which is especially interesting in case of private vehicles due to their low energy demand and long standstill times. The driving profiles of taxis however consist of long driving durations and short standstill times. Hence, smart charging algorithms had a much smaller degree of freedom to improve the charging process. Therefore, smart charging is not taken into account in this thesis.

2.4 Driving profile data

The main objective of this work is to present a method for designing a charging infrastructure that is tailored to the mobility patterns of today's taxi drivers. Thus, a detailed understanding of taxi driving profiles is essential. Therefore, three types of data sets were taken into account: logger, status, and revenue data. All data concerns taxis in Singapore. The logger data was recorded in collaboration with the public transport company SMRT Corporation Ltd (SMRT, 2017), while the status and revenue data sets were provided by SMRT as well.

2.4.1 Logger data

The data set with the highest recording frequency and accuracy is denoted as *logger data set*. To record this data set, *Columbus V-990* GPS data loggers (Columbus, 2017) were installed in 50 taxis over a period of six month. The data recording period spanned from 9.6.2014 to 13.4.2015 [2].

The accuracy stated by the manufacturer is 5.0 m/CEP (95%) (CEP: Circular Error Probability), which means that 95% of all data points fall below a circular error of 5.0 m. The GPS logger records one data point per second, thereby each data point includes the observables: *index, date, time, latitude, longitude* and *speed*. The device is plugged into the cigarette lighter socket and is turned on automatically when the vehicle's on board power supply was switched on.

Table 2.3: Logger data excerpt

Index	Date	Time	Latitude [deg]	Longitude [deg]	Speed [km/h]
56	140609	033503	01.449803N	103.795596E	0
57	140609	033504	01.449801N	103.795598E	0
58	140609	033505	01.449798N	103.795600E	4
59	140609	033506	01.449761N	103.795621E	6
60	140609	033507	01.449743N	103.795631E	8

Table 2.3 depicts an example subset of five recorded data points. The *index* is the consecutive data point number, the *date* format is interpreted as *yymmdd* and the *time* format is *hhmmss* (e.g. the first row's timestamp means 9.6.2014 3:35:03). The field *speed* contains the speed value between two data points in the unit of km/h.

Figure 2.2 shows a recorded trajectory where the data points are coloured with respect to the recorded speed. This trajectory is based on the raw data without any pre-processing. It matches very well to the underlying street network (Open Street Map, 2017a), which reflects the GPS logger's high accuracy with remarkably detailed depiction. Furthermore, the speed information is plausible as the highest speed was reached on express-ways whereby other streets had predominantly speed values below 50 km/h. As the recording frequency was constantly one point per second, the distance

[2] not all taxis entered the study period from the start

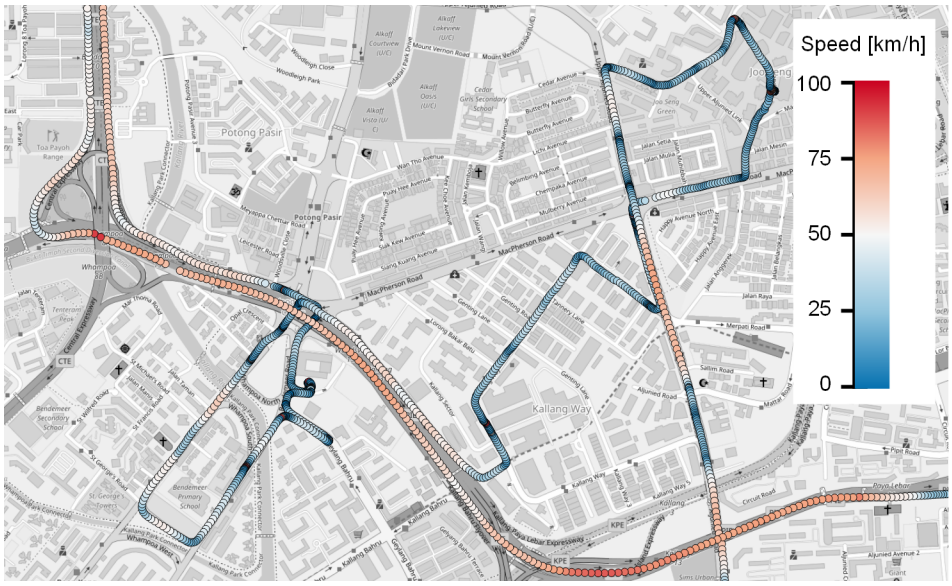

Figure 2.2: Trajectory sample

of consecutive data points correlates very well with the recorded speed. The higher the speed, the farther the data points were apart from each other.

In general, the data quality was very good, albeit with some occasional inaccuracies. For example, in the above figure, there are two instances, one in the north east and one in the west whereby the distance between data points is uncommonly big. Obviously, there is at least one data point missing. As the logger recorded the time as well, these cases were easily identified and interpolated values were used to fill these gaps.

Another inaccuracy appeared in the very west where the driver changed from one express-way to another. There are two data points in this area with a notable high speed of 89 km/h although the trailing and successive points had a speed of 71 km/h. It is most unlikely that the driver increased and decreased its speed by 18 km/h within two seconds. Hence, the recorded speed of these points must be incorrect. Apparently, the car drove underneath a bridge when theses points were recorded, which certainly affected the recording quality. These cases are detected by computing the vehicle's acceleration between two consecutive data points. Whenever a threshold was violated, data points were replaced by interpolated values.

2.4.2 Status data

The *status data set* contains the taxis' operational status at a certain point in time and location. It was obtained through the Mobile Data Terminal (MDT), each taxi is equipped with. The MDT continuously captures the taxi's position, timestamp (format: *mm/dd/yyyy hh:mm:ss*) and status information with an approximate sampling period of three minutes. The driver manually changes the status on the MDT. Table 2.4 lists a description of all statuses.

The status of all taxis was transmitted to SMRT and got stored in a database. An excerpt is listed in Table 2.5.

Table 2.4: Taxi status description

Status	Description
hired	taxi has customer on board
STC	soon to clear: taxi finishes trip with customer soon and can receive new bookings
payment	taxi arrived at customer's destination, taxi meter is stopped
for hire	driver is searching for next customer
on call	driver accepted booking and drives to pick-up point
arrived	taxi arrived at pick-up point
no show	customer did not appear at pick-up point, booking is cancelled
busy	driver is having a private trip
change shift	driver ends shift and drives to shift change location
log off	taxi is inactive

Table 2.5: Status data excerpt

License plate[a]	Latitude [deg]	Longitude [deg]	Status	Datetime
SHB59XXX	1.289653	103.8544	hired	6/30/2014 13:23:56
SHB1XXX	1.448395	103.7947	log off	6/30/2014 13:24:01
SHB12XXX	1.280097	103.8495	for hire	6/30/2014 13:26:31
SHB55XXX	1.346845	103.8592	hired	6/30/2014 13:26:33
SHB1XXX	1.333402	103.8950	busy	6/30/2014 13:26:34

[a] the last three digits were anonymised to protect the drivers' privacy

2.4.3 Revenue data

Additional to the *status data set*, SMRT provided a *revenue data set* which contains the information which taxi (identified by *license plate*) started a hired trip at what time and the amount of money charged at the end of the trip. Table 2.6 shows a sample of the *revenue data set*.

2.5 Street network

A street network of Singapore was used to analyse the driving profiles in greater detail in Chapter 3 and to simulate the agent's driving profiles in Chapter 5. Therefore, Singapore's street network was downloaded from Open Street Map (OSM) (Open Street Map, 2014), all pre-processing steps to make the downloaded data usable for this work were described in (Moecker, 2014).

Figure 2.3 illustrates some definitions of the pre-processed street network. Only

Table 2.6: Revenue data excerpt

License plate[a]	Datetime	Amount paid [SGD]
SHF4XXX	8/10/2014 0:02	8.36
SHC40XXX	8/10/2014 0:03	35.73
SHC45XXX	8/10/2014 0:06	47.60
SHFXXX	8/10/2014 0:08	13.65
SHD62XXX	8/10/2014 0:11	10.99

[a]the last three digits were anonymised to protect the drivers' privacy

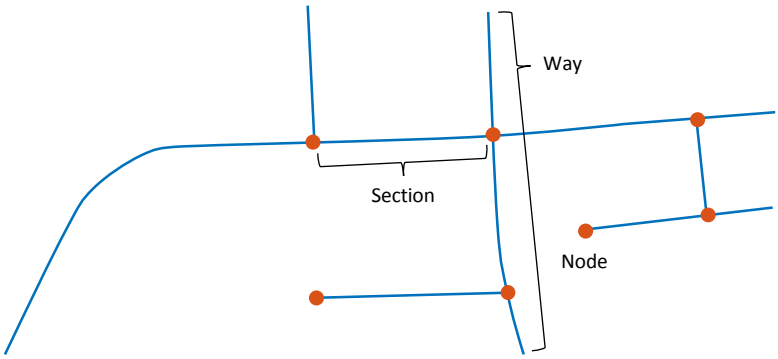

Figure 2.3: Street network definitions

intersections and end of roads are represented by nodes, all other nodes from the OSM which are used to describe the shape of the road were removed. Each node has a geographical position (latitude and longitude) and a corresponding OSM *Node ID* as property. Sections refer to road segments connecting two neighbouring nodes with each other. The information, which sections are directly connected with each other was stored in a connectivity matrix. Each section has following features: OSM *Node IDs* of connected nodes, length, and OSM *Way ID*. All sections belonging to the same street have the same *Way ID*. Moreover, all streets are classified with respect to their street type (e.g. *motorway*, *residential*, ..). A description of all street types can be found in Appendix A.

Some key figures of the street network are listed in Table 2.7. There are more nodes than sections since the street network has many dead ends which are represented by nodes as well. Each *way* consists of only 1.9 sections on average. The reasons for that are twofold. First, the street network consists of many small residential streets with unique *Way* IDs. *S*econd, major roads and express-ways are represented by two different *ways* with opposite directions and different IDs.

Table 2.7: Key figures of street network

Number of *nodes*	46,291
Number of *sections*	39,177
Number of *ways*	20,260
Number of street types	14
Total length [km]	5,123

All *ways* were classified into 14 different street types, whereby *service* was the most common class with 6,206 *ways* and *residential* was the type with the highest total length of 1,467 km. The total length of the street network is 5,123 km, which is significantly higher than the official street network length of 3,496 km provided by the LTA (LTA, 2014b). Again, this can be explained by the split of main roads into two *ways* of opposite directions which resulted in double counting the length of these roads.

Figure 2.4: Street network of Singapore

The complete street network is shown in Figure 2.4, where the six most common street types are represented by one colour each and all remaining classes were grouped as *other*. The network of express-ways (denoted by *motorway*) coincides very well with Figure 2.1 but also with other maps like Google Maps (Google, 2017). Also, the layout of the *primary* streets which are major roads with multiple lanes in each direction fits well together with these maps.

However, the declaration of smaller roads (*secondary*, *residential*, and *service*) is in some areas not consistent. For example, there are several areas with a mixture of these street types whereby the street network's topology does not indicate explicitly whether there is a different hierarchy among these types. Furthermore, there are *residential* streets in Tuas at the very south west of Singapore, although Tuas is a purely industrial

district. Hence, it is unclear whether the street type classification is sufficiently reliable to allow quantitative distinctions among the smaller street's type. Another problem of the OSM street network is that the fifth most common street type is *unclassified*, meaning that these streets were not assigned to any class.

These inaccuracies are inherent to crowd-sourced data such as OSM. Due to the huge number of users who are entitled to edit the maps without major restrictions, different interpretations are combined, which compromises consistency (Moecker, 2014). Despite these issues, the used street network is comprehensive and well connected. Hence, it constitutes a good basis for the analysis and simulation of driving profiles.

Chapter 3

Driving profile analysis

This chapter describes the analysis of taxi driving profiles. First, Chapter 3.1 summarises all pre-processing steps and explains the merging of the original data sets into two data sets. Subsequently in Chapter 3.2, *standstill periods* are extracted from the driving profiles and classified. Based on that, *shift schedules* are derived which describe the taxi drivers' activity patterns. Next, in Chapter 3.3 the taxis' trips are classified and analysed with respect to the taxis' status. Furthermore, the algorithm to match the driving profiles to Singapore's street network is introduced. Finally, traffic statistics are derived from the map-matched trips in Chapter 3.4 in order to estimate the energy consumption of electric vehicles and to estimate travel durations.

3.1 Pre-processing and merging of data sets

The taxis' driving profile analysis was made on two data sets which were derived from the raw data sets introduced in Chapter 2.4. The first data set was generated by merging the *logger*, *status*, and *revenue data sets* and is denoted as High Frequency Data set (HFD) due to the high recording frequency of the logger data. The HFD includes driving profiles of 50 taxis over a period of six months. The second data set comprised only of status data and covered 2,973 taxis over one month. Due to the lower recording frequency of the status data (one data point every 3 min), this data set is denoted as Low Frequency Data set (LFD).

Both data sets were essential for the analysis of the taxis' driving profiles. On basis of its high accuracy, the HFD allowed the investigation of route choices, trips, and traffic conditions in great detail. Whereas the LFD contains a significantly higher number of taxis and thereby enabled a more representative analysis on the drivers' activity schedules, *shift change*, and *break location* choices.

Before the *logger data set* was integrated into the HFD, following pre-processing steps were applied to improve its quality:

1. outlier detection (spatial and dynamic),
2. interpolation, and
3. smoothing.

As the first step, it was checked if the recorded data points were plausible. This was done with respect to their location (spatial) and their correlation with neighbouring

data points (dynamic). The spatial outlier detection ascertained whether the recorded points were located within Singapore's boundaries. The dynamic detection considered the speed and acceleration derived from the data point's location and recorded speed values. Each data point which speed exceeded 150 km/h or which acceleration was outside the range of -6 to $+4\,m/s^2$ was detected as outlier and consequently, deleted.

All gaps in the data set caused by either deleted outliers or missing recordings were filled by interpolated values. Here, the *Piecewise Cubic Hermite Interpolating Polynomial Method* (Fritsch and Carlson, 1980) was applied. Finally, a *moving window low pass filter* was applied to smooth the speed profile. All pre-processing steps are explained in detail in (Moecker, 2014).

The outlier detection was also applied to the *status data sets*. However, since its recording frequency was much lower, fewer outliers could be detected. Outliers were removed and not replaced by interpolations as the lower recording frequency made it very difficult to find reasonable substitutions.

After the pre-processing, the HFD was created by merging the *logger*, *status*, and *revenue data sets*. Therefore, the *logger data set* was used as basis and got extended with the features *status* and *revenue*. The status of all *logger data set* points which time was exactly the same as the time in the status data was set to the corresponding value of the *status data set*. This status information was copied to all successive data points until the next data point with a status value originating from the *status data set* was reached (Moecker, 2014). As the *revenue data set* contained the exact time when a *hired* trip started, this information was also used to alter the status feature. The information on the amount of taxi fare, charged after the trip, was added to the corresponding data point when the hired trip started. All other data points' revenue entries remained vacant.

Table 3.1: Key figures of data sets

	Unit	HFD	LFD
Recording frequency	1/s	1	1/180
Number of taxis	-	50	2,973
Recording period	d	184	31
Mileage	km	2,521,055	31,285,627
Number of data points	-	304,914,091	35,819,968

Some key figures of the HFD and LFD are listed in Table 3.1. Due to its much higher recording frequency, the HFD contains 8.5 times the number of data points compared to the LFD. However, as the LFD covers many more taxis, the total recorded mileage of this data set is considerably higher (a description on how the mileage of the LFD was estimated follows in Chapter 3.3). Nevertheless, the HFD contains more than 2.5 million km of high quality driving profiles and constitutes a good basis for the following analysis.

Both data sets are stored in databases that design is presented in Appendix D.

3.2 Standstill periods

In order to identify locations where charging is possible and to simulate the charging behaviour of taxi drivers, it is essential to gain a detailed understanding of the taxis' *standstill periods*. A *standstill period* is defined as a time period when the taxi is stationary. These events could be used to recharge the taxis' battery. To distinguish these events from stops which were caused by traffic conditions (traffic jam, red light, ...) the required minimum standstill duration was set to 5 min.

3.2.1 Detection

Regarding the HFD, *standstill periods* were identified by analysing the speed profiles. Anytime the speed of all data points within a period of at least 5 min was zero, a *standstill period* has been detected.

Since the LFD contains much less information than the HFD, a different approach was applied to identify *standstill periods*. Therewith, the first step was to classify data points as *standstill* if at least one of the following conditions was fulfilled:

Condition 1: duration to next data point greater than 15 min

Condition 2: average speed to next data point below 0.25 km/h

Condition 3: status is *log off*

Condition 1 takes into account that there are big gaps in the data set when the taxi was switched off. Hence, a *standstill period* must be assigned at each of these events. Condition 2 considers if the taxi remained at almost the same location of the previous data point. Usually, when taxis are parked, the status is switched to *log off*, this case is respected by Condition 3. Next, data points classified as *standstill* which were not farther apart than 10 min were combined to one *standstill period*. Data points between two combined *standstill periods* were classified as *standstill* as well. Finally, all *standstill periods* shorter than 5 min were removed.

3.2.2 Classification

Standstill periods of both data sets were classified as *break* or *shift change*. *Breaks* are short interruptions of *shifts* when drivers have a rest or eat, whereas *shift changes* are periods when the taxi is parked for a longer duration (typically several hours) until either the same or another driver uses the taxi to start a new *shift*.

This classification is important in the context of simulating the charging behaviour of electric taxi drivers. During *breaks,* public charging stations with high charging power are required to minimise the drivers' loss of time. However, if public charging stations could be used during the drivers' *shift change* as well, the charging station utilisation would be considerably lower, as *shift change* durations are typically much longer than the time to fully recharge the battery. As a result, charging stations would be blocked by taxis which would have completed their charging process already long time ago. Furthermore, this classification also allows to analyse the option of using cheaper low power AC charging stations at the drivers' *shift change location* to recharge during the *shift change*.

The *standstill period* classification was done in four steps:

Step 1: Assign *shift change* to all *standstill periods* which are longer than two hours

Step 2: Assign *shift change* to *standstill periods* subject to location, standstill duration, and *shift* duration

Step 3: Assign additional *shift changes* to *standstill periods* of *shifts* which are longer than 16 hours

Step 4: Assign *break* to all *standstill periods* which were not classified as *shift change*

It is assumed that no taxi driver has *breaks* longer than two hours, thus all these *standstill periods* were classified as *shift change* in Step 1. After this assignment, a set of *shifts* was extracted, whereby each *shift* is defined as a set of consecutive *standstill periods* between two *shift changes*.

In Step 2, within each *shift*, candidate *standstill periods* for an assignment of *shift change* were searched for. Each candidate had to fulfil three conditions:

Condition 1: The *standstill* duration must be longer than 30 min

Condition 2: The duration of both resulting *shifts* must be at least four hours if *shift change* was assigned to the candidate *standstill period*

Condition 3: The candidate *standstill period* must have taken place within the area with the most *shift changes* of the considered taxi

These conditions shall ensure that the resulting *shifts* and *shift changes* are not too short and that the *shift change locations* are not too far away from the place where the taxi drivers are usually having their *shift changes*.

For all *shifts* which had more than one candidate, a decision had to be made which of these candidates was assigned as *shift change*. Therefore, for each candidate a total weight w_{Total} was calculated while the candidate with the highest weight was selected. The total weight is calculated by cumulating five normalised weights:

$$w_{Total} = w_{Duration} + w_{Area} + w_{Activity} + w_{ShiftChangeHistory} + w_{ShiftMiddle} \quad (3.1)$$

Thereby, the weights take following aspects into account (all weights were calculated for each taxi individually):

Duration: The higher the *standstill* duration the higher the weight. Durations of two hours got a weight of one.

Area: Singapore got divided into 306 areas. If the candidate location was in the same area where most of the taxi's *shift changes* took place, the weight was one. Otherwise it was set to zero.

Activity: It is expected that drivers followed certain mobility patterns and had *shift changes* at times when they were least active. Therefore, time intervals of one hour were defined and for each time interval the ratio of *standstill* duration to the interval duration was calculated. The weight was set to the ratio of the time interval in which the candidate *standstill period* occurred.

Shift change history: Furthermore, it was calculated how many *shift changes* started in each time interval. This weight was set to the ratio of the number of *shift changes* at the candidate's time interval to the maximum number of *shift changes* over all time intervals.

Shift middle: To avoid the assignment of *shift changes* shortly after or before another *shift change*, this weight is one if the candidate *standstill* event took place in the exact middle of two *shift changes* and decreases with respect to the time difference to the closest *shift change*.

After the assigning *shift changes* to the candidate *standstill periods* with respect to the total weight of equation 3.1 in Step 2, Step 3 checks if there are any *shifts* left which were longer than 16 hours. *Shifts* exceeding this duration are considered as not possible and were split into several *shifts* by assigning additional *shift changes* within these *shifts*. In contrast to Step 2, no conditions were applied to constrain the selection of candidates. The decision which candidate was assigned as *shift change* was again made with respect to the total weights of equation 3.1.

Finally in Step 4, all *standstill periods* which were not classified as *shift change* got assigned as *breaks*.

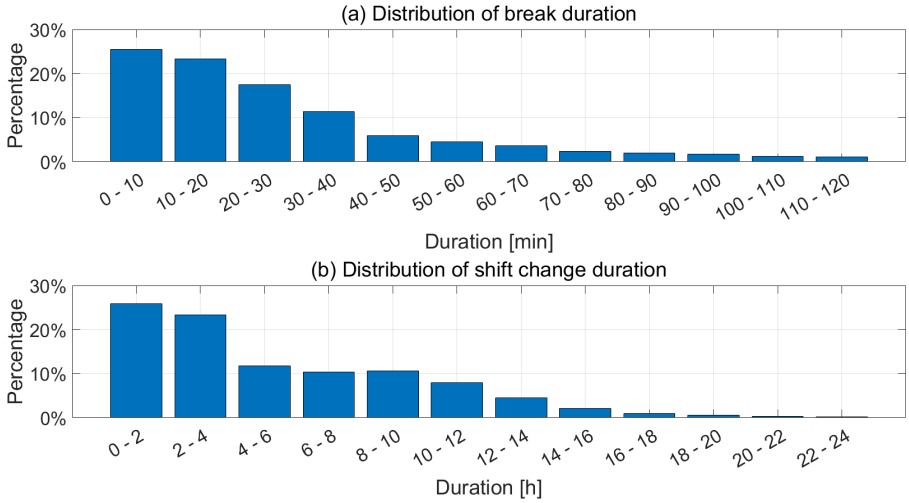

Figure 3.1: Distribution of *break* (a) and *shift change* (b) duration

Figure 3.1 shows the distribution of *break* and *shift change* durations of the LFD set. The frequency of *breaks* decreased with respect to the *break* duration whereby *breaks* with a duration between 5 and 10 min were with 25% most common. The average *break* duration was 28 min which would be sufficient to recharge 23 kWh with a charging power of 50 kW. This amount of energy would allow to drive another 137 km at an energy consumption of 170 Wh/km. As taxis had 1.9 *breaks* per *shift* on average, and the average mileage per *shift* was 195 km, *breaks* alone would be sufficient to recharge the taxis' energy demand.

The frequency of *shift changes* also decreased continuously with respect to the *shift change* duration whereby durations up to two hours occurred in 26% of all cases. The

average *shift change* duration was 6.0 h. If a taxi with a battery capacity of 50 kWh would use a 50 kW charging station during the *shift change*, the battery could have been fully charged after approximately 1.0 h[1] which would have resulted in blocking the charging station for the next 5.0 h. Hence, the utilisation of the charging station would have been only 17% during the *shift change*.

Another interesting aspect is that if the battery could be charged by an AC charging station with a charging power of 6 kW, 36 kWh could be recharged during the *shift change* on average. This would be enough to drive 212 km which is more than the average mileage per *shift*.

Hence, both charging concepts could be viable solutions. However, these estimations were only made for average values, whereby the distributions show that there is a big variance in *break* and *shift change* durations. In order to take the big variety of taxi driving profiles into account, a taxi driving profile simulation model was developed (see Chapter 5).

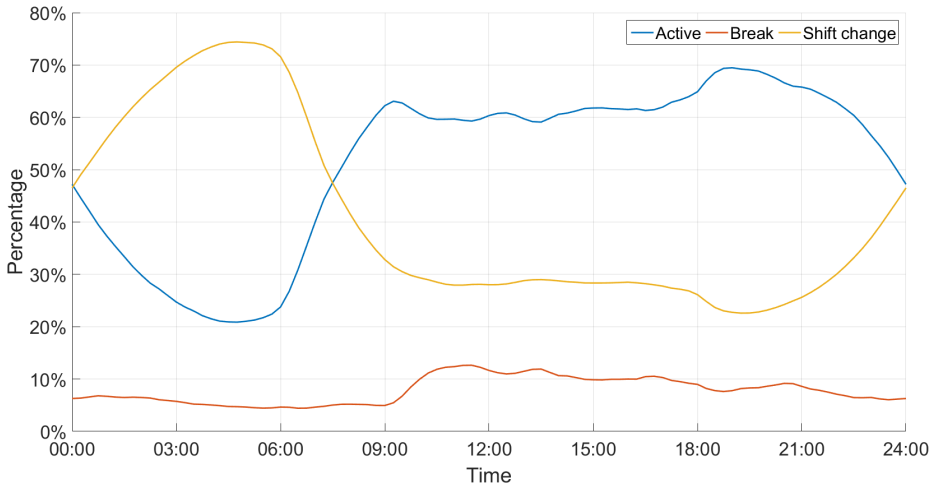

Figure 3.2: Activity of taxi fleet with respect to time

Apart from the duration of *standstill periods*, it is also important to take into account when these events occurred. Therefore, Figure 3.2 visualises which percentage of the taxi fleet of the LFD set was active (taxi was driving) or had a *break* or *shift change* with respect to time. At 4:45 the lowest percentage (21%) of the taxi fleet was active whereby the highest share of active taxis was reached at 19:00 with 69%. This peak is reached as the percentage of taxis having *shift changes* decreased from 28% at 17:00 to 23% at 19:00. One reason why many drivers started their *shift* at that time could be that as of 18:00 an evening surcharge of 25% is added to the standard fare (LTA, 2017a).

The percentage of taxis having *breaks* varied only between 5 and 7% throughout the whole night while it significantly increased from 5 to 12% between 9:00 and 11:00. This increase may be explained by the ending of the morning peak hour surcharge at 9:30, which could cause drivers to have a rest.

[1] the duration would be slightly longer as the charging power decreases after the battery's charging level exceeds 80%

The drivers' activity patterns are an important information for the planning of the charging infrastructure in order to estimate the taxis' charging demand with respect to time and to derive the required number of charging stations to supply that demand. Therefore, the driving profile simulation model is designed to reproduce these patterns.

3.2.3 Location clustering

Another essential aspect for the charging infrastructure planning is to identify locations where charging stations shall be installed. In order to reach a high acceptance of the drivers, it is vital to give them the chance to recharge their taxi at locations where they would stop anyway to have a *break*. Therefore, a clustering algorithm was applied to derive *candidate charging locations* for the placement of charging stations from the set of all *standstill period locations*.

The main requirement for the clustering algorithm was to identify locations with the highest density of *standstill* events whereby events outside these hotspots did not have to be matched to any cluster. The *density-based spatial clustering of applications with noise* (DBSCAN) algorithm (Tran et al., 2013) fulfils these requirements. It identifies clusters where at least n_{min} data points are within a maximum radius of ε.

The parameters ε and n_{min} have to be adjusted with respect to the application. In order to limit the size of each cluster to the size of car parks or parking houses, ε was set to 50 m. The minimum number of data points per cluster n_{min} was set in order to get approximately 300 clusters in total. This number was defined as approximately 50 *charging locations* with 5 charging stations each would be required for an electric taxi fleet of 3,000 vehicles. In order to give the optimisation some freedom to choose locations, a six fold higher number of clusters was targeted. After clustering all 457,657 *standstill* events of the LFD with different values of n_{min}, a value of 180 was finally chosen which generated 291 clusters.

In order to embed the clusters to the street network, each cluster was assigned with the node ID of the *street network node* which was nearest to the cluster's centroid.

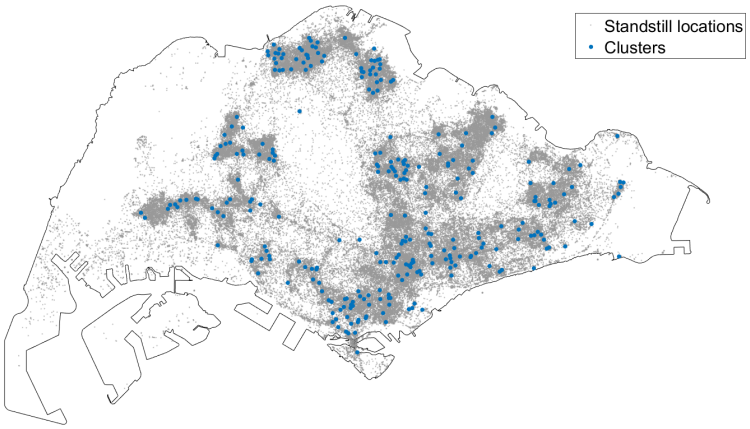

Figure 3.3: Map with *common standstill clusters*

Figure 3.3 shows the locations of all *standstill* events and the found clusters. There was a high density of clusters in the south at the Central Business District (CBD) which can be explained by the general high density of taxis in this area. Apart from that, there was also an area in the very north with a high number of clusters. This is due to the fact that many drivers are living in this area, and that many drivers had their *shift change* or *breaks* near their home. The airport in the very east was another place where many *standstill* events took place.

Additionally to these clusters which were based on the *standstill periods* of all taxis, clusters were derived for each taxi individually. To distinguish these types of clusters, the clusters derived from all taxis are denoted as *common standstill clusters* whereby the latter are named *individual standstill clusters*. Although the *common standstill clusters* are representative as they are based on the driving profiles of all taxis, they may not be sufficient to reflect the taxi drivers' individual choice of *standstill locations*. For example, it could be that a driver has a *break* at the same location every day but as he or she might be one of very few drivers who prefer this place it would not be among the *common standstill cluster* locations. Therefore, *individual standstill clusters* are very useful to understand the behaviour of each driver in more detail.

Since the data set to identify *individual standstill clusters* is much smaller, the maximum radius ϵ was increased to 200 m and the required minimum number of points per cluster n_{min} was reduced to six. With these parameters the average number of *individual standstill clusters* per taxi was 3.7 whereby 3,705 *individual standstill clusters* were found in total. Each *individual standstill cluster* was also assigned with one *street network node* ID. For all *individual standstill clusters* which had one *standstill period* in common with a *common standstill cluster*, the *common standstill cluster's* node ID was used. Otherwise, the cluster's centroid was calculated and matched to the nearest *street network node*.

3.2.4 Shift schedules

Shift schedule sets were derived from the LFD to summaries the activity pattern of each taxi[2]. Thereby, each *shift schedule* represents one *shift* and contains following information:

- start time
- start location
- end time
- end location
- *shift change* duration

whereby the start and end location is described by a *street network node* ID. Furthermore, each *shift schedule* contains a *break set* which includes the information of all *breaks* which were executed during the *shift*. Each *break set* contains following features:

- start time

[2]taxis can be operated by more than one driver, hence *shift schedules* may cover the behaviour of not only one driver

- duration
- driving distance to *break location*
- location

The feature "driving distance to *break location*" contains the taxi's driving distance after it finished the last *hired* trip until it arrived at the *break location*. Based on this feature it is possible to assess whether the driver had the intension to stop at a specific location or chose an arbitrary location nearby. The "location" feature includes the node ID if the taxi stopped at an *individual standstill cluster* location or is empty otherwise. The generated *shift schedules* are an essential input for the driving profile simulation model to reproduce the taxis' driving profiles in great detail.

3.3 Trips

Apart from *shift schedules*, trips are the other main statistical input of the driving profile simulation. In order to simulate the driving profiles of electric taxis it is necessary to estimate the energy consumption of each trip. Therefore, only trips of the HFD were used as only this data set contains detailed information about the vehicles' speed profiles.

3.3.1 Status and classification

A trip is defined as a set of consecutive data points of the same status which are not interrupted by any *standstill periods*.

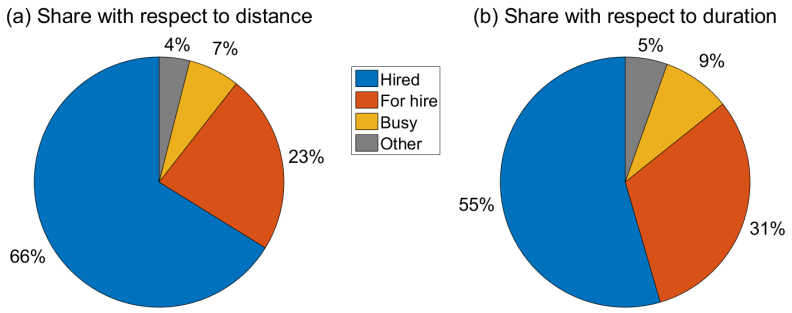

Figure 3.4: Share of status with respect to driving distance (a) and duration (b)

Figure 3.4 shows the frequency of the trips' status with respect to the driving distance (a) and the duration (b) extracted from the HFD. In both cases the status *hired* was clearly dominant, followed by the statuses *for hire* and *busy*. All other statuses combined had a share of 4 respectively 5%. The share of *hired* trips was with respect to the driving distance with 66% clearly higher than with respect to the duration (55%). This can be explained by the trips' average speed: *hired trips* had an average speed of 36.2 km/h while *for hire trips* were considerably slower with 22.2 km/h. The reason for this difference is that in case of *hired trips*, the driver had a defined destination which he or she tried to reach as fast as possible. In contrast, during *for hire trips* the driver circles around and has to reduce the speed in order to find the next passenger.

Due to these significant differences in the driving profiles with respect to the trips' status, two classes of trips were defined: *engaged trips* and *search trips*. *Engaged trips* are trips with customer on board, hence the status must be *hired*, *soon to clear (STC)*, or *payment* (Chapter 2.4.2). Directly connected trips of these statuses without any *standstill periods* in between were combined to one *engaged trip*. However, it must be considered that the taxis' status information was only recorded every three minutes and that it is possible that the driver could have found the next customer in less than that time. In this case two separate *engaged trips* were detected with the help of the *revenue data set* which contains all points in time whenever a new trip started. Thus, *engaged trips* can be directly connected with each other. The second trip of these pairs was additionally tagged as *instant pickup trip*.

A *search trip* is defined as a set of directly connected trips of the statuses *for hire*, *on call*, and *arrived* without any *standstill periods* in between. Moreover, to ensure that a customer was found after a *search trip*, an *engaged trip* must have directly followed after these trips. All trips neither classified as *search* or *engaged trip* were not further taken into account.

Table 3.2: Statistics of *search* and *engaged trips* of the HFD

	Unit	*Search trips*	*Engaged trips*
Number	-	90,899	137,072
Average distance	km	3.6	10.6
Average duration	min	10.8	17.6
Average revenue	SGD	-	14.1

Table 3.2 contains some statistics of the extracted trips. The number of *engaged trips* is higher than the number of *search trips* due to *instant pickup trips*. Although taxis are actively searching for passengers by driving around, the distance of *engaged trips* was on average 2.9 times higher than that of *search trips*. This reflects the high demand for taxis in Singapore. The average revenue per *engaged trip* was 14.1 SGD.

Figure 3.5 shows the spatial-temporal frequency of origins and destinations of *engaged trips*. Each map represents on a different time interval, whereby each time interval covers one hour with the displayed time being exactly in the middle of the time interval (e.g. the 3:00 map shows trips between 2:30 and 3:30). The colour of each area is subject to the difference of the number of originating and arriving *engaged trips*. It is red if more trips started than arrived (surplus of origins) and blue if the opposite is true (surplus of destinations). In case the number of starting and arriving trips is equal, the colour is white. The bigger the difference, the darker the colour.

Map (a) shows the origin-destination map at 3:00, where the majority of trips started from the CBD in the south of Singapore (origin - red) and went to outer - mainly residential areas (destination - blue). During that time it is likely that taxis came back to the CBD without a passenger on board once they finished a trip farther away.

In contrast, at 8:00 (b) taxis came from outer areas to the CBD and the airport. Based on the analysis of *shift change locations* of all taxis, it is assumed that most of the drivers lived in the areas which had the highest surplus of starting trips. Most likely, they were starting their *shift* at that time and went to the CBD or airport since the customers' travel demand to these areas was very high.

Figure 3.5: Origin-destination map of *engaged trips* for different times of the day

Later at 13:00 (c) most of the areas' colours are bright, which means that the number of starting and arriving trips was roughly equal in each area. During that time there is no specific direction of the customers' travel demand visible - most taxis were searching in the same area for the next customer where they dropped the last one.

In the evening at 19:00 (d) the colours of most areas were inverted compared to the 8:00 map, it seems that many people who went to the CBD or airport in the morning came back home at that time.

These maps show that the taxis' driving patterns are dependent on time and space. These effects need to be taken into account in order to simulate driving profiles as realistic as possible.

3.3.2 Mileage and revenue estimation

Regarding the HFD, the driving distances were calculated by integrating the recorded speed with respect to time. Although all trips were extracted from the HFD, it was also necessary to have mileage and revenue estimations of the LFD in order to extract *shift schedules* and to validate the driving profile simulation model in Chapter 5.8.

One possibility to estimate the driving distance of the LFD would be to map-match all data points to the street network and calculate the length of shortest paths connecting these points. However, this would be extremely time consuming as the LFD contains a total mileage of many million km.

Hence, a computationally more efficient approach was chosen. Therefore, the whole recording area was divided into squares with a side length of 780 m and each data point was assigned to one square with respect to its location (see Figure 3.6). The driving distance d_{drive} from one data point in cell i to the consecutive point in cell j was estimated with respect to the euclidean distance $d_{euclidean}$ between these points:

$$d_{drive} = a_{ij} d_{euclidean} + b_{ij} \tag{3.2}$$

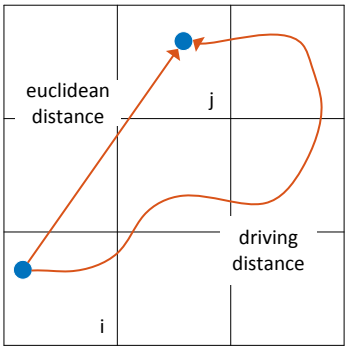

Figure 3.6: Driving distance estimation

As it is not possible to drive directly from square *i* to *j*, the parameter b_{ij} takes the street network's topology into account. The data points' location within the squares is taken into account by a_{ij}. To obtain the parameters a_{ij} and b_{ij} for each combination of origin square *i* and destination square *j*, 1.4 million data point pairs with a time difference of three minutes each were extracted from the HFD. Since the driving distance between data points of the HFD is known, the parameters a_{ij} and b_{ij} were fitted for each set of data point pairs.

Since no revenue data was available for the LFD, the revenue of each trip had to be estimated as well. Taxi fares in Singapore consist of a flag down fare which has to be paid at the start of each trip plus duration and distance dependent fares. Furthermore, a surcharge factor is multiplied to the basic fare if the trip took place in the late night or during peak hours (LTA, 2017a). First of all, the revenue of non *engaged trips* was set to 0 SGD. The *engaged trips'* revenue *r* was estimated with respect to the trip's driving distance d_{drive}, duration Δt, and the time of the day *t*. The surcharge factor is taken into account by the function $f_s(t)$:

$$r = (k_d d_{drive} + k_t \Delta t + k_0) \cdot f_s(t) \tag{3.3}$$

Again, the HFD was used to fit the parameter k_d, k_t, and k_0. Thereby, it was considered that the data set included different vehicle types for which different fares applied (SMRT, 2015). The fitted parameter values are listed in Table 3.3.

Table 3.3: Revenue estimation parameter

Vehicle type	k_d [SGD/km]	k_t [SGD/min]	k_0 [SGD]
Chevrolet Epica	0.71	0.15	1.92
Toyota Prius	0.76	0.14	1.87

The mileage and revenue of all taxis of the LFD were estimated. The resulting distributions of daily mileage (a) and revenue (b) per taxi are shown in Figure 3.7.

Both distributions show a wide spread between the least and the most active taxis. On average, the daily mileage of *Prius* taxis was 365 km which was higher than the average daily mileage of *Epica* taxis of 342 km. It is suspected that this was due to

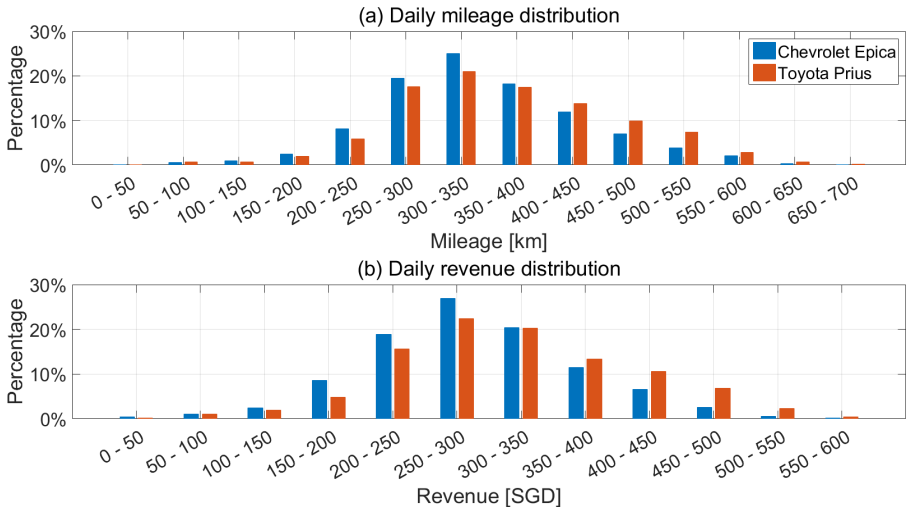

Figure 3.7: Distribution of average daily mileage (a) and revenue (b) per taxi

the lower fuel consumption (Chevrolet, 2009; Toyota, 2015) and the higher rental fee (SMRT, 2015) of the *Prius* compared to the *Epica*. This makes *Prius* taxis economically more profitable for higher daily mileage. There was a significant increase in the proportion of taxis having a daily mileage between 200 - 250 km and those between 250 and 300 km. That can be explained by the LTA's taxi availability standard[3] (LTA, 2016a) which regulated the percentage of taxis which have to meet a daily mileage of at least 250 km.

Figure 3.7(b) shows the average daily revenue distribution. The average revenue of the *Prius* taxis was with 318 SGD higher than that of *Epica* taxis which was 289 SGD. This difference was caused by the higher average mileage of *Prius* taxis and the different fare schemes that favours the *Prius* as well (SMRT, 2015).

These distributions illustrate the heterogeneity of taxi driving profiles very well. It is essential to simulate taxis with different *shift schedules* to reproduce this variety of driving profiles.

3.3.3 Map-matching

In order to extract traffic statistics, all data points of the HFD were matched to the street network of Singapore. Therefore, all *sections* of the street network were assigned with an unique ID and each data point was tagged with the ID of the *section* which the taxi traversed when it was recorded.

For this task, the ST (Spatial-Temporal) map-matching algorithm was applied (Lou et al., 2009). This algorithm takes spatial and temporal (speed) information of the data points and the street network's topology into account. A detailed description on how this algorithm was applied to the HFD can be found in (Moecker, 2014).

In order to reduce the computation time, only every 60^{th} data point (one point per minute) was matched to the street network. The *sections* of the remaining data points were assigned with respect the shortest path connecting matched data points.

[3] this standard was valid during the data recording but was abolished on 1.1.2017

The transition probability P_{total} that data point p_i matches to *section* c_i^s was calculated with respect to the matching of the previous data point p_{i-1} to *section* c_{i-1}^t by following product:

$$P_{total}\left(c_{i-1}^t \to c_i^s\right) = P_{point}\left(p_i, c_i^s\right) \cdot P_{path}\left(c_{i-1}^t \to c_i^s\right) \cdot P_{speed}\left(c_{i-1}^t \to c_i^s\right) \quad (3.4)$$

Thereby, following aspects were taken into account:

point: Projected distance of data point p_i to *section* c_i^s. The lower the distance, the higher the probability to match p_i to c_i^s.

path: Length of shortest path on street network from *section* c_{i-1}^t to *section* c_i^s. The shorter the length the higher the probability. This aspect ensures that the matched *sections* are closely connected with each other.

speed: Similarity between expected speed per *section*[4] on the path from c_{i-1}^t to c_i^s and the average speed from p_{i-1} to p_i. This feature ensures that suitable *sections* are selected with respect to the recorded speed. This is important if there are two parallel roads close to each other with different speed limits (e.g. express-way and residential street).

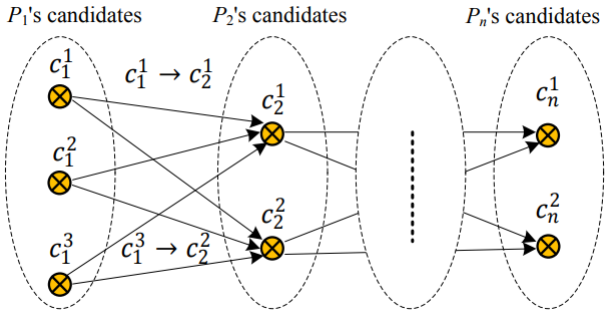

Figure 3.8: Map matching graph with candidate *section* and transition probabilities (Lou et al., 2009)

Transition probabilities P_{total} were calculated for the three nearest *sections* of each data point. Next, a graph with all candidate *sections* and transition probabilities was created (see Figure 3.8). Based on that graph the combination of candidate *sections* with the highest total transition probability was selected.

3.4 Traffic statistics

The map-matched driving profiles of the HFD allow to extract time dependent speed related statistics of street types, roads, and *street network sections*. These statistics were used in Chapter 4 to estimate the energy consumption for given paths and in Chapter 5 to simulate travel times.

[4]this speed was either derived from recorded trajectories or speed band sensor data (LTA, 2014a)

3.4.1 Choice of street types

Due to the map-matching of all data points it can be easily analysed which street types were chosen by the taxi drivers.

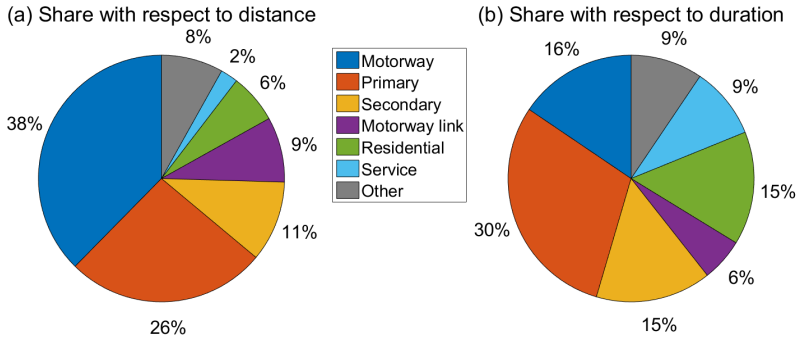

Figure 3.9: Usage share of street types with respect to driving distance (a) and driving duration (b)

Figure 3.9 shows how often each street type was used with respect to driving distance (a) and driving duration (b). The most commonly used street type with respect to driving distance is *motorway* (equivalent to express-ways) with 38%, additionally, *motorway links* which are connecting other streets with express-ways or express-ways with each other contributed another 9%. Hence, 47% of the total mileage was recorded on express-way related street types. The shares of other street types decreased with their size: starting with *primary* and *secondary* roads to the small *residential* and *service* roads. Although *unclassified* roads were the fifth most common street type in terms of length, their usage share with respect to driving distance was only 1.9%. Thus, the issue of not knowing the type if these streets is neglectable.

Regarding the usage share with respect to the driving duration (b), the share of express-way related roads decreased from 47% to 22% whereby the share of smaller roads increased significantly. In case of *service* roads, the share changed from 2% with respect to driving distance to 9% with respect to driving duration. The reason for these changes is that roads of different type were traversed with very different speeds. *Motorway* was with 72 km/h on average the street type with by far the highest speed whereby *primary* roads had a value of 26 km/h and *service* roads had the lowest average speed of 7 km/h. The average speed on express-ways during peak hours[5] was according to (LTA, 2014c) 64.1 km/h which matches very well with the extracted value of 62.6 km/h for these time windows.

Since the comparison of street types and average speeds is sound, it can be assumed that first, the street type classification is logical and second, that the map-matching algorithm produced reasonable results.

3.4.2 Speed profiles

The average speed over all street types throughout the day was 29.8 km/h, to analyse the taxis' speed in more detail, the average speed with respect to the time of the day is

[5] 8:00 - 9:00 and 18:00 - 19:00

shown by Figure 3.10.

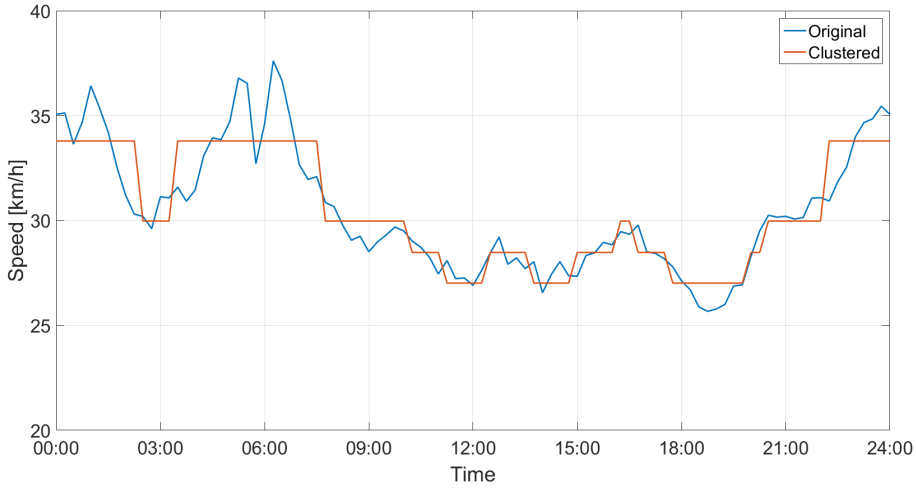

Figure 3.10: Average speed profile with respect to time of the day

The highest speed was reached at 6:15 with 37.6 km/h while the lowest speed was recorded with 25.7 km/h during the evening peak at 18:45.

Interestingly, the average speed during the morning peak is higher than during the day, e.g. the speed reduced from 30.7 km/h to 27.9 km/h between 8:00 and 13:00. This can be explained by the usage of express-ways: at 8:00 18.8% of all active taxis drove on express-ways while this percentage dropped to 13.5% at 13:00. This behaviour could be a result of the travel patterns discussed by Figure 3.5 where at 8:00 many taxis drove from outer areas to the CBD or airport and had disproportionate long *engaged trips* of 11.9 km on average. Later, at 13:00 the average *engaged trip* distance dropped to 9.5 km which may affected the share of taxis using express-ways.

During the evening peak hour at 19:00 only 15.5% of all active taxis used express-ways, which could have been a result of relatively short *engaged trips* of 9.9 km on average. Additionally, due to the high traffic volume at that time, the average speed dropped to the lowest value throughout the day.

Another interesting aspect of the speed profile is the deep and narrow valley at 5:45 where the average speed dropped and increased by more than 4 km/h within one hour. A separation of the speed profiles by the trips' statuses revealed that the speed of *engaged trips* did not drop at that time. An explanation why the speed of the other trips dropped could be that many taxi drivers started their *shift* at that time (see Figure 3.2) and therefore had to drive through small streets with low speed until they reached major roads to search for their first customer.

In order to take different traffic situations into account for the following analysis, four time dependent *speed clusters* (named as *low*, *medium*, *high*, and *very high speed*) were derived from the speed profile. The time windows of the *speed clusters* were designed in the way that approximately the same number of recorded data points was covered by each cluster. As a result, the validity of the generated statistics of each cluster was comparable.

The *speed clusters* are represented by the red line in Figure 3.10. It shows that e.g.

the *very high speed cluster* covers the time periods from 3:23 until 7:38 and 22:08 until 2:23. The total time window duration of this cluster is the longest as it covers almost the whole night when the fewest number of data points was recorded as the smallest share of the taxi fleet was active at that time. The time windows of all speed clusters are listed in Appendix B.

In order to analyse the driving profiles in greater detail, *pass-through speeds* for each *street network section* were extracted. *Pass-through speeds* are defined as the average speed of consecutive data points which were matched to one *section*. For each event when a taxi drove through a *section*, another *pass-through speed* was calculated.

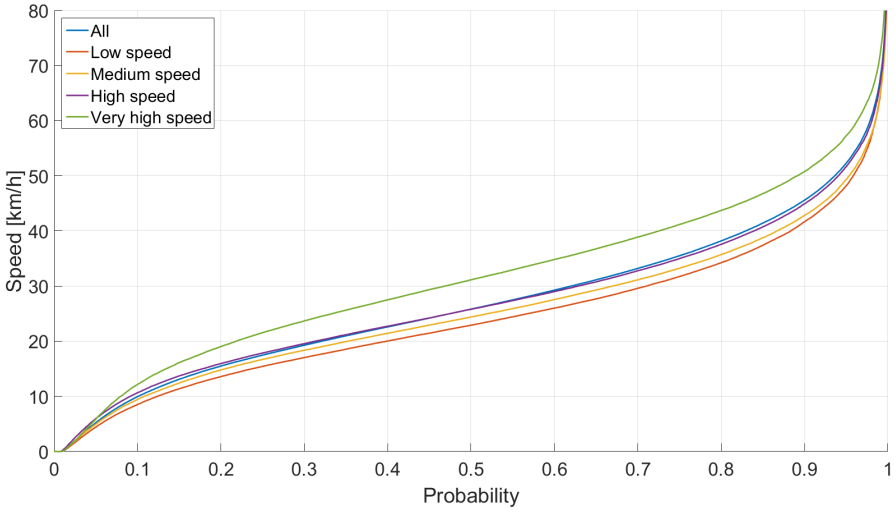

Figure 3.11: Inverse cumulative frequency distribution of *pass-through speeds* for *sections* of type *primary* and all *speed clusters*

The inverse cumulative frequency distribution of *pass-through speeds* for *sections* of the type *primary* is shown by Figure 3.11. These distributions were created for each *speed cluster* separately and additionally for all clusters combined (represented by "All"). The diagram shows e.g. that the *pass-through speed* of the very *high speed cluster* was with a probability of 80% lower than 43.7 km/h.

Singapore has a speed limit of 50 km/h on all roads except express-ways (LTA, 2017b). This limit was exceeded by 10.9% of all *pass-throughs* of the *very high speed cluster* while due to the higher traffic volume during the *low speed cluster*, this limit was only exceeded in 4.2% of all cases. The probability of *pass-through speeds* of 0 km/h ranged from 0.7% to 0.9%. Obviously, these values are not sensible and must have originated from either recording or map-matching errors.

In order to make these distributions easier to handle, the parameters *a* to *e* were fitted to estimate the *pass through speed* $\overline{v}$ with respect to the probability *p* for each *speed cluster* individually (the upper index α refers to the *speed cluster*):

$$\overline{v}^{\alpha}(p) = a^{\alpha} \cdot p - b^{\alpha} \cdot (\exp(-c^{\alpha} \cdot p) - 1) + d^{\alpha} \cdot (\exp(e^{\alpha} \cdot p) - 1) \tag{3.5}$$

This function is designed to be greater than zero for every probability higher than zero. Thus, the discussed inaccuracy of 0 km/h speeds found in the data is not repro-

duced by the fit function.

If at least 30 *pass-throughs* could be extracted, the parameters of this function were fitted for each *section*, all *sections* with the same *way* ID, and all *sections* of the same street type individually. The resulting fit parameters are listed in Appendix C. In the next chapter, these functions are used to obtain the *pass-through speed* per *section* with respect to a random number between zero and one.

3.4.3 Acceleration

Additionally to the speed distributions, accelerations were analysed with respect to the *pass-through speed* for each *section*, *way*, and street type for all *speed clusters*. Figure 3.12 shows the extracted accelerations of all *sections* of type *primary*.

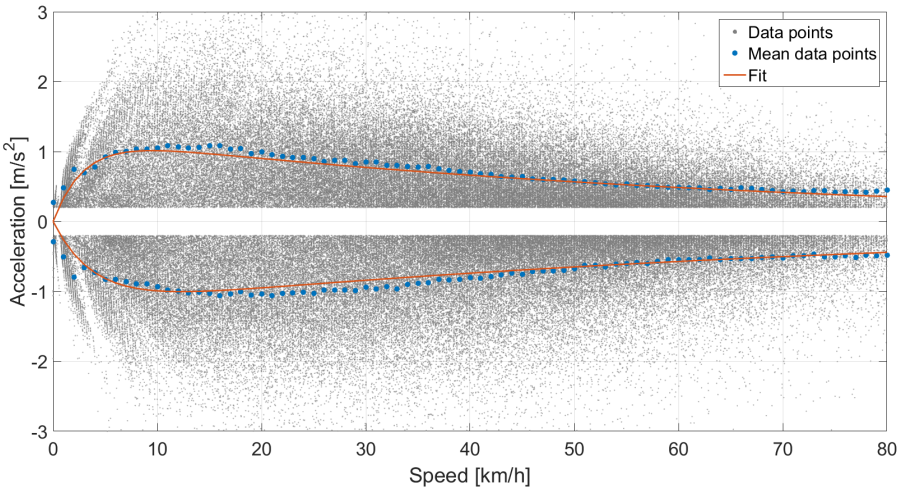

Figure 3.12: Fit of acceleration with respect to *pass-through speed* of all *primary sections*

The diagram distinguishes between positive and negative accelerations: positive accelerations must have been at least $0.2\,\mathrm{m/s^2}$ and negative accelerations equal or smaller $-0.2\,\mathrm{m/s^2}$. All values between these thresholds were considered as no acceleration and excluded.

The reason for choosing $0.2\,\mathrm{m/s^2}$ was that the speed was recorded in intervals of $1\,\mathrm{km/h}$ with a frequency of one value per second. Hence, the lowest measurable acceleration was $0.28\,\mathrm{m/s^2}$. As the speed profile was smoothed during the pre-processing, the threshold was set a little below this value.

The figure contains more than one million data points (grey dots), which makes it very difficult to identify any trend in their distribution. Therefore, mean values over intervals of $1\,\mathrm{km/h}$ were calculated and displayed by the blue dots[6]. It can be seen that the positive acceleration increased fast at very low speeds, reached its maximum of $1.1\,\mathrm{m/s^2}$ at $16\,\mathrm{km/h}$ and decreased slowly with higher speeds. The negative acceleration profile is almost exactly mirrored to the positive accelerations.

The reason for having low accelerations at low speeds could be that drivers gradually press the acceleration pedal when starting from standstill. Later, when the driver reaches

[6]these dots are only used as reference, the parameters were fitted to the original data (grey dots)

the targeted speed he or she slowly lifts off the pedal in order not to overshoot the targeted speed.

Again, to handle the acceleration profiles easier, the parameters *a* to *c* of following function were fitted to the positive and negative acceleration data separately with respect to the *pass-through speed* $\bar{v}$:

$$\dot{v}^{\alpha}(\bar{v}) = a^{\alpha}\left(\exp\left(-b^{\alpha}\cdot\bar{v}\right) - \exp\left(-c^{\alpha}\cdot\bar{v}\right)\right) \tag{3.6}$$

This approach of fitting the acceleration profiles with respect to the *pass-through speed* was also applied in (Kraschl-Hirschmann and Fellendorf, 2012; Moecker, 2014). The difference to this work is that their fits were not individually made for time windows reflecting different traffic conditions (*speed-clusters*). Furthermore, (Kraschl-Hirschmann and Fellendorf, 2012) used a linear fit function which significantly overestimated accelerations at low speeds. (Moecker, 2014) used equation 3.6 and added the term $d\cdot\exp\left(-\frac{1}{\bar{v}}\right)$. On the one hand, the higher variance of the fit function increased the chance to achieve lower estimation errors, on the other hand higher variance always bares the risk that the algorithm which optimises the fit parameter gets stuck at a local optimum which is significantly worse than the global optimum. As this function was fitted to thousands of data sets it was not possible to check whether the results of each fit were reasonable. Therefore, a simpler and more reliable function was chosen in this work. The fitted parameters for acceleration and deceleration are listed in Appendix C.

3.4.4 Driving shares

In order to analyse the vehicles' driving status, all data points were classified to four categories with respect to their speed v and acceleration $\dot{v}$:

Idle: $v = 0$

Acceleration: $v > 0 \ \wedge \ \dot{v} > 0.2\frac{\mathrm{m}}{\mathrm{s}^2}$

Deceleration: $v > 0 \ \wedge \ \dot{v} < -0.2\frac{\mathrm{m}}{\mathrm{s}^2}$

Cruise: $v > 0 \ \wedge \ -0.2\frac{\mathrm{m}}{\mathrm{s}^2} \leq \dot{\mathrm{v}} \leq 0.2\frac{\mathrm{m}}{\mathrm{s}^2}$

Based on that, *driving shares* were defined as the ratio of the number of data points classified to one category to the total number of data points of one *pass-through* (Kraschl-Hirschmann and Fellendorf, 2012).

Figure 3.13 shows the four *driving shares* of all *primary sections* with respect to the *pass-through speed*. Again, due to the high number of data points, mean values for speed intervals of 1 km/h are shown by the blue dots.

Logically, the *idle share* (a) was very high at low speeds and decreased monotonously with respect to speed. Nevertheless, the *idle share* at a *pass-through speeds* of 60 km/h was still 2.5%. This can be explained by the high range of *section* lengths: while the average length of one *section* is 132 m, 3.8% of all *sections* were longer than 500 m. Thus, at these long *sections* it is possible to reach a high average speed while having a short stop in between.

Due to the high value of the *idle share* at low speeds, all other shares were small and increased with higher speeds. The *acceleration* and *deceleration share* curves were very

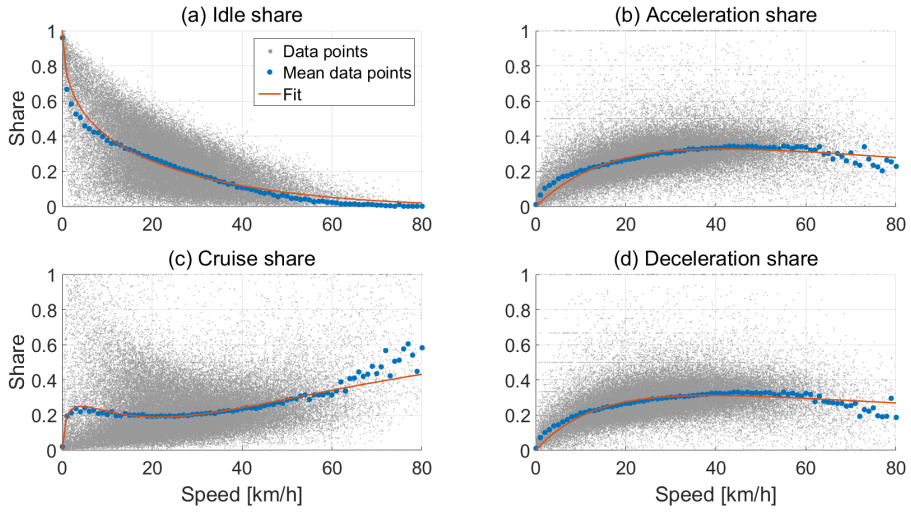

Figure 3.13: *Driving shares* of *sections* of street type *primary* with respect to *pass-through speed*

similar. Both shares decreased slightly at speeds above 60 km/h while the *cruise share* (c) increased further.

Following fit functions were defined to estimate the shares with respect to the *pass-through speed* $\bar{v}$ (*acc* refers to acceleration, *dec* to deceleration, the upper index α refers to the *speed-cluster*):

$$f^{\alpha}_{idle}(\bar{v}) = \exp\left(-\left(a^{\alpha}_{idle} \cdot \sqrt{\bar{v}} + b^{\alpha}_{idle} \cdot \bar{v}^2\right)\right) \tag{3.7}$$

$$f^{\alpha}_{acc}(\bar{v}) = a^{\alpha}_{acc}\left(\exp\left(-b^{\alpha}_{acc} \cdot \bar{v}\right) - \exp\left(-c^{\alpha}_{acc} \cdot \bar{v}\right)\right) \tag{3.8}$$

$$f^{\alpha}_{dec}(\bar{v}) = a^{\alpha}_{dec}\left(\exp\left(-b^{\alpha}_{dec} \cdot \bar{v}\right) - \exp\left(-c^{\alpha}_{dec} \cdot \bar{v}\right)\right) \tag{3.9}$$

$$f^{\alpha}_{cruise}(\bar{v}) = 1 - \left(f^{\alpha}_{idle}(\bar{v}) + f^{\alpha}_{acc}(\bar{v}) + f^{\alpha}_{dec}(\bar{v})\right) \tag{3.10}$$

In contrast to (Kraschl-Hirschmann and Fellendorf, 2012; Moecker, 2014), these definitions ensure that the *driving shares* are normalised:

$$f^{\alpha}_{idle}(\bar{v}) + f^{\alpha}_{acc}(\bar{v}) + f^{\alpha}_{dec}(\bar{v}) + f^{\alpha}_{cruise}(\bar{v}) = 1 \tag{3.11}$$

The parameters of all share functions were fitted in parallel, meaning a function was created which output was a four-column matrix whereby each column corresponded to one type of share. The total error of the fit was calculated by comparing the result of the fit function with the *driving shares* extracted from the data. This approach ensured that all *driving share* fits were close to the data. In contrast, if one share function was fitted at a time it would have been expectable that the first fitted functions correlated very well to the real data whereby the last share function had significant deviations. The results of these fits are given in Appendix C.

Following, in Chapter 4.1.3 it will be explained how the fitted acceleration and share functions were used to estimate the vehicles' energy consumption with respect to a given route.

Chapter 4

Vehicle energy model

Due to the limited range of electric vehicles it is essential to precisely estimate the vehicle's battery energy level and therewith the remaining range. Therefore, this chapter introduces the energy models which are integrated into the driving profile simulation model. First, in Chapter 4.1 an energy consumption model is presented which is used to estimate the required battery's energy flow in order to execute a trip. Next, in Chapter 4.2 a charging model is introduced which estimates how much energy is recharged with respect to the battery energy level, charging power, and charging time.

4.1 Energy consumption model

The energy consumption model is used to estimate how much energy would be discharged from the battery to execute a trip with respect to vehicle specific parameters. This model is capable of estimating the energy consumption with respect to a given speed profile (speed-based) and a given route with *pass-through speeds* per *street network section* (route-based). The nomenclature of this section is given in Table 4.1.

Table 4.1: Nomenclature of energy consumption model

Symbol	Unit	Description
A	N	dynamometer coefficient
B	Ns/m	dynamometer coefficient
C	Ns^2/m^2	dynamometer coefficient
E_{bat}	Ws	battery discharge energy
η_{Bat}	-	battery efficiency
η_{Conv}	-	converter efficiency
η_{Inv}	-	inverter efficiency
η_{Motor}	-	motor efficiency
η_{Trans}	-	transmission efficiency
$\eta_{Wheel-Bat}$	-	efficiency wheel to battery
f_{acc}	-	acceleration share
f_{cruise}	-	cruise share

Symbol	Unit	Description
f_{dec}	-	deceleration share
f_{idle}	-	idle share
g	m/s^2	gravitational acceleration
$\dot{h}$	m/s	derivation of altitude profile
k_m	-	rotational inertial factor
l	m	section length
$m_{vehicle}$	kg	weight of vehicle
$\bar{P}$	W	average power
P_0	W	standstill power
P_{AC}	W	air conditioning power
P_{acc}	W	acceleration power
P_{aero}	W	power of aerodynamic drag
P_{aux}	W	auxiliary consumer power
P_{bat}	W	battery power
P_{cruise}	W	power in cruise state
P_{dec}	W	power in deceleration state
P_{drive}	W	power to drive vehicle
P_{grad}	W	gradient resistance power
P_{idle}	W	power in idle state
P_{Inv}	W	inverter power
P_{road}	W	road load power
P_{roll}	W	power of rolling resistance
t	s	time
v	m/s	speed
$\bar{v}$	m/s	pass-through speed
$\dot{v}$	m/s^2	acceleration
$\dot{v}_{acc}$	m/s^2	average positive acceleration
$\dot{v}_{dec}$	m/s^2	average negative acceleration

4.1.1 Model and parameter

The applied vehicle model to simulate the energy consumption is depicted in Figure 4.1.

In order to drive the vehicle, the battery's discharge current is inverted from DC to AC by the inverter. Next, the electric motor transforms the electrical power to mechanical power which flows through the transmission to the wheels to overcome the driving resistances. The design of electric vehicles allows *regenerative braking* meaning that while braking kinetic energy can be transformed by the motor to electric energy which can be used to supply auxiliary consumers and recharge the battery. The inverter also supplies the air conditioning system directly with AC current, whereby the converter

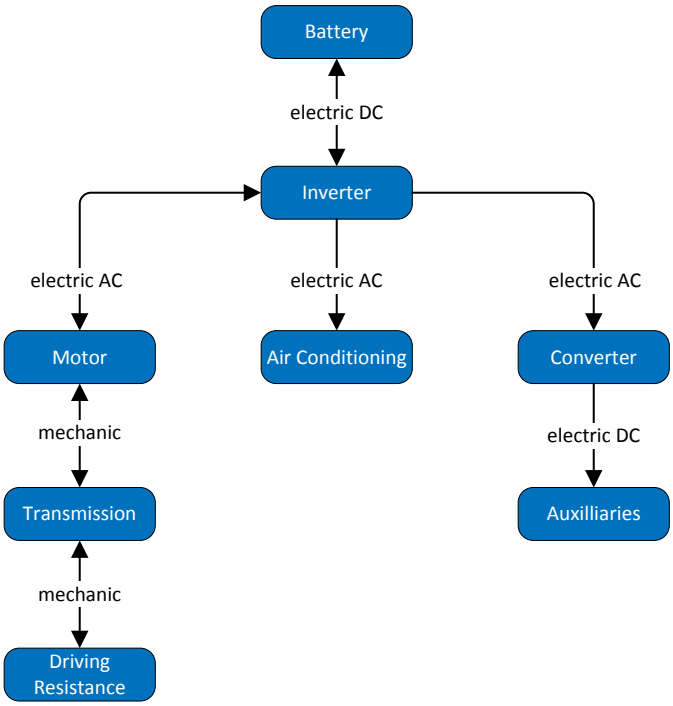

Figure 4.1: Power flow diagram of electric vehicle

transforms the current to DC (at a much lower voltage than the battery's voltage) to supply all auxiliary consumers (infotainment, lights, control units, ...).

The electric power consumption of the air conditioning system P_{AC} of EVA in Singapore was estimated to 810 W in (Reuter et al., 2014), whereby the the average power consumption of all auxiliary consumers P_{aux} was assumed to be 700 W. The driving resistance power with respect to the vehicle's speed v and acceleration $\dot{v}$ is calculated by (Simpson, 2005):

$$P_{drive}\left(v,\dot{v}\right) = P_{aero}\left(v\right) + P_{roll}\left(v\right) + P_{acc}\left(v,\dot{v}\right) + P_{grade}\left(v\right) \tag{4.1}$$

The road load power combines the aerodynamic drag P_{aero} and the rolling resistance P_{roll} and is calculated with following formula (Giannelli et al., 2005):

$$P_{road}\left(v\right) = P_{aero}\left(v\right) + P_{roll}\left(v\right) = \left(A + B \cdot v + C \cdot v^2\right) v \tag{4.2}$$

The parameter *A*, *B*, and *C* are dynamometer coefficients which were measured for each vehicle except EVA by (EPA, 2016). In case of EVA the coefficients were calculated with respect to its frontal area (2.8 m^2), drag resistance coefficient (0.31), total weight (1636 kg), and rolling resistance coefficient (0.008). All coefficients are listed in Table 4.2.

As the rolling resistance is predominantly speed independent whereby the drag resistance depends on the squared speed, the coefficient *A* is representative for the rolling resistance and *C* for the drag resistance. The coefficient *B* was fitted to improve the

Table 4.2: Dynamometer coefficients (EPA, 2016)

Vehicle	A [N]	B [Ns/m]	C [Ns^2/m^2]
BYD e6	270.3	6.588	0.4443
EVA[a]	128.4	0	0.5317
Kia Soul EV	101.4	3.265	0.4860
Nissan Leaf SV	133.1	0.7563	0.4886
Tesla Model S 70D	161.2	1.897	0.3887

[a] coefficients estimated

simulation of road loads on a dynamometer and can be understood as a mixture of rolling and drag resistance. According to this interpretation, the BYD e6 has the highest rolling resistance which can be explained by its high weight of 2,495 kg and the Tesla Model S has the lowest drag resistance which is due to its low frontal area (2.3 m^2) and drag coefficient (0.24) (Sherman, 2014).

The required power to accelerate the vehicle at speed v with acceleration $\dot{v}$ is calculated by (Simpson, 2005):

$$P_{acc}\left(v, \dot{v}\right) = k_m m_{vehicle} \cdot v \cdot \dot{v} \tag{4.3}$$

Thereby $m_{vehicle}$ is the weight of the vehicle and k_m is a factor which accounts the rotational inertia of the powertrain and the wheels. This factor was estimated for the Nissan Leaf to 1.066 with respect to a wheel radius of 31.5 cm (Hayes and Davis, 2014) and a total moment of inertia of 10 kg m^2 (Hayes et al., 2011).

The gradient resistance P_{grade} is calculated with respect to derivation of the altitude by time $\dot{h}$ (g is the gravitational acceleration):

$$P_{grade}\left(\dot{h}\right) = m_{vehicle} \cdot g \cdot \dot{h} \tag{4.4}$$

To assess the impact of the gradient resistance on the total energy consumption, 65,476 km of taxi driving profiles were matched to an elevation map of Singapore (Moecker, 2014). The inclusion of the gradient resistance increased the total energy consumption by only 0.9%.

Reasons why the impact of the gradient resistance was so low are that Singapore has moderate elevation changes and that taxis predominantly start and end their *shift* at the same location so that the resulting elevation change throughout the *shift* is neutral.

Due to its low impact it was decided to neglect the gradient resistance in the context of Singapore. However, in case of cities with higher elevation changes this decision must be carefully assessed.

Apart from estimating the power to drive the vehicle, the efficiencies of all components of Figure 4.1 are taken into account as well. Among others, the components' efficiencies depend on the power output. However, for simplicity all efficiencies of this model were assumed to be constant. As it is very difficult to get specific values for each vehicle type, only values for the Nissan Leaf were selected and applied to all other vehicle types. Table 4.3 lists all chosen efficiencies.

Table 4.3: Efficiencies of components

Component	Symbol	Efficiency	Citation
Battery	η_{Bat}	97.1%	(Genovese et al., 2015)
Converter	η_{Conv}	98%	(Hayes et al., 2011)
Inverter	η_{Inv}	98%	(Hayes et al., 2011)
Motor	η_{Motor}	95%	(Hayes et al., 2011)
Transmission	η_{Trans}	97%	(Hayes et al., 2011)

4.1.2 Speed-based approach

The purpose of the speed-based approach is to estimate how much energy needs to be discharged from the battery to follow a given *speed profile* $v(t)$ and its derivative, the *acceleration profile* $\dot{v}(t)$. First, it is calculated how much power would be required to overcome the driving resistance of equation 4.1. Next, all component efficiencies are taken into account to compute how much power would be needed to discharge the battery in order to supply the inverter. Hereby, the power consumption of the air conditioning system and all auxiliaries are included as well. During *regenerative braking* ($P_{drive}(v(t), \dot{v}(t)) < 0$), it is calculated how much power would flow from the motor to the inverter to supply other consumers and recharge the battery.

The total efficiency from the wheel to the battery is:

$$\eta_{Wheel-Bat} = \eta_{Trans} \cdot \eta_{Motor} \cdot \eta_{Inv} \tag{4.5}$$

The power flow from the inverter to the air conditioning system and the auxiliary consumers is:

$$P_0 = P_{AC} + \frac{P_{aux}}{\eta_{Conv}} \tag{4.6}$$

If power is required to drive the vehicle ($P_{drive}(v(t), \dot{v}(t)) \geq 0$), the input power to the inverter is:

$$P_{Inv}(v(t), \dot{v}(t)) = \frac{P_{drive}(v(t), \dot{v}(t))}{\eta_{Wheel-Bat}} + \frac{P_0}{\eta_{Inv}} \tag{4.7}$$

Otherwise, the power flow from the battery to the inverter is:

$$P_{Inv}(v(t), \dot{v}(t)) = \eta_{Wheel-Bat} \cdot P_{drive}(v(t), \dot{v}(t)) + \frac{P_0}{\eta_{Inv}} \tag{4.8}$$

To calculate the battery power it must be distinguished if the battery is discharged ($P_{Inv}(t) \geq 0$) or charged ($P_{Inv}(t) < 0$). In case of discharging the power output must be divided by the root of the battery efficiency, while during charging the power input is multiplied by the root of the battery efficiency.

$$P_{bat}(v(t), \dot{v}(t)) = \begin{cases} \frac{P_{Inv}(v(t), \dot{v}(t))}{\sqrt{\eta_{Bat}}} & \text{if } P_{Inv}(v(t), \dot{v}(t)) \geq 0 \\ \sqrt{\eta_{Bat}} \cdot P_{Inv}(v(t), \dot{v}(t)) & \text{otherwise} \end{cases} \tag{4.9}$$

The battery efficiency is defined over one charging and discharging cycle, as only either one or the other is taken into account by equation 4.9, the battery efficiency's square root is taken. Finally, the total energy consumption of the whole speed profile is calculated by integrating the battery power:

$$E_{bat} = \int P_{bat}\left(v\left(t\right), \dot{v}\left(t\right)\right) \mathrm{d}t \tag{4.10}$$

To validate this model, the energy consumption was simulated for two driving cycles: the Urban Dynamometer Driving Schedule (UDDS) and the Highway Fuel Economy Test Driving Schedule (HWFET) (EPA, 2017). The simulation results were compared with the measured values from (EPA, 2016). Air conditioning was not used during these measurements, therefore P_{AC} was set to zero. Table 4.4 gives an overview of the results (measured values are shown in brackets):

Table 4.4: Energy consumption of driving cycles: simulated (measured)

	BYD e6	Nissan Leaf SV
Energy consumption HWFET [Wh/km]	219 (225)	141 (145)
Deviation from measurements HWFET	-2.7%	-2.8%
Energy consumption UDDS [Wh/km]	189 (234)	118 (119)
Deviation from measurements UDDS	-19.2%	-0.8%

The in (EPA, 2016) measured energy consumption of the Kia Soul and Tesla Model S was higher than 800 Wh/km, which is unreasonable for electric cars. Thus, the simulation results of these vehicles could not be validated.

The simulation results of the Nissan Leaf matched very well with the measurements for both driving cycles. In case of the BYD e6, the simulated energy consumption for the HWFET was similar to the measured value, whereby the simulation model significantly underestimated the consumption of the UDDS compared to the measured value. It is notable that the measured energy consumption of the BYD was higher for the urban UDDS driving cycle (234 Wh/km) than for the highway-based HWFET cycle (225 Wh/km) whereby the opposite trend appeared for the Nissan Leaf. Electric vehicles are expected to be more energy efficient on urban driving cycles as lower speeds cause lower driving resistances and *regenerative braking* is especially beneficial at stop-and-go traffic conditions.

Nevertheless, it is difficult to assess whether this difference was caused by a measurement error or if the BYD e6 is because of technical reasons less efficient at urban driving cycles. However, since the deviation of all other values is low, it can be presumed that the speed-based simulation model is capable of reproducing the energy consumption with acceptable accuracy.

To analyse the energy demand of all vehicles with respect to driving profiles of taxis in Singapore, the simulation model was applied to all speed profiles of the High Frequency Data set (HFD). The simulated average energy consumption per vehicle is listed in Table 4.5.

In contrast to the UDDS and HWFET cycle, air conditioning was included in the simulation of HFD trips to generate more realistic results. As a consequence, the energy consumption of the Nissan Leaf and BYD e6 was significantly higher than compared to

Table 4.5: Simulated energy consumption on Singapore driving profiles

Vehicle	Energy consumption [Wh/km]
BYD e6	236
EVA	160
Kia Soul EV	164
Nissan Leaf SV	162
Tesla Model S 70D	173

the UDDS cycle. The results also show that the vehicles with the lowest weights (EVA: 1,636 kg, Kia Soul: 1,644 kg, Nissan Leaf: 1,701 kg) had the lowest energy consumption. The BYD e6 had clearly the highest energy consumption which was partly caused by its high weight of 2,495 kg. However, comparing its energy consumption with that of the 2,286 kg Tesla Model S suggests that this is not the only reason why the BYD e6 performs considerably worse. Its appreciably higher dynamometer coefficient A (Table 4.2) must also be a result of a significantly higher rolling resistance.

4.1.3 Route-based approach

The route-based energy estimation is used to quantify the vehicle's energy consumption with respect to a set of *street network sections* and the *pass-through speed* $\bar{v}$ of each *section*. Thereby, the energy consumption of the route is calculated by cumulating the energy consumption of each *section*. The energy per *section* is calculated with respect to the average power $\bar{P}(\bar{v})$ to pass-through the *section* and the *section's* length l:

$$E_{bat} = \bar{P}(\bar{v}) \frac{l}{\bar{v}} \tag{4.11}$$

The average power consists of a weighted sum of the required power per *driving share* (Kraschl-Hirschmann and Fellendorf, 2012) (*driving shares* were introduced in Chapter 3.4.4):

$$\bar{P}(\bar{v}) = f_{idle}(\bar{v}) \cdot P_{idle}(\bar{v}) + f_{cruise}(\bar{v}) \cdot P_{cruise}(\bar{v}) + f_{acc}(\bar{v}) \cdot P_{acc}(\bar{v}) + f_{dec}(\bar{v}) \cdot P_{dec}(\bar{v}) \tag{4.12}$$

The share functions are defined by equations 3.7 - 3.10 whereby the fit parameter of these functions were selected with respect to the *section's* street type and the *speed-cluster* (Chapter 3.4.2) associated with the time of the day when the *section* was passed through. It would be possible to make a more detailed selection of the fit parameters with respect to the *section's way ID* or even choose parameters which were indipendnetly fitted for each *section*. However, in order to limit the complexity of this estimation model it was decided to work on the street type level.

The power per *driving share* is calculated with respect to equation 4.9:

$$P_{idle}(\bar{v}) = P_{bat}(0, 0) \tag{4.13}$$
$$P_{cruise}(\bar{v}) = P_{bat}(\bar{v}, 0) \tag{4.14}$$
$$P_{acc}(\bar{v}) = P_{bat}(\bar{v}, \dot{v}_{acc}) \tag{4.15}$$
$$P_{dec}(\bar{v}) = P_{bat}(\bar{v}, \dot{v}_{dec}) \tag{4.16}$$

With the idea that during *idle* the vehicle is not moving, hence speed and acceleration is zero so that only the air conditioning and the auxiliary consumers withdraw power from the battery. During *cruise*, the vehicle moves with constant speed so that the acceleration power is zero. In case of the *acceleration* and *deceleration share*, it is assumed that the vehicle accelerates with the constant acceleration $\dot{v}_{acc}$ respectively $\dot{v}_{dec}$. The values of these accelerations are calculated via equation 3.6. The fit parameters of this function were again selected with respect to the *section's* street type and *speed-cluster*.

This approach was validated by simulating the energy consumption of each vehicle type for all trips of the HFD with respect to the map-matched *sections* of each trip. Thereby, the simulated energy consumption of EVA was 150 Wh/km which was 6.3% lower than the simulated energy consumption by the speed-based approach. The root mean square error of the energy consumption per trip was 25 Wh/km.

One reason for the underestimation of the average energy consumption is that it is assumed that the vehicle drives with constant speed through each *section*. This leads to an underestimation of the road load power (equation 4.2) as it includes square and cubic speed terms.

Apart from that, when comparing the results of these models, it must be kept in mind, that even if the route-based approach is applied with the exact *pass-through speed* derived from the speed profile, it uses average accelerations and *driving shares* of all pass-throughs which were recorded at any *section* of the same street type. Thus, as these statistics deviate from the speed profile which was simulated by the speed-based approach, the estimated energy consumption deviates as well.

In order to reduce the estimation error, the correction factors of Table 4.6 were added to the vehicle's energy consumption. The standard deviation error of EVA was reduced from 25 Wh/km to 22 Wh/km by applying the correction factor.

Table 4.6: Route-base energy consumption correction factors

Vehicle	Correction [Wh/km]
BYD e6	21.9
EVA	10.2
Kia Soul EV	11.2
Nissan Leaf SV	11.4
Tesla Model S 70D	18.3

Apart from the application in this work, this approach could also be applied to estimate emissions of conventional vehicles with respect to the extracted traffic statistics. Instead of estimating the battery's discharge power, it would be necessary to estimate how much torque the internal combustion engine would have to deliver at which rotation speed. The rotation speed could be derived from the vehicle's speed and transmission

ratio. Engine maps could be applied to estimate emissions with respect to torque and rotation speed.

4.2 Charging model

The charging model is used to estimate how much energy can be recharged within a given charging duration and how long it takes to reach a certain charging level. Thereby, battery characteristics are taken into account. The nomenclature of this section is given by Table 4.7.

Table 4.7: Nomenclature of charging model

Symbol	Unit	Description
α	-	open circuit voltage parameter
E	J	battery energy
E_{max}	J	maximum battery energy
e	J	energy of cell
e_{max}	J	maximum cell energy
I	A	charging current
k_i	V	open circuit voltage parameter
N_p	-	number of parallel cell series
N_s	-	number of cells in one series
N_{total}	-	number of cells
P	W	charging power
P_{max}	W	maximum charging power
Q	As	charge of battery
Q_{max}	As	maximum charge of battery
q	As	charge of cell
q_{max}	As	maximum charge of cell
R	Ω	battery resistance
SOC	-	state of charge
SOC_{CPend}	-	SOC when CP charging ends
t	s	time
u	V	cell voltage
U_{max}	V	maximum battery voltage
U_t	V	terminal voltage
U_{oc}	V	battery open circuit voltage
u_{oc}	V	cell open circuit voltage

4.2.1 Charging curve

As an example, Figure 4.2 shows the simulated voltage, current, and charging power of a 50 kWh battery with respect to time. This charging profile can be separated in two parts: *constant power* (CP) and *constant voltage* (CV) charging (Chan, 2000).

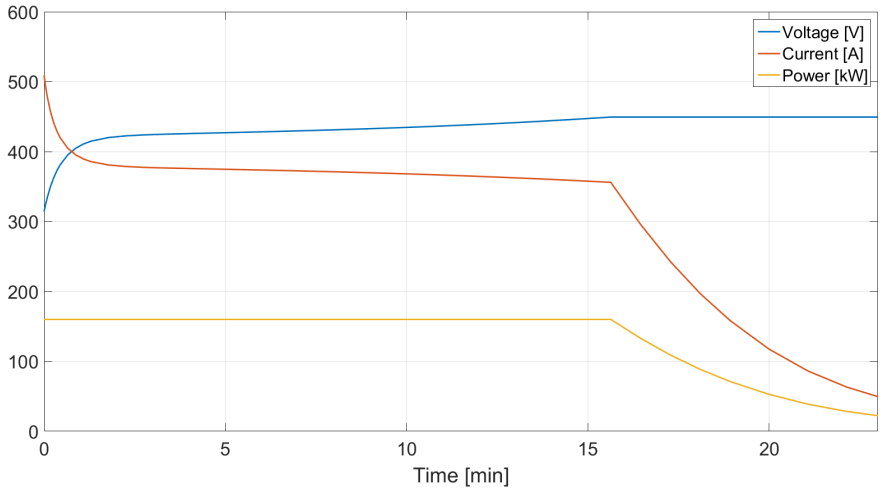

Figure 4.2: Example of battery pack charging curve

The first 16 minutes the battery was charged with a constant power of 160 kW. As the battery's *open circuit voltage* (OCV) increases with higher State of Charge (SOC), the *terminal voltage* supplied by the charger was increased as well. The OCV is the battery's voltage which would be measured if the battery was disconnected from any circuit - no current flows in or out of the battery.

The CP phase ended when the maximum battery pack voltage of 450 V was reached. A further increase of the *terminal voltage* would harm the battery, thus as of this point the *terminal voltage* was kept constant - CV charging started. As the SOC still increases and therewith the OCV, the difference between the *terminal voltage* and the battery's OCV became smaller. A smaller voltage difference results in lower charging current and further, in a decrease of the charging power.

The consequence of this characteristic is that a constant charging power can only be presumed before the *terminal voltage* reaches the battery pack's maximum voltage. Thereafter, it must be considered that the charging power decreases gradually. To reproduce this characteristic, the introduced charging model is capable of simulating the battery's energy content with respect to time for CP and CV charging.

4.2.2 Model and parameter

The used battery pack model to simulate the charging process is depicted in Figure 4.3. The battery pack consists of N_p parallel series of battery cells whereby each series contains N_s cells. Battery cells are represented by resistances. It is assumed, that all cells have the same SOC at any time. The battery pack is recharged by the charger which supplies a current I with a *terminal voltage* U_t.

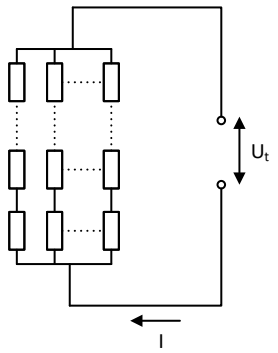

Figure 4.3: Simplified battery pack model

As this model is applied to simulate the charging of batteries with different maximum energy content E_{max}, the first step is to define the battery pack design - total number of cells, number of series in parallel and number of cells per series. Therefore, the energy content e_{max} of one cell is calculated (lower case variables are associated with cells whereby variables on battery pack level have capital letters). The OCV of a Li-ion battery cell is estimated with following formula (Chen and Rincon-Mora, 2006):

$$u_{oc}\left(SOC\left(t\right)\right) = \sum_{i=0}^{3} k_i \cdot SOC\left(t\right)^i + k_4 \cdot \exp\left(\alpha \cdot SOC\left(t\right)\right) \tag{4.17}$$

The parameter values are listed in Table 4.8.

Table 4.8: Open circuit voltage parameter (Chen and Rincon-Mora, 2006)

Symbol	Unit	Value
k_0	V	3.685
k_1	V	0.2156
k_2	V	-0.1178
k_3	V	0.3201
k_4	V	-1.031
α	-	-35

The SOC is defined as the ratio of the stored charge q over the maximum charge q_{max} of one cell (which is assumed to be 40 Ah):

$$SOC\left(t\right) = \frac{q\left(t\right)}{q_{max}} \tag{4.18}$$

Thus, equation 4.17 can also be written as:

$$u_{oc}\left(q\right) = \sum_{i=0}^{3} k_i \cdot \left(\frac{q}{q_{max}}\right)^i + k_4 \cdot \exp\left(\alpha \cdot \frac{q}{q_{max}}\right) \tag{4.19}$$

The amount of energy $e(q)$ which is stored in a battery cell can be calculated with respect to the OCV and the charge q of the cell:

$$e(q) = \int_0^q u_{oc}(q')\,\mathrm{d}q' \tag{4.20}$$

$$\Longleftrightarrow e(q) = \sum_{i=0}^{3} \frac{1}{i+1} k_i \frac{q^{i+1}}{q_{max}^i} + \frac{1}{\alpha} k_4 q_{max} \left(\exp\left(\alpha \frac{q}{q_{max}} \right) - 1 \right) \tag{4.21}$$

Thus, the maximum amount of energy which can be stored in one cell is:

$$e_{max} = e(q_{max}) = q_{max} \left(\sum_{i=0}^{3} \frac{1}{i+1} k_i + \frac{1}{\alpha} k_4 \left(\exp(\alpha) - 1 \right) \right) \tag{4.22}$$

Therefore, the total number of cells can be calculated by:

$$N_{total} = \frac{E_{max}}{e_{max}} \tag{4.23}$$

Next, N_p and N_s must be calculated. Hereby, it is assumed that the battery pack is designed for a maximum voltage U_{max} of 450 V. As the voltage of a battery pack is defined by the sum of the voltage of all cells in series, N_s and N_p are calculated as follows:

$$N_s = \frac{U_{max}}{u(SOC = 1)} \tag{4.24}$$

$$N_p = \left\lceil \frac{N_{total}}{N_s} \right\rceil \tag{4.25}$$

As a battery pack with a non-integer number of parallel series does not make sense, N_p is rounded up to the next higher integer. Therefore, N_s must be adjusted:

$$N_s = \frac{N_{total}}{N_p} \tag{4.26}$$

In case of N_s it is for simplicity reasons neglected that it is a non-integer number since N_s is much higher than N_p due to the low maximum cell voltage of 4.1 V compared to the maximum pack voltage of 450 V. Thus, the battery pack's OCV is:

$$U_{oc}(SOC) = N_s u_{oc}(SOC) \tag{4.27}$$

4.2.3 Charging process

Next, it is derived how the total amount of energy $E(t)$ changes with respect to time during CP charging. Therefore, equations 4.23, 4.21, and 4.18 are combined:

$$E(t) = N_{total} \cdot e(t) = N_{total} \cdot e(q(t)) = N_{total} \cdot e(q_{max} \cdot SOC(t)) \tag{4.28}$$

Hence, to calculate $E(t)$ it is necessary to know how the SOC changes with respect to time. Therefore, it is used that current is the derivative of charge with respect to time:

$$I\left(SOC\left(t\right)\right) = \frac{\mathrm{d}Q\left(t\right)}{\mathrm{d}t} = Q_{max}\frac{\mathrm{d}SOC\left(t\right)}{\mathrm{d}t} \tag{4.29}$$

The battery pack's maximum charge Q_{max} depends on the number of cell series in parallel N_p and the maximum charge of one cell q_{max}:

$$Q_{max} = N_p \cdot q_{max} \tag{4.30}$$

The charging current is derived from the equations for the *terminal voltage* $U_t\left(SOC\right)$ and the charging power $P\left(SOC\right)$ (Marra et al., 2012):

$$U_t\left(SOC\left(t\right)\right) = U_{oc}\left(SOC\left(t\right)\right) + R \cdot I\left(SOC\left(t\right)\right) \tag{4.31}$$
$$P\left(SOC\left(t\right)\right) = U_t\left(SOC\left(t\right)\right) \cdot I\left(SOC\left(t\right)\right) \tag{4.32}$$

where R is the total resistance of the battery pack. Combining equations 4.31 and 4.32 leads to:

$$P\left(SOC\left(t\right)\right) = \left(U_{oc}\left(SOC\left(t\right)\right) + R \cdot I\left(SOC\left(t\right)\right)\right) \cdot I\left(SOC\left(t\right)\right) \tag{4.33}$$
$$\Rightarrow I\left(SOC\left(t\right)\right) = \frac{-U_{oc}\left(SOC\left(t\right)\right) + \sqrt{U_{oc}^2\left(SOC\left(t\right)\right) + 4 \cdot R \cdot P\left(SOC\left(t\right)\right)}}{2 \cdot R} \tag{4.34}$$

as the charging power P during CP charging is constant, its dependency on the SOC can be removed:

$$I\left(SOC\left(t\right)\right) = \frac{-U_{oc}\left(SOC\left(t\right)\right) + \sqrt{U_{oc}^2\left(SOC\left(t\right)\right) + 4 \cdot R \cdot P}}{2 \cdot R} \tag{4.35}$$

The resistance *R* is quantified by taking into account that CP charging ends once the *terminal voltage* reaches to maximum battery pack voltage $U_{oc}\left(SOC = 1\right)$, thereby the considered charging power is the maximum power P_{max} the battery pack is designed to be charged with:

$$U_{oc}\left(SOC = 1\right) = U_{oc}\left(SOC_{CP\,end}\right) + R \cdot I\left(SOC_{CP\,end}\right) \tag{4.36}$$

by inserting equation 4.32 follows:

$$R = U_{oc}\left(SOC = 1\right) \cdot \frac{U_{oc}\left(SOC = 1\right) - U_{oc}\left(SOC_{CP\,end}\right)}{P_{max}} \tag{4.37}$$

Most car manufacturers quantify the fast charging capability of their vehicle by giving the charging duration until a SOC of 80% is reached. Therefore, $SOC_{CP\,end}$ is set to this value. By inserting equation 4.35 and 4.30 into 4.29, results in following differential equation:

$$\frac{\mathrm{d}SOC\left(t\right)}{\mathrm{d}t} = \frac{-U_{oc}\left(SOC\left(t\right)\right) + \sqrt{U_{oc}^2\left(SOC\left(t\right)\right) + 4 \cdot R \cdot P}}{2 \cdot N_p \cdot q_{max} \cdot R} \tag{4.38}$$

which is a first order non-linear differential equation. This equation was numerically solved with the explicit Runge-Kutta (4,5) algorithm (Dormand and Prince, 1980;

Shampine and Reichelt, 1997). The battery's energy content during CP charging was then calculated via equation 4.28.

During CV charging, the *terminal voltage* (equation 4.31) is set to the battery's maximum voltage $U_{oc}\left(SOC = 1\right)$. Hence, the charging current is:

$$I\left(SOC\left(t\right)\right) = \frac{U_{oc}\left(SOC = 1\right) - U_{oc}\left(SOC\left(t\right)\right)}{R} \tag{4.39}$$

Thus, the differential equation for the SOC is:

$$\frac{\mathrm{d}SOC\left(t\right)}{\mathrm{d}t} = \frac{U_{oc}\left(SOC = 1\right) - U_{oc}\left(SOC\left(t\right)\right)}{N_p \cdot q_{max} \cdot R} \tag{4.40}$$

and was again solved with the Runge-Kutta (4,5) algorithm.

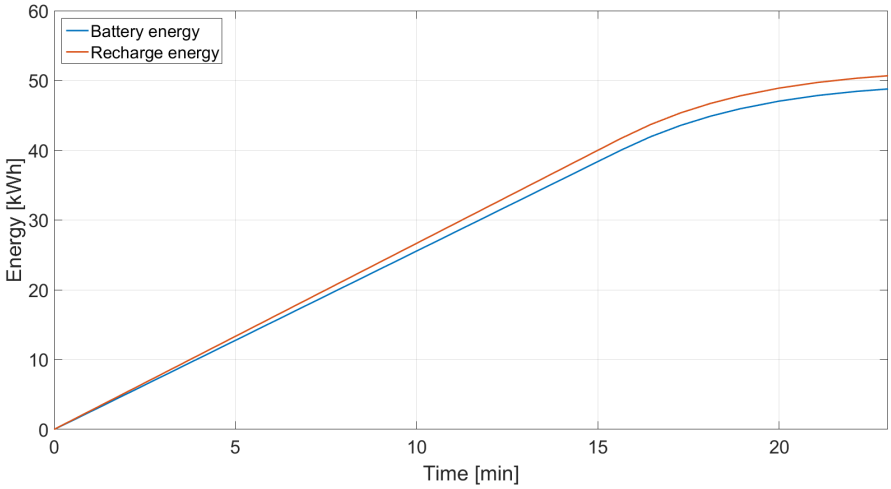

Figure 4.4: Charging energy with respect to time

The calculated battery and recharge energy with respect to time for a 50 kWh battery and a charging power of 160 kW during CP charging is shown in Figure 4.4. "Battery energy" refers to the amount of energy which was stored in the battery, whereby "recharge energy" is the the energy output of the charger. The difference between these lines is caused by the battery resistance.

The simulated charging process started with a completely empty battery, during CP charging, the amount of energy increased linearly. This phase ended after 16 min when the *terminal voltage* reached its maximum and CV charging started. During CV charging, the charging power was continuously reduced which flattened the curves.

This charging model was integrated in the driving profile simulation (Chapter 5). In order to improve the computation time, it was avoided to solve the differential equations 4.38 and 4.40 for each simulated charging event. Instead, lookup-tables were created for the calculated recharge energy curves. The lookup-tables used linear interpolation to estimate the amount of recharged energy with respect to the battery energy content and the charging time as well as the required charging time with respect to a targeted energy amount at the end of the charging process.

Chapter 5

Driving profile simulation

This chapter introduces the driving profile simulation model (Sellmair and Schelo, 2018). With respect to the statistics derived in Chapter 3, this model is capable of reproducing driving profiles of taxi drivers with conventional vehicles. Furthermore, the integrated *charging behaviour model* allows to simulate electric taxis subject to the taxis' vehicle type and the charging infrastructure design. Based on the simulation results, the charging demand of an electric taxi fleet is derived and used as an essential input for the charging infrastructure optimisation presented in Chapter 7.

This chapter is structured as follows: First Chapter 5.1 gives a literature review over approaches to simulate driving profiles of electric taxis. The basic concept of the agent-based approach which was chosen for this work is introduced in Chapter 5.2.

All *actions* which the agents can execute are explained in Chapter 5.3. Next, Chapter 5.4 and Chapter 5.5 present the *shift schedule pool* and the *trip generator*. The *shift schedule pool* assigns *shift schedules* to the agents in order to ensure that their activity patterns correlate with that of real taxis while the *trip generator* assigns trips to the agents which they have to execute next. Following, Chapter 5.6 introduces the concept of the *agent memory* which individually records key values of all *actions* each agent executed. The behaviour models, which decide which *action* the agents have to execute next are explained in Chapter 5.7.

The chapter concludes with a validation for the simulation of conventional taxis in Chapter 5.8 and a discussion of case studies to highlight certain properties of the simulation model in Chapter 5.9.

5.1 Literature review

There are several papers which introduced agent-based electric taxi simulation models already. All these papers followed a demand-based approach, which means that the demand for taxis was used as input and an agent-based model was applied to simulate driving profiles of electric taxis supplying that demand. The demand was either derived from real data or synthesised and the taxi agents were travelling on a street network which was either taken from an existing city or synthesised as well. The mentioned papers mainly differ with regards to the introduced dispatch strategies, scenario definitions, and the criteria to assess the performance of an electric taxi fleet.

In (Lee et al., 2014), taxis were ordered to return to a charging facility after each *engaged trip* to recharge the battery and wait for the next job. The assignment of

the charging facility depended on the taxi's location, battery energy level, and expected demand at the charging facility. The simulated scenario was based on the currently existing charging infrastructure in Jeju city. The authors analysed how often electric taxis would have to recharge for the given scenario.

The strategy, that taxis had to return to taxi stands for recharging was also applied in (Bischoff and Maciejewski, 2014). However, in their implementation taxis only needed to return if there was no current customer request or the battery energy level was too low. Customer requests were matched to the nearest waiting taxi with sufficient battery energy level. The paper presented scenarios with different numbers of charging stations, different dispatching strategies, and different demand. The customer waiting time, number of taxis which were simultaneously charging and the taxis' mileage of these scenarios was analysed.

Apart from electric taxis, (Jung et al., 2012) also investigated the concept of taxi sharing. Hence, their proposed dispatching algorithm did not only include the scheduling of customer requests and charging events but also the altering of routes in order to serve different customer requests by the same taxi at the same time. They analysed the number of completed customer requests, average customer waiting time, and taxi mileage with respect to different charging types (*battery swapping* and fast charging). Furthermore, the effect of different *share detour ratios* were analysed. This ratio defines the distance that a taxi is allowed to extend its initial route to pick up another group of customers.

The dispatching strategy in (Lu et al., 2012) took the battery energy level, expected demand, and availability of charging stations at the requested destination into account to match customer requests with available taxis. This strategy was compared with a random matching of requests with taxis. Furthermore, *battery swapping* and fast charging concepts were considered in this approach as well. The authors assessed the performance of electric taxis via waiting time per charging event and number of executed trips.

In contrast to the above mentioned papers, (Gacias and Meunier, 2015) not only took booking requests (customers send a request with pickup and drop off location) into account, but also street hailings (customers flag down taxis passing by). The introduced dispatch strategy combined the scheduling of all customer trips with the recharging of taxis. Moreover, different charging station placement methods were presented and their performance with respect to the number of executed trips, number of fulfilled bookings, percentage of available taxis, and percentage of taxis which were waiting to be charged was assessed.

An advantage of demand-based approaches is that it is easy to asses if the same number of electric taxis is able to serve the demand as conventional taxis or how many more electric taxis would be required. Furthermore, by analysing customer waiting times, it is also possible to quantify the effect of electric taxis on the customers' experience and satisfaction. Moreover, it is possible to quantify these criteria for a changing demand in the future.

However, one of the biggest challenges of the demand-based approach is that it is very difficult to accurately quantify the spatial-temporal demand for taxis. Hereby, demand generated by bookings as well as street hailings must be taken into consideration. The booking demand is recorded by taxi operators or third party taxi booking service providers. However, booking requests of a whole city are typically divided among several competitors, which makes it difficult to get access to the complete data set.

The street hailing demand can be extracted from taxi driving profiles. Unfortunately, this data set only contains the demand that was met, customers who waited for taxis until they resigned and took another mode of transport would not be included (the street hailing demand in Gacias and Meunier (2015) was synthesised and not derived from real data).

Another aspect the introduced approaches did not take into account is respecting driver individual activity patterns. Instead, it was assumed that taxis are active throughout the whole day or that the whole fleet follows the same activity pattern. Considering individual activity patterns is especially important when taxi drivers are self-employed and are free to decide when to work. This accounts for Singapore.

5.2 Approach and model design

In this thesis, the chosen approach to simulate driving profiles of electric taxi agents is a supply-based approach. Here, the basic idea is to reproduce the driving profiles of conventional taxis as close as possible and to make changes only when the simulated agent needs to recharge. The statistical background of this model consists of *engaged trips*, *search trips*, and *shift schedules* which were extracted in Chapter 3.

All these extracted trips and *shift schedules* represent the behaviour of taxi drivers with conventional vehicles. To model an electric taxi fleet, the following hypothesis was defined: drivers of electric taxis mimic the behaviour of conventional taxi drivers as close as possible. Meaning, they start and end their *shifts* at the same time, and have *breaks* at the same time of the day and location with equal duration as conventional taxi drivers. Additionally, their search strategies to find the next customer are identical. Their behaviour only deviates from that of conventional taxi drivers when their vehicle's battery energy level is low and they have to extend their *breaks* or add *breaks* to recharge the battery.

Based on this hypothesis, an agent-based simulation model was designed in a two-step process: First, a conventional taxi model was developed which was then calibrated and validated based on the recorded data. In the second step, the model was expanded with electric vehicle models, a charging infrastructure, and a *charging behaviour model*.

This simulation is a discrete event simulation, meaning that agents are executing *actions* one at a time. As these *actions* have different durations, each agent has a different *simulation time* while running a scenario. The *simulation time* is the time which progresses within the simulated scenario, it must not be confused with the time to perform the computational process.

A high-level representation of the model's architecture and processes can be seen in Figure 5.1. The *controller* handles the overall sequence of all simulation steps from initialisation to execution until termination. During the initialisation, each agent gets a set of *shift schedules* which exclusively originated from the driving profiles of one recorded taxi. The first schedule to be executed is randomly selected from that set. The initial spatio-temporal state of each agent is then set according to the location and time information taken from the respective *shift schedule*. This initial state of the physical world is then altered in an iterative process.

This process is illustrated by the following layers that are handled in sequence:

Physical layer: The *physical layer* describes the current state of the physical world in

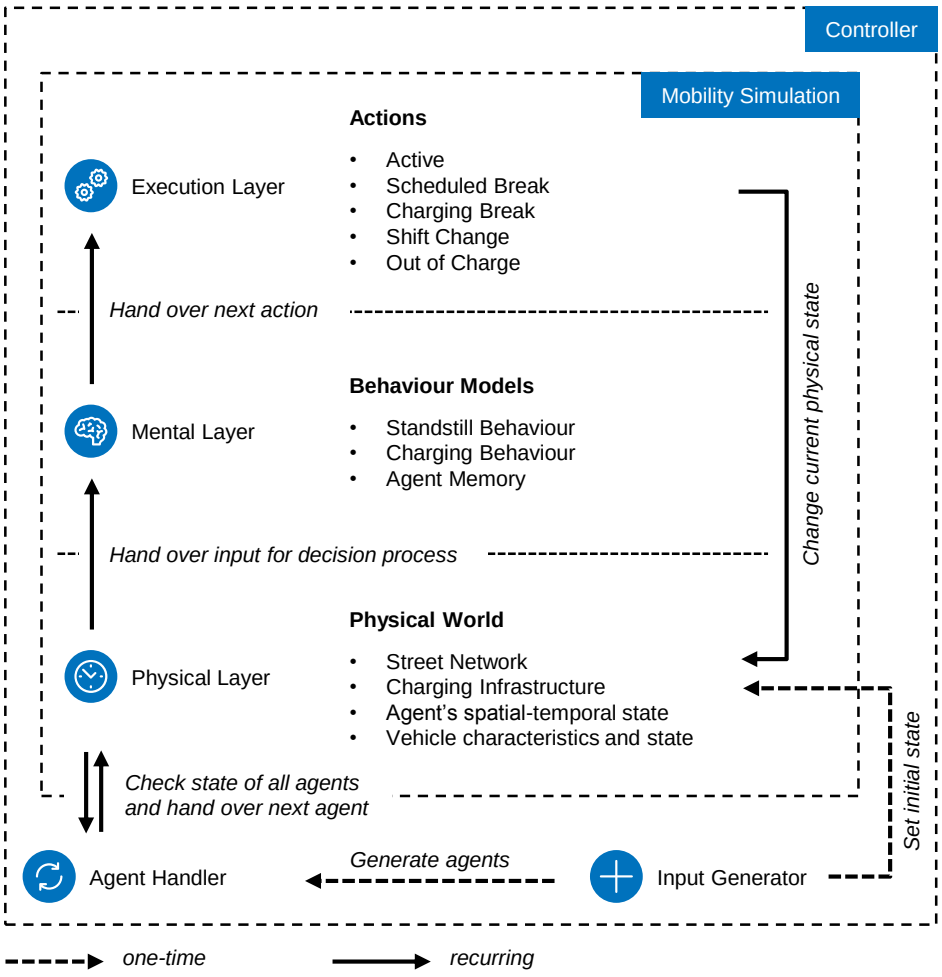

Figure 5.1: Model design (Sellmair and Schelo, 2018)

the model for each agent and charging station. It includes the street network (introduced in Chapter 2.5) where the location of each agent and charging station is represented by the corresponding *street network node* ID[1]. Furthermore, this layer consists of the vehicle energy model (Chapter 4).

Mental layer: At the *mental layer*, information from the *physical layer* is taken into account for the decision process that defines the next *action*. Based on its *standstill behaviour model* the agent decides whether or not it should take a *scheduled break* or make a *shift change*. The *charging behaviour model* decides when and where to charge the vehicle's battery by taking into account the agent's experience stored in the *agent memory*.

Execution layer: At the *execution layer* all *actions* are executed by changing the current state of the *physical layer*. Therefore, the *agent handler* selects one agent at a time and hands it over to the mobility simulation for the next *action*. The

[1]in reality charging stations cannot be placed at intersections, for simplicity this fact is neglected and it is assumed that the effect of placing charging stations at street segments instead is not significant

characteristic that during the simulation each agent has a different *simulation time* becomes important whenever agents are interacting with each other. The only interaction between agents in this model occurs when agents queue to use a charging station. In order to calculate how long each agent has to wait until it can use a charging station, it must be known what all other agents did at that time. To have that information, the *agent handler* always chooses the agent with the lowest *simulation time* to be handled next.

The simulation is terminated by the *controller* once each agent's *simulation time* exceeded the defined simulation duration. Due to the random assignment of trips and *shift schedules*, several simulated days are required until the average values of the simulation results converge. The convergence also depends on the number of simulated taxis - the more taxis are simulated, the fewer days are necessary. Simulation durations of 8 to 60 days have proven to sufficiently reduce statistical fluctuations.

The definition of the simulated scenarios and all executed *actions* are recorded in log files and imported to a database. The design of this database is introduced in Appendix D. The model's class diagram is presented in Appendix E.

In contrast to the demand-based approach, the data requirement of the supply-based approach is less ambitious since only tracking data, including the taxi's status of a representative sample of the whole taxi fleet is required. The assignment of recorded trips with respect to time and space automatically takes real traffic conditions into account. Furthermore, the vehicle energy model (Chapter 4) is applied to make realistic energy consumption estimations of the agents' trips. Additionally, it is possible to predict revenue of electric taxis by summing up the recorded revenue of all executed trips.

5.3 Actions

The *agent handler* selects the next agent which has to execute an *action* with respect to the agent's *simulation time*. Which *action* this agent executes is decided by the agent's behaviour models. An overview of all *actions* is given in Figure 5.2. Flow diagrams describing the functional design of each *action* are presented in Appendix F.

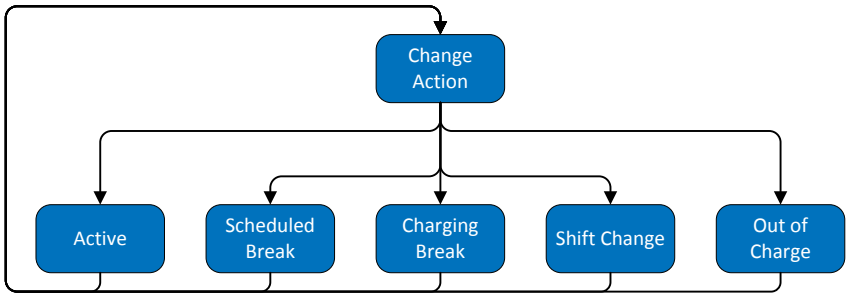

Figure 5.2: *Actions* agents can execute

Change Action: *Change action* is a transition *action* which is called after every other *action*. During this *action* the *standstill* and *charging behaviour model* decide

which *action* must be executed next. This decision is made with respect to the current time, the *shift schedule,* and the battery's state of energy (SOE). If the next *action* contains a *standstill period* (which is the case for the *actions*: *scheduled break*, *charging break*, *shift change*, and *out of charge*) a trip is generated and executed to the respective location.

***Active*:** After *change action*, *active* is the most frequently executed *action*. This *action* reproduces the taxi driver's procedure of searching for a customer and transporting him or her to the requested destination. Therefore, *search* and *engaged trips* are sampled by the *trip generator* with respect to the agent's *simulation time* and location. These trips are executed if the battery's SOE is sufficient, otherwise the agent switches back to *change action* directly.

***Scheduled Break*:** During the *scheduled break action*, the agent is executing *breaks* which are included in the *shift schedule*. If the *charging behaviour model* requires the agent to recharge during the *break*, the agent would have to queue in case all charging stations are in use at the time of arrival. Thus, due to waiting times and the following charging process the agent may have to exceed the scheduled break duration.

***Charging Break*:** In contrast, the *charging break action* is exclusively used to recharge the battery. The agent exits this *action* once its battery has reached the SOE required by the *charging behaviour model*.

***Shift Change*:** Other than the *break actions*, for *shift change* the agent must come to the location which is defined in the *shift schedule*. During the *shift change action* the agent waits until the *shift change* duration is over and gets a new *shift schedule*[2] randomly assigned by the *shift schedule pool* with respect to the time and location. If there is a charging station at the *shift change* location, the battery is recharged as well (charging during the *shift change* is denoted as *home charging*).

***Out of Charge*:** This *action* handles the case if the agent ran out of energy and cannot reach any charging station. In this case, the agent is moved to the closest charging station and has to wait there without charging until a time penalty of two hours is over. This penalty takes the loss of time caused by towing the car into account. The *charging behaviour model* was designed to minimise the occurrence of this case. Among the analysed scenarios of this work, more than 1,700 simulation days on average were necessary until this case occurred once per taxi. Although this case occurred very rarely it is important to handle it, otherwise the simulation model could be stuck in an infinite loop.

There are two ways of charging: *public charging* and *home charging*. *Public charging* is executed at *scheduled breaks* and *charging breaks* whereby all charging stations are accessible by every agent. This causes waiting times if all charging stations are in use when an agent arrives. Due to the short duration of these *breaks*, only charging stations with at least 40 kW charging power are considered for *public charging*.

[2] the new *shift schedule* must have been derived from the same recorded taxi as the previous schedule

Home charging is an additional option which can only be made during *shift changes*. In this case it is assumed that one charging station is installed at each agent's most common *shift change location*. Each charging station is considered as private and can only be used by one specific agent. Since *shift changes* are much longer than *breaks*, the charging power of these stations is set to 6 kW in order to reduce costs.

The *actions* are designed to mimic the behaviour of real taxi drivers in great detail. The sampling of *search trips* during the *active action* allows to reproduce the drivers' search strategies. Furthermore, as the trips are sampled with respect to the agent's *simulation time* and location, the temporal-spatial demand for taxis is indirectly respected as well. For example, if the agent is currently in an area with low demand, it is very likely that the sampled *search trip* will be longer than average. Moreover, since the agents are following the sampled trips' *speed profiles*, real traffic conditions are taken into account as well.

Another important aspect is that the *actions* are designed to respect real drivers' activity patterns by following the *shift schedules*. Thus, agents will have *breaks* and *shift changes* at the same time and place as the real taxi driver from whose driving profiles the *shift schedule* was derived from. As a result, the pattern that the lowest share of the taxi fleet is active in the night while during peak hours the highest share of the fleet is active (compare Figure 3.2) is reproduced by the simulation as well.

The design of this model allows a fair comparison between conventional and electric taxis. Electric taxi agents have to follow exactly the same *shift schedules* as conventional taxis. Hence, key values like average mileage or revenue per day of electric taxis cannot exceed those of conventional taxis. Additionally, electric taxi agents have to respect the constraint of not running out of charge. Therefore, charging events have to be included in *scheduled breaks* and (if *home charging* is enabled) in *shift changes*. If these events cannot be executed within the scheduled time or if the agent has to include additional *charging breaks*, it will loose time. The same accounts for additional detours electric taxi agents may have to make to reach the next charging station.

Thus, simulated driving profiles of electric taxis are very similar to those of conventional taxis as long as detours, waiting times for available charging stations, and charging times are low. The stronger the impact of these factors becomes, the more electric taxi driving profiles will deviate and the lower their revenue will be.

5.4 Shift schedule pool

All *shift schedules* which originated from the same taxi of the recorded data set were combined to one *shift schedule set*. At the initialisation of the simulation the *shift schedule pool* assigns *shift schedule sets* to agents whereby each set can only be assigned to one agent. The first *shift schedule* which the agent has to follow is randomly sampled from this set. Whenever the agent completes its *shift schedule*, the *shift schedule pool* assigns another schedule from the agent's *shift schedule set*. Thereby, the new *shift schedule* must fulfil following conditions:

Temporal condition: The end of the *shift change* of the previous *shift* must not be further apart than 30 min from the start of the new *shift*.

Spatial condition: The start location of the new *shift* must not be more than 200 m (driving distance on street network) away from the end location of the previous

shift.

Shifts which fulfil both conditions are considered as connected. The temporal condition is essential to ensure that the *shift change* durations are respected, e.g. it does not make sense to connect a *shift* which starts at 18:00 to a *shift* which *shift change* ended at 5:00. Additionally, it is also important to take spatial considerations into account, e.g. it could have happened that the driver brought the car to service and collected it afterwards. Assuming that the standstill time was longer than two hours, this event would have been considered as *shift change*. It is expectable that the following *shift* was different than a *shift* starting from the driver's home. Therefore, these two *shifts* should be executed in this order, which is most likely ensured by respecting the temporal and spatial condition.

To apply these conditions it must first be ensured that there is at least one *shift* connected to another and it must be avoided that only a subset of the whole set of *shift schedules* can be used. This problem is illustrated by a simplified *shift schedule set* in Figure 5.3.

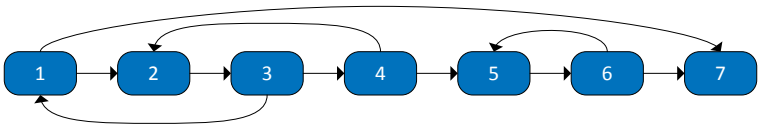

Figure 5.3: Connected *shift schedule set*

Each *shift* is represented by one block whereby the arrows show which *shifts* are connected with each other. As all *shifts* were recorded in sequence, one *shift* is always connected with its consecutive *shift*. Additionally, it is also possible that *shifts* are connected with other *shifts*, e.g. this is the case for *shift* 3 and *shift* 1.

By checking the *shifts'* connections it is notable that *shift* 7 is not connected with any other *shift*. Hence, if the agent executed this *shift schedule* it would not be possible to assign any following *shift schedule*. In order to rule this case out, *shift* 7 would be removed from the *shift schedule set*.

Another problem of this *shift schedule set* is that once *shift* 5 was selected, the algorithm could only assign the subset of *shift* 5 and *shift* 6, all other *shifts* are not reachable any more. To prevent this case, *shift* 5 and 6 would have been removed from the *shift schedule set* as well. The criteria for removing subsets is that *shifts* are removed as long as there is no sequence of *shifts* connecting the last *shift* of the set with the set's first *shift*. Thus, *shift* 4 would not be removed since *shift* 1 can be reached via *shift* 2 and *shift* 3.

An important aspect when removing *shifts* from the set is that the representativeness of the remaining *set* must not be affected. Hence, this approach is only viable if only a small percentage of all *shifts* is removed.

Furthermore, it was required that after the removal, each *shift schedule set* must contain at least ten *shift schedules*. This criteria was not fulfilled by 24 taxis so that the maximum number of taxis which can be simulated was reduced to 2,949. In total there were 159,805 *shifts* extracted from these taxis, whereby after the removal 149,960 *shifts*

remained. Which means that a moderate share of 6.2% of all *shifts* was removed. It is assumed that this reduction did not harm the representativeness.

The reason why only a small percentage of *shifts* had to be removed is that the *shifts* are well connected with each other. As an example, Figure 5.4 shows the connectivity matrix of one *shift schedule set* consisting of 52 *shifts* in total.

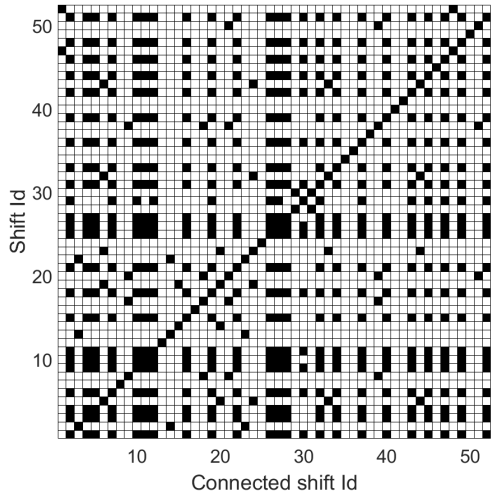

Figure 5.4: *Shift* connectivity matrix

Each row of this matrix represents one *shift*, if column *j* of row *i* is black then *shift i* is connected with *shift j*. The average number of connections per shift was 11.3. The diagonal from the bottom left to the top right shows that consecutive *shifts* are always connected with each other. Since *shift* 52 was connected with *shift* 1, there was at least one sequence of *shifts* connecting each *shift* with any other *shift*. Hence, it is not possible that the agent gets stuck into a subset of *shifts*.

After the pre-processing of the *shift schedule sets*, another important question is how to make a representative selection of these sets if fewer than the maximum number of taxis shall be simulated. Since there is a big variance in the average daily mileage of the recorded taxis (compare Figure 3.7) a random selection could especially for a small number of agents mean that key values of this subset could significantly differ from the average over the whole fleet. To handle this issue, each *shift schedule set* got features which were calculated by averaging the following values over all *shifts*:

- *shift* duration a_1
- number of *shifts* per day a_2
- *break* duration a_3
- number of *breaks* per day a_4

The average values of these features over the whole *shift schedule set* are listed in Table 5.1.

Table 5.1: Averages and standard deviation of features over all *shift schedule sets*

Feature	Average	Standard deviation
Shift duration [min]	309	132
Number of *shifts* per day	2.33	0.767
Break duration [min]	28.5	6.74
Number of *breaks* per day	4.45	2.35

A sample of *shift schedule sets* is characterised by the average μ_{1-4} and standard deviation σ_{1-4} over each *shift schedule set's* features a_{1-4}. These values are compared with the averages $\bar{\mu}_{1-4}$ and standard deviations $\bar{\sigma}_{1-4}$ over all *shift schedule sets.* Following formula is used to quantify the overall deviation δ:

$$\delta = \sum_{i=1}^{4} \left(\frac{\mu_i}{\bar{\mu}_i} - 1 \right)^2 + \sum_{i=1}^{4} \left(\frac{\sigma_i}{\bar{\sigma}_i} - 1 \right)^2 \tag{5.1}$$

To start the selection of sets, δ was calculated for each pair of *shift schedule sets*, while the pair with the lowest δ was selected. Next, every combination of the selected pair with any other *shift schedule set* was evaluated and the *shift schedule set* with the lowest resulting δ was added to the selection. This procedure was repeated until all *shift schedule sets* were added. The *shift schedule pool* uses this order of *shift schedule sets* to assign sets to a given number of agents.

A comparison between the selected *shift schedule sets* and the whole *shift schedule set* regarding the differences of averages $(\mu_i - \bar{\mu}_i)$ and standard deviations $(\sigma_i - \bar{\sigma}_i)$ for 10, 100, and 1,000 selected sets is shown in Table 5.2.

Table 5.2: Difference of average and standard deviation (STD) between selected *shift schedule sets* and all *shift schedule sets*

Number of sets	10	100	1,000
Average *shift* duration [min]	10.10	0.50	0.04
Average *shifts* per day	$32.89 \cdot 10^{-3}$	$6.74 \cdot 10^{-3}$	$-0.09 \cdot 10^{-3}$
Average *break* duration [min]	$-57.15 \cdot 10^{-3}$	$74.12 \cdot 10^{-3}$	$1.94 \cdot 10^{-3}$
Average *breaks* per day	$52.11 \cdot 10^{-3}$	$7.83 \cdot 10^{-3}$	$1.58 \cdot 10^{-3}$
STD *shift* duration [min]	-2.81	-0.02	-0.06
STD *shifts* per day	$7.58 \cdot 10^{-3}$	$-0.73 \cdot 10^{-3}$	$-0.17 \cdot 10^{-3}$
STD *break* duration [min]	$-105.6 \cdot 10^{-3}$	$2.60 \cdot 10^{-3}$	$0.09 \cdot 10^{-3}$
STD *breaks* per day	$-24.52 \cdot 10^{-3}$	$-7.87 \cdot 10^{-3}$	$0.66 \cdot 10^{-3}$

As expected, the differences decreased with the number of selected sets. For 10 sets the relative difference per feature was between -2.1% and 3.3%, whereby the differences for 1,000 sets were less than $\pm 0.1\%$. The relative differences of each feature among a selection of *shift schedule sets* is around even, which means that no feature is considerable worse represented than others. Taking into account that 10 sets are only 0.3% of the whole set of *shift schedules*, the found differences are moderate. Hence, it can be

expected that also a small number of agents can represent the variety of all taxi driving profiles on an acceptable level.

5.5 Trip generator

The *trip generator* has two tasks: it has to synthesise trips from an origin to a destination *street network node* and it has to sample *search* and *engaged trips* from the High Frequency Data set (HFD) (introduced in Chapter 3.1). Approximately 81% of the agents' simulated mileage origins from sampled trips.

Most of the *search trips* and all *engaged trips* are sampled. The sampling of trips has the advantage that the agents are following exactly the same *route* (set of *street network sections*) and speed profiles of a real taxi. However, if the agent has to arrive at a specific destination, which is the case to execute *scheduled break*, *charging break*, and *shift change actions*, it is very unlikely that a recorded trip can be found which started at the agent's current location and ended at the required destination. For this purpose trips are synthesised.

5.5.1 Trip synthetisation

The required input to synthesise trips is the time when the trip starts and the origin's and destination's *street network node* ID. The A* algorithm (Moeller, 2014) is used to find the fastest *route* connecting these *nodes*. To assign the trip's duration, *pass-through speeds* are randomly sampled with respect to speed distributions (Chapter 3.4.2 equation 3.5) associated to the *sections'* street type and the *speed-cluster* chosen with respect to the trips' start time. The speed distribution functions allow to generate an average speed value for each *section* with respect to a random number r between zero and one (the higher the number the higher the speed).

The two most obvious options to generate r are:

Option 1: generate a random number for each *section* individually

Option 2: generate one random number which is applied for all *sections*

The main criteria to assess which of these options is better applicable is whether the driving through one *section* can be seen as an independent event or if the *pass-through speed* depends on speeds which occurred at previous *sections*. Since the average length of one *section* is 132 m there must be a correlation between the speeds of two consecutive *sections*, e.g. if the vehicle drove with very low speed of 10 km/h through one *section* it could not reach a *pass-through speed* of 80 km/h at the following *section*. Thus, using independent random numbers for each *section* would result in unreasonable high speed fluctuations.

Moreover, it must be kept in mind that a trip with the length of 10 km consists of 76 *sections* on average. Hence, 76 random numbers would be generated to simulate the trip's average speed. Due to the law of great numbers it must be expected that high and low *pass-through speeds* will balance out so that the average speed of all synthesised trips will be very similar. This does not agree with the observed speed distribution of the recorded trips.

On the other hand, Option 2 means that if a low random number was generated the agent drives through each *section* with disproportionately low speed[3]. Low values of r could be associated with traffic jams, however it is unlikely that a vehicle got stuck in a traffic jam at each street it passed through. Therefore, Option 2 is also not an ideal solution.

Nevertheless, it is chosen in this work, as it is considered to be more realistic than Option 1. In order to avoid that the agent drove with unreasonable low or high speed through each *section*, the range of r was reduced to be between 0.33 and 0.93. This means that the lowest speed which can be assigned as *pass-through speed* must not be lower than the 33rd percentile of all recorded speeds of the respective *sections'* street type and the highest possible speed must not exceed the 93rd percentile.

To validate the speed assignment, 10,000 trips were randomly sampled from the HFD. The *routes* and the time of the day of these trips were given to the *trip generator* as input to apply the introduced method of assigning *pass-through speeds* to each *section*. Due to the random speed assignment, it cannot be expected that the resulting average speed of each trip would be similar to the original trip. However, in order to simulate realistic driving behaviours, it is necessary to reproduce similar distributions of the average speeds per trip. A comparison of these distributions is depicted in Figure 5.5.

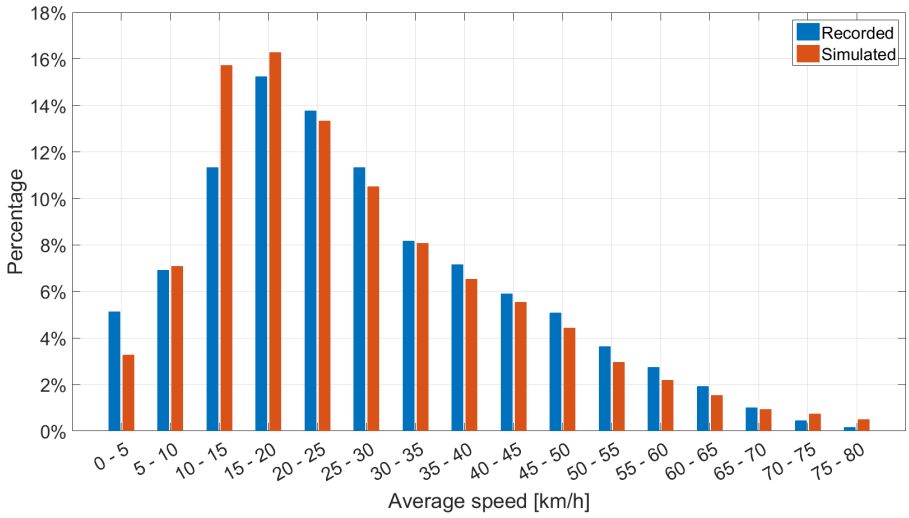

Figure 5.5: Distribution of recorded and simulated average speed per trip

The average speed of the recorded trips was 27.1 km/h with a standard deviation of 15.8 km/h. The range of the random variable r (0.33 to 0.93) was adjusted in order to reproduce this distribution. The resulting average speed distribution of the simulated trips had an average value of 26.6 km/h and a standard deviation of 16.5 km/h.

Interestingly, the range of r was asymmetrically reduced - 33% of the lowest speeds were neglected while only 7% of the highest speed values cannot be chosen. A reason for that could be that the derived speed distributions overestimated the probability of low speeds. It was discussed in Chapter 3.4.2 that 0.7 to 0.9% of the extracted *pass-*

[3]as speed distribution functions are selected with respect to the *sections'* street type not necessarily every *section* would be passed through with the same speed

through speeds had a value of 0 km/h. Possibly, low speeds greater than zero were also overrepresented in the data which could have caused the overestimation of low speeds by the fitted speed distribution functions. A reason for the overrepresentation of low speeds could be measurement and map-matching errors.

The *trip generator's* synthesised trips are given to the route-based energy consumption model (Chapter 4.1.3) to estimate the required amount of energy to execute these trips with an electric vehicle.

5.5.2 Trip sampling

The procedure of generating *search* and *engaged trips* during the *active action* is shown in Figure 5.6.

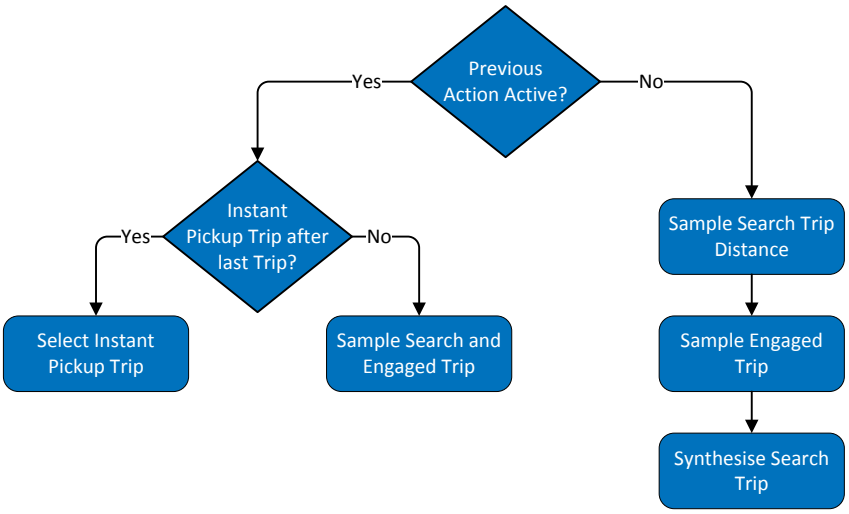

Figure 5.6: Generation of trips within *active action*

First it is checked whether the last *action* [4] was *active* or if an *action* with a *standstill period* (*scheduled break, charging break,* or *shift change*) was executed. If the last *action* was *active*, it is further checked if an *instant pickup trip* is connected to the last executed *engaged trip*. *Instant pickup trips* are *engaged trips* which immediately followed after another *engaged trip* without a *search trip* in between (10.6% of all *engaged trips* are *instant pickup trips*). If there is an *instant pickup trip*, this trip is assigned to the agent as the next *engaged trip* and no *search trip* is generated. It is important to handle this case, otherwise the agents would always have to execute a *search trip* and loose more time for searching than real taxis. Consequently, their generated revenue would be less.

If no *instant pickup trip* is connected to the last *engaged trip*, a *search trip* which is not farther away than 200 m (driving distance on street network) from the agent's location is sampled with respect to the current time of day. The sampling of the *engaged trip* is done in the same way, whereby its start *node* must not be farther away than 200 m from the end *node* of the sampled *search trip*. If necessary, trips are synthesised to connect the agent with the *search trip* and the *search trip* with the *engaged trip*.

[4] excluding *change action* which is called after each other *action*

If the previous *action* was not *active*, a *search trip* is sampled in the same way as above. The driving distance of this trip is denoted as d_{ST}. In contrast to the previous method, this trip will not be assigned to the agent. Instead, the driving distance d_k from the agent's current location to the start location of any *engaged trip k* is calculated. The difference of the driving distance to reach the start location and the sampled search distance d_{ST} is calculated for each *engaged trip*. All *engaged trips* which difference is below the tolerance δ of 250 m are selected:

$$|d_k - d_{ST}| \leq \delta \tag{5.2}$$

If no *engaged trip* is found, δ is doubled as long as at least one trip is found. In case that more than one *engaged trip* is found, one among these trips is sampled with respect to the time of the day. Finally, the assigned *search trip* is synthesised by connecting the agent's location with the start *node* of the sampled *engaged trip*.

The difference between method 1 of sampling a *search trip* (after *active action*) and method 2 of synthesising a *search trip* (after a *standstill action*) is that method 1 assigns *search trips* that are more realistic as they were derived from real data and that the computation time is lower. However, the variety of selectable *engaged trips* is larger when applying method 2. As agents usually have *standstill periods* at a relatively small number of locations, this drawback could become critical and may cause agents to repeat the same sequence of trips many times. Thus, less realistic trips and higher computation time is accepted by applying method 2 after *standstill periods*, while the benefits of method 1 are exploited after *active actions*. The energy consumption of all sampled trips is estimated via the speed-based energy model introduced in Chapter 4.1.2.

A test scenario was defined and simulated in order to analyse whether the *trip generator* is capable of sampling a big variety of different trips instead of frequently assigning the same sequence of trips. This scenario consisted of 200 agents which all had to make their *shift change* at the same location. Hence, every agent started its *shift* on the same *street network node*. To assess the variety of generated trips, it was evaluated how many different *engaged* trips were sampled at the kth trip of each *shift*. The results are illustrated in Figure 5.7.

The number of unique trips is shown by the blue dots while the red dots represent how many *shifts* consisted of at least *k engaged trips*. As each *shift* contained at least one *engaged trip*, this value is shown by the red dot for the first trip. Each *shift* had a duration of several hours, hence the number of *shifts* remained almost constant for the next seven trips. Afterwards, more and more agents reached the end of the scheduled *shift* duration and consequently did not execute any further trips. Thus the number of *shifts* decreased rapidly between 7 and 20 trips. The highest number of trips per *shift* was 31.

In total 751 different *engaged trips* were sampled at the first trip of all *shifts* (blue dot). Which is quite a high number considering that each agent started from exactly the same location and that a strict spatial constraint was applied for the sampling. The number of unique trips increased to 3,322 and 6,463 for the second, respectively third trip of each *shift* and reached its maximum of 9,065 for the sixth trip. Afterwards, the number of unique trips decreased which was caused by the decreased number of *shifts*.

Nevertheless, the percentage of unique trips at the kth trip of each *shift* (purple dots) still increased thereafter and eventually reached 100%, meaning that at this point every sampled trip was different. The decrease of the percentage from the 23rd until

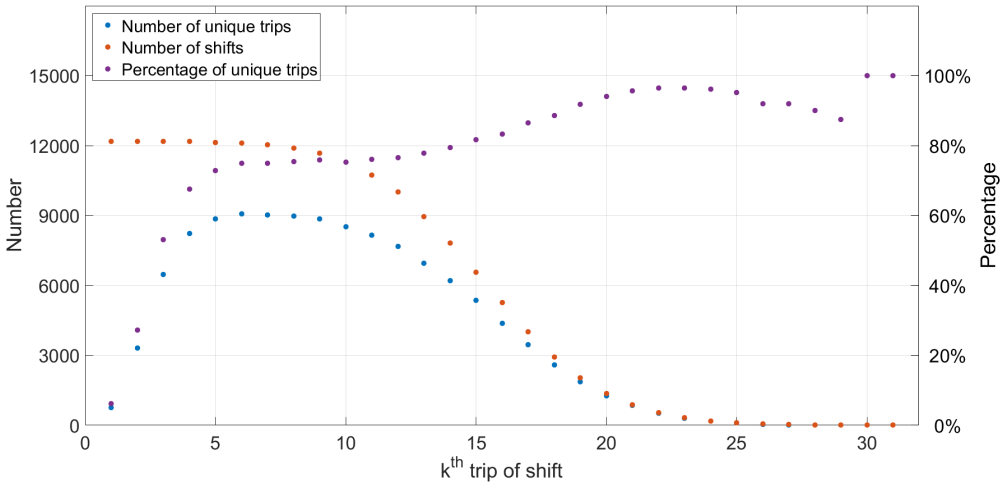

Figure 5.7: Number and percentage of unique *engaged trips* for k^{th} trip of *shift*

the 29^{th} trip was most likely caused by the low number of remaining *shifts* when even a small number of agents executing the same sequence of trips had a significant effect on the overall percentage.

A very important aspect which can be derived from these curves is that after the first time when the sampling of *search trips* (method 1) was applied to generate the second trip of each *shift*, the number of unique trips increased by a factor of 4.4. Assuming that all of the first 751 trips ended at different locations this means that from each location on average 4.4 different trips were sampled. As a result, the number of unique trips was increased by 2,571 to 3,322 which was a significant increase in the variety of trips. However, if method 1 would have been applied to sample the first trip of the *shift,* only four to five different trips would have been selected. Even if this number was multiplied each time for the following trips of the *shift*, the variety of trips would still have been much lower than for the analysed scenario. Thus, applying method 2 after each *standstill period* is vital to reach a high variety of sampled trips.

As the results of this simulation model are later used to derive the taxis' charging demand and based on that to optimise the placement of charging stations it is very important to reproduce a high variety of driving profiles. Otherwise, the charging demand would be too heterogeneous. That would result in placing too many charging stations at charging demand hot spots while underestimating the required number of charging stations in other areas.

To simulate the charging demand for the infrastructure optimisation, each agent will get a unique set of *shift schedules* (Chapter 5.4). Thus, the variety of simulated trips will be significantly higher than at the scenario visualised by Figure 5.7 as almost each agent will start its *shift* at a different location. Nevertheless, the synthesising of *search trips* after *standstill periods* (method 2) still remains important since many agents will have *scheduled breaks* or *charging breaks* at a small number of locations which are equipped with charging stations.

5.6 Agent memory

The agent's behaviour models have to make several estimation-based decisions. Humans would make those decisions based on their experience. The idea of the *agent memory* is to collect a set of average values which are derived from previously executed *actions* that are accessible by the behaviour models to make experience-based estimations. Hereby, each agent has individual memory values which are exclusively derived from its own executed *actions*. Every time the agent executed another *action*, its memory values are updated. The *agent memory* is a set of the following average values:

- duration of *active action* Δt^M_{Active}
- driving distance to *shift change* d^M_{sc}, *scheduled break* d^M_{sb}, and *charging break* d^M_{cb} location
- charging power P^M_c
- waiting time for available charging station w^M_j and number of charging events n^M_j at location *j*
- speed v^M
- energy consumption η^M

The *active action* duration, driving distances to *standstill locations* and the speed are important for the *standstill behaviour model* to decide if the agent has enough time left to execute another *active action* before the next *scheduled break* or *shift change action*. To accurately plan recharging, the *charging behaviour model* relies on the average charging power, the waiting time per *charging location*, and the vehicle's energy consumption.

Hereby, the waiting time per *charging location* is especially interesting, as it is used to select *charging locations*. Locations with high waiting times can be rejected even if they are closer to the agent's current location. As each agent has its individual memory, previous waiting times influence their decision, which results in preferring or avoiding certain *charging locations*. This is comparable with the behaviour of humans who prefer locations where they made good experiences while avoiding others.

Due to the stochastic nature of charging events, the waiting time at a specific location fluctuates very strongly, e.g. if the agent arrives shortly before a group of other agents that want to recharge at the same location, the waiting time of this agent would be significantly lower as if it arrived after that group. Thus, the waiting time estimation with respect to the memorised values must be carefully handled especially when only a small number of charging events was executed so far.

In case that no charging event was recorded at location *j*, the estimated waiting time w^E_j at this location is set to the average over all *charging locations i*:

$$w^E_j = \bar{w}^M = \frac{\sum_i n^M_i w^M_i}{\sum_i n^M_i} \tag{5.3}$$

In case no waiting time was recorded yet, it is assumed that the waiting time at each location is zero. If fewer than *k* events were recorded at location *j*, the estimated waiting time is calculated by a weighted sum of the waiting time at this location w^M_j and the average waiting time over all locations $\bar{w}$:

$$w_j^E = \begin{cases} \frac{n_j^M \cdot w_j^M + (k - n_j^M)\bar{w}^M}{k} & \text{if } n_j^M < k \\ w_j^M & \text{otherwise} \end{cases} \tag{5.4}$$

This method allows to damp the fluctuations of the memorised waiting times when few information for this location is available while more and more weight is put to this value with an increased amount of information.

To evaluate which effect different values of k have on the agent's *charging location* choice, three test scenario with different values of k (1, 3, and 5) and a simulation duration of 31 days were simulated. If k is one, no weighted sum is calculated and the memory value is exclusively used after the first charging event at the respective location. The scenarios consisted of 200 agents and four *charging locations*. How often each agent chose one of these locations for recharging is shown by Figure 5.8.

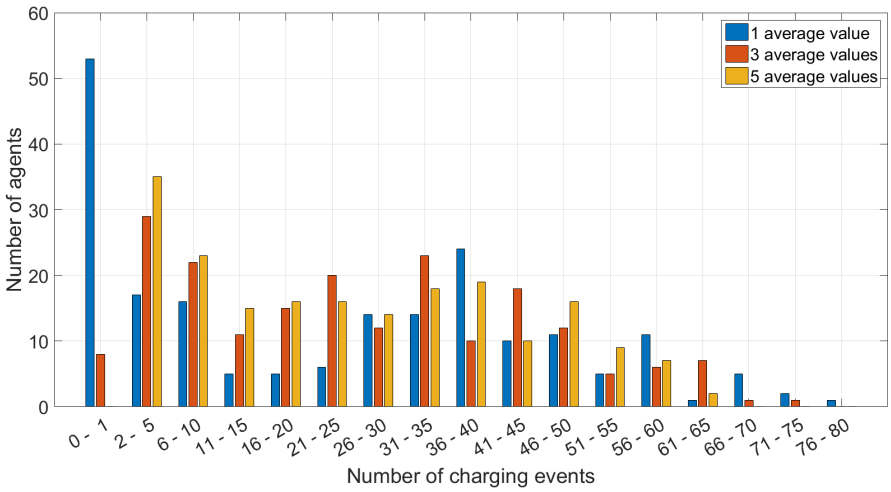

Figure 5.8: Number of charging events per agent at one *charging location*

The blue bars represent the scenario with k=1. Here, it can be seen that 53 out of 200 agents had no or only one charging event at the chosen *charging location*. As it is very unlikely that agents never chose this location it is expected that these 53 agents had exactly one charging event at this location where they had to wait very long for an available charging station. As a result, the stored waiting time in the agent's memory was very high so that these agents never chose this location again. Moreover, eight agents had more than 65 charging events at the same location while only two agents for k=3 (red bars) and no agent for k=5 (yellow bars) exceeded this number. Hence, it seems that in case of k=1 there were agents which almost exclusively chose one location and rejected all others most likely because their memory value for all other locations was much higher than for the analysed location. Choosing one location exclusively means that the agents will have to accept high detours. It is very unlikely that electric taxi drivers would behave in this way. Thus, k=1 is no reasonable choice.

The distributions for k=3 and k=5 are similar. In order to decide for one parameter value it must be taken into account that the higher k is, the longer it would take until the agents exclusively rely on location specific memory waiting time. As a consequence

it could take longer until a convergence of the agent behaviour is reached which in turn could also increase the necessary simulation duration. Thus, k=3 was chosen to estimate the waiting time at *charging locations*.

5.7 Behaviour models

All of the agent's decisions are made by the *standstill* or *charging behaviour model*. The *standstill behaviour model* decides with respect to the agent's *shift schedule* when and where *scheduled breaks* and *shift changes* have to be made. This model ensures that the agent's activity patterns correlate with that of real taxi drivers.

Due to limitations in range and charging time, agents with electric vehicles may not be able to follow the same activity patterns as conventional taxi drivers. Therefore, the *charging behaviour model* has to ensure that the agent is not running out of energy by deciding when and where it has to recharge the battery. Since this has a higher priority than respecting the agent's *shift schedule*, the *charging behaviour model* can overrule decisions of the *standstill behaviour model*. The fewer decisions are overruled, the more similar the agent will behave like a taxi driver with a conventional vehicle.

The nomenclature of this section is given by Table 5.3.

5.7.1 Standstill behaviour

Each time *change action* is executed, the *standstill behaviour model* must decide if the agent continues with an *active action* or if it should stop to execute a *scheduled break* or a *shift change action*. Furthermore, when a *scheduled break action* must be done, the *standstill behaviour model* selects the location as well.

First of all, the model decides if a *shift change action* shall be made. Therefore, the current time t and the scheduled end time of the *shift* t_{sc} are required. If the agent exceeded the end of the *shift* already $(t > t_{sc})$, the next *action* is *shift change.* Otherwise, the *shift* end time is projected for the case that the agent is driving to the *shift change location* immediately (equation 5.5) and for the case that the agent executes another *active action* and drives to the *shift change location* afterwards (equation 5.6):

$$t_1 = t + \frac{d_{sc}^M}{v^M} \tag{5.5}$$

$$t_2 = t_1 + \Delta t_{Active}^M \tag{5.6}$$

The next *action* will be *shift change* if t_1 is closer to the scheduled *shift change* time than t_2:

$$|t_{sc} - t_1| < |t_{sc} - t_2| \tag{5.7}$$

If this condition is not fulfilled, no *shift change action* will be executed and it will be checked if the next *action* shall be *scheduled break*. Therefore, the same method as for *shift change* is used, whereby t_{sc} is replaced by the scheduled time of the next *break* and d_{sc}^M is replaced by the memorised driving distance to a *scheduled break* d_{sb}^M. The *standstill behaviour model* decides to execute another *active action* if neither *shift change* nor *scheduled break actions* are required.

Table 5.3: Nomenclature of behaviour models

Symbol	Unit	Description
d_j	km	driving distance to location *j*
d_{min}	km	minimum remaining range
d_{sb}	km	scheduled driving distance to *break*
d_{sb}^M	km	driving distance to *break* in memory
d_{sc}^M	km	driving distance to *shift change* in memory
Δt_{Active}^M	h	duration of *active action* in memory
Δt_i^{break}	h	scheduled duration of ith break
e	kWh	current battery energy
e_i^C	kWh	recharge energy at ith *break*
e_i^{drive}	kWh	driving energy between i-1th and ith *break*
e_i^{target}	kWh	energy target of ith *break*
η^M	kWh/km	energy consumption in memory
l_A	-	location of agent
l_{sb}	-	location of *scheduled break*
n_b	-	number of *breaks*
P^{M}	kW	charging power in memory
P_j	kW	charging power at location *j*
T_j	h	total time of *break action* at location *j*
t	h	current time
t_i	h	scheduled time of ith *break*
t_{sc}	h	scheduled *shift change* time
v^M	km/h	speed in memory
$\bar{w}^M$	h	average waiting time in memory
w_j^M	h	waiting time at location *j* in memory

In the case that the *scheduled break action* must be executed, the *standstill behaviour model* also decides at which location this *break* must be made (in case of *shift change* the location is already defined in the *shift schedule*). Thereby, the driving distance to the *break* location d_{sb} and, if available,[5] the standstill location l_{sb} defined in the *shift schedule* are taken into account.

The problem of modelling the *break* location choice of agents is that the agents have to choose their *break* location from a different start location than the taxi driver of whom the *shift schedule* was derived from. Hence, if agents had to strictly select the *break* locations in the *shift schedule*, their average driving distance to *breaks* would be too high. Therefore, the scheduled location and the driving distance are taken into account when selecting *break* locations. To do so, two tolerances (δ_1 and δ_2) are used to decide at which location a *scheduled break* shall be made. First, it is checked if l_{sb} is

[5] standstill locations are defined in the *shift schedule* if the driver of whom the schedule was derived from stopped at an *individual standstill cluster* (Chapter 3.2.3)

defined in the *shift schedule* and if the driving distance from the agent's current location l_A to that location does not exceed d_{sb} by more than δ_1:

$$\text{distance}\,(l_A, l_{sb}) - d_{sb} \leq \delta_1 \tag{5.8}$$

If this is fulfilled, the *scheduled break* has to be executed at location l_{sb}. In any other case (either l_{sb} is not defined or the tolerance is exceeded), it is checked if any other location of the agent's *individual standstill cluster* l_{sc} (Chapter 3.2.3) can be reached within the tolerance δ_2:

$$|\text{distance}\,(l_A, l_{sc}) - d_{sb}| \leq \delta_2 \tag{5.9}$$

In that case, the location l_{sc} which distance from the agent's current location is closest to d_{sb} will be selected. Finally, if no location is found, the location with a driving distance closest to d_{sb} among the *individual standstill clusters* of all agents is selected.

In order to set the tolerances δ_1 and δ_2, two criteria have to be taken into account: first, the share of *breaks* executed at the agents' specific *individual standstill clusters* must be similar to that extracted from the recorded data of real taxi drivers and second, the agents' driving distances to *break* locations must match the recorded data as well. The values which satisfied these criteria the best were: $\delta_1 = 8.0\,\text{km}$ and $\delta_2 = 1.5\,\text{km}$.

In order to assess how the criteria were fulfilled with respect to the parameter choice, a simulation with all 2,949 agents over five simulation days was run. The simulated agents made 35.3% of all *breaks* at their *individual standstill clusters* while the share extracted from the taxi driving profiles was 36.2%. The simulated and recorded distributions of driving distances to clustered, respectively non-clustered *break* locations is depicted by Figure 5.9.

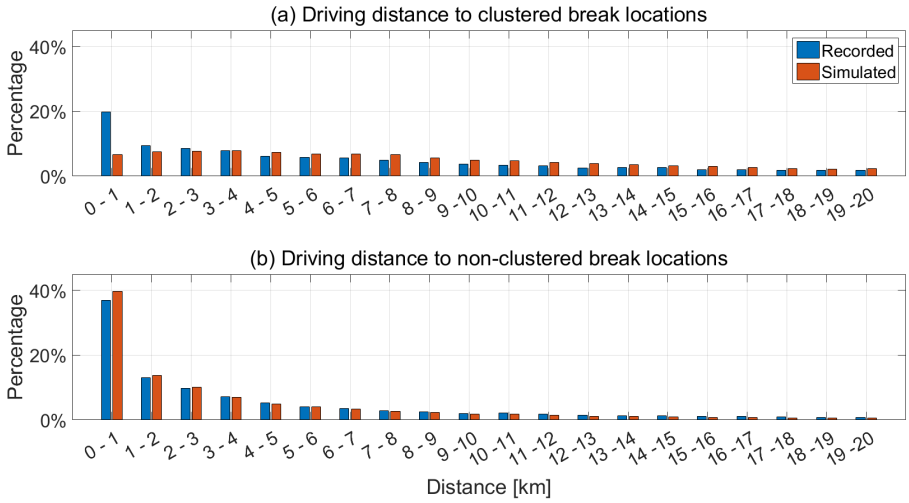

Figure 5.9: Recorded and simulated driving distance to clustered (a) and non-clustered (b) *break locations*

The recorded average driving distance to clustered *break* locations was with 8.6 km higher than the distance to non-clustered location which was 5.3 km. This observation makes sense as it can be expected that taxi drivers accept longer driving distances

to reach a place they probably like and therefore visit more frequently. The simulation results matched the recorded data very well with an average driving distance to clustered *break* locations of 9.5 km and 4.6 km to non-clustered locations.

Also the recorded and simulated driving distance distributions shown in Figure 5.9 (a) and (b) fit in general well together. However, there is one significant deviation between the recorded and simulated frequency of driving distance to clustered *break* locations below 1 km (19.9% and 6.7%). The high percentage of the recorded data gives an indication that drivers do not only decide to have a *break* with respect to the time but also take their current position into account. Meaning that if they finish an *engaged trip* nearby a location which they prefer, they have a *break* at that location although it is out of their usual rhythm of having *breaks*.

Since the introduced *standstill behaviour model* takes only temporal conditions into account to decide when a *break* shall be made, the described behaviour cannot be reproduced with this approach. Certainly, a more complex model would be required to consider temporal and spatial conditions. However, as the other distributions and average values match very well for the implemented model, it was decided to hold on this model.

5.7.2 Charging behaviour

The aim of the *charging behaviour model* is to alter the activity patterns defined in the *shift schedules* as little as possible while ensuring that the agent's vehicle is not running out of energy. Therefore, *scheduled breaks* are used to recharge as much energy as possible and *charging breaks* shall only be made when unavoidable. At the beginning of each *shift*, a *charging schedule* is created which contains the amount of energy that can be recharged during each break i. The recharge energy is calculated as follows:

$$e_i^C = \begin{cases} \left(\Delta t_i^{break} - \bar{w}^M\right) P^M & \text{if } \Delta t_i^{break} > \bar{w}^M \\ 0 & \text{otherwise} \end{cases} \tag{5.10}$$

where Δt_i^{break} is the duration of break i defined in the *shift schedule*. The average waiting time over all *charging locations* $\bar{w}^M$ is derived from the *agent memory*. Based on the estimated driving energy e_i^{drive} between two *standstill periods*, the amount of remaining battery energy at the beginning of each break, e_i is estimated (e_0 is the battery energy at the start of the *shift*):

$$e_i^{drive} = \left(t_i - \left(t_{i-1} + \Delta t_{i-1}^{break}\right)\right) \cdot v^M \cdot \eta^M \tag{5.11}$$

$$e_i = e_{i-1} + e_{i-1}^C - e_i^{drive} \tag{5.12}$$

here, t_i is the time when *break* i is scheduled. If these energy levels are sufficient to maintain a minimum range d_{min} at the beginning of each *standstill period* the *charging schedule* is finalised:

$$e_i \geq \frac{d_{min}}{\eta^M} \ \forall i \tag{5.13}$$

During the *shift*, the minimum range is set to 35 km which should be sufficient to reach a charging station from any location in Singapore. At the end of the *shift* before

the *shift change*, a remaining range of at least 80 km is required. The increasing of this limit avoids that the agent would have to make a *charging break* right at the beginning of the following *shift*.

If equation 5.13 is not fulfilled, the *break* durations can be extended so that the battery can be charged until the *fast charging limit* is reached. The *fast charging limit* is defined as the amount of energy when *constant power charging* ends and the charging power has to be reduced (Chapter 4.2.1). It is not considered to recharge the battery beyond this point as the charging power would gradually decrease and the agent would loose disproportionally more time to fully charge the battery. If the extension of *breaks* is still not sufficient to ensure the minimum range before each *standstill period*, additional *charging breaks* are added to the *shift schedule* and the *charging schedule*.

Finally, *energy targets* e_i^{target} that must be reached at the end of each *break* (n_b being the total number of *breaks*) are calculated:

$$e_{n_b}^{target} = \frac{d_{min}}{\eta^M} + e_{n_b}^{drive} \tag{5.14}$$

$$e_i^{target} = e_{i+1}^{target} + e_i^{drive} - e_{i+1}^{C} \tag{5.15}$$

To illustrate how a *charging schedule* is generated, Figure 5.10 shows a simplified example of a *shift* with one *scheduled break*.

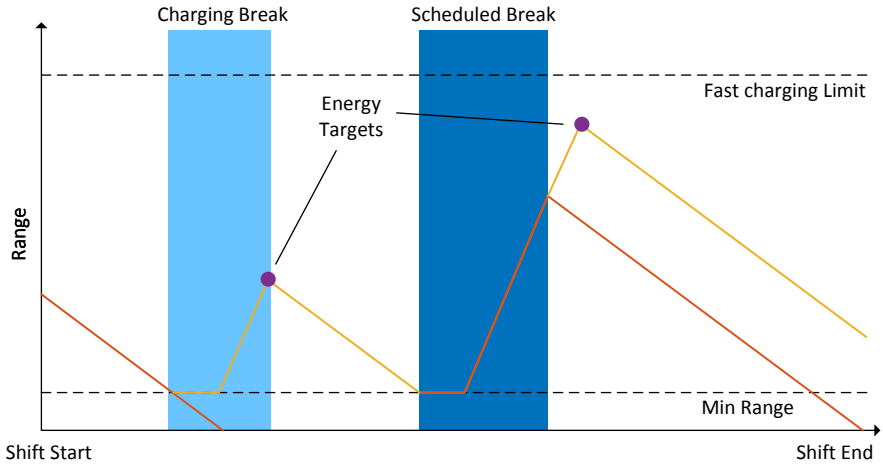

Figure 5.10: *Charging schedule* generation

The x-axis represents the time from the start of the *shift* until the end of the *shift*, while the y-axis represents the remaining range of the agent's vehicle. The lower dashed line depicts the minimum range during the *shift* (35 km) which must never be undercut and the upper dashed line represents the range corresponding to the *fast charging limit*. The *charging behaviour model* must not define any *energy targets* which would exceed this limit. Furthermore, it must ensure that a minimum range of 80 km is available at the end of the *shift*. The dark blue box represents the only *scheduled break* of this *shift*.

The first attempt to create the *charging schedule* is to assume that the agent exclusively uses the *scheduled break* to recharge the battery. How the vehicle's range would

evolve in this case is shown by the orange line, whenever the vehicle is driving, the range decreases while during the *scheduled break* it first remains constant which is caused by waiting for an available charging station and increases once the charging started. The graph shows that the vehicle's remaining range would fall below the minimum range before the *scheduled break* and before the end of the *shift*. Hence, it is not possible to execute this *shift* without any modifications.

Due to the low remaining range of the vehicle at the beginning of the *shift* in this example, a *charging break* must be included in order to reach the *scheduled break* thereafter. It is planned that the *charging break* starts when the remaining range reaches the minimum range. After including the waiting time $\bar{w}^M$ the battery is charged until the remaining range is sufficient to reach the beginning of the *scheduled break*. The corresponding amount of energy of this range is defined as *energy target*.

The recharged energy at the *scheduled break* is not sufficient to maintain the required minimum range of 80 km at the end of the *shift*. Therefore, it is assumed that the *scheduled break* was extended so that the range after the charging event would fulfil this requirement. Subject to this range the second *energy target* is defined. It is important to notice that the duration of the *scheduled break* in the *shift schedule* will not be changed although it is expected that the defined *energy target* will not be met within the scheduled time. The reason for this is that at the beginning of the *shift* it cannot be expected for certain that the *scheduled break* will have to be extended, e.g. if no waiting occurred the *energy target* would be met.

During the simulation, the *energy targets* are used to calculate if and how much energy must be recharged at each *break* with respect to the current SOE. As the *charging schedules* are only created based on average values derived from the *agent memory*, the simulated SOE will differ from the projections. To overcome these inaccuracies, the *charging schedule* is updated after each *break*.

Furthermore, it must be considered that agents must not interrupt *active actions* and therefore are not able to make a *scheduled break* or *charging break* at the exact scheduled time. Hence, the required recharge energy must be adjusted accordingly. For example if the agent executes the next *break* earlier than scheduled, it must reach a higher SOE as the driving duration after the *break* will be longer. Therefore, the recharge energy of an agent reaching the *i*th *break* with battery energy e at time t is calculated as follows:

$$e^C = e_i^{target} + (t_i - t)\, v^M \eta^M - e \tag{5.16}$$

A negative recharge energy e^C means that charging is not required at the respective *break*. In that case, the *charging behaviour model* would not change the location choice of the *standstill behaviour model*, and a *charging break* would be skipped. Otherwise, the *charging behaviour model* checks with respect to the selected location's average waiting time and charging power if it is possible to recharge the required energy within the *scheduled break* duration Δt_i^{break}. If that is possible, no amendments are made. If not, the *charging behaviour model* selects the *charging location* j which promises the shortest total time T_j with respect to the driving distance d_j from the current location, the memorised waiting times w_j^M, and the charging power P_j :

$$T_j = \frac{d_j}{v^M} + w_j^M + \frac{e^C}{P_j} \tag{5.17}$$

The implemented *charging behaviour model* is only one of many possible approaches. An introduction and evaluation of different strategies based on this work's driving profile simulation model can be found in (Czypulovski, 2017). The analysed charging strategies were modified in three ways compared to this work's approach:

information level: additional information regarding the availability of charging stations was included in the agent's decision process

charge full: the required recharge energy of the *energy targets* was set to the *fast charging limit* for all charging events

charging breaks only: all *scheduled breaks* were skipped and the agents made only *charging breaks* when running low on energy

The results showed that the *information level* could only increase the average revenue by 1% compared to this work's charging strategy. Adding the *charge full* method caused an increase of 5% in total. Combining all three modification resulted in a revenue increase of 16%.

The analysed scenarios of this study were different to that discussed in this thesis. First, all agents of this study had to follow the same set of *shift schedules,* meaning that they had to charge at the same time in the base line scenario and second, the number of charging stations per taxi was lower than what this thesis found out to be ideal.

As a result waiting times were significantly higher in this study which increased the importance of a more sophisticated charging strategy. Thus, it is expected that if these charging strategies were applied on this thesis' scenarios, the gain in revenue would be smaller. Moreover, these strategies would require that the drivers had to change their habits while this thesis focuses on analysing a system in which the drivers would have to change their behaviour as little as possible.

5.8 Validation

As no data regarding driving profiles of electric taxis was available, this model was validated with respect to driving profiles of 2,949 conventional taxis extracted from the LFD. The driving profiles of each of these taxis were simulated over a period of 31 days and compared with the recorded data. Therefore, the vehicles' energy consumption was set to zero[6] and the *charging behaviour model* was disabled.

The simulated distribution of daily mileage (a) and revenue (b) per taxi are compared with the recorded data in Figure 5.11.

The recorded and simulated distributions are similar: The average recorded daily mileage was 346 km with a standard deviation of 145 km, while the simulated mileage was 335 km with a standard deviation of 138 km. The average recorded daily revenue was 294 SGD with a standard deviation of 134 SGD and the simulated revenue was 292 SGD with a standard deviation of 133 SGD. Hence, the average deviation between recorded data and simulation results was 3.2% in terms of mileage and 0.7% regarding revenue.

The biggest deviation between recorded and simulated mileage was in the range of 200 to 250 km per day. Here, the recorded frequency was 7.2% whereby the simulated value was 9.7%. The reason for this gap is that at the time of the data recording there

[6] the refuelling of conventional vehicles was neglected

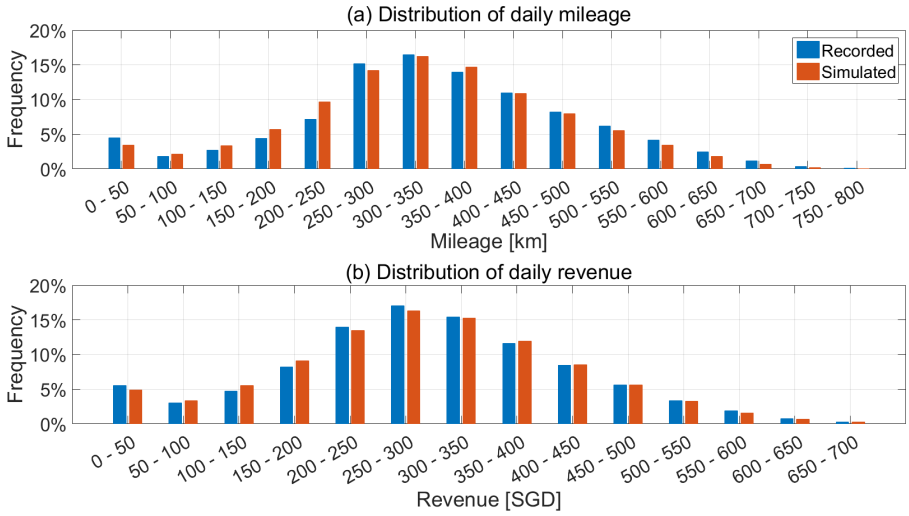

Figure 5.11: Distribution of recorded and simulated daily mileage (a) and revenue (b)

was a regulation in Singapore which required the majority of a taxi fleet to drive at least 250 km a day (LTA, 2016a). Thus, taxi drivers who did not meet this mark at the end of the day would have extended their *shift* until the requirement was met. That also explains the steep jump of the recorded frequency to 15.2% within the 250 to 300 km per day range. The *shift schedule pool* assigns *shift schedules* randomly without imposing a minimum daily mileage limit on the agents. As a result, more agents failed to meet this requirement.

A comparison of daily average values and standard deviations (in brackets) of more distribution is listed in Table 5.4.

Table 5.4: Comparison of recorded and simulated daily averages and (standard deviations)

	Unit	Recorded	Simulated	Difference
Daily mileage	km	346 (145)	335 (137)	-10.3 (-7.7)
Daily revenue	SGD	294 (134)	292 (133)	-1.7 (-1.5)
Daily driving duration	h	11.8 (4.6)	11.7 (4.45)	-0.10 (-0.19)
Daily *break* duration	h	1.57 (1.26)	1.47 (1.22)	-0.100 (-0.037)
Daily number of *breaks*	-	3.33 (2.22)	3.00 (2.09)	-0.324 (-0.132)
Daily *shift change* duration	h	10.5 (4.97)	10.8 (4.84)	+0.27 (-0.13)
Daily *shift change* number	-	1.76 (0.82)	1.70 (0.82)	-0.056 (+0.007)

The average and standard deviations of the simulation results deviate by less than 10% between the recorded data and the simulation results among all distributions. The highest deviations was found for the average number of *breaks* per day which was 9.7% lower than the recorded value. As a consequence, the simulated average duration of all *breaks* within one day was with 6.4% also lower. In contrast, the simulated *shift change* duration was 2.6% above the reference value. Thus, it seems that the simulation skipped a few *breaks* which were shorter than average and instead slightly extended *shift changes*.

This observation can be very well explained by the implementation of the *standstill behaviour model* which first checks if a *shift change* is scheduled and considers *breaks* only when this is not the case. Hence, it is possible that *scheduled breaks* may not be executed and instead the agent could make a *shift change* earlier than scheduled. It is more likely that rather shorter than longer *scheduled breaks* are affected since the time difference between the start of a long *break* and the end of the *shift* is higher. This would explain why the relative deviation regarding the break duration (6.4%) was lower than the deviation in the number of *breaks* (9.7%).

As all deviations are relatively low, it can be expected that the simulation model is capable of reproducing driving profiles of conventional taxis with high accuracy. Nevertheless, it must be kept in mind that no validation regarding electric taxis could be made. Thus, it is not possible to quantify how well the assumptions made for the *charging behaviour model* would reflect the actual usage of electric vehicles by taxi drivers. Therefore, the uncertainty of simulating this use case is clearly higher than for the case of conventional taxis.

5.9 Case studies

The purpose of this section is to discuss characteristics of the introduced driving profile simulation model by analysing simulation results of different scenarios. The charging infrastructures (power, placement, and number of charging stations) of these scenarios were chosen in order to highlight certain features of the model. Therefore, predominantly infrastructures with fewer than the ideal number of charging stations were defined. A discussion of simulation results for optimised charging infrastructures will follow in Chapter 8.

One of the most important features of this model is that due to the design of the behaviour models, agents with electric vehicles will act similar to conventional taxi drivers as long as limitations regarding detours to charging stations, waiting times, and charging times are negligible. The more these factors affect the agents the more their driving profiles will diverge from that of conventional taxis.

In order to investigate this effect, a charging infrastructure (40 charging stations of 160 kW charging power and 6 kW charging station at each agents' *shift change location* (*home charging*)) was chosen which allowed a small number of agents with EVA vehicles to follow the same driving profiles as conventional vehicles. To analyse the effect of waiting times, the number of agents was increased step by step until the maximum number of agents (2,949) was reached while the charging infrastructure remained unchanged for each simulated scenario. To quantify the similarity of the driving profiles, the simulated revenues of conventional and electric taxis were compared. Revenue is considered to be a better indicator than mileage since if electric taxis have to make detours to reach the next charging station, their total mileage could be the same than that of conventional taxis while the revenue would decrease due to the lower amount of time electric taxis can search for and transport customers. The results of this experiment or depicted in Figure 5.12.

The dashed line shows the simulated revenue of conventional taxis. The revenue was not constant with respect to the number of taxis since each agent got assigned to a different *shift schedule set* (Chapter 5.4). Due to the high charging power and the low average waiting time per charging event of 1.1 min for 300 taxis, the agents with electric

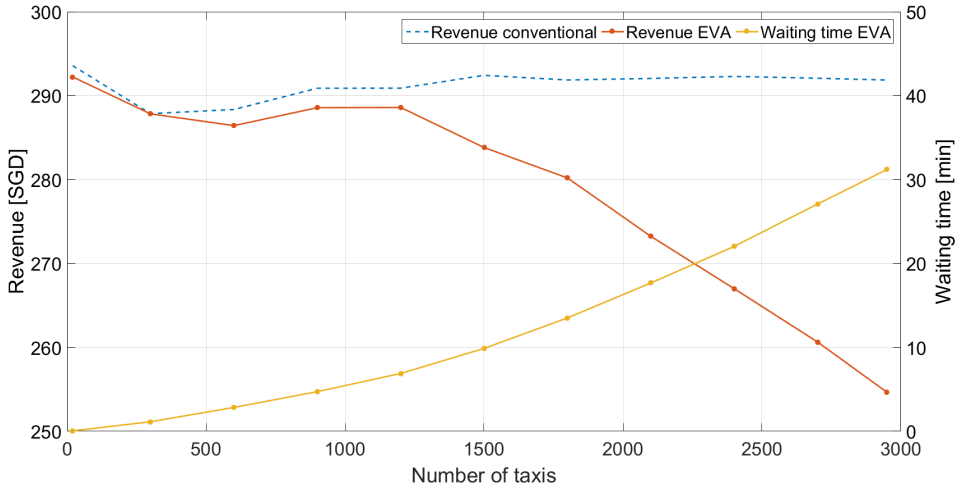

Figure 5.12: Average revenue per day and taxi and waiting time of conventional and EVA vehicles with respect to the number of simulated taxis

vehicles lost almost no time compared to conventional taxi agents which allowed them to reach nearly equal revenues.

In case of 1,200 taxis, the average waiting time increased to 6.9 min which caused a revenue decrease of 2.3 SGD per day compared to conventional taxis. After this point, waiting times increased rapidly which significantly reduced achievable revenue. For 2,949 taxis the average waiting time per charging event reached 31.2 min which resulted in a massive revenue decrease of 36.4 SGD per day.

Although it was not possible to validate the *charging behaviour model*, it can be expected that as long as the effect of electric vehicle specific constraining factors such as charging times, waiting times, and detours are small, the simulation results should be reasonable. The simulation results for optimised charging infrastructures presented in Chapter 8.3 showed as an example that the Nissan Leaf could reach on average 93% of conventional taxis' mileage. Thus, the effect of the electric vehicle constraining factors is moderate and as a consequence it can be expected that the developed simulation model is a good basis to be used to optimise the charging infrastructure for electric taxis.

In order to analyse the effect of different charging infrastructure designs on the agents' driving profiles, two charging infrastructures with 40 charging stations each and a charging power of 40 kW were chosen. For the first charging infrastructure, all charging stations were located at one place which was also the *shift change location* of all agents. The other charging infrastructure had 25 charging stations at the *shift change location* while the remaining 15 charging stations were equally distributed among three other locations. In contrast to the previous example, all agents were assigned to the same *shift schedule set* and as a consequence had their *shift changes* and *breaks* at the same time of the day. The BYD e6 was chosen as simulated vehicle. The simulation results of these scenarios are shown in Figure 5.13.

The upper diagram (a) shows the generated daily revenue with respect to the number of simulated vehicles. Again, the revenue per taxi decreases since more and more agents had to share the same number of charging stations. In contrast to the previous

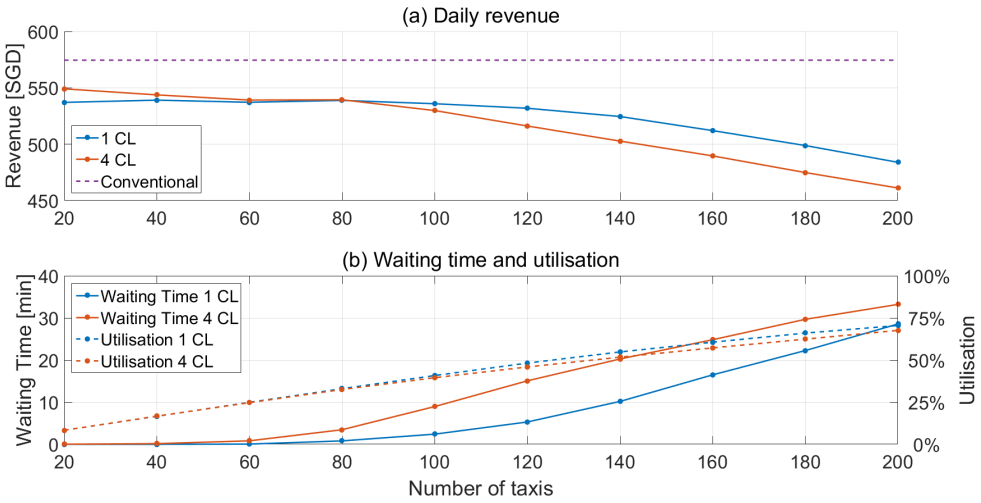

Figure 5.13: Revenue per day and taxi (a), waiting time and charging station utilisation (b) for charging infrastructures with one and four *charging locations* (CL)

example even a small number of only 20 agents could not reach the simulated revenue of conventional taxis which was primarily caused by significantly longer charging times as the charging power was only 40 kW.

The revenue curves show that for 20 taxis the charging infrastructure with four *charging locations* (CL) allows to generate 12.0 SGD per day and taxi more than the infrastructure with only one CL. The gap between these infrastructures became smaller with higher number of taxis and diminished at 80 taxis. Afterwards, agents using the charging infrastructure with only one CL generated more revenue and exceeded the others by 22.8 SGD per taxi and day in case of 200 agents.

The reason why only one CL allows to generate more revenue than four CL at higher numbers of taxis is that the average waiting time per charging event increased slower for one CL than for four CL (diagram (b)). This condition remained even though the charging station utilisation was slightly higher for one CL. This observation can be explained by the probability of getting an available charging station at a specific location, which is the higher the more charging stations (possibilities) are available.

Lower waiting times allow agents to drive longer which results in higher mileage and a higher energy demand. As this additional amount of energy must be recharged at charging stations, their utilisation is higher than in case of four CL. For less than 80 taxis almost no waiting times occurred, hence charging stations utilisations and mileage were the same for both charging infrastructures. Therefore, the difference in revenue can be explained by shorter detours agents had to make when having the choice to choose one out of four locations.

Regarding the optimisation of the number of charging stations, this example shows that reducing detours by distributing the same number of charging stations among more locations is only an efficient measure as long as the charging station utilisation is low. The higher the utilisation, the better it is to have a smaller number of *charging locations*. This means that in order to reduce detours and increase revenue more charging stations in total and therewith higher infrastructure investment costs must be accepted.

These two effects are balanced by the infrastructure optimisation algorithm introduced in Chapter 7. The results presented in Chapter 8.3 showed that from an economical point of view it is best to install a high number of charging stations which utilisation ranged only between 16 and 32%. The high infrastructure costs were compensated by small detour and waiting time costs.

To understand the effect of waiting times on detours to charging stations in more detail, waiting times and driving distances were extracted from the previous example for each of the four *charging locations* individually and are depicted in Figure 5.14.

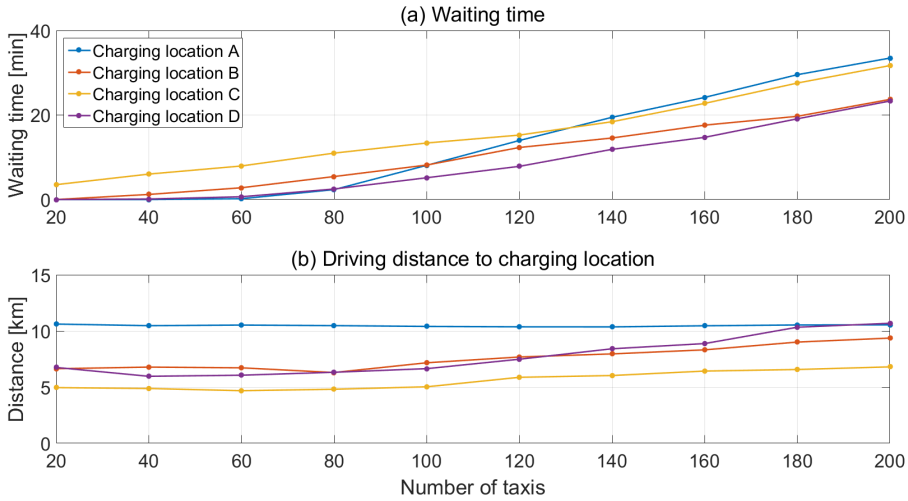

Figure 5.14: Waiting times (a) at and driving distances (b) to each *charging location* with respect to the number of taxis

Charging location A (CL A) was located in the middle of Singapore, was equipped with 25 charging stations, and had to be used as *shift change location* for all agents. These charging stations could also be used to recharge during the *shift change*. The other *charging locations* (B, C, and D) were equipped with five charging stations each, whereby CL B was located near the airport in the east of the island, CL C was in the south close to the Central Business District (CBD) and CL D was placed in the north of Singapore.

Due to its proximity to the CBD where the density of taxis is the highest, CL C was chosen more frequently than CL B and CL D. As a consequence, the waiting times increased at this location more rapidly than at any other location. Since all agents had to choose CL A to recharge during *shift changes*, the majority of all charging events appeared at this location. Nevertheless, due to the high number of charging stations, waiting times appeared only once the number of taxis increased to 80.

The lower diagram (b) shows the average driving distance of agents from the point when they decided to drive to a *charging location* until they arrived. The driving distances to CL A were the longest since agents had to come to this location for *shift change* regardless of their current location. In contrast, CL C had the lowest driving distances since many agent chose this location when they were in the CBD.

The driving distances to the *charging locations* B-D increased with respect to the number of taxis. This was caused by the increase of waiting time at each location.

Agents record their individual waiting times at each *charging location* and choose the location which promises the shortest combination of driving and waiting time. Due to statistical fluctuations of waiting times it is likely that each agent experienced significantly different waiting times and therefore selects not always the closest *charging location*. The more waiting times increase on average the stronger this effect becomes and the further detours to *charging locations* increase.

This example shows that apart from their direct effect, waiting times can also bias the taxi drivers' decisions and further downgrade the efficiency of a taxi fleet. Thus, in cases with very high waiting times it could be better not to include memorised waiting times in the decision to select the next *charging location*.

However, the application of the *agent memory* concept can also be beneficial. Without their memory, agents would always choose the closest *charging location* regardless of the demand and the number of charging stations. As a result, *charging locations* near hotspots like the airport could become overloaded while other locations slightly farther away may be ignored by the agents. In this example the *agent memory* would be very helpful to balance the charging demand among these locations.

Chapter 6

Economic model

This chapter introduces two economic models which are used to parametrise the objective function of the charging infrastructure optimisation in Chapter 7 and to quantify the economic potential of electric taxis including charging infrastructure costs in Chapter 8. Therefore, a Total Cost of Ownership (TCO) approach was chosen which covers the whole costs of a product from acquisition to operation until the product's end-of-life (EoL).

The TCO models of taxis and charging stations are presented in Chapter 6.1 and 6.2. The derivation of cost factors for the optimisation objective function and the calculation of the taxi's profit is explained in Chapter 6.3.

6.1 TCO of taxis

The model presented in (Kochhan, 2017) was used in this thesis to calculate the TCO of taxis in Singapore. Unless declared otherwise, all parameter values were taken from this source as well. The TCO is calculated with respect to three main components:

- Acquisition costs
- Operation costs
- End-of-life value

The following sections explain these components in more detail.

6.1.1 Acquisition costs

The acquisition costs include the vehicle's purchasing price and all registration fees to operate a vehicle as taxi in Singapore. The vehicle's Open Market Value (OMV) is used as basis for the tax calculation. The OMV can be understood as the vehicle's value when it arrives in Singapore. Since no electric vehicles are so far registered in Singapore, there are no official OMVs for the vehicles analysed in this thesis. To estimate the OMV of these vehicles, a regression model was built to estimate the OMV of conventional vehicles with respect to their price in other countries. This regression model was applied to estimate the OMV of the electric vehicles with respect to their price in the respective country. As EVA is not on the market, its OMV was derived by balancing costs of electric vehicle and conventional vehicle components on basis of the price of a comparable

conventional vehicle (Kochhan et al., 2014). Table 6.1 lists the OMVs of all vehicles analysed in this thesis:

Table 6.1: OMV of vehicle types in Singapore (Kochhan et al., 2014; Kochhan, 2017)

Vehicle Type	OMV [SGD]	Battery Capacity [kWh]
BYD e6	47,000	61.4
EVA	50,982	50
Kia Soul EV	33,087	27
Nissan Leaf SV	35,253	30
Tesla Model S 70D	93,809	70
Toyota Prius	35,683	1.3[a]

[a] battery is only used to buffer electrical energy during driving and cannot be charged externally

Comparing the OMV with the vehicles' battery capacity shows that these values are correlated with each other - the higher the battery capacity the more expensive the vehicle. This underlines that the battery is one of the main cost factors of an electric vehicle. However, the high price difference of the Tesla Model S to all other vehicles is not only caused by its high battery capacity but is also attributed to the fact that this vehicle is more luxurious than the others.

With respect to the OMV, goods and service tax (GST) of 7% (Inland Revenue Authority of Singapore, 2017) and excise duty (ED) of 20% (Singapore Customs, 2017) have to be paid. Furthermore, an Additional Registration Fee (ARF) must be paid which accounts to 100% of the OMV for the first 20,000 SGD of the OMV, 140% for the following 30,000 SGD and 180% for the remaining OMV exceeding 50,000 SGD (LTA, 2017c).

In order to promote low-emission vehicles, a Carbon Emission-Based Vehicle Scheme (CEVS) grants rebates to vehicles with low emissions and imposes surcharges on high emission vehicles. The highest rebate for taxis is 45,000 SGD if the vehicle's CO_2 emissions are not higher than 95 g/km (LTA, 2015a).

To register a private vehicle in Singapore, a ten years valid Certificate of Entitlement (COE) must be obtained via a bidding system. Between the years 2013 to 2015 the average price of a COE ranged between 62,195 and 77,703 SGD. Taxis are only allowed to be operated for eight years, thus only 80% of the price of a private vehicle's COE needs to be paid in this case.

6.1.2 Operation costs

In Singapore, vehicles are not allowed to be operated longer than eight years as taxis. The total operation costs for this period consist of following factors:

- Operating taxes
- Energy costs (fuel or electricity)
- Service and maintenance costs

- Insurance costs
- Parking costs
- Battery replacement costs (electric and hybrid vehicles only)

In contrast to (Kochhan, 2017), charging infrastructure costs are not included in this calculation. This cost factor is estimated separately in Chapter 6.2.

The operating taxes contain taxes for using streets in the Central Business District (CBD) which are automatically charged via an Electronic Road Pricing (ERP) system whenever a vehicle enters this area. Furthermore, a general road tax must be paid which accounts for taxis to 1,020 SGD per year (LTA, 2017c).

Electric taxis' energy costs are calculated with respect to the simulated energy demand (Chapter 4.1) and a charging station efficiency of 92.6% (Genovese et al., 2015). The applied electricity tariff is 0.24 SGD/kWh which is assumed to increase by an annual rate of 2%.

Service and maintenance costs include all costs (except replacing the battery) which are required to keep the vehicle in perfect working condition. The costs for electric vehicles are set to 0.044 SGD/km.

The vehicle insurance costs were set to 12,000 SGD per year for each vehicle type.

Typically, it is not allowed to park along roads in Singapore. Therefore, taxi drivers have to use car parks and pay for the usage. According to a taxi driver survey, the average annual parking costs are 789 SGD.

Due to the high mileage of taxis it cannot be expected that the battery will last throughout the whole vehicle operation period. The battery is one of the most expensive component of the vehicle which makes this cost factor an important part of the operation costs. It is expected that a battery must be exchanged after 2,000 cycles[1]. With respect to the vehicle's battery capacity and energy consumption it is calculated after which mileage a replacement is required. The costs of the new battery are calculated with respect to the projected battery price at the time of replacement and the vehicle's battery capacity.

6.1.3 End-of-life value

The EoL value is the vehicle's value at the end of its operation period. Usually, this value is positive so that the TCO is reduced by the EoL value. This value includes tax returns as well as the residual value of the vehicle and its battery.

Tax returns are applied for the ARF and CEVS. When the vehicle is deregistered just before the end of the eighth year of usage 60% of the ARF are returned (LTA, 2017c). As the CEVS grants rebates to low emission vehicles, a part of these rebates would have to be returned after eight years as well.

The residual value of the battery is estimated with respect to the ratio of executed discharge cycles and the maximum number of charging cycles (2,000). While the residual value of the vehicle is assumed to be 1,000 SGD for each vehicle type.

[1] one cycle is defined by fully discharging and charging the battery

6.1.4 Cost comparison of vehicle types

Figure 6.1 compares the TCO values of all electric vehicles with that of the Toyota Prius which is operated as taxi in Singapore. For this example, the average daily mileage was set to the average mileage of the whole taxi fleet, which is 335 km. The TCO was cumulated over an operation period from 2017 until 2025[2].

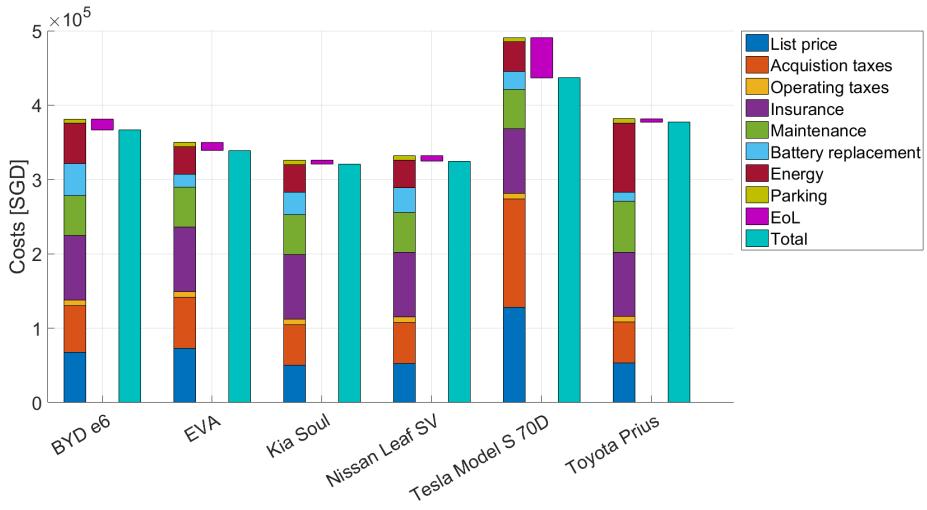

Figure 6.1: TCO by cost category for all vehicle types

The respective left bar of each vehicle type represents the sum of all acquisition and operation costs, the middle bar the cost reduction by the EoL, and the right bar the resulting TCO of each vehicle. The list price contains the OMV, GST, and ED plus a retailer margin of 7,500 SGD for each vehicle, while the acquisition taxes include the COE, ARF, and CEVS.

The results show that the Kia Soul EV was the vehicle with the lowest TCO of 320,674 SGD, while the Tesla Model S was most expensive with 436,560 SGD. The Toyota Prius which is used as reference vehicle had total costs of 376,976 SGD and was therewith more expensive than all other electric vehicles except the Tesla Model S. The acquisition of the Tesla Model S was significantly more expensive than for all other vehicles due to its much higher OMV and the therewith coupled taxes. Although the returned amount of these taxes included in the EoL value is considerably higher, the TCO remained the highest at the end.

The main advantage of electric vehicles over conventional vehicles in terms of costs is their higher energy efficiency which results in significantly lower energy costs, e.g. the energy costs of the Toyota Prius are 150% higher than that of the Kia Soul. Taking into account that the Prius is a fuel efficient vehicle with an average consumption of 5.3 l/100km it is expectable that non-hybrid vehicles have even higher energy costs.

How the TCO of these vehicles evolved with respect to the average daily mileage is shown by Figure 6.2.

Due to the mileage dependent energy and maintenance costs, all TCO curves constantly increased with higher mileage. There were some mileages where the slope of

[2]the results differ with respect to the year of usage as the TCO model applies different prices with respect to the year

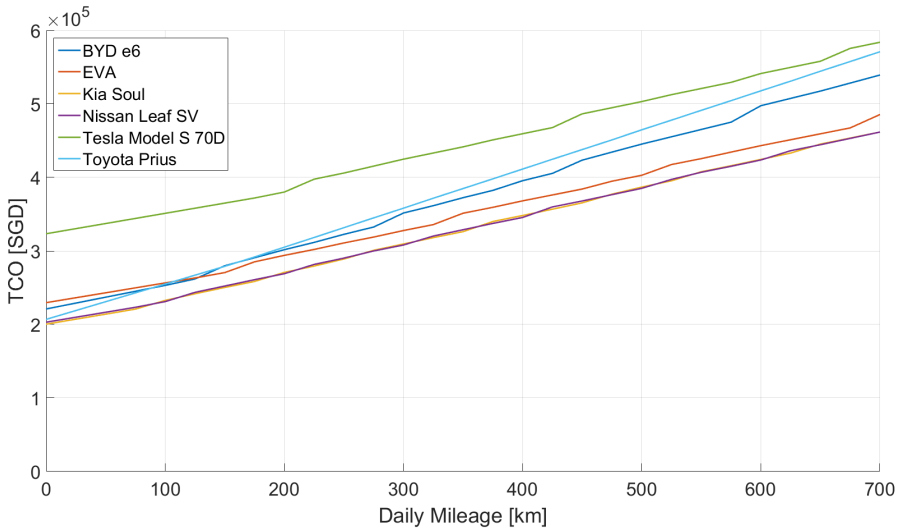

Figure 6.2: TCO with respect to daily mileage

the costs of electric vehicles increased. Theses were the critical points when one more replacement battery was required throughout the whole period of operation.

The costs of the Kia Soul and Nissan Leaf were the lowest for any daily mileage. Since both vehicles had almost identical OMVs and energy consumptions, their costs curves were hardly distinguishable. Due to their lower energy costs, the BYD e6 and EVA undercut the costs of the Toyota Prius at a daily mileage of 90 respectively 110 km. These values are far below the average mileage of taxis which means that almost each BYD or EVA taxi could be more cost efficiently operated than a conventional vehicle.

This diagram also underlines the importance of the vehicle's energy consumption: EVA had a higher TCO value than the BYD e6 at very low mileage. However, due to its high energy efficiency, it undercut the costs of the BYD e6 at 130 km per day and was by 54,300 SGD cheaper at an average mileage of 600 km per day.

Although most electric taxis had lower TCO values than conventional taxis, it must be kept in mind that charging infrastructure costs were not included in this calculation. Furthermore, due to their limitation in range and charging time, electric taxis will generate less revenue than conventional taxis. A comprehensive analysis taking all theses aspects into account follows in Chapter 8.4.

6.2 TCO of charging stations

The TCO of charging stations consist of three components:

- Installation costs
- Equipment costs
- Operational costs

The installation costs include all costs associated with setting up a charging station and connecting it to the electricity grid. These costs strongly depend on the required power

and the location where the charging station shall be set up, e.g. an important factor is how far the charging station will be away from the connecting point to the grid and how much effort it takes to lay the cables. Detailed information of the electricity grid would be required to accurately estimate these costs. For simplicity reasons this information was not used in this thesis, thus it must be expected that the generalised costs may significantly deviate from the actual costs at specific locations.

Beside the charging power, equipment costs also depend on the station's current output type (AC or DC) and whether the charging station shall be publicly accessible. DC charging stations are significantly more expensive than AC charging stations due to the integrated transformer which converts AC current from the grid to DC current to charge the battery directly. Public charging stations need to be protected against vandalism and have to have an integrated billing system which makes them more expensive than private charging stations. In this thesis, all charging stations which can be used during the *shift* are considered as public charging stations, while charging stations used during the *shift change* (*home charging*) are private charging stations.

The operational costs include costs for renting the space where the charging station is installed, maintenance costs to keep it in perfect working condition, as well as costs related to the billing system (i.a. communication, contract management, and IT) (Nationale Platform Elektromobilitaet, 2015).

Table 6.2 summarises costs extracted from a literature research.

Table 6.2: Costs of charging stations (Thoma, 2014; Schroeder and Traber, 2012; ERI@N, 2016; Nationale Platform Elektromobilitaet, 2015)

Power [kW] (type)	Equipment [SGD]	Installation [SGD]	Operation [SGD/a]
6.6 (AC)	1,319	16,200	1,128
43 (AC)	13,414	27,300	-
50 (DC)	39,715	30,000	3,383
100 (DC)	58,769	-	-
250 (DC)	90,226	-	-

It was not possible to find a set of cost values for all charging stations which are considered in this thesis. Therefore, regression models were created to estimate these costs.

The equipment costs c_{eq} of DC charging stations and installations costs c_{ins} of all charging stations were estimated by a constant factor and a factor proportional to the output power P:

$$c_{eq}(P) = a_{eq} + b_{eq} \cdot P \tag{6.1}$$

$$c_{ins}(P) = a_{ins} + b_{ins} \cdot P \tag{6.2}$$

The fitted parameter values are listed in Table 6.3.

Regarding the operation costs per year c_{op} it was assumed that these are proportional to the equipment costs:

$$c_{op}(e_{eq}) = a_{op} + b_{op} \cdot c_{eq} \tag{6.3}$$

Table 6.3: Fitted parameter for charging station equipment and installation costs

Cost type	a [SGD]	b [SGD/kW]
Equipment (eq)	30,548	243
Installation (ins)	14,085	314

Here, the fitted parameter values were: $a_{op} = 1,015\,\text{SGD/a}$ and $b_{op} = 0.0787\,1/\text{a}$.

The total operating costs $c_{op\,total}$ over the whole period of operation Δt_{op} of 15 years (Engholm et al., 2013) with an interest rate *i* of 3% (Kochhan, 2017) are calculated as follows:

$$c_{op\,total} = \sum_{y=1}^{\Delta t_{op}} c_{op} \left(\frac{1}{1+i}\right)^{y-1} \tag{6.4}$$

An overview of all cost components and the TCO for a use duration of 15 years for all charging stations used in this thesis is given by Table 6.4.

Table 6.4: TCO of charging stations in SGD

Charging Power [kW] (type)	Equipment	Installation	Operation	TCO
6.6 (AC)	1,319	15,967	14,480	31,766
40 (AC)	13,424	26,633	26,802	66,848
40 (DC)	40,355	26,633	54,145	121,033
50 (DC)	42,682	29,770	56,617	129,068
60 (DC)	45,108	32,906	59,090	137,104
100 (DC)	54,815	45,454	68,978	169,247
120 (DC)	59,668	51,728	73,923	185,319
160 (DC)	69,375	64,275	83,811	217,462

The table shows that the higher the charging station's power output is the higher the TCO becomes. However, comparing 40 and 160 kW DC charging stations shows that although 160 kW charging stations could recharge four times more vehicles at the same time, their TCO is only 80% higher. Thus, it can be expected that these charging stations are more cost efficient.

However, an important aspect which must be considered is how these charging stations are utilised. First, it cannot be expected that directly after one vehicle leaves the charging station another vehicle starts a new charging process. Moreover, it must be considered that the higher the charging power is the shorter the time to fully charge the battery will be. Thus, the chance that a vehicle reaches the end of the charging process and unnecessarily blocks the charging station until the driver ends the *break* and continues driving increases with the charging power. These two aspects downgrade the economic potential of expensive charging stations with high power. The driving profile simulation model (Chapter 5) takes these aspects into account so that a realistic comparison of charging infrastructures with different charging power can be made in Chapter 8.4.

The comparison of 40 kW charging stations with AC or DC current output shows that the equipment costs of AC charging stations are due to their simpler design by 26,931 SGD cheaper than DC charging stations with the same power output. Moreover, as operational costs were estimated with respect to the equipment costs, AC charging stations have a significant cost advantage in this category as well. Overall, the TCO of DC charging stations was 81% higher than that of AC charging stations.

Although this comparison clearly favours AC charging stations, it must be kept in mind that in order to utilise these charging stations, the vehicle internal onboard charger must be capable of transforming the supplied current to DC. To save costs, space, and weight, most electric vehicles are only equipped with onboard chargers with a maximum power of 6 kW. In contrast, the BYD e6 is capable of using AC charging power of up to 40 kW. Therefore, AC charging stations are considered for this vehicle while the analysed charging infrastructures of all other vehicles consist of more powerful and expensive DC charging station.

An overall economic assessment where charging infrastructure costs are balanced with the costs caused by the loss of time due to charging follows in Chapter 8.4.

6.3 Cost factors and profit

The charging infrastructure optimisation presented in Chapter 7 optimises the placement and number of charging stations by minimising waiting time, detour, and charging infrastructure costs. Following cost factors are derived in order to quantify the effect of each of these cost categories on the overall costs:

***Waiting time cost factor* (C_w):** Due to waiting for an available charging station the driver looses time to search for and serve the next customer. This factor is used to quantify the lost amount of revenue with respect to the drivers' waiting time.

***Detour cost factor* (C_d):** Costs caused by detours the driver has to make in order to reach a *charging location*. This factor quantifies the loss of revenue with respect to the driving distance to *charging locations*.

***Charging station* cost *factor* (C_c):** TCO of one charging station per day.

The *waiting time* and *detour cost factors* are calculated with respect to the vehicle's TCO and the taxi's average daily mileage $\bar{m}$, revenue $\bar{r}$, energy consumption $\bar{\eta}$, and driving duration $\Delta\bar{t}_{drive}$. These values are obtained from a simulation run with the respective vehicle, while the TCO model (Chapter 6.1) is applied to calculate the vehicle's mileage dependent costs (maintenance costs, energy costs, and battery replacement costs) $C_v\left(\bar{m}, \bar{\eta}\right)$ in SGD per km with respect to the mileage and energy consumption. Therefore, the *waiting time cost factor* is calculated by:

$$C_w = \frac{\bar{r}}{\Delta\bar{t}_{drive}} - C_v\left(\bar{m}, \bar{\eta}\right) \frac{\bar{m}}{\Delta\bar{t}_{drive}} \tag{6.5}$$

The first term of equation 6.5 takes the loss of revenue due to waiting into account while the second term deducts driving costs which do not apply when the vehicle is stationary. In contrast, since the taxi is also moving when driving detours to *charging locations*, only the loss of revenue is considered for the *detour cost factor*:

$$C_d = \frac{\bar{r}}{\bar{m}} \tag{6.6}$$

To set the cost factors for each vehicle type, driving profile simulations were run with the maximum number of agents and an unlimited number of charging stations at each *candidate charging location*. The derived charging demand of these scenarios were used as input for the first charging infrastructure optimisation step (Chapter 7.6.1). Table 6.5 lists the cost factors which were calculated based on the simulation results.

Table 6.5: Waiting time and detour costs factors of all vehicle types

Vehicle type	C_w [SGD/min]	C_d [SGD/km]
BYD e6	0.331	0.870
EVA	0.361	0.873
Kia Soul	0.344	0.868
Nissan Leaf SV	0.349	0.869
Tesla Model S 70D	0.356	0.874

Since all scenarios were simulated with the same charging infrastructure, detours to *charging locations* were similar for each vehicle type. Moreover, since the same fares were applied for each vehicle type it is expectable that the ratio of the average revenue per day to the daily mileage or driving duration is similar for each vehicle type. As a result, the variance of the *detour cost factor* is very low among all vehicles.

In contrast, the variance regarding the *waiting time cost factor* is significantly higher as specific vehicle costs are included in this factor. EVA is the vehicle with the best energy efficiency and therewith the lowest mileage dependent costs which is reflected by the highest *waiting time cost factor*. In contrast, the BYD e6 has the highest energy consumption and consequently the lowest waiting time costs.

The *charging station cost factors* C_c are simply calculated by dividing the TCO of each charging station by the number of days of operation.

In Chapter 8.4, the economic profit is assessed per taxi and day. Thereby, vehicle and charging infrastructure costs are balanced with the taxi's revenue. Following formula is used to calculate the profit per taxi with respect to the simulated revenue, mileage and energy consumption:

$$p\left(\bar{r}, \bar{m}, \bar{\eta}\right) = \bar{r} - \frac{TCO_v\left(\bar{m}, \bar{\eta}\right)}{\Delta t_{op}} - \frac{n_s}{n_{ET}} C_c \tag{6.7}$$

Thereby, the vehicle's TCO is calculated by calling the function $TCO_v\left(\bar{m}, \bar{\eta}\right)$ and Δt_{op} is the operation duration of the vehicle in days. It is assumed that the charging infrastructure costs are equally distributed among all taxis, hence C_c is multiplied by the total number of charging stations n_s and divided by the total number of taxis n_{ET}. If *home charging* is considered, the TCO of one 6.6 kW charging station which is 5.80 SGD per day is additionally deducted from the taxi's profit.

Chapter 7

Infrastructure Optimisation

This chapter describes the developed method to optimise the placement and number of charging stations with respect to the charging power, number of taxis, and vehicle type. First, the charging infrastructure concept to be optimised is introduced in Chapter 7.1. Criteria to assess the quality of charging infrastructure optimisation methods are derived in Chapter 7.2. Following, Chapter 7.3 gives a classified literature review and discusses the matching of each approach with the optimisation criteria. In Chapter 7.4 the optimisation approach of this work is introduced. Since the estimation of waiting times with respect to the *charging demand* and the number of charging stations is a very important detail of the introduced approach, Chapter 7.5 covers this aspect. Finally, the mathematical formulation of the charging infrastructure optimisation is presented in Chapter 7.6.

7.1 Infrastructure concept

Private vehicles in Singapore have an average annual mileage of 17,500 km (LTA, 2015b). Assuming that they are used six days a week, the average daily mileage is 41 km, that translates to a daily driving time of 68 minutes at an average speed of 36.1 km/h. Hence, one charging event per vehicle with low charging power is sufficient to cover the users' mobility patterns. Therefore, low power charging stations could be placed at the workplace or at home to ensure sufficient energy supply.

Although the average mileage of private vehicles is much lower than that of taxis, it must be kept in mind that due to their much higher number of 536,882 compared to 28,736 taxis, their contribution to the total mileage driven by vehicles is 40.8%, whereas taxis contribute only 16.2% (LTA, 2015b). Therefore, charging concepts which require higher investment costs like battery swapping or *dynamic inductive charging* could be considered for private cars whereas taxis alone might not utilise these infrastructure concepts sufficiently to compensate the high investment costs.

As taxis have much higher mileage and much shorter standstill times, several short charging events per day are required to supply the vehicles' energy demand. In order to make charging as convenient as possible it would be ideal to enable drivers to recharge their car during *breaks*. Therefore, charging stations with high power shall be placed at the taxi drivers' most common *standstill locations* (the selection of *candidate charging locations* was described in Chapter 3.2). Since drivers use many different locations, the most suitable locations have to be identified for the placement of charging stations.

7.2 Optimisation criteria

In this section eleven criteria are derived which should be taken into account in order to optimise a charging infrastructure with respect to the specific needs of electric taxis:

real taxi driving profiles: It is most important to extract statistics from real world taxi driving profiles in order to derive charging infrastructure design requirements.

temporal-spatial *charging demand*: As the density of taxis in a city varies with time and space the *charging demand* does so as well. It must be taken into account whether enough charging stations are available to supply not only the average but also the peak *charging demand*.

SOE dependent *charging demand*: Apart from the temporal-spatial variance of the *charging demand*, the vehicles' state of energy (SOE) has another important effect on the *charging demand*, e.g. if taxis had the possibility to recharge during *shift changes*, their *charging demand* at the beginning of the *shift* would be significantly lower.

re-routing: Due to the limited number of *charging locations* and high mileage, electric taxis will not be able to follow the same trajectories as conventional taxis. Therefore, it must be taken into account that electric taxis have to alter their *routes* in order recharge the battery. Additional mileage and lost of time shall be considered in order to find the ideal *charging location* choice.

street network: The accessibility of *charging locations* is an important aspect in order to reduce detours. Therefore, the calculation of driving distances shall be based on a real street network and not be estimated with the Euclidian or Manhattan distance.

individual driving patterns: Driving patterns of different taxis vary a lot in terms of working hours, mileage, and choice of *standstill locations*. Hence, it is necessary to consider a variety of individual driving patterns instead of one single pattern which all taxis are following.

discrete *charging locations*: It is very helpful to get a coordinate for each *charging location* instead of identifying the number of charging stations per area. Considering areas does not allow to determine among how many *charging locations* the optimised number of charging stations shall be assigned to.

economic assessment: To justify the installation of additional charging stations in order to reduce waiting times or detours, it is essential to balance the charging infrastructure costs with the waiting time and detour costs of taxis. Therefore, the objective function shall minimise the total costs of these three aspects.

number of charging stations: For the overall economic assessment it is important to know how many charging stations are ideal for a given number of electric taxis. Hence, the total number of charging stations shall be a result and not a constraint of the optimisation.

waiting time: In order to economically optimise the number of charging stations, the opportunity costs of waiting times shall be balanced with the charging station costs. Hence, the effect of charging station utilisation on waiting times should be respected in the optimisation.

assessment solution quality: Another important aspect is whether it is possible to assess the closeness of the found solution to the global optimum. There are standard solvers for linear problems which ensure that the global optimum is found. In contrast, heuristics like greedy or genetic algorithm may only find a local optimum which could be far away from the global optimum. Therefore, linear problems or analytical models are favourable in this context.

7.3 Literature review

Many different approaches have been applied to optimise the placement of charging stations for electric taxis. All approaches are introduced and classified in this section. Following, an overview on which optimisation criteria is met by which approach is given. Appendix G complements this section by giving more details on the reviewed approaches.

7.3.1 Flow-capturing model

The ideal placement of charging or refuelling facilities from the consumers' perspective would be if these facilities were placed along the users' driving paths so that they would not need to alter their routes at all. The flow-capturing model is an approach to optimise the placement of facilities in order to maximise the served refuelling or *charging demand* along given travel paths (Hodgson, 1990). Based on this model, e.g. (Kuby and Lim, 2005; Hwang et al., 2017; de Vries and Duijzer, 2017) optimised the locations of refuelling stations for alternative-fuel vehicles. Furthermore, this model was also applied to locate fast charging stations for private electric vehicles in (Chung and Kwon, 2015; Cruz-Zambrano et al., 2013; Jiang et al., 2012; Wu and Sioshansi, 2017). When applying this approach for electric vehicles it must be kept in mind that their recharging times are significantly longer than refuelling times of conventional or hydrogen vehicles. Hence, even if consumers do not have to make any detours to reach a charging station, it could be very inconvenient for them to interrupt their planned trip for a long recharging stop. An innovative approach to overcome this problem could be the use of *dynamic inductive charging* which allows to recharge the battery while driving. A method to optimise the placement of this charging infrastructure with the flow-capturing model is presented in (Riemann et al., 2015). However, due to its high investment costs, this technology would require a higher number of users than only taxis.

The only application of the flow-capturing model to optimise a charging infrastructure for electric taxis is presented in (Shahraki et al., 2015). The authors extracted trajectories of 11,880 taxis from GPS data and formulated a mixed-integer linear problem to assigned charging stations near *standstill locations* by maximising the vehicles' mileage. Hereby, it was assumed that a taxi is charged if its *standstill location* was no farther than one mile away from a charging station. The maximum number of *charging locations* was defined as a constraint. The selected locations had no capacity limitation, meaning that an unlimited number of vehicles could recharge at each location at the same time.

7.3.2 P-median problem

The objective of the p-median problem is to locate a given number of facilities in order to minimise the total travel distances or travel times from all demand points to the nearest facility (ReVelle and Swain, 1970).

In (Li et al., 2015) a bi-level optimisation heuristic was presented which first selected regions where charging stations shall be placed and optimised the number of charging stations for each selected region in the second step. The input of the optimisation were origins of real electric taxi trips to charging stations. A p-median problem was formulated to minimise the total travel distance from all origins to charging stations. After selecting a set of *charging locations*, the number of charging stations per location was optimised. Hereby, the total number of charging stations was defined and the charging station utilisation at each location was minimised with a greedy algorithm.

7.3.3 Maximum covering problem

The maximum covering problem optimises the location of a given number of facilities in order to maximise the demand which is covered by at least one facility. The demand was defined by points with weights and is considered as covered if it is not farther than a maximum distance away from a facility (Church and ReVelle, 1974).

In (Gacias and Meunier, 2015) origin/destination pairs of the taxi customer travel demand was synthesised. There were three options analysed to locate the *charging demand*: either at the trip's origin, the trip's destination, or to both. The weight of each trip's *charging demand* was defined by the ratio of the trip's energy consumption over the charging power. The objective was to maximise the *charging demand* which was covered by a given number of facilities within a defined distance β_{close}. A constraint required that the total *charging demand* had to be covered within the distance β_{far}.

The *charging demand* points in (Asamer et al., 2016) were extracted from origins and destinations of recorded taxi trips. Hereby, the demand of each trip was equally weighted. Hexagons with a diameter of 1 km were defined to cover the whole area of recorded data. Each hexagon was assigned with the total number of covered origin and destination points. The objective was to select a defined number of hexagons which covered the highest *charging demand*. Thereby, for each selected hexagon the demand of directly neighbouring hexagons was considered as covered as well.

The potential state of charge (SOC) of an electric taxi fleet was estimated based on recorded trips of conventional taxis in (Ko et al., 2017). Every time when the SOC dropped below 10% a demand point was created. The optimisation objective was to place a defined number of charging stations to cover the maximum number of demand points. Thereby, the maximum distance between demand points and charging stations to consider demand as covered was varied from 0.5 to 5 km. A greedy algorithm was applied to solve this problem.

7.3.4 Analytical model

An analytical model to optimise the density of charging stations was presented in (Ahn and Yeo, 2015). Therefore, the whole data recording area was divided into cells with a length between 0.5 and 4 km. The *charging demand* of each cell was assumed to be proportional to the number of taxis which passed through the cell within a given time.

The length of detours drivers would have to make in order to reach a charging station was estimated with respect to the cell's charging station density (number of charging stations over cell area). Waiting times until a charging station could be used were estimated with respect to the ratio of the total recharging time of all vehicles λ over the service rate of all charging stations μ. Thereby, it was assumed that waiting times were zero if $\lambda \leq \mu$. A formula, including waiting time costs, detour costs, charging station and *charging location* costs with respect to the density of charging stations was derived. The optimal charging station density per cell was found by computing the root of the formula's derivative.

7.3.5 Simulation-based heuristic

An approach is considered as simulation-based heuristic if a simulation model is used to evaluate the objective function and a metaheuristic (e.g. evolutional algorithm) is iteratively applied to find a local optimum.

This approach was applied in (Sellmair and Hamacher, 2014) to optimise the placement of inductive charging stations at taxi stands. This charging concept allowed drivers to combine their waiting time for the next customer with recharging the battery. Therefore, an event-based model was developed which simulates driving profiles of electric taxis by sampling trips and waiting times with respect to the taxi stand where the simulated taxi waits for the next customer. A greedy algorithm was applied to identify how many charging stations per taxi stand were necessary in order to maximise the economic profit per taxi. Therefore, vehicle costs and charging infrastructure costs were subtracted from the estimated taxi's revenue.

Trajectories of conventional taxis were used in (Han et al., 2016) to simulate the SOC of electric taxis. Whenever the SOC dropped below 15%, the simulated taxi left its historic trajectory, drove to the nearest charging station, charged the battery, and rejoined the historic trajectory at the same place where it left. An evolutionary algorithm was applied to minimise charging infrastructure, waiting time, and detour costs by placing a maximum number of charging stations. Constraints were defined to limit the maximum driving distance to charging stations, the maximum waiting time, and the number of charging stations per location. As in (Ahn and Yeo, 2015), waiting times were estimated to be zero if $\lambda \leq \mu$.

In (Tu et al., 2016) an event-based simulation model was introduced which assigned recorded *engaged trips* to simulated electric taxis with respect to time and location. Whenever the taxis' SOC was not sufficient to execute the next trip, they had to select the nearest *charging location* to recharge the battery. If all charging stations at this location were occupied the taxis had to wait until the next station was available. A genetic algorithm was applied to optimise the placement of a maximum number of charging stations in order to maximise the taxis' mileage and minimise their waiting times.

7.3.6 Multiple server location problem

The aim of the multiple server location problem is to optimise the placement of a given number of servers on a network in order to minimise travel times to the servers and waiting times until a server is available (Berman and Drezner, 2007).

A bi-level simulation-optimisation model to optimise the placement of charging stations was presented in (Jung et al., 2014). Therefore, a model was developed to simulate the *charging demand* which was defined as the set of all origins of trips when the simulated taxis went to charging stations. The *charging demand* was given as input to the multiple server location problem to minimise travel times and waiting times. The charging duration of each event was randomly sampled from a normal distribution and the waiting time for an available charging station was estimated by the following formula:

$$W_k(\lambda, k) = \frac{\lambda}{(k\mu - \lambda)^2 \left(a_k + \frac{\lambda}{k\mu - \lambda}\right)} + \frac{1}{\mu} \tag{7.1}$$

with

$$a_1 = 1;\ a_i = 1 + \frac{\mu}{\lambda}(i-1)\, a_{i-1} \tag{7.2}$$

where k is the number of charging stations, μ is the service rate of each charging station, and λ is the arrival rate. The optimisation constraints were that each *charging demand* point must be allocated to the nearest charging station and that the total number of charging stations was limited. A greedy algorithm was applied to find the ideal charging station placement. This algorithm was only applicable when the total number of charging stations is much higher than the number of candidate locations where charging stations could be placed.

Another approach to apply the multiple server location problem was presented in (Yang et al., 2017). The authors analysed driving profiles of taxis and divided the recording area into cells. Each cell was assigned with the number of standstill events. The number of charging stations per cell was optimised by minimising the charging infrastructure costs while limiting the rate of rejected charging events to 5 - 25%. A charging event was considered as rejected if all charging stations and parking slots at a location were occupied.

7.3.7 Matching of optimisation criteria

Table 7.1 shows which of the discussed approaches meets the criteria described in Chapter 7.2.

All approaches, except Gacias and Meunier (2015) based their analysis on real taxi data sets. The only approach that took individual driving patterns into account is (Shahraki et al., 2015) where it was assumed that electric taxis would strictly follow the same trajectories as conventional taxis. Due to that restriction, re-routing or delays caused by occupied charging stations were not taken into consideration.

The table also shows that simulation-based heuristics are the approaches which satisfy the most of the defined criteria. By using agent-based simulations it would be possible to take even more criteria into account like individual driving patterns. However, the main drawback of these approaches is that only heuristics can be applied to minimise the objective function which makes an assessment of the quality of the found solution very difficult.

In contrast, the analytic model introduced in (Ahn and Yeo, 2015) has the advantage that the global optimum can be found by calculating the root of the objective function's derivative. However, for this approach it is very difficult to include more complex features

Table 7.1: Matching of optimisation criteria of each approach

Citation	Classification	real taxi driving profiles	temporal-spatial *charging demand*	SOE dependent *charging demand*	re-routing	street network	individual driving patterns	discrete *charging locations*	economic assessment	number of charging stations	waiting time	assessment solution quality
Shahraki et al., 2015	flow capturing problem	X		X			X					X
Li et al., 2015	p-median problem	X		X	X			X				
Gacias and Meunier (2015)	maximum covering problem							X				X
Asamer et al., 2016	maximum covering problem	X										X
Ko et al., 2017	maximum covering problem	X		X		X		X				
Ahn and Yeo, 2015	analytical model	X			X				X	X	X	X
Tu et al., 2016	simulation-based heuristic	X	X	X	X	X		X			X	
Han et al., 2016	simulation-based heuristic	X	X	X	X			X	X		X	
Sellmair and Hamacher, 2014	simulation-based heuristic	X	X	X	X			X	X	X		
Yang et al., 2017	multiple server location problem	X								X		X
Jung et al., 2014	multiple server location problem	X		X	X	X		X			X	

like temporal-spatial *charging demand*, individual driving patterns, or discrete *charging locations*.

The only other class of approaches which includes waiting times and therefore allows to respect economic considerations is the multiple server location problem. In this context, (Jung et al., 2014) presented a method to include the majority of the optimisation criteria and (Yang et al., 2017) formulated a mixed integer linear program to optimise the charging infrastructure.

7.4 Approach

The aim of this work is to introduce an approach which satisfies all optimisation criteria of Chapter 7.2. Therefore, as well as in (Jung et al., 2014), a bi-level simulation-optimisation multiple server location problem is formulated. The simulation part is executed by the simulation model introduced in Chapter 5.

In contrast to (Jung et al., 2014), the objective function includes detour costs, waiting time costs, and charging infrastructure costs. This formulation allows to optimise the number of charging stations instead of setting this number as constraint. In order to take temporal effects into account, the *charging demand* is discretisised into time intervals. Waiting times are estimated with respect to the *charging demand* per location and the number of charging stations. To formulate a linear program, a different estimation of waiting times than the recursive equation 7.1 is derived in the next section.

Figure 7.1 depicts the optimisation procedure. The input of the optimisation is the number and vehicle type of the electric taxis as well as the charging station's power (all charging stations must have the same power).

The first step of the optimisation is to simulate the driving profiles of electric taxis with an unlimited number of charging stations at each *candidate charging location* (Chapter 3.2.3). This scenario allows to analyse when and where taxis would recharge in the absence of any disturbing influences like waiting times or long detours to reach a charging station. This is important as the agents have individual memories (Chapter 5.6) that record waiting times at each *charging location* and causes them to adjust their charging strategy accordingly. The *charging demand* which is defined by the origin of trips (represented by *street network nodes*) to charging stations and the duration how long a charging station has been used is extracted from the simulation results.

In the next step, a mixed integer linear program is used to select all locations where charging stations shall be placed. Therefore, the allocation of the *charging demand* to *candidate charging locations* and the number of charging stations per location are optimised by minimising the costs of detours and the charging infrastructure. Waiting time costs are excluded from the objective function as a constraint requires zero waiting times. All *candidate charging locations* without any charging stations are dismissed for the rest of the procedure.

Afterwards, a second simulation is executed with unlimited number of charging stations at each of the selected *charging locations*. In contrast to the first run, the *charging demand* is directly extracted for each *charging location*. Hence, the agents' *charging location* choice is considered as fixed and no re-routing is taken into account in this step. The reason for simulating the *charging demand* again instead of using the optimised *charging demand* allocation is that agents have individual preferences regarding

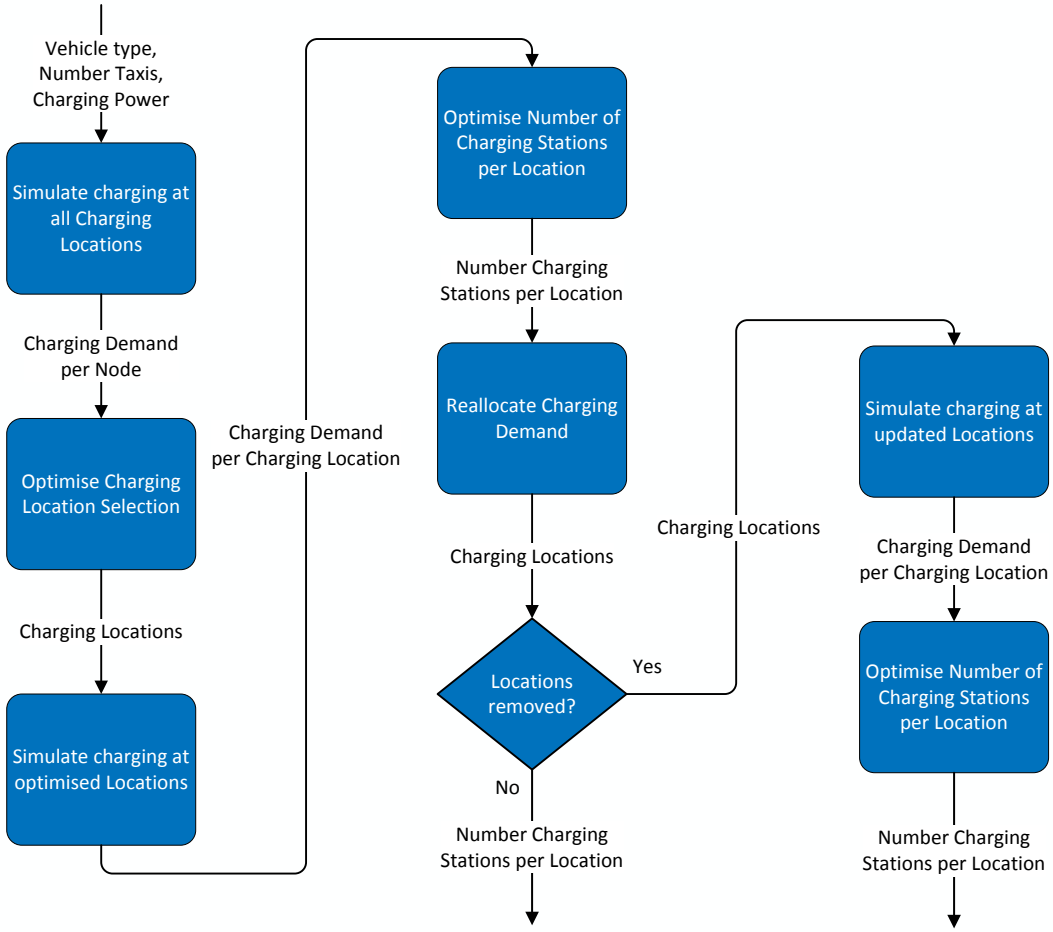

Figure 7.1: Optimisation approach

the *charging location* choice (see definition of *shift schedules* in Chapter 3.2.4) and may deviate from the optimised choice.

Next, the number of charging stations per location is optimised. Since the demand is already allocated to *charging locations*, the number of charging stations can be optimised for each location independently. Thus waiting times can be estimated with respect to the demand and the number of charging stations. The objective is to balance the waiting time costs with charging infrastructure costs.

As the allocated *charging demand* of the first optimisation step to select *charging locations* is different from the simulated *charging demand* of the previous step, the initial choice of *charging locations* may not be ideal any more. Therefore, the next step updates the location choice by checking if it is economically more efficient to remove a *charging location* A and allocating the *charging demand* to another location B. Hereby the agents' travelling costs from location A to B and the costs of additional charging stations at location B are considered.

If no location was removed, the optimisation is completed and the number of charging

stations per location are returned. Otherwise, another simulation is executed with the updated *charging locations* and the number of charging stations is optimised based on the simulated *charging demand*. Thereafter the optimisation is completed.

7.5 Waiting time estimation

In this section a formula is derived to estimate the waiting time of a taxi for the next available charging station at location j and time t with respect to the *charging demand* Λ_{jt} and the number of charging stations s_j. The *charging demand* Λ_{jt} is defined as the total use duration of charging stations at location *j* and time interval *t*. The nomenclature of this section is given by Table 7.2.

Table 7.2: Nomenclature of waiting time estimation

Symbol	Unit	Description
a_i	-	waiting time sub function
a_i^{lin}	-	linear waiting time sub function
a_i^{quad}	-	quadratic waiting time sub function
α_i	-	waiting time parameter
Δt	min	duration of time interval
ϵ	-	adjustment parameter
j	-	*charging location*
Λ_{jt}	min	*charging demand* at location *j* and time *t*
$\bar{\Lambda}_{jt}$	min	weighted *charging demand* at location *j* and time *t*
m_i	min	slope of waiting time straight
s_j	-	number of charging stations at location *j*
s'_j	-	adjusted number of charging stations at location *j*
t	-	time interval
u_{jt}	-	charging station utilisation at location *j* and time *t*
W	min	waiting time
w_k	-	weight of time interval *k*

As agents have to queue at *charging locations* until a charging station is available the waiting time of time interval t depends not only on the current *charging demand* Λ_{jt} but also on the demand of previous time interval $(t-1,\ t-2,\ t-3)$. Hence, a weighted sum of the *charging demand* over these time intervals is calculated:

$$\bar{\Lambda}_{jt} = \sum_{k=0}^{3} w_k \Lambda_{jt-k} \tag{7.3}$$

while the weights w_k are normalised:

$$w_0 = 1 - \sum_{k=1}^{3} w_k \text{ with } w_k \geq 0 \,\forall k \tag{7.4}$$

Waiting times $W\left(u_{jt}, s'_j\right)$ are either estimated as zero or by linear equations with respect to the charging station utilisation u_{jt}:

$$u_{jt} = \frac{\bar{\Lambda}_{jt}}{s'_j \Delta t} \tag{7.5}$$

where Δt is the duration of a time interval (the used time intervals have a duration of one hour):

$$W\left(u_{jt}, s'_j\right) = \begin{cases} 0 & \text{if } u_{jt} \leq a_1\left(s'_j\right) \\ \left(u_{jt} - a_1\left(s'_j\right)\right) m_1 & \text{if } a_1\left(s'_j\right) < u_{jt} \leq a_2\left(s'_j\right) \\ \left(a_2\left(s'_j\right) - a_1\left(s'_j\right)\right) m_1 + \left(u_{jt} - a_2\left(s'_j\right)\right) m_2 & \text{otherwise} \end{cases} \tag{7.6}$$

s'_j is defined as:

$$s'_j = s_j + \varepsilon \tag{7.7}$$

to avoid division by zero if no charging stations are assigned to location j. The parameter ε is set to 10^{-10} in order to estimate very high waiting times if the charging station utilisation is greater than zero while s_j is zero.

The functions a_1 and a_2 are used to decide which equation shall be evaluated with respect to the charging station utilisation and number of charging stations. Two different formulations are used for these functions:

$$a_1^{lin}\left(s'_j\right) = \alpha_2 + \frac{\alpha_3}{s'_j} \tag{7.8}$$

$$a_2^{lin}\left(s'_j\right) = \alpha_5 + \frac{\alpha_6}{s'_j} \tag{7.9}$$

and

$$a_1^{quad}\left(s'_j\right) = \alpha_1 s'_j + \alpha_2 + \frac{\alpha_3}{s'_j} \tag{7.10}$$

$$a_2^{quad}\left(s'_j\right) = \alpha_4 s'_j + \alpha_5 + \frac{\alpha_6}{s'_j} \tag{7.11}$$

In contrast to a_1^{quad}, the definition of a_1^{lin} allows to derive a linear condition when waiting times are zero:

$$\frac{\bar{\Lambda}_{jt}}{s'_j \Delta t} \leq \alpha_2 + \frac{\alpha_3}{s'_j} \tag{7.12}$$

$$\Leftrightarrow \alpha_2 s'_j + \alpha_3 - \frac{\bar{\Lambda}_{jt}}{\Delta t} \geq 0 \tag{7.13}$$

On the other hand, the additional parameters α_1 and α_4 in a_1^{quad} and a_2^{quad}enable a more precise estimation.

The driving profile simulation model was used to simulate 109,393 charging events in total at *charging locations* with 1, 2, 4, 9, 16, and 40 charging stations in order to fit the

parameters $w_{1,2,3}$, $\alpha_{1,2..6}$, and $m_{1,2}$ for the linear conditions (7.8, 7.9) and the quadratic conditions (7.10, 7.11) separately. Due to the higher degree of freedom, the root mean square error of the waiting time fit with the quadratic condition is with 7.55 min slightly lower than the error of the fit with the linear condition which is 7.57 min.

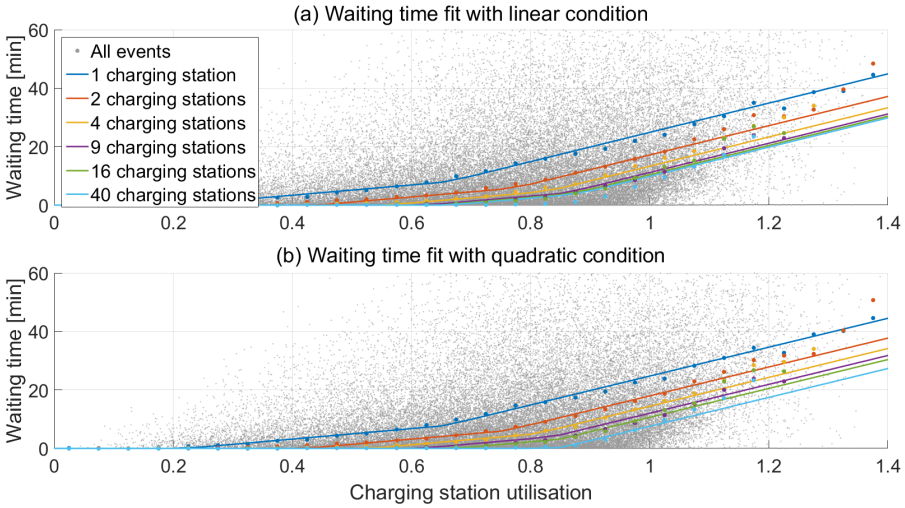

Figure 7.2: Fit of waiting time with respect to the charging station utilisation and the number of charging stations with linear condition (a) and quadratic condition (b)

Figure 7.2(a) shows the results of the fit with linear condition and Figure 7.2(b) with quadratic condition. The waiting time with respect to the charging station utilisation of the simulated charging events are represented by the grey dots. The high variance of waiting times at equal charging station utilisations is caused by the stochastic nature of arriving taxis at *charging locations*. High waiting times occur when taxis arrive at almost the same time and the latter arriving taxi has to wait until the first taxi finished the charging process. In contrast, the waiting time would be zero if the second taxi arrives at the time when the first taxi leaves the *charging location*. In both cases the *charging demand* would be the same. This explains the relatively high root mean square error of both fits.

The coloured dots depict the average waiting time of all charging events within an charging station utilisation interval of ± 0.025 for different number of charging stations per location. Comparing these dots with the fitted functions represented by the coloured lines shows that average waiting times are very well estimated over a wide range of charging station utilisation and number of charging stations.

The average waiting time remains zero until a certain charging station utilisation is reached. The critical utilisation when waiting times start to increase strongly depends on the number of charging stations. The more charging stations are installed at a location the higher the critical charging station utilisation. This characteristic is very important as the optimisation algorithm can increase the utilisation while having zero waiting time costs until the critical utilisation is reached. The waiting time estimation is capable of reproducing these critical points very accurately.

The main difference between using linear or quadratic conditions becomes apparent in case of high numbers of charging stations. Here, for the linear condition the estimated

waiting times for 9, 16, or 40 charging stations are almost equal, whereby the quadratic condition differentiates these cases significantly better.

The fitted parameter values for the linear conditions (7.8, 7.9) and quadratic conditions (7.10, 7.11) are listed in Table 7.3.

Table 7.3: Waiting time fit parameter values

Parameter	Unit	Value for linear condition	Value for quadratic condition
w_1	-	0.533	0.525
w_2	-	0.211	0.211
w_3	-	0.0379	0.0409
α_1	-	-	$5.97 \cdot 10^{-3}$
α_2	-	0.676	0.604
α_3	-	-0.468	-0.387
α_4	-	-	$2.36 \cdot 10^{-14}$
α_5	-	0.885	0.860
α_6	-	-0.222	-0.203
m_1	min	17.6	17.9
m_2	min	50.0	49.4

The parameter values of the fit with linear respectively quadratic condition are very similar (highest relative deviation is 21%). The values of the weights $w_{1,2,3}$ are decreasing with the time difference of the corresponding time interval to the time interval for which the waiting time is estimated. Which makes sense as charging events which occurred long time before must have a smaller effect than resent events. As w_3 is less than 5%, a consideration of more than four time intervals (including interval t) is not expected to improve the estimation further. Interestingly, the *charging demand* at time interval $t-1$ has an even bigger effect than the *charging demand* at the time interval t for which the waiting time is estimated. This is can be explained as due to queuing, all events of $t-1$ can affect taxis at time interval t, whereby a taxi which arrives at the end of interval t cannot affect the waiting time of another taxi which arrived earlier.

The main difference between both fits is caused by the parameter α_1, whereby the very low values of α_4 has hardly any effect. Another important aspect regarding the optimisation is that since α_1 is positive, it is not possible to formulate a convex constraint to require zero waiting times with the quadratic condition:

$$\alpha_1 s_j'^2 + \alpha_2 s_j' + \alpha_3 - \frac{\bar{\Lambda}_{jt}}{\Delta t} \geq 0 \tag{7.14}$$

7.6 Optimisation problem

This section contains the mathematical formulation of the *charging location* optimisation, the optimisation of the number of charging stations per location, and the algorithm to reallocate *charging demand*. The nomenclature of this section is given by Table 7.4.

Table 7.4: Nomenclature of optimisation problem

Symbol	Unit	Description
α_k	-	waiting time estimation parameter
C_c	SGD	charging station costs
C_d	SGD/km	driving distance costs
C_w	SGD/min	waiting time costs
c_{AB}	SGD	driving costs from location A to B
d_{ij}	km	driving distance from cluster *i* to location *j*
Δt	min	time interval duration
i	-	cluster
j	-	*charging location*
l_j	-	selection of *charging location j*
Λ_{jt}	min	*charging demand* at location *j* and time *t*
λ_{it}	min	*charging demand* of cluster *i* at time *t*
$\bar{\lambda}_{it}$	min	scaled *charging demand* of cluster *i* at time *t*
N_j	-	total number of charging events at location *j*
n_{day}	-	number of simulated days
n_{ETsim}	-	number of simulated taxis
n_{ETopt}	-	number of taxis to optimise infrastructure for
n_{it}	-	number of charging events of cluster *i* at time *t*
$\bar{n}_{it}$	-	scaled number of charging events of cluster *i* at time *t*
s_j	-	number of charging stations at location *j*
t	-	time interval
W	min	waiting time
Y_{ij}	-	*charging demand* allocation of cluster *i* to location *j*

7.6.1 Charging location optimisation

The most important requirement of the optimisation is to take the spatial-temporal *charging demand* of electric taxis into account. In order to find out from which location and at what time taxis start trips to charging stations and how long charging stations are used, a simulation is run with unlimited number of charging stations at each *candidate charging location*.

The origins of all trips leading to charging stations are represented by *street network node* IDs (Chapter 2.5). The *charging location* optimisation has to allocate the *charging demand* of each trip to a *charging location*. Since the used street network has in total 45,364 nodes, a huge number of decision variables would be required to do so. In order to significantly reduce that number, the k-means++ algorithm (Arthur and Vassilvitskii, 2007) is used to combine all nodes to 900 clusters with respect to the node's geographical location. Each cluster is represented by the node which is closest to the cluster's centroid. These nodes are denoted as *cluster centre nodes*. All remaining nodes are matched to their closest *cluster centre node*, whereby the driving distance on the street network is

taken into account. Figure 7.3 shows a map of all clustered nodes, the colours are used to distinguish the clusters (not each cluster has an unique colour).

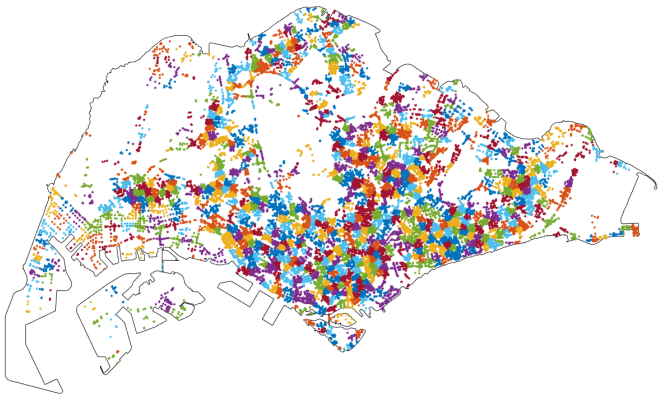

Figure 7.3: Clustered *street network nodes*

The total simulation duration is divided into time intervals with a duration of one hour. All trips originating from the same cluster *i* within the same time interval *t* are merged to one set. For each set the total duration of all following charging events λ_{it} is calculated. The average use duration over all time intervals which correspond to the same time of the day (*t*, *t*+24, *t*+48, ...) is scaled with respect to the number of taxis n_{ETopt} for which the charging infrastructure shall be optimised:

$$\bar{\lambda}_{it} = \frac{n_{ETopt}}{n_{ETsim} n_{day}} \sum_{k=0}^{n_{day}-1} \lambda_{it+24k} \quad \forall t = 1, 2, .., 24 \tag{7.15}$$

The same is done for the number of charging events:

$$\bar{n}_{it} = \frac{n_{ETopt}}{n_{ETsim} n_{day}} \sum_{k=0}^{n_{day}-1} n_{it+24k} \quad \forall t = 1, 2, .., 24 \tag{7.16}$$

The number of simulated taxis n_{ETsim} is 2,949 which is the total number of *shift schedule sets* (Chapter 5.4), the number of simulation days n_{day} is set to 30. The scaling with respect to the number of optimised taxis allows to generate an average *charging demand* which reflects the driving profiles of all taxis although the number of taxis for which the infrastructure shall be optimised can be different. With this approach a solution is found which should work well for many different selections of *shift schedule sets*. At the same time however, the found solution will not be ideal for a specific selection of *shift schedule sets*. Apart from that, the scaling also enables to optimise a charging infrastructure for more than the maximum number of agents.

In order to obtain the *charging demand* per *charging location j* and time interval *t* Λ_{jt}, the *charging demand* of each cluster *i* must be allocated to one or several *candidate charging locations*. Therefore, the allocation matrix Y_{ij} is used:

$$\Lambda_{jt} = \sum_i Y_{ij} \bar{\lambda}_{it} \tag{7.17}$$

whereby:

$$\sum_j Y_{ij} = 1 \quad \forall j \tag{7.18}$$

and

$$Y_{ij} \geq 0 \quad \forall i, j \tag{7.19}$$

The binary decision variable l_j describes if charging stations shall be placed at location *j*. Thus, the number of charging stations at location s_j have to fulfil following condition:

$$l_j \leq s_j \leq l_j n_{ETopt} \quad \forall j \tag{7.20}$$

This condition requires the number of charging stations to be zero if no charging stations shall be placed at location *j* and that at least one charging station must be placed in case that l_j is equal one. Hence, s_j cannot get any value between zero and one. Therefore, s_j can be a continuous number as only the selection of *charging locations* but not the number of charging stations is a required input for the next optimisation step.

The decision variables of this problem are Y_{ij}, l_j, and s_j. As Y_{ij} allocates 900 clusters to 291 *candidate charging locations*, the complexity of this problem is relatively high, which makes it important in terms of calculation time and solution quality to use a linear formulation. Therefore, the waiting time costs which would be evaluated with the non-linear function 7.6 are not included in the objective function. In order to respect capacity limitations nevertheless, the condition:

$$\alpha_2 s'_j + \alpha_3 l_j - \frac{\bar{\Lambda}_{jt}}{\Delta t} \geq 0 \quad \forall j, t \tag{7.21}$$

is derived from equation 7.13 to require zero waiting time at all *charging locations*. Since α_3 is negative, it is multiplied by l_j in order to allow s_j to be zero if no *charging demand* is allocated to *charging location j* ($\bar{\Lambda}_{jt} = 0$).

The objective function includes the travelling costs from all *cluster centre nodes i* to all *charging locations j* during all time intervals *t*:

$$C_d \sum_i \sum_j \sum_t Y_{ij} d_{ij} \bar{n}_{it} \tag{7.22}$$

and the charging infrastructure costs:

$$C_c \sum_j s_j \tag{7.23}$$

where C_d is the *detour cost factor*, C_c the *charging station cost factor* (Chapter 6.3), and d_{ij} is the driving distance from cluster *i* to *charging location j*.

The complete optimisation problem is formulated as:

$$\min\ C_d \sum_i \sum_j \sum_t Y_{ij} d_{ij} \bar{n}_{it} + C_c \sum_j s_j \tag{7.24}$$

subject to:

$$\sum_j Y_{ij} = 1 \quad \forall j \tag{7.25}$$

$$Y_{ij} \geq 0 \quad \forall i, j \tag{7.26}$$

$$l_j \in \{0, 1\} \tag{7.27}$$

$$l_j \leq s_j \leq l_j n_{ETopt} \quad \forall j \tag{7.28}$$

$$\alpha_2 s'_j + \alpha_3 l_j - \frac{\bar{\Lambda}_{jt}}{\Delta t} \geq 0 \quad \forall j, t \tag{7.29}$$

whereby Y_{ij}, l_j, and s_j are the decision variables. This problem was solved by applying the solver of (Gurobi Optimization, Inc., 2016).

7.6.2 Charging station optimisation

Due to the constraint of having no waiting times at all (equation 7.13), the number of charging stations is overestimated by the previous step. Therefore, in this step the number of charging stations is optimised with respect to the waiting time costs.

Again, a simulation is run with unlimited number of charging stations at the *charging locations* which were selected in the previous step. The reason for simulating the driving profiles again is that due to the minimising of travelling costs at the previous step, taxis are most likely allocated to the closest *charging location* although the driver might have preferred a different location farther away. As the drivers' preferences are respected by the agents' behaviour model (Chapter 5.7), another simulation run generates a more realistic *charging demand* for the reduced number of *charging locations*.

The used output of this simulation run is the *charging demand*: λ_{jt} and the number of charging events n_{jt} at each *charging location j* and time interval *t*. In contrast to equations 7.15 and 7.16, the scaled *charging demand* Λ_{jt} and scaled number of charging events $\bar{n}_{jt}$ are not averaged over time intervals which corresponded to the same time of the day:

$$\Lambda_{jt} = \frac{n_{ETopt}}{n_{ETsim}} \lambda_{jt} \tag{7.30}$$

$$\bar{n}_{jt} = \frac{n_{ETopt}}{n_{ETsim}} n_{jt} \tag{7.31}$$

The reason for averaging the demand for the location optimisation but not for the charging station optimisation is that the waiting times are constraint to zero for the location optimisation. Due to this constraint, the design of the optimised charging infrastructure strongly depends on the highest *charging demand* at one time interval. In order to avoid that only the highest peak throughout the whole simulation duration would define the charging infrastructure design, the *charging demand* is smoothed by averaging the simulated demand over all days.

Due to the inclusion of waiting times in the objective function of this optimisation step, the highest *charging demand* peak affects the total costs, however it does not force the optimisation to place an inappropriately high number of charging stations only to avoid waiting times. Therefore, the solution at this step is more cost efficient and a reduction of the *charging demand* variability due to averaging over all days is not necessary.

The total waiting time costs are:

$$C_w \sum_j \sum_t \bar{n}_{jt} W\left(u_{jt}, s'_j\right) \tag{7.32}$$

whereby the charging station utilisation u_{jt} is calculated with equation 7.3 and 7.5 with respect to Λ_{jt}. To improve the accuracy of the waiting time estimation, the quadratic conditions 7.10 and 7.11 are used in $W\left(u_{jt}, s'_j\right)$. The *waiting time costs factor* C_w (Chapter 6.3) quantifies the drivers' loss of revenue caused by waiting.

The charging infrastructure costs are calculated with equation 7.23 and are multiplied by the number of simulated days as the waiting time costs are also cumulated over the whole simulation duration. As the number of charging stations is used as output of this step, s_j must be an integer.

Hence, the formulation of this optimisation problem is:

$$\min\ C_w \sum_j \sum_t \bar{n}_{jt} W\left(u_{jt}, s'_j\right) + n_{day} C_c \sum_j s_j \tag{7.33}$$

subject to:

$$s_j \in \mathbb{N}_0 \quad \forall j \tag{7.34}$$

In contrast to the objective function 7.24, this formulation does not include the allocation matrix Y_{ij}. Thus, all objective equations are uncoupled and can be optimised separately.

Therefore, the lowest number of charging stations with zero waiting time s_{max} is calculated by rounding up the root of equation 7.14 to the next integer. The ideal number of charging stations is found by evaluating equation 7.33 with each value of s_j between zero and s_{max} and selecting the value with the lowest costs.

7.6.3 Charging demand reallocation

In contrast to the first optimisation step, waiting times are allowed to occur for the optimised charging infrastructure of the second step. Thus, the total number of charging stations gets reduced and a more cost efficient solution is found. According to the waiting time estimation (Figure 7.2), a lower number of charging stations means that the *charging demand* per charging station must be reduced to keep waiting times at the same level. In other words: the efficiency of a *charging location* decreases by reducing the number of charging stations. Hence, the question is whether the optimised selection of *charging locations* at the first step is still ideal after reducing the number of charging stations or if the number of *charging locations* should be reduced as well.

Therefore, this step is used to check if it is economically better to remove *charging locations* and to reallocate the *charging demand* of the removed locations to other locations nearby. In order to assess if the reallocation of *charging demand* from location

A to location B is beneficial, charging station costs, travelling costs of all taxis from location A to B, and the change of waiting time costs is taken into account. The reallocation is checked for every pair of *charging locations*.

To optimise the new number of charging stations at location B s_B^*, the *charging demand* at location A Λ_{At} is added to the demand at B Λ_{Bt}:

$$\Lambda_{Bt}^* = \Lambda_{At} + \Lambda_{Bt} \tag{7.35}$$

The objective function 7.33 is minimised with the above method to find s_B^* with respect to the new *charging demand* Λ_{Bt}^*. The driving costs from A to B are:

$$c_{AB} = C_d \sum_t \bar{n}_{At} d_{AB} \tag{7.36}$$

where d_{AB} is the driving distance from A to B on the street network.

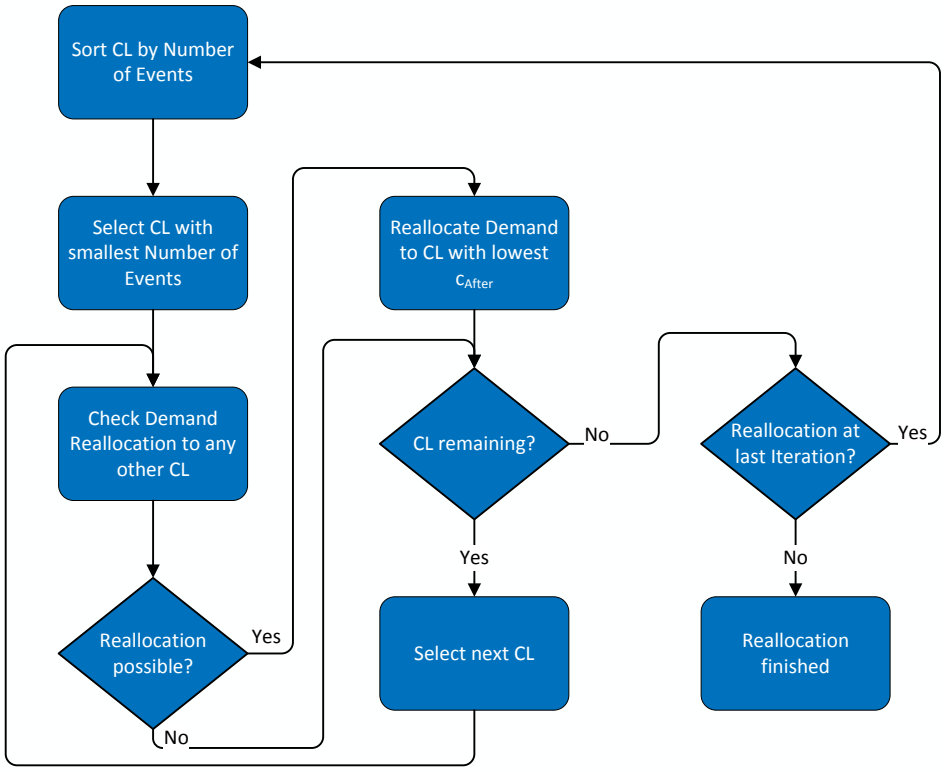

Figure 7.4: Algorithm to reallocate *charging demand* among *charging locations* (CL)

The costs before the reallocation are:

$$c_{before} = C_w \sum_t \left(\bar{n}_{At} W\left(u_{At}, s_A\right) + \bar{n}_{Bt} W\left(u_{Bt}, s_B\right)\right) + n_{day} C_c \left(s_A + s_B\right) \tag{7.37}$$

and after:

$$c_{after} = c_{AB} + C_w \sum_t \left(\bar{n}_{At} + \bar{n}_{Bt}\right) W\left(u^*_{Bt}, s^*_B\right) + n_{day} C_c s^*_B \tag{7.38}$$

If c_{after} is smaller than c_{before}, *charging location* A is removed and s^*_B charging stations are placed at location B. Otherwise the charging infrastructure is not changed. It can be expected that the change of waiting times after the reallocation is marginal, which means that reallocations are mostly done if the total number of charging stations can be reduced.

A flow chart of the reallocation algorithm is depicted in Figure 7.4. First, all *charging locations* are sorted by the total number of charging events over all time intervals *t*:

$$N_j = \sum_t \bar{n}_{jt} \tag{7.39}$$

Next, the *charging locations* are selected in the sorted order starting with the smallest number of charging events. The reason for following this order is that a reallocation of the *charging demand* of location A to location B could be possible as well as a reallocation from B to A. Due to the travelling costs it is always better to reallocate *charging demand* from the location with the smaller number of charging events to the location with the higher number. Therefore, the algorithm selects *charging locations* in ascending order.

After the reallocation of all *charging locations* was considered, the algorithm starts a new iteration if the demand of any location was reallocated at the this iteration. This procedure is repeated as long as no reallocation was made within one iteration.

Chapter 8

Results

This chapter discusses the results of the infrastructure optimisation and presents the analysis of the simulated taxi driving profiles for these infrastructures. First, Chapter 8.1 introduces the analysed scenarios. The results of the infrastructure optimisation of these scenarios are presented in Chapter 8.2. The simulated driving profiles are analysed in Chapter 8.3, whereby an economic assessment is done in Chapter 8.4.

8.1 Scenario definition

The designed scenarios consist of two groups:

Group I concerns charging infrastructure expansion scenarios where it is analysed how to expand a charging infrastructure for 50 taxis up to the maximal fleet size of 2,949 taxis. Thereby, it is ensured that charging stations of an optimised scenario with a lower number of taxis must remain at the same place at all following scenarios. Hence, the condition:

$$s_{jk} \leq s_{jk+n} \quad \forall j, n \geq 1 \tag{8.1}$$

must be fulfilled, whereby s_{jk} is the number of charging stations at location *j* after the k^{th} step of increasing the number of taxis. This condition is ensured by including the number of charging stations of the previous iteration in the constraint equation 7.20.

Moreover, the possibility of *home charging* is analysed in this scenario group as well. *Home charging* means, that additionally to the public charging stations, an AC charging station with a charging power of 6.6 kW is placed at the most frequent *shift change location* of each agent and is used to charge the battery whenever the agent is having a *shift change* at that location.

Scenario group II is designed to analyse the effect of different battery capacities and public charging power on the infrastructure design, the driving profiles, and the economics of electric taxis. In order to produce representative results, these parameters were varied for one vehicle type. EVA was chosen for this purpose as it is the vehicle with the best known technical parameters. The selected charging power was 40, 50, 60, 100, 120, and 160 kW[1] and the analysed battery capacities ranged from 30 to 100 kWh. Combinations with low battery capacity (< 50 kWh) and high charging power (> 60 kW)

[1] these are the maximum charging power of each analysed vehicle in this thesis (120 kW is the output power of Tesla's superchargers)

may not be realisable today due to technical limitations. Nonetheless, they were analysed in this study to investigate if these settings could make sense from an economical point of view.

In order to make a fair comparison between configurations with different battery capacities, the batteries' weight difference was taken into account. As EVA's 50 kWh battery has a weight of 500 kg (Bender et al., 2014), it is assumed that the battery weight changes by 10 kg per kWh. With respect to the adjusted weight, the vehicle's energy consumption was updated by simulating all trips with all considered battery capacities. The adjusted energy consumptions and ranges of the analysed vehicle configurations were taken into account by the driving profile simulation model introduced in Chapter 5.

Furthermore, changing the battery capacity also affects the vehicles' economics. Therefore, EVA's Open Market Values (OMV) was adjusted by 391 SGD/kWh (Kochhan, 2017) with respect to the selected battery capacity. The effect of the OMV on the total costs is especially important in the context of taxis in Singapore as the payable Additional Registration Fee (ARF) ranges from 100 to 180% of the OMV (Chapter 6.1).

All chosen scenario configurations of group I and II are summarised in Table 8.1.

Table 8.1: Scenario definition

Group	Vehicle type	Battery capacity [kWh]	Charging power [kW]	Number of taxis	Home charging
I	BYD e6	61.4	40	50 - 2,949	yes / no
I	EVA	50	160	50 - 2,949	yes / no
I	Kia Soul	27	100	50 - 2,949	yes / no
I	Nissan Leaf	30	50	50 - 2,949	yes / no
I	Tesla Model S	70	60	50 - 2,949	yes / no
II	EVA	30 - 100	40 - 160	2,949	no

8.2 Infrastructure design

This section discusses the results of the infrastructure optimisation for different vehicle types (group I) and vehicle configurations (group II) regarding the number and placement of charging stations.

Figure 8.1 shows the optimised numbers of charging stations and locations for a taxi fleet of 2,949 taxis for different vehicle types without (a) and with *home charging* (b). Obviously, the charging power had a big effect on the results. In case of no *home charging,* EVA required 278 charging stations with 160 kW power whereby for the same fleet size of BYD e6 taxis 2.7 times more 40 kW charging stations were ideal. The main reason for this difference is that the charging times increase with lower charging power which means that a higher number of charging stations is necessary to supply the same number of vehicles. Furthermore, it can be seen that there is a correlation between the number of charging stations and the number of *charging locations*. The more charging stations were required, the more *charging locations* were chosen.

Other aspects which also caused a difference in the numbers of charging stations were that 40 kW charging stations are significantly cheaper which allowed to install more charging stations in order to reduce waiting times and detours (Chapter 6.2).

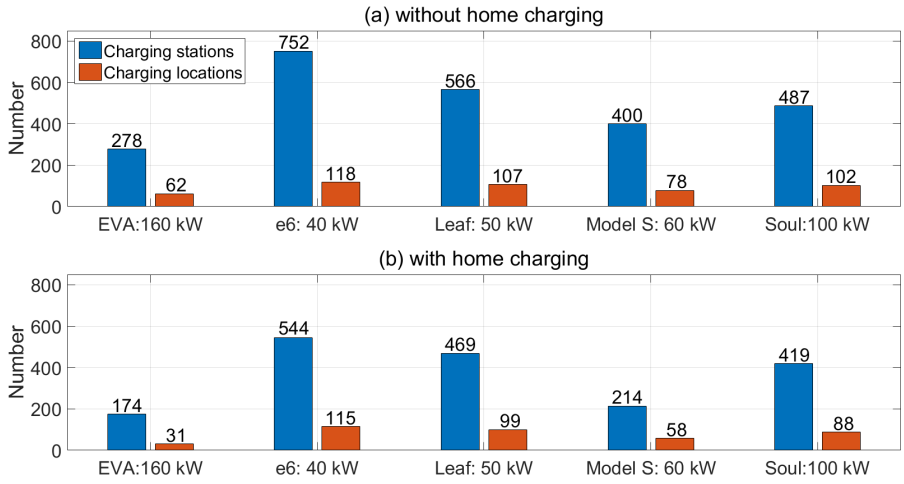

Figure 8.1: Optimised number of charging stations and locations for different vehicle types without *home charging* (a) and with *home charging* (b)

Furthermore, it must be kept in mind that BYD's energy consumption is higher than EVA's, which increased the total energy demand and therewith required more charging stations.

If *home charging* was available, the number of public charging stations was significantly reduced for all vehicle types. Recharging during *shift changes* even with low charging power means that taxis started their *shift* with a higher State of Energy (SOE) which reduced the *charging demand* during the *shift* and in turn the number of charging stations.

There was a big difference regarding the ratio of reduced charging stations among the different vehicle types. The highest reduction was achieved for the Tesla Model S with 46% whereby the number of charging stations got only reduced by 14% for the Kia Soul. The reason for these big differences is that the Tesla Model S has with 70 kWh the highest battery capacity whereby the Soul's battery size is the smallest with 27 kWh. Thus, Tesla taxis could recharge much more energy during *shift changes* which reduced their *charging demand* during the *shift* disproportionally compared to the other vehicle types.

The number of charging stations (a) and the number of charging locations (b) with respect to the number of taxis for all vehicle types without *home charging* is depicted in Figure 8.2. The number of charging stations increased linearly with the number of taxis, whereby the increase of the number of *charging locations* became smaller with higher number of taxis. Hence, more and more charging stations were placed at the same locations.

The optimisation method prioritised the reduction of detour costs first by placing charging stations at many different locations. However, the more locations were chosen, the smaller the effect on detours became. Therefore, at higher numbers of taxis, waiting time costs were reduced by increasing the number of charging stations per location.

This switch of priorities appeared at around 500 taxis. Thus, this number seems to be a critical fleet size for which a cost efficient charging infrastructure network can

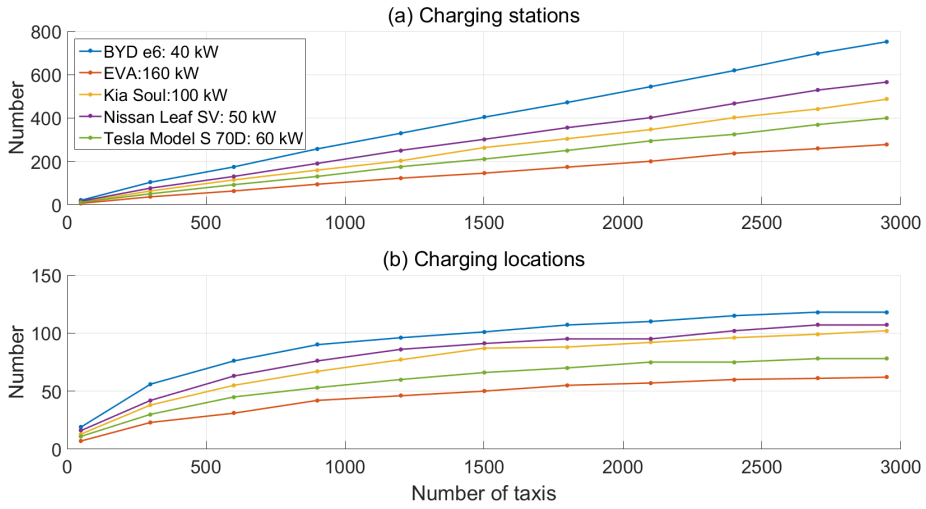

Figure 8.2: Number of charging stations (a) and *charging locations* (b) with respect to the taxi fleet size without *home charging*

be provided. For bigger fleets, the ratio of charging stations per taxi and therewith the infrastructure costs per taxi did not considerably improve.

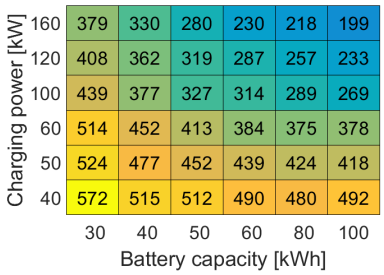

Figure 8.3: Number of charging stations with respect to battery capacity and charging power

Figure 8.3 shows the optimised numbers of charging stations for scenario group II. As well as for group I, the number of charging stations decreased with the charging power. The number of charging stations was reduced by 11.8% on average when the charging power got increased from 40 to 50 kW. Another increase of the charging power by 10 kW reduced the number of charging stations by only 8.8% on average. Thus, the efficiency of the charging infrastructure can be significantly improved by increasing the charging power to at least 50 kW.

Regarding the battery capacity, there are two effects which influence the ideal number of charging stations. On the one hand, a higher battery capacity allows the agents to recharge more energy during their *breaks*, which improves the charging station utilisation and therewith reduces the required number of charging stations. On the other hand, higher battery capacities increase the vehicle's weight and therewith the energy consumption and *charging demand* which would require a higher number of charging stations. The results show that the number of charging stations was reduced with in-

creasing battery capacity. Hence, the first effect dominates the latter. However, there was a turnaround in case of high battery capacities and low charging power ($\leq$60 kW). For these scenarios the number of charging stations was slightly increased by 1% when the battery capacity was increased from 80 to 100 kWh. The reason why this turnaround occurred at high battery capacities and low charging power is that the *break* duration of many charging events were not long enough to fully recharge a 80 kWh battery. Hence, there was no benefit in having an even bigger battery in these scenarios.

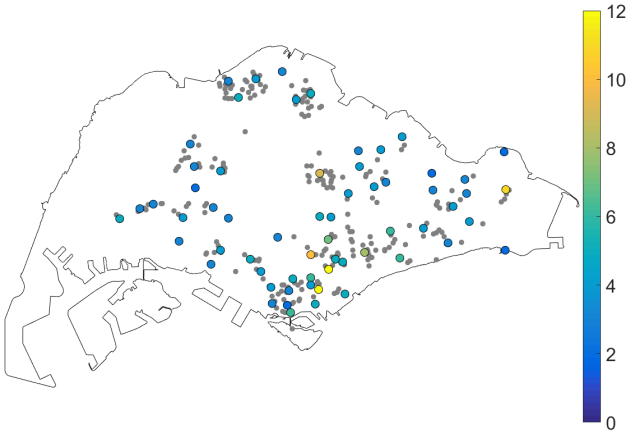

Figure 8.4: Charging station map for 2,949 EVA taxis and 160 kW charging power without *home charging*

A map with all optimised *charging locations* for 2,949 EVA taxis with 160 kW charging stations is depicted in Figure 8.4. The colour of the dots corresponds to the number of charging stations. *Candidate charging locations* (Chapter 3.2.3) which were not chosen for the placement of charging stations are represented by grey dots.

The map shows a homogeneous distribution of *charging locations* over the whole island (excluding areas with very low population density in the west and the middle of the island). However, *charging location*s at the city centre in the south of the island have higher numbers of charging stations (up to twelve) than *charging locations* at outer areas. This is mainly caused by the fact that the Central Business District (CBD) is the area with the highest density of taxis. The location with the highest number of charging stations outside the CBD is the airport in the very east with eleven charging stations.

A very interesting aspect is, that the lowest number of charging stations per location is two - no location has only one charging station. Certainly, this was caused by the waiting time estimation which disproportionally reduced waiting times if more than one charging station is located at the same place.

A detailed analysis of the optimised selection of *charging locations* showed that mainly locations were chosen with big car parks which are close to shopping malls or food centres. Thus, this selection should be convenient for the drivers as it would allow them to combine their lunch or dinner *breaks* with the recharging of their vehicle.

The optimised locations of other vehicle types were very similar to the shown charging infrastructure. The main difference was that more charging stations were placed at

mainly the same locations.

8.3 Driving profile analysis

All optimised charging infrastructures were given as input to the driving profile simulation model in order to analyse the charging behaviour of taxis and to quantify what mileage and revenue electric taxis can achieve.

First of all, the simulation results were used to compare the waiting times estimated by the optimisation method with the simulated waiting times. The optimised waiting time per event $W\left(u_{jt}, s'_j\right)$ was calculated with respect to the optimised number of charging stations s_j, the number of charging events $\bar{n}_{jt}$, and the charging station utilisation u_{jt} per *charging location j* and time interval *t* (see Chapter 7.6.1):

$$\bar{W}_{opt} = \frac{\sum_j \sum_t \bar{n}_{jt} W\left(u_{jt}, s'_j\right)}{\sum_j \sum_t \bar{n}_{jt}} \tag{8.2}$$

The variables $\bar{n}_{jt}$ and u_{jt} were obtained from a simulation run which was executed during the optimisation with the maximum fleet size of $n_{ETsim} = 2,949$. To adjust the *charging demand* to the number of taxis for which the infrastructure had to be optimised (n_{ETopt}), the *charging demand* was scaled via equation 7.15. Thus, the resulting infrastructure should work well for various selections of *shift schedule sets* (Chapter 5.4) but is not ideal for one specific choice of *shift schedule sets*.

In order to evaluate the difference, another optimisation was executed based on an unscaled demand, meaning that the number of simulated taxis was set to the number of taxis for which the charging infrastructure had to be optimised ($n_{ETsim} = n_{ETopt}$).

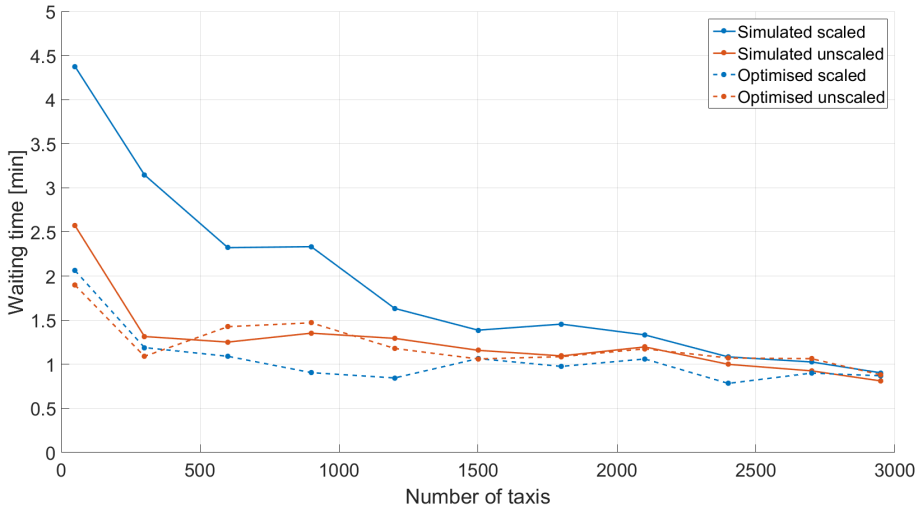

Figure 8.5: Optimised and simulated waiting time per charging event for EVA with scaled and unscaled *charging demand* without *home charging*

The optimised and simulated waiting times of these different approaches are shown in Figure 8.5 with respect to the fleet size. The simulated waiting times were calculated by averaging the waiting times of all charging events.

The simulated and optimised waiting times based on scaled demand deviated by 2.3 min for 50 taxis and converged to the same value for 2,949 taxis. The reason why the deviation decreased with higher number of taxis is that the scaled *charging demand* became more and more similar to the *charging demand* of the simulated taxis by increasing the number of taxis. Hence, the optimisation could adjust the infrastructure more accurately to the charging requirement of the simulated taxis and therewith reduce waiting times.

In contrast, the unscaled *charging demand* was derived from exactly the same *shift schedule sets* which were simulated after the optimisation. As a result, the deviation between optimised and simulated waiting times was smaller for all fleet sizes. These small deviations show that the introduced waiting time estimation in Chapter 7.5 is very accurate. However, as the infrastructures resulting from unscaled demand optimisations are especially tailored to a specific selection of *shift schedule sets*, it can be expected that it would fit considerably worse to any other selection. Therefore, in order to have a more stable solutions, all analysed charging infrastructures of this chapter were optimised with the scaled *charging demand*.

Apart from that, another important aspect which can be drawn from this diagram is that the average waiting time per charging event is very low - for 2,949 taxis it was only 0.9 min on average. Hence, from an economical point of view it is best to minimise waiting time costs to a very small amount by investing a high amount of money into a well-developed charging infrastructure. Moreover, the low waiting times also justify the chosen optimisation approach where waiting times were constraint to zero at the first step.

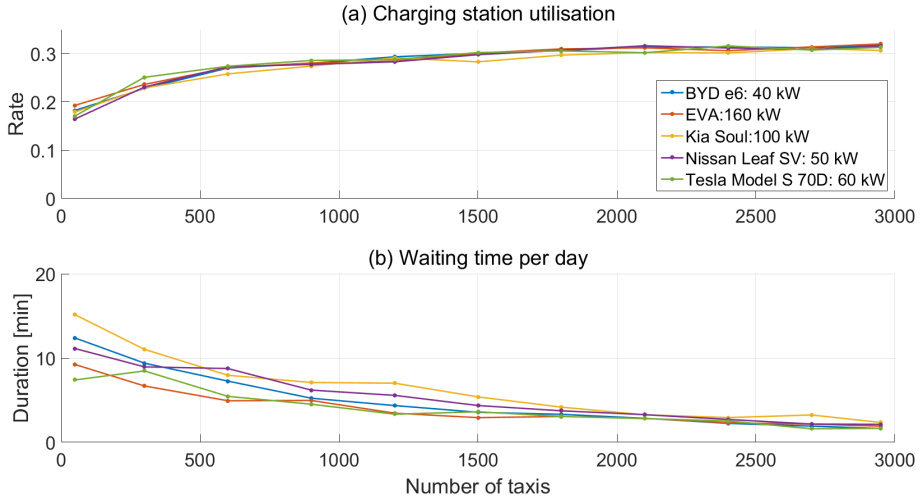

Figure 8.6: Charging station utilisation (a) and waiting time per day (b) with respect to the number of taxis without *home charging*

Figure 8.6 shows the average charging station utilisation (a) and the average waiting time per taxi and day (b) with respect to the number of taxis.

A charging station was considered as utilised when a vehicle was connected with it, this included the time when the battery was charged as well as the time when the charging process was finished until the agent continued its *shift*. Although the charging

infrastructures were optimised for different vehicle types with different *charging demand* and for charging stations with various charging power and costs, the charging station utilisation was for each scenario almost identical. For only 50 taxis it ranged between 16 and 19% and reached 31 to 32% for the whole fleet of 2,949 taxis. The utilisation did not significantly increase once a number of 500 taxis was reached.

Although the charging station utilisation increased with respect to the taxi fleet size, the average waiting times per day were decreased from 7 - 15 min for 50 taxis down to 1 - 2 min for 2,949 taxis. This was due to the increased number of charging stations per location which allowed to utilise the charging stations more efficiently.

The Kia Soul was the taxi with the highest simulated waiting times, which was mainly caused by its configuration of high charging power (100 kW) and low battery capacity (27 kWh). Due to this combination, only a relatively small proportion of the *break* durations could be used to recharge the battery as the maximum charge level was reached very soon. Therefore, more charging events per *shift* were required which meant that agents had to queue more often and therewith increased the total waiting time. Due to the high costs of 100 kW charging stations, increasing the number of charging stations in order to reduce waiting times was not cost efficient.

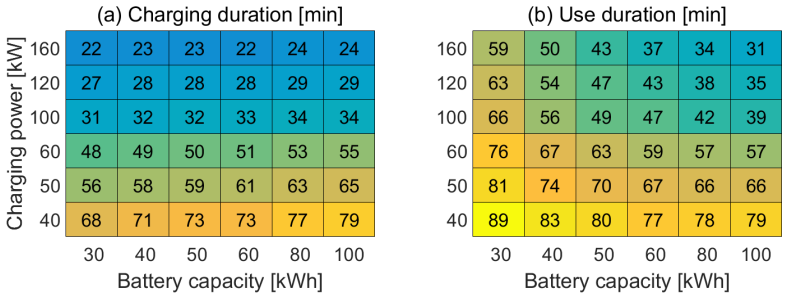

Figure 8.7: Charging and use duration of charging stations per taxi and day

In order to analyse in more detail how charging stations were used by agents with different vehicle configurations, Figure 8.7 shows the daily charging duration (a) and use duration (b) of EVA taxis with different battery capacity and charging power.

The charging duration decreased with higher charging power and increased with respect to the battery capacity due to the higher energy consumption. In contrast, the use duration, which is the time a vehicle was connected with a charging station became smaller when the battery capacity was increased. The reason for this is that in case of lower battery capacities, more charging events are necessary, which increases the chance that the battery got fully charged before the agent ended the break and continued its *shift*.

Due to these effects, the best ratio of charging duration to use duration is almost 100% for vehicles with 100 kWh battery capacity and 40 kW charging power, whereby the other extreme configuration with 30 kWh battery capacity and 160 kW charging power had the worst ratio of only 37%. The later case means that with a probability of 63% a charging station was blocked by a taxi which was not charged any more.

Although configurations of low charging power and high battery capacity allowed the best utilisation of charging stations during charging events, these configurations are not ideal from an economic point of view. First of all, low charging power would force the

agents to expand their *breaks* in order to recharge enough energy before the next *break*. Hence, less time would be left for driving to gain revenue. Furthermore, bigger batteries also increase the vehicle costs and therefore downgrade the economic potential.

A holistic evaluation of these aspects from an economic point of view follows in Chapter 8.4.

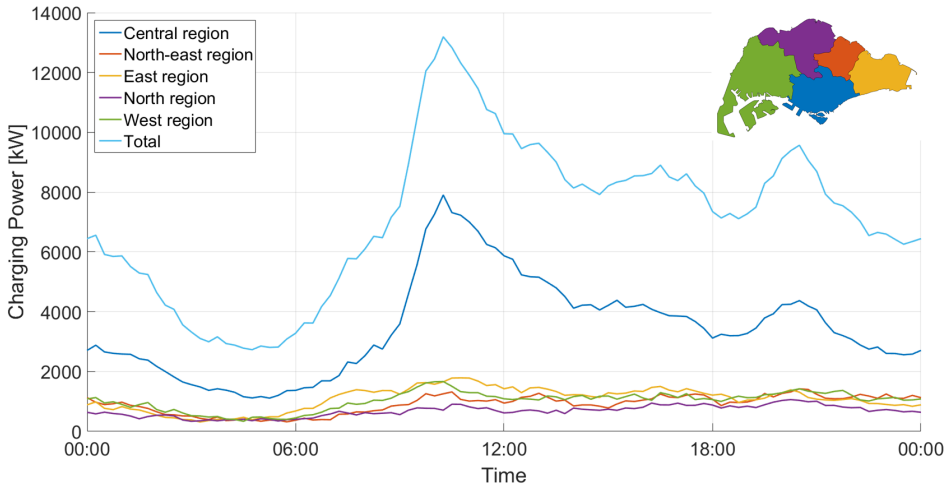

Figure 8.8: Charging load per region with respect to time for 2,949 EVA taxis without *home charging*

The cumulated charging load of all 2,949 EVA taxis with a charging power of 160 kW with respect to the time and region where charging events occurred is depicted in Figure 8.8.

It shows that the simulated charging load ranged from 2.7 MW at 4:45 to 13.1 MW at 10:30. The main reason why the charging load reached its maximum at this time is that a high percentage of all taxi drivers are having *breaks* at that time. Which is most likely because the morning rush hour ends at that time and the demand for taxis is comparably low. A similar pattern occurred after the evening peak hour at 20:30 when the charging load reached another peak of 9.6 MW. The lowest load at 4:45 can be explained by the fact that the lowest percentage of the taxi fleet is active at that time.

The disaggregation of the charging load into regions shows that by far the highest charging load throughout the day occurred in the central region which also includes the CBD. This is plausible as the spatial density of taxis is the highest in this region. The highest load with 7.9 MW appeared at 10:30 as well which contributed 60% of the total load. Interestingly, the evening peak at 20:30 is much smoother and contributed only 45% of the total load. This can be explained by the taxi travelling demand: in the morning, many customers take a taxi to go from an outer region to the central region which results in a disproportional high density of taxis in that region after the morning peak hours (Chapter 3.3). In contrast, at the evening a high percentage of customers wants to go back to an outer region which reduces the taxi density in the central region and therewith the *charging demand* at that time.

The implemented *charging behaviour model* (Chapter 5.7) which is designed to recharge as much energy as possible during *breaks* had a big effect on the simulated

load curves. More intelligent strategies which take the temporal and spatial utilisation of charging stations into account could cause significantly different load curves.

These strategies could be favourable from the drivers' as well as a charging infrastructure provider's point of view. Drivers could adjust their charging pattern in order to minimise waiting times, which would result in a smoother load curve with lower peaks. Lower peak loads favour an infrastructure provider as a smaller number of charging stations would be required to keep waiting times at an acceptable level.

A discussion of these results in the context of electrifying the road transport of Singapore can be found in (Massier et al., 2017).

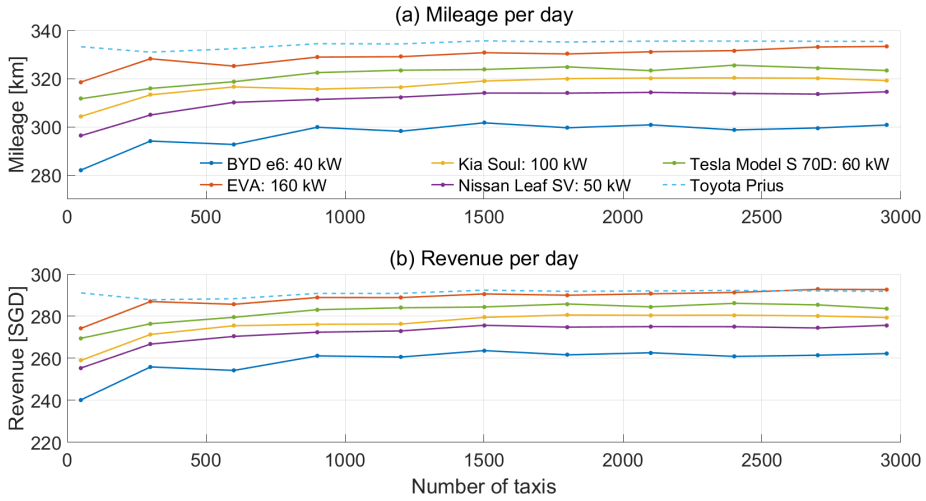

Figure 8.9: Mileage (a) and revenue (b) per day with respect to the number of taxis without *home charging*

Figure 8.9 shows the simulated mileage (a) and revenue (b) of all analysed vehicle types with respect to the number of taxis. The mileage and revenue of conventional taxis is represented by the dashed line. These values slightly varied with respect to the number of taxis as different sets of *shift schedules* were chosen for each number of taxis. In order to make the results comparable with electric taxis, exactly the same sets were chosen for each vehicle type.

When comparing the mileage and revenue values it must be kept in mind that these are averages over all taxis of the whole fleet. This means that in order to reach the same average values of conventional taxis, electric taxis would even have to reproduce driving profiles of the busiest taxis which reach around 650 km per day on average.

The simulated mileage and revenue of electric taxis increased slightly from 50 to 300 taxis and saturated afterwards. The lower values for 50 taxis were mainly caused by higher waiting times. EVA is the vehicle type which reached almost exactly the same values as conventional taxis. The biggest gap occurred for BYD e6 taxis which daily mileage and revenue were 35 km respectively 30 SGD per day lower than that of conventional taxis. Since the BYD has an even higher battery capacity than EVA, the performance gap must have been caused by its higher energy consumption and lower charging power.

8.4 Economic analysis

In this section, the optimised charging infrastructures and driving patterns are analysed from an economic point of view. Therefore, charging infrastructure costs, vehicle costs, and revenue are balanced in order to evaluate the potential profit with respect to different infrastructure concepts, vehicle types, and vehicle configurations. The profit calculation is explained in Chapter 6.3.

All revenue, costs, and profit values are given per day. Hereby, it should be kept in mind that even small differences of e.g. 2 SGD per day and taxi are significant. A taxi driver in Singapore has an average income of 2,076 SGD per month (Kochhan, 2017). Earning 2 SGD more per day would cumulate to 730 SGD per year which is the income of 10.5 days. Considering that most taxi drivers are working seven days a week having this amount of additional spare time would be very attractive to them.

A taxi operator with 3,000 taxis that could save 2 SGD per day and taxi would gain 2.2 million SGD per year. If this amount would be invested in the charging infrastructure, 255 additional charging stations with 50 kW charging power could be installed.

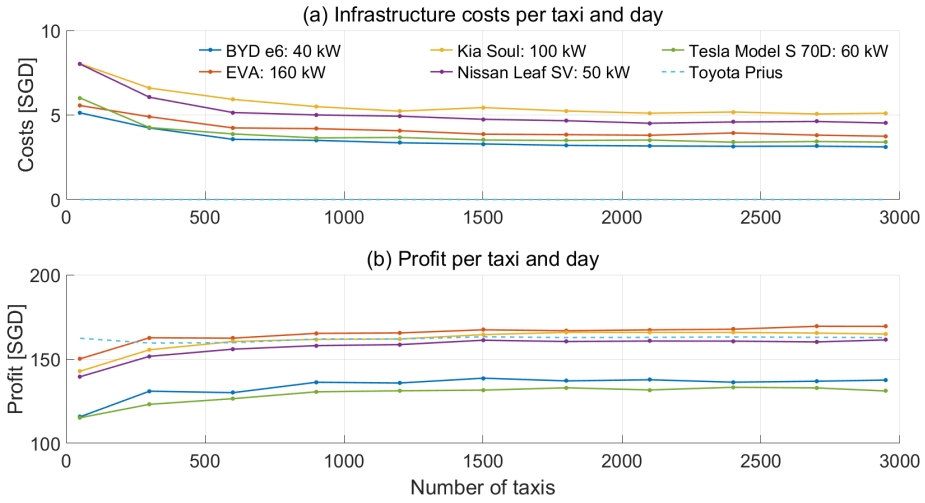

Figure 8.10: Infrastructure costs (a) and profit (b) per taxi and day without *home charging*

Figure 8.10 shows the charging infrastructure costs (a) and the profit (b) per taxi and day with respect to the number of taxis.

The charging infrastructure costs decreased with the number of taxis until a saturation at around 500 taxis was reached. This is due to the fact that the charging infrastructure costs are proportional to the number of charging stations and that the optimisation decreased the number of charging stations per taxi for bigger fleet sizes.

The infrastructure costs for the maximum fleet size of 2,949 taxis were the highest for the Kia Soul with 5.1 SGD per day which is attributed to the high waiting times which were described in Figure 8.6(b). The optimisation counteracted these waiting times by placing more charging stations which increased the infrastructure costs. In contrast, despite requiring the highest number of charging stations (752), the infrastructure costs for BYD e6 taxis were the lowest with 3.1 SGD per day which is possible due to the low costs of 40 kW AC charging stations (Chapter 6.2). The investment costs to install

the optimised charging infrastructures for 2,949 taxis ranged from 30 to 49 million SGD with respect to the vehicle type.

The taxis' profit was calculated by subtracting the vehicle and infrastructure costs from the revenue (Figure 8.9(b)), the drivers' labour costs are not included in this calculation. To compare the results with today's operating taxis, the estimated profit of Toyota Prius taxis is depicted by the dashed line.

The estimated profit of the Nissan Leaf, Kia Soul, and EVA ranged from 161 to 169 SGD per day for the maximum fleet size. Although the Nissan Leaf and Kia Soul had lower revenue and higher infrastructure costs, their profit was very close to EVA's. This can be explained by their estimated OMV which is with 35,253 respectively 33,087 SGD significantly lower than EVA's 50,982 SGD. Due to the ARF, this price difference becomes especially important in the context of Singapore (Chapter 6.1).

Apart from that, the estimated profit of BYD e6 and Tesla Model S taxis is 32 respectively 38 SGD per day lower than EVA's. In case of the BYD e6 this was caused by its significantly lower revenue and in case of the Tesla Model S by its much higher OMV of 93,809 SGD which massively increases the vehicle costs.

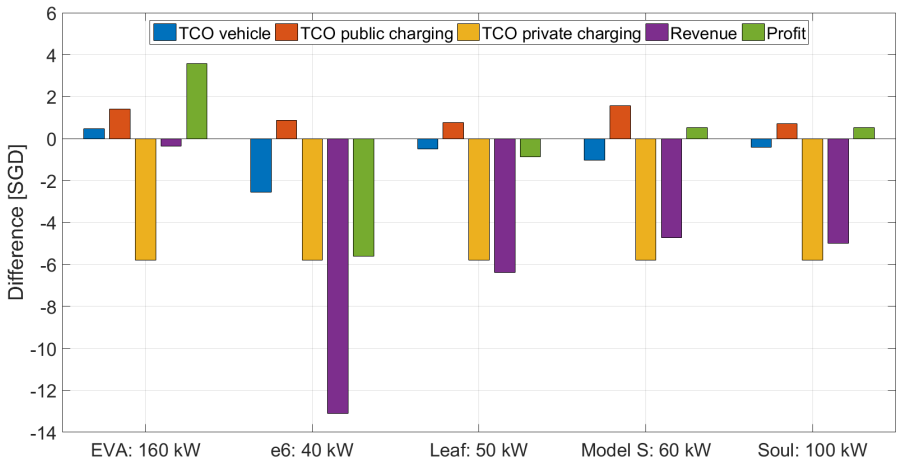

Figure 8.11: Difference in economic key values per taxi and day between charging infrastructures without and with *home charging* for 2,949 taxis

A comparison between charging infrastructures with and without *home charging* regarding vehicle costs, infrastructure costs, revenue, and profit is shown in Figure 8.11. The values for optimised infrastructures with *home charging* were subtracted from these without *home charging*. Hence, positive differences mean that the value without *home charging* is higher.

The yellow bars represent the difference in the Total Costs of Ownership (TCO) of the private charging infrastructure which is zero in case of no *home charging* and include the costs of one 6.6 kW charging station per taxi in case of *home charging*. Since the costs of one of these charging stations were estimated to 5.80 SGD per day, the overall charging infrastructure costs were significantly increased by this option. However, as agents had the chance to recharge the battery during *shift changes*, the *charging demand* at *public charging stations* was reduced and therewith their required number and costs. The

public charging infrastructure savings (red bars) ranged from 0.7 to 1.6 SGD per day and taxi.

Moreover, *home charging* also allowed agents of all vehicle types (except EVA) to reach higher mileage and revenue. Due to the higher mileage, the vehicle costs increased by 0.4 to 2.6 SGD per day, while the revenue increased by 4.7 to 13.1 SGD per day. The reason why EVA's mileage and revenue almost remained the same is that its onboard charger is only designed for 3.3 kW (Bender et al., 2014), hence it benefited much less from *home charging* than all other vehicle types.

Balancing all costs with the revenue changes showed that *home charging* could significantly increase the profit of BYD e6 taxis by up to 5.6 SGD per day, while Nissan Leaf, Kia Soul, and Tesla Model S taxis would generate almost the same profit ($\pm$0.9 SGD per day). Due to EVA's onboard charging limitation, taxis of this type would generate 3.6 SGD per day less profit with *home charging*.

The reason why *home charging* only significantly improved the profitability of BYD e6 taxis is that agents of this vehicle would have to expand their usual *breaks* significantly due to the higher energy consumption and lower public charging power of 40 kW. Thus, *home charging* reduced the charging time during *shifts* considerably which would give the agents more time to generate revenue.

Considering that *home charging* would require to place one charging station at each driver's home which causes significant effort and higher investment costs, this option is only favourable if the overall profit can be increased. This was only the case for BYD e6 taxis.

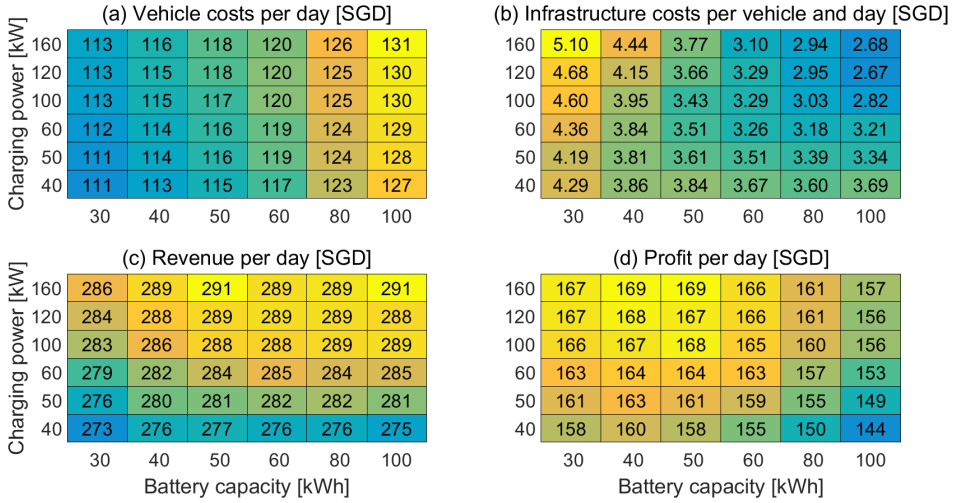

Figure 8.12: Vehicle costs (a), infrastructure costs (b), revenue (c), profit (d) per taxi and day with respect to battery capacity and charging power

An overview of economic key figures with respect to the taxis' battery capacity and charging power for 2,949 EVA taxis without *home charging* is depicted by Figure 8.12. Part (a) shows the vehicle costs per day, (b) the charging infrastructure costs per taxi and day, the simulated revenue per day is shown in (c), and (d) depicts the profit per day.

The vehicle costs increased with respect to the battery capacity due to increased

battery costs and with respect to the charging power as the mileage and therewith the energy costs increased.

The costs per taxi to use the charging infrastructure (excluding energy costs) ranged between 2.68 and 5.10 SGD per day. Hence, although the optimised charging station utilisation was with 29 to 33% relatively low, the charging infrastructure costs per taxi amounted only 2.0 to 4.5% of the vehicle costs. As the number of charging stations decreased with higher battery capacities (see Figure 8.3), the infrastructure costs decreased as well. Between taxis with 30 and 100 kWh batteries, these costs decreased by 47% for 160 kW charging stations.

Interestingly, the charging power with the lowest infrastructure costs increased with the battery capacity. For 30 kWh batteries, the lowest costs were 4.19 SGD per day for 50 kW charging power, whereby in case of 60 kWh the lowest costs were 3.10 SGD per day for 160 kW charging stations. This is because there is an intercept in the charging station costs estimation which reduces the costs per kW with increasing charging power. Hence, charging stations with high power are more cost efficient. However, as discussed by Figure 8.7, the ratio of charging duration over total use duration increased with respect to the battery capacity and decreased with the charging power. Thus, for small battery sizes, the latter effect outweighs the first, whereas its influence decreases with higher battery capacities which led to lower infrastructure costs for higher charging power.

Figure 8.12(c) shows that electric taxis with a battery capacity of at least 40 kWh and charging power of at least 100 kW could reach almost the same revenue as conventional taxis (292 SGD per day). The most significant revenue increase of 4.8 SGD per day appeared when the charging power was increased from 40 to 50 kW. Whereby, another increase to 60 kW caused a smaller revenue increase of only 2.8 SGD per day.

The profit per taxi and day in (d) was calculated by deducting the vehicle and infrastructure costs from the revenue. It shows that the highest profit was reached for a battery capacity of 50 kWh and a charging power of 160 kW. Nevertheless, the profit with a charging power of 100 kW and the same battery capacity was only 0.8 SGD per day lower. Taken into account that the battery would deteriorate faster with higher charging power (Trippe et al., 2014), this configuration should have a higher practical relevance. Comparing other battery capacities shows that an increase from 100 kW to 160 kW charging power had in general very little effect on the revenue.

While taxis with 40 or 50 kWh batteries had very similar profit, the profit decreased for 60 kWh or higher battery capacities. This is due to the ARF which is 180% for the OMV exceeding an amount of 50,000 SGD (Chapter 6.1). As EVA's OMV was estimated to 50,982 SGD for a battery capacity of 50 kWh, every increase in battery costs is taxed with 180%. This significantly downgrades the economic potential of configurations with higher battery capacities.

Chapter 9

Summary and discussion

This chapter finalises this thesis. Chapter 9.1 summarises the approach and the main findings of this thesis. Following, Chapter 9.2 discusses its main uncertainties while Chapter 9.3 suggests extensions of the presented approach to reduce these uncertainties. Finally, Chapter 9.4 presents the conclusion of this thesis.

9.1 Summary

This thesis proposed a method to optimise a charging infrastructure for electric taxis and applied this method in the context of Singapore. Thereby, the ideal number of charging stations per location is optimised by minimising waiting time and detour costs of electric taxi drivers as well as charging infrastructure costs. To optimise the charging infrastructure, a bi-level simulation-optimisation approach was chosen. Therefore, an agent-based driving profile simulation model was developed to estimate the taxis' *charging demand*.

In order to simulate driving profiles of electric taxis, a detailed understanding of the driving patterns of conventional taxis is essential. To gain this knowledge, two data sets were analysed. The first data set consists of 50 taxis which were equipped with GPS loggers that recorded the taxis' location and speed with a frequency of one data point per second over a period of six months. Additionally this data set was synchronised with the taxis' status and revenue. Due to the high recording frequency, this data set is denoted as High Frequency Data set (HFD). The second data set, denoted as Low Frequency Date set (LFD) contains status and location information of 2,973 taxis over a period of one month with an average recording frequency of one data point every three minutes.

The taxi drivers' activity pattern are described by *shift schedules* which were derived from the LFD. *Shift schedules* contain the information when and where a driver started and ended his or her *shift* as well as when, where, and how long drivers interrupted their *shift* to have *breaks*. In total, 149,960 *shift schedules* were extracted. Furthermore, a density clustering algorithm was applied on all *breaks* and *shift change locations* to identify the drivers' most frequently chosen locations. In order to ensure that drivers can combine their *breaks* with recharging the vehicle's battery, the infrastructure optimisation is constraint to place charging stations at only these locations.

In order to get more detailed insights into the drivers' behaviour, in total 227,971 *search* and *engaged trips* were extracted from the HFD. Due to the high recording frequency, these trips contain detailed information about the taxis' route choices and

driving speeds. To emulate the driving behaviour of the simulated agents, these trips are assigned to the agents with respect to their location and time. Thereby, not only real traffic conditions but also the demand for taxis is considered by sampling recorded trips. For example, if the agent is currently in an area with low demand it is likely that a long *search trip* will be assigned to it next.

Furthermore, all data points of the HFD were map-matched to Singapore's street network. On basis of *street network segments* which directly connect two intersections with each other, statistics regarding the distribution of *pass-through speeds*, accelerations, and *driving shares* were created.

Due to their limited range and long charging times, it is very important to accurately simulate the energy consumption and charging process of electric vehicles. Therefore, a speed-based approach was proposed which estimates the energy consumption with respect to a given speed profile extracted from the recorded data. The simulated energy consumption of this model deviated by less than 3% from the measured consumption of the Nissan Leaf.

Moreover, a route-based approach was proposed which utilises the extracted traffic statistics. This model estimates the energy consumption with respect to a selected route and the *pass-through speeds* of each *street segment*. Compared to the speed-based model, this approach requires much less detailed information, in turn its root mean square error is approximately 14% higher than that of the speed-based approach. This model is applied in the driving profile simulation whenever agents have to drive to a specific location and the sampling of recorded trips is not possible.

The agent-based driving profile simulation model was built on a supply-based approach. Meaning that it uses the recorded driving profiles of conventional taxis as input and reproduces them unless the agents need to recharge the battery. Therefore, a *standstill behaviour model* and a *charging behaviour model* was implemented to simulate the agent's behaviour. The *standstill behaviour model* is responsible that the agent follows the activity pattern described by the *shift schedule* which is assigned to the agent. Hence, it decides when and where the agent has to make a *break* or *shift change*.

The *charging behaviour model* has to ensure that the agent never runs out of energy. Therefore, it decides when and where the agent has to recharge which amount of energy. Since maintaining a minimum range at any time has a higher priority than respecting the *shift schedule*, the *charging behaviour model* may overrule the *standstill behaviour model*. The more critical electric vehicle specific restrictions regarding range and charging time become, the more often the *charging behaviour model* overrules the *standstill behaviour model* and the stronger electric taxi driving profiles diverge from that of conventional taxis.

Due to the lack of data regarding electric taxi driving profiles, the driving profile model could not be directly validated for electric taxis. However, conventional taxis were simulated by ignoring the vehicle's energy consumption and disabling the *charging behaviour model*. The comparison of the simulation results with the recorded data showed that the introduced model is capable of accurately reproducing driving profiles of conventional taxis, i.a. the average simulated mileage diverged by less than 3% from the recorded mileage.

Furthermore, a case study showed that for a specific charging infrastructure which allows short detours, charging times, and waiting times, the simulated electric taxis reached almost equal revenue as conventional taxis. However, by increasing the number

of agents utilising this infrastructure, the simulated revenue monotonically decreased. Thus, the intended divergence of the simulated driving profiles of electric taxis due to increasing obstacles is well illustrated by this case study.

In order to assess the overall economic potential of electric taxis including infrastructure costs, Total Cost of Ownership (TCO) models for taxis (Kochhan, 2017) and charging stations were used. Comparing the TCO of electric taxis with conventional taxis showed that all vehicles considered in this thesis (excluding Tesla Model S) have lower total costs than the Toyota Prius which is commonly used as taxi in Singapore today. Thereby, the main advantage of electric vehicles are their energy costs which are up to 60% lower than that of the Toyota Prius. Vehicle individual cost parameter were derived from the TCO models to parametrise the objective function of the charging infrastructure optimisation.

The infrastructure optimisation is formulated as a multiple server allocation problem and decides how many charging station shall be placed at each *candidate charging location* in order to minimise the taxis' detour and waiting time costs as well as the charging infrastructure costs. The optimisation is done in three steps while at the beginning of each step a simulation is executed to extract the taxis' spatial-temporal *charging demand* which is described by the required use duration of charging stations.

First, among the pre-defined *candidate charging locations* a subset of locations is chosen where charging stations shall be placed. Therefore, the allocation of the *charging demand* to each *charging location* is optimised at the same time. The problem is formulated as a mixed-integer linear program which minimises detour and charging infrastructure costs. Waiting times are considered by a linear constraint which requires a sufficient number of charging stations to ensure zero waiting time.

After the selection of *charging locations*, another simulation is run in order to quantify the time dependent *charging demand* at each selected *charging location*. As no *charging demand* allocation is required in this step, the ideal number of charging stations can be optimised for each location independently. Therefore, a non-linear objective function including waiting time costs is used.

The optimisation results showed that the optimised charging infrastructures ensured average waiting times of less than 2.1 min per charging event. Hence, it is expected that although constraining the waiting times to zero at the first optimisation step, the selection of locations should have been already close to the global optimum. Nevertheless, a *charging demand* reallocation step is executed to check if the resulting increase of detour costs by removing *charging locations*, can be overcompensated by an overall lower number of charging stations and therewith lower infrastructure costs. If *charging locations* are removed, the second optimisation step is repeated, otherwise the optimisation is finished.

The optimised number of charging stations for 2,949 taxis ranged from 278 for EVA to 752 for BYD e6 taxis. The main reason for this wide spread is that EVA taxis are considered to be charged with 160 kW while BYD e6 taxis had a charging power of only 40 kW. Regarding the chosen locations it was found out that a homogeneously dense network of *charging locations* is ideal. Spatial differences are mainly reflected by the number of charging stations per location: near the city centre and at the airport were the *charging locations* with the highest number of charging stations (up to 12 for EVA taxis) while *charging locations* in outer regions had only two to four charging stations.

Furthermore, infrastructure extension scenarios were analysed. Within these scen-

arios first a charging infrastructure for a small number of taxis was optimised and afterwards extensions of this infrastructure were optimised for an increasing number of taxis. These scenarios showed in general that for small fleet sizes of 50 taxis disproportionately high numbers of charging stations were selected so that the average charging station utilisation ranged between 16 and 19%. The charging station utilisation increased with higher numbers of taxis while its slope continuously decreased. Apparently, at approximately 500 taxis, this ratio saturated. The charging infrastructure investment costs for a fleet of 2,949 taxis ranged for different vehicle types between 30 and 49 million SGD.

Simulations were run for all optimised charging infrastructures to analyse the taxis' driving profiles and their economic potential for different vehicle types and fleet sizes. The average mileage and revenue of electric taxis significantly increased between 50 and 300 taxis and saturated thereafter. EVA taxis reached almost the same values of conventional taxis while BYD e6 taxis had the highest mileage and revenue deviation of 35 km and 30 SGD less per day and taxi. These differences were mainly caused by their higher energy consumption and lower charging power.

The economic profit per taxi is calculated by balancing the taxis' revenue with vehicle costs and charging infrastructure costs. Due to the lower achievable revenue, the estimated profit per day of BYD taxis was 32 SGD below that of Toyota Prius taxis. The estimated profit of Tesla Model S taxis was even 38 SGD per day lower than that of the Prius. However, this difference was caused by the Tesla's higher price which has due to the high registration taxes in Singapore a very strong impact on the total costs. The difference of the profit of EVA, Kia Soul, and Nissan Leaf taxis to the Toyota Prius ranged between 1 SGD less and 7 SGD more per day whereby EVA was the taxi with the highest profit. Although the simulated revenue of EVA taxis was up to 17 SGD per day higher than that of the Kia Soul and Nissan Leaf, its economic profit was diminished by the higher purchasing price and the therewith related higher taxes.

To understand the effect of the vehicle's battery capacity and charging power on the taxis driving profiles and ultimately on the achievable profit, multiple infrastructures were optimised for vehicles with different battery capacities and charging stations of different power. Simulations were run to evaluate the taxis' driving profiles and potential profit. The results showed that taxis of a battery capacity of 50 kWh and a charging power of 100 kW would have the best economic potential. This configuration allows to closely reproduce the same driving profiles of conventional taxis. Hence, higher battery capacities or charging power would unnecessarily increase vehicle or charging infrastructure costs.

9.2 Main Uncertainties

From an economic point of view, lower energy costs are the main advantage of electric taxis over conventional taxis. Hence, the comparison of these vehicle concepts is highly sensitive on fuel and electricity prices. Since especially the oil price fluctuates strongly and the estimated economic potential of conventional and electric taxis was found to be roughly equal, future changes in the energy prices could cause significant differences among these concepts.

An aspect which is important in the context of Singapore is that so far no electric vehicles are on the market. Therefore, there are no official values for their Open Market Value (OMV). The OMV was used as basis for the calculation of the vehicle acquisition

taxes. As these taxes considerably exceed 100% of the OMV, the vehicle's total costs are very sensitive with respect to the OMV. In this thesis the OMV is estimated on basis of a price comparison between conventional vehicles in other country and their OMV in Singapore and the price of electric vehicles in the respective countries. These estimations may significantly deviate from the OMV of electric vehicles once they are available on the Singaporean market.

Another important cost factor are the charging station installation costs. In this thesis it was assumed that these costs solely depend on the charging station's power, whereby cost reductions due to installing several charging stations at the same place or location specific considerations (e.g. cable length to grid connection point) were neglected for reasons of simplicity. If cost reductions for several stations at the same location were considered the optimised total number of *charging locations* would have been smaller. Furthermore, it is expectable that the inclusion of location specific consideration would have caused a different selection of *charging locations*.

Apart from cost uncertainties, a further source of uncertainty is the battery ageing. The applied vehicle TCO model only considers mileage related battery ageing while the effect of the charging power is not taken into account. As a wide range of different charging powers from 40 kW to 160 kW was analysed in this thesis it must be expected that batteries charged with higher power will degrade considerably faster. As a result, these vehicles would require more battery replacements which as a consequence downgrades their economic competitiveness. Taking this into account, it is expectable that EVA's economic advantage over the Kia Soul and Nissan Leaf would become smaller and may vanish completely. Furthermore, the recommended vehicle configuration of a 50 kWh battery and 100 kW charging power may need to be adjusted towards higher battery capacity and lower charging power.

The implemented charging behaviour is based on the assumption that drivers would stick to the same activity patterns (*shift schedules*) as if they used a conventional vehicle and combine their *breaks* by recharging the battery. This assumption could not be proofed due to the lack of electric taxi driving profile data. Hence, it is certainly possible that electric taxi drivers would alter their activity patterns in order to recharge their vehicle at different times and locations. These changes affect their driving profiles and achievable revenue, which in turn have an effect on the economic competitiveness of electric taxis. Furthermore, a different *charging demand* would result from these changes which impose other requirements on the charging infrastructure and as a consequence lead to a different charging infrastructure design.

Last but not least, it must be kept in mind that the implemented driving profile simulation model is calibrated to reproduce today's taxi driving profiles. An evolution of these driving profiles induced by i.a. changing customer travel demand, urban planning alterations, or regulation changes are not taken into consideration. In the context of Singapore there is a number of aspects which either today or in future will influence the taxi business i.a.:

- Regulation changes on the taxi availability standard (LTA, 2016a)
- Competition by private hire car drivers (Cheng, 2017)
- Launch of autonomous taxis (The Online Citizen, 2017)
- Extension of Mass Rapid Transit (MRT) network (LTA, 2013a)

– Setting up a second Central Business District (CBD) (The Straits Times, 2017)

It is expected that all these aspects will have an effect on the economic competitiveness of electric taxis and the ideal charging infrastructure design.

9.3 Future Work

The introduced driving profile simulation model is capable of producing load curves for each *charging location* individually. These load curves could be given as input to a power flow simulation model (Ciechanowicz et al., 2017) in order to evaluate the effect of charging an electric taxi fleet on the power grid. The results of this simulation could be used to derive constraints regarding location individual maximum number of charging stations. These constraints in turn could be integrated in the charging infrastructure optimisation in order the ensure the grid stability of the found solution.

Moreover, it is also possible to extract time dependent charging and discharging currents of the vehicle's battery and the battery's State Of Charge (SOC) from the simulation results. These curves could be given as input to a battery ageing model (Trippe et al., 2014) in order to evaluate the effect of the chosen charging power on the battery degradation. The results could be forwarded to the vehicle TCO model to balance charging time costs with battery replacement costs.

A significant improvement of the proposed driving profile simulation model would be to calibrate and validate the *charging behaviour model*. Therefore, driving profiles of electric taxi drivers are indispensable. There is an electric taxi test bed running in Singapore already (Lim, 2016). However, in contrast to all other Singaporean taxi drivers, the participating drivers of this test are employed by a company and have to follow pre-defined *shift schedules*. Thus, data from this test would not allow to analyse how self-employed drivers who are free to choose when and how long they want to work would alter their driving profiles when using an electric vehicle.

In order to get better insights on how taxi drivers would adapt their behaviour, it would be very helpful to first record and analyse their driving profiles while using a conventional vehicle. Afterwards, their usage of an electric vehicle shall be recorded as well. Thereby, it is important to not only track the driving profiles but also the battery's SOC in order to get the chance to analyse which of the driver's decisions were triggered by the SOC and how much energy the driver recharged at charging events. The comparison of conventional and electric taxi driving profiles would allow to i.a. extract how drivers would change their activity patterns, when and where they prefer to recharge the battery, and at which remaining range they decide to recharge the battery.

The implemented supply-based approach of the driving profile simulation model is restricted to reproduce the taxi customer demand at the time of the data recording. Thus, future developments mentioned in the previous section cannot be taken into account with this approach. In order to study the implications of these developments on electric taxis a more general demand-based approach would be necessary.

Therefore, the commuters' travelling demand would have to be given as input to the taxi simulation model which had to simulate how the taxi driver agents serve this demand. Thereby, search strategies of taxi agents to find the next customer would have to be implemented while the assignment of recorded trips is not possible any more. As a consequence, the simulation model would become more complex. Therefore,

computational performance challenges may have to be tackled when integrating this model in the charging infrastructure optimisation.

The taxi commuter travel demand could be generated by a multi-modal simulation model like MATSim (Horni et al., 2016). Thereby, plenty of aspects like demographic changes, urban planning alterations, and transportation network extensions can be reflected in the generated demand for taxis. Ideally, the taxi simulation model could be integrated in a multi-modal simulation to feedback commuter waiting times, travel durations, and costs so that the travel mode choice of the simulated commuter agents could be iteratively adjusted with respect to the quality of the taxi service.

9.4 Conclusion

The simulation results showed that electric vehicles which are already available on the market have the potential of covering 95%[1] of the mileage of today's conventional taxis in Singapore. Therefore, a charging infrastructure which is especially designed for this application is essential. An economically ideal operation is only possible if enough charging stations are available to reduce average waiting times below two minutes per charging event. Although the consequence of this requirement is that the average charging station utilisation would be less than 32%, the therewith related infrastructure costs can be overcompensated by the additional revenue electric taxi drivers can achieve.

Electric taxi drivers can cover a high share of the conventional taxis' mileage while following the same activity patterns of conventional taxi drivers. Breaks can be made at the same time and with the same duration and no additional working time would be required. Thus, if a suitable charging infrastructure is available, it is expectable that electric taxi drivers would not have to experience significant inconveniences caused by range limitations or long charging times. A pure electric taxi fleet in Singapore (27,534 taxis) could save 694,000 tons of CO_2 emissions per year (electricity production related emissions included) compared to an entirely diesel fuelled fleet and 150,000 tons per year compared to a fleet exclusively consisting of hybrid vehicles.

By taking achievable revenue as well as vehicle and charging infrastructure costs into account, today's electric vehicles would enable taxi drivers to generate the almost identical profit as conventional taxi drivers. Thereby, the lower achievable revenue of electric taxis would be compensated by up to 60% lower energy costs. Nevertheless, it must be kept in mind that the investment costs for a charging infrastructure designed for 2,949 taxis ranges between 30 and 49 million SGD. Hence, there is a considerable risk of investment which could not be justified by a higher profitability of today's electric vehicles.

However, a new generation of electric vehicles will be soon or is already available on the market. Most relevant for the use case of taxis would be the Chevrolet Bolt (Chevrolet, 2017), Tesla Model 3 (Tesla, 2017a) and the next generation Nissan Leaf (Nissan, 2017b). These vehicles offer higher range and charging power for comparable prices to the vehicles analysed in this thesis.

Although taxi driving profiles impose due to their high mileage and short standstill times challenging requirements on electric vehicles, it is expectable that the overall economic potential of these vehicle models will surpass that of conventional vehicles.

[1] simulation result of Kia Soul taxis with a charging infrastructure optimised for 600 taxis

Due to that progress and higher production figures which are related to lower prices, mass market electric vehicles have a higher potential to prevail in this use case than custom designed vehicles with significantly lower production figures.

Even though battery prices are anticipated to fall further, the purchasing prices of electric vehicles are not expected to fall below conventional vehicle prices before 2025 (Wu et al., 2015). This means in the context of Singapore that higher registration taxes would have be to be paid for electric vehicles due to the Additional Registration Fee (ARF) which amounts to at least 100% of the vehicle's Open Market Value (OMV). Furthermore, the scheme of the ARF significantly affects the competitiveness of electric taxis which are more expensive due to higher battery capacities. However, the simulation results showed that vehicles with higher battery capacities could utilise the charging infrastructure more efficiently and therewith save up to 47% of charging infrastructure costs.

There is a Carbon Emission-Based Vehicle Scheme (CEVS) in Singapore which grants incentives to low-emission vehicles. However, the lowest tier granting the highest incentives is 95 gCO_2/km (LTA, 2015a) which can also be undercut by hybrid vehicles. Further tax incentives for electric vehicles could be justified by their additional CO_2 saving potential compared to hybrid vehicles. Therefore, one option could be to exclude an amount relative to the vehicle's battery capacity from the ARF calculation. Thereby, the economic competitiveness of electric taxis with high battery capacities would not be affected and charging infrastructure costs could be saved.

Bibliography

Ahn, Y., Yeo, H., 2015. An analytical planning model to estimate the optimal density of charging stations for electric vehicles. PloS One 10 11.
URL http://journals.plos.org/plosone/article?id=10.1371/journal.pone.0141307

Arthur, D., Vassilvitskii, S., 2007. K-means++: The advantages of careful seeding. In: Proceedings of the Eighteenth Annual ACM-SIAM Symposium on Discrete Algorithms. SODA '07. Society for Industrial and Applied Mathematics, Philadelphia, PA, USA, pp. 1027–1035.
URL http://dl.acm.org/citation.cfm?id=1283383.1283494

Asamer, J., Reinthaler, M., Ruthmair, M., Straub, M., Puchinger, J., 2016. Optimizing charging station locations for urban taxi providers. Transportation Research Part A: Policy and Practice 85, 233 – 246.
URL http://www.sciencedirect.com/science/article/pii/S0965856416000239

Association Tokyo Hire-Taxi, 2015. Tokyo's taxis. Tech. rep.
URL http://www.taxi-tokyo.or.jp/english/datalibrary/pdf/hakusyo2015all_en.pdf

Bender, S., Pannirsilvam, V., Khoo, R., Hidalgo, P. L., Tschochner, M., Pratik, S., Osswald, S., Gleyzes, D., Ng, H. W., Lienkamp, M., 2014. Concept of an electric taxi. In: 3rd Conference on Future Automotive Technology (CoFAT'14).

Berman, O., Drezner, Z., 2007. The multiple server location problem. Journal of the Operational Research Society 58 (1), 91–99.
URL http://dx.doi.org/10.1057/palgrave.jors.2602126

Bi, Z., Kan, T., Mi, C. C., Zhang, Y., Zhao, Z., Keoleian, G. A., 2016. A review of wireless power transfer for electric vehicles: Prospects to enhance sustainable mobility. Applied Energy 179, 413 – 425.
URL http://www.sciencedirect.com/science/article/pii/S0306261916309448

Bischoff, J., Maciejewski, M., 2014. Agent-based simulation of electric taxicab fleets. Transportation Research Procedia 4, 191 – 198.
URL http://dx.doi.org/10.1016/j.trpro.2014.11.015

BYD, 2014. BYD Magazine.
URL bydeurope.com/downloads/download.php?filename=BYDAUTOMagazine8.pdf

BYD, 2015. BYD brings world leading pure electric taxi to Brussels. Retrieved on 3.8.2017.
URL http://www.bydeurope.com/news/news.php?action=readnews&page=2&nid=192

BYD, 2017. Byd e6. Retrieved on 3.8.2017.
URL http://www.byd.com/ap/images/e6/download/e6%20brochure.pdf

Carspring, 2017. 2017 taxi price index. Retrieved on 2.8.2017.
URL https://www.carspring.co.uk/taxi-price-index-usd/

Chan, H. L., 2000. A new battery model for use with battery energy storage systems and electric vehicles power systems. In: 2000 IEEE Power Engineering Society Winter Meeting. Conference Proceedings (Cat. No.00CH37077). Vol. 1. pp. 470–475 vol.1.

Chen, M., Rincon-Mora, G. A., June 2006. Accurate electrical battery model capable of predicting runtime and i-v performance. IEEE Transactions on Energy Conversion 21 (2), 504–511.

Cheng, K., 2017. Comfortdelgro's taxi fleet down to seven-month low. Retrieved on 3.10.2017.
URL http://www.todayonline.com/singapore/comfortdelgros-taxi-fleet-down-seven-month-low

Chevrolet, 2009. Chevrolet launches diesel powered Capative and Epica. Press release, retrieved on 17.11.2015.
URL http://chevrolet.com.sg/pr/local/PR-09-02-26-Chevrolet_Captiva_Diesel_and_Epica_Diesel.pdf

Chevrolet, 2017. Bolt EV 2017. Retrieved on 5.10.2017.
URL http://www.chevrolet.com/content/dam/chevrolet/na/us/english/index/shopping-tools/download-catalog/02-pdf/2017-chevrolet-bolt-ev-catalog.pdf

Choi, S. Y., Gu, B. W., Jeong, S. Y., Rim, C. T., March 2015. Advances in wireless power transfer systems for roadway-powered electric vehicles. IEEE Journal of Emerging and Selected Topics in Power Electronics 3 (1), 18–36.

Chung, S. H., Kwon, C., 2015. Multi-period planning for electric car charging station locations: A case of Korean expressways. European Journal of Operational Research 242 (2), 677 – 687.
URL http://www.sciencedirect.com/science/article/pii/S0377221714008509

Church, R. L., ReVelle, C., 1974. The maximum covering location problem. Papers in Regional Science 32.

Ciechanowicz, D., Pelzer, D., Bartenschlager, B., Knoll, A., May 2017. A modular power system planning and power flow simulation framework for generating and evaluating power network models. IEEE Transactions on Power Systems 32 (3), 2214–2224.

Columbus, 2017. Columbus V-990. Retrieved on 5.8.2017.
URL http://www.columbus-gps.de/produkte/columbus-v-990-gps-logger/

Commission Taxi & Limousine, 2014. Taxicab factbook. Tech. rep.
URL http://www.nyc.gov/html/tlc/downloads/pdf/2014_taxicab_fact_book.pdf

Crowe, P., 2013a. 15 Nissan Leaf for Rio de Janeiro taxi duty. Retrieved on 3.8.2017.
URL http://www.hybridcars.com/15-nissan-leaf-for-rio-de-janeiro-taxi-duty/

Crowe, P., 2013b. Mexico's Leaf taxi pilot program well received. Retrieved on 3.8.2017.
URL http://www.hybridcars.com/mexicos-leaf-taxi-pilot-program-well-received/

Crowe, P., 2014. Nissan EV taxis for Madrid and Barcelona. Retrieved on 3.8.2017.
URL http://www.hybridcars.com/nissan-ev-taxis-for-madrid-and-barcelona/

Cruz-Zambrano, M., Corchero, C., Igualada-Gonzalez, L., Bernardo, V., May 2013. Optimal location of fast charging stations in Barcelona: A flow-capturing approach. In: 2013 10th International Conference on the European Energy Market (EEM). pp. 1–6.

Czypulovski, L., 2017. Analysis of charging strategies for electric taxis. Master's thesis, Technical University of Munich.

de Vries, H., Duijzer, E., 2017. Incorporating driving range variability in network design for refueling facilities. Omega 69, 102 – 114.
URL http://www.sciencedirect.com/science/article/pii/S030504831630490X

Department of Statistics Singapore, 2016a. Population trends 2016. Tech. rep.
URL http://www.singstat.gov.sg/docs/default-source/default-document-library/publications/publications_and_papers/population_and_population_structure/population2016.pdf

Department of Statistics Singapore, 2016b. Singapore in figures 2016. Tech. rep.
URL https://www.singstat.gov.sg/docs/default-source/default-document-library/publications/publications_and_papers/reference/sif2016.pdf

Dormand, J., Prince, P., 1980. A family of embedded Runge-Kutta formulae. Journal of Computational and Applied Mathematics 6 (1), 19 – 26.
URL http://www.sciencedirect.com/science/article/pii/0771050X80900133

Edelstein, S., 2013. Nissan's Leaf will make Zurich's taxi fleet greener, but not how you think. Retrieved on 3.8.2017.
URL https://www.digitaltrends.com/cars/nissans-leafs-will-make-zurichs-taxi-fleet-greener-but-not-how-you-think/

Egbue, O., Long, S., 2012. Barriers to widespread adoption of electric vehicles: An analysis of consumer attitudes and perceptions. Energy Policy 48, 717 – 729, special Section: Frontiers of Sustainability.
URL http://dx.doi.org/10.1016/j.enpol.2012.06.009

Energy Market Authority, 2016. Singapore energy statistics 2016.
URL https://www.ema.gov.sg/cmsmedia/Publications_and_Statistics/Publications/SES/2016/Singapore%20Energy%20Statistics%202016.pdf

Engholm, A., Johansson, G., Persson, A. A., 2013. Life cycle assessment of solelia green-tech's photovoltaic based charging station for electric vehicles. Tech. rep., Uppsala Universitet.
URL http://www.diva-portal.org/smash/get/diva2:626019/FULLTEXT01.pdf

EPA, 2016. Data on cars used for testing fuel economy. Retrived on 10.8.2016.
URL https://www.epa.gov/compliance-and-fuel-economy-data/data-cars-used-testing-fuel-economy

EPA, 2017. Dynamometer driving schedules. Retrieved on 23.8.2017.
URL https://www.epa.gov/vehicle-and-fuel-emissions-testing/dynamometer-drive-schedules

ERI@N, 2016. E-mobility technology roadmap. Tech. rep.
URL https://www.nccs.gov.sg/sites/nccs/files/Roadmap_E-M_1.pdf

Falvo, M. C., Sbordone, D., Bayram, I. S., Devetsikiotis, M., June 2014. EV charging stations and modes: International standards. In: 2014 International Symposium on Power Electronics, Electrical Drives, Automation and Motion. pp. 1134–1139.

Fritsch, F. N., Carlson, R. E., 1980. Monotone piecewise cubic interpolation. SIAM Journal on Numerical Analysis 17 (2), 238–246.
URL https://doi.org/10.1137/0717021

Gacias, B., Meunier, F., 2015. Design and operation for an electric taxi fleet. OR Spectrum 37 (1), 171–194.
URL http://dx.doi.org/10.1007/s00291-014-0362-y

Genovese, A., Ortenzi, F., Villante, C., 2015. On the energy efficiency of quick DC vehicle battery charging. In: EVS28.

Giannelli, R. A., Nam, E. K., Helmer, K., Younglove, T., Scora, G., Barth, M., 11 2005. Heavy-duty diesel vehicle fuel consumption modeling based on road load and power train parameters. In: SAE Technical Paper. SAE International.
URL http://dx.doi.org/10.4271/2005-01-3549

Glanzer, G., Sivaraman, T., Buffalo, J. I., Kohl, M., Berger, H., May 2011. Cost-efficient integration of electric vehicles with the power grid by means of smart charging strategies and integrated on-board chargers. In: 2011 10th International Conference on Environment and Electrical Engineering. pp. 1–4.

Google, 2017. Singapore. Retrieved on 8.8.2017.
URL https://www.google.com.sg/maps/place/Singapore/

Gurobi Optimization, Inc., 2016. Gurobi optimizer reference manual.
URL http://www.gurobi.com

Hadzhistoykov, M., 2015. First electric taxi in Sofia - Kia Soul EV is now an official Yellow Taxi. Retrieved on 3.8.2017.
URL http://www.ecars.bg/en/1216-kia-soul-ev-electric-yellow-taxi

Han, D., Ahn, Y., Park, S., Yeo, H., 2016. Trajectory-interception based method for electric vehicle taxi charging station problem with real taxi data. International Journal of Sustainable Transportation 10 (8), 671–682.
URL http://dx.doi.org/10.1080/15568318.2015.1104565

Hanley, S., 2015. Taxelco will provide all electric taxi service to Montreal. Retrieved on 3.8.2017.
URL https://ecomento.com/2015/11/27/taxelco-will-provide-all-electric-taxi-services-to-montreal/

Hayes, J. G., Davis, K., June 2014. Simplified electric vehicle powertrain model for range and energy consumption based on EPA coast-down parameters and test validation by Argonne National Lab data on the Nissan Leaf. In: 2014 IEEE Transportation Electrification Conference and Expo (ITEC). pp. 1–6.

Hayes, J. G., de Oliveira, R. P. R., Vaughan, S., Egan, M. G., Sept 2011. Simplified electric vehicle power train models and range estimation. In: 2011 IEEE Vehicle Power and Propulsion Conference. pp. 1–5.

Hodgson, M. J., 1990. A flow-capturing location-allocation model. Geographical Analysis 22 (3), 270–279.
URL http://dx.doi.org/10.1111/j.1538-4632.1990.tb00210.x

Horni, A., Nagel, K., Axhausen, K., 2016. The Multi-Agent Tranport Simulation MATSim. Ubiquity Press.

Huifeng, H., 2015. Shenzhen offers new incentives to boost switch to electric taxis. Retrieved on 3.8.2017.
URL http://www.scmp.com/tech/innovation/article/1775381/shenzhen-offers-new-incentives-boost-switch-electric-taxis

Hwang, S. W., Kweon, S. J., Ventura, J. A., 2017. Locating alternative-fuel refueling stations on a multi-class vehicle transportation network. European Journal of Operational Research 261 (3), 941 – 957.
URL http://www.sciencedirect.com/science/article/pii/S0377221717301583

Inland Revenue Authority of Singapore, 2017. Goods and Service Tax (GST): What it is and how it works. Retrieved on 18.10.2017.
URL https://www.iras.gov.sg/IRASHome/GST/GST-registered-businesses/Learning-the-basics/Goods-and-Services-Tax--GST---What-It-Is-and-How-It-Works/

Jiang, Y., Zhang, Y., Zhang, C., Fan, J., 2012. Capacitated deviation-flow fueling location model for sitting battery charging stations. In: CICTP 2012. pp. 2771 – 2778.
URL http://ascelibrary.org/doi/abs/10.1061/9780784412442.282

Jones, P. T., Onar, O., Dec 2014. Impact of wireless power transfer in transportation: Future transportation enabler, or near term distraction. In: 2014 IEEE International Electric Vehicle Conference (IEVC). pp. 1–7.

Jung, J., Chow, J. Y., Jayakrishnan, R., Park, J. Y., 2014. Stochastic dynamic itinerary interception refueling location problem with queue delay for electric taxi charging stations. Transportation Research Part C: Emerging Technologies 40, 123 – 142.
URL http://www.sciencedirect.com/science/article/pii/S0968090X14000126

Jung, J., Jayakrishnan, R., Choi, K., 2012. Shard-taxi operations with electric vehicles.
URL http://www.its.uci.edu/its/publications/papers/ITS/UCI-ITS-WP-13-1.pdf

Kerns, J., 2016. Could battery swapping ease range anxiety for EV owners? Retrieved on 4.8.2017.
URL http://www.machinedesign.com/automotive/could-battery-swapping-ease-range-anxiety-ev-owners

Kia, 2017. The new Kia Soul EV. Retrieved on 3.8.2017.
URL http://www.kia.com/worldwide/vehicles/catalogue/PS-EV.pdf

Ko, J., Kim, D., Nam, D., Lee, T., 2017. Determining locations of charging stations for electric taxis using taxi operation data. Transportation Planning and Technology 40 (4), 420–433.
URL http://dx.doi.org/10.1080/03081060.2017.1300243

Kochhan, R., 2017. Techno-economic evaluation of battery-electric taxis. Ph.D. thesis, Ulm University.

Kochhan, R., Fuchs, S., Reuter, B., Burda, P., Matz, S., Lienkamp, M., 02 2014. An overview of costs for vehicle components, fuels and greenhouse gas emissions. Published on ResearchGate.

Kochhan, R., Sellmair, R., 2016. Economic evaluation of electric taxis in megacities - example of Singapore. In: 29th International Electric Vehicle Symposium 2016.

Kraschl-Hirschmann, K., Fellendorf, M., June 2012. Estimating energy consumption for routing algorithms. In: 2012 IEEE Intelligent Vehicles Symposium. pp. 258–263.

Kuby, M., Lim, S., 2005. The flow-refueling location problem for alternative-fuel vehicles. Socio-Economic Planning Sciences 39 (2), 125 – 145.
URL http://www.sciencedirect.com/science/article/pii/S0038012104000175

Lambert, F., 2016. Tesla to deliver its largest privately-owned supercharger station to a taxi fleet in montreal. Retrieved on 4.8.2917.
URL https://electrek.co/2016/10/03/tesla-to-deliver-its-largest-privately-owned-supercharger-station-to-a-taxi-fleet-in-montreal/

Lee, J., Park, C. J., Park, G.-L., 2014. Design of a Performance Analyzer for Electric Vehicle Taxi Systems. Springer International Publishing, Cham, pp. 237–244.
URL http://dx.doi.org/10.1007/978-3-319-05458-2_25

Li, Y., Luo, J., Chow, C. Y., Chan, K. L., Ding, Y., Zhang, F., April 2015. Growing the charging station network for electric vehicles with trajectory data analytics. In: 2015 IEEE 31st International Conference on Data Engineering. pp. 1376–1387.

Lim, A., 2016. October roll-out for all-electric fleet of taxis. Retrieved on 2.8.2017.
URL http://www.straitstimes.com/singapore/transport/october-roll-out-for-all-electric-fleet-of-taxis

Lou, Y., Zhang, C., Zheng, Y., Xie, X., Wang, W., Huang, Y., November 2009. Map-matching for low-sampling-rate GPS trajectories. In: ACM SIGSPATIAL GIS 2009. ACM SIGSPATIAL GIS 2009.
URL https://www.microsoft.com/en-us/research/publication/map-matching-for-low-sampling-rate-gps-trajectories/

LTA, 2013a. Bringing new and extended rail lines to you by 2025/2030. Tech. rep.
URL https://www.lta.gov.sg/content/dam/ltaweb/corp/PublicationsResearch/files/ReportNewsletter/Connect/Connect-2013-Feb_FA.pdf

LTA, 2013b. Land transport master plan 2013. Tech. rep.
URL https://www.lta.gov.sg/content/dam/ltaweb/corp/PublicationsResearch/files/ReportNewsletter/LTMP2013Report.pdf

LTA, 2014a. Mytransport.sg:data mall: Traffic related data. Retrieved on 24.9.2014.
URL http://www.mytransport.sg/content/mytransport/home/dataMall.html#Traffic_Related

LTA, 2014b. Road length in kilometer. Retrived on 7.8.2017.
URL https://www.lta.gov.sg/content/dam/ltaweb/corp/PublicationsResearch/files/FactsandFigures/Road%20Length-km.pdf

LTA, 2014c. Traffic flow. Retrieved on 16.8.2017.
URL https://www.lta.gov.sg/content/dam/ltaweb/corp/PublicationsResearch/files/FactsandFigures/Traffic%20Flow.pdf

LTA, 2015a. Revised carbon emissions-based vehicle scheme (CEVS) from 1 july 2015. Retrieved on 6.10.2017.

URL https://www.lta.gov.sg/apps/news/page.aspx?c=2&id=8aa03b88-409f-4852-b2df-09077e101468

LTA, 2015b. Statistics in Brief 2015.
URL https://www.lta.gov.sg/content/dam/ltaweb/corp/PublicationsResearch/files/FactsandFigures/Statistics%20in%20Brief%202015%20FINAL.pdf

LTA, 2016a. Taxi availability framework simplified in response to changing taxi operating environment.
URL https://www.lta.gov.sg/apps/news/page.aspx?c=2&id=8d105be4-5fa5-4837-b346-300533288a03

LTA, 2016b. Taxi info 2016. https://www.lta.gov.sg/content/dam/ltaweb/corp/PublicationsResearch/files/FactsandFigures/taxi_info_2016.pdf.

LTA, 2017a. Fares & payment methods. Retrieved on 11.8.2017.
URL https://www.lta.gov.sg/content/ltaweb/en/public-transport/taxis%20and%20private%20hire%20cars/fares-and-payment-methods.html

LTA, 2017b. Road regulations. Retrieved on 17.8.2017.
URL https://www.lta.gov.sg/content/ltaweb/en/roads-and-motoring/road-safety-and-regulations/road-regulations.html

LTA, 2017c. Tax structure for taxis. Retrieved on 18.10.2017.
URL https://www.lta.gov.sg/content/ltaweb/en/roads-and-motoring/owning-a-vehicle/costs-of-owning-a-vehicle/tax-structure-for-taxis.html

Lu, J. L., Yeh, M. Y., Hsu, Y. C., Yang, S. N., Gan, C. H., Chen, M. S., March 2012. Operating electric taxi fleets: A new dispatching strategy with charging plans. In: 2012 IEEE International Electric Vehicle Conference. pp. 1–8.
URL 10.1109/IEVC.2012.6183233

Marra, F., Yang, G. Y., Traeholt, C., Larsen, E., Rasmussen, C. N., You, S., July 2012. Demand profile study of battery electric vehicle under different charging options. In: 2012 IEEE Power and Energy Society General Meeting. pp. 1–7.

Massier, T., Recalde, D., Sellmair, R., Gallet, M., Hamacher, T., 2017. Electrification of road transport in singapore and its integration into the power system. Energy Technology, n/a–n/a.
URL http://dx.doi.org/10.1002/ente.201700652

Moecker, S., 2014. Driving profile and energy demand analysis for electrical vehicles based on gps trajectories. Master's thesis, Technical University of Munich.

Moeller, C., 8 2014. Routing on openstreetmap. http://www.osm2po.de/.

Nationale Platform Elektromobilitaet, 2015. Charging infrastructure for electric vehicles in Germany. Tech. rep.
URL http://nationale-plattform-elektromobilitaet.de/fileadmin/user_upload/Redaktion/AG3_Statusbericht_LIS_2015_engl_klein_bf.pdf

Nissan, 2017a. 2017 Leaf. Retrieved on 3.8.2017.
URL https://www.nissanusa.com/content/dam/nissan/request-brochure/en/2017/pdf/2017-nissan-leaf-en.pdf

Nissan, 2017b. Overview: 2018 Nissan LEAF. Retrieved on 5.10.2017.
URL http://nissannews.com/en-US/nissan/usa/releases/overview-2018-nissan-leaf

Ogden, J., Anderson, L., 2011. Sustainable transportation energy pathways. Tech. rep., University of California.

Open Street Map, 2014. Retrieved on 4.2014.
URL http://www.openstreetmap.org/about

Open Street Map, 2017a. Retrieved on 2.8.2017.
URL https://www.openstreetmap.org/#map=11/1.3289/103.7157&layers=H

Open Street Map, 2017b. Map features. Retrieved on 7.8.2017.
URL http://wiki.openstreetmap.org/wiki/Map_Features#Highway

Parkinson, G., 2015. First Tesla taxi/limousine service in Australia launched in Sydney. Retrieved on 3.8.2017.
URL https://cleantechnica.com/2015/07/09/first-tesla-taxilimousine-service-australia-launched-sydney/

Plugless Power, 2015. Plugless power website. Retrieved on 6.2015.
URL https://www.pluglesspower.com

Ranarison, T., Rakotomalala, M., Rajoharison, J. W., May 2017. Statistics on plug-in electric cars sales in the world from 2011 to 2016 and overview of the evolution of their performances. International Journal of Precious Engineering Research and Applications 2 (2), 01–08.

Reuter, B., Schonsteiner, K., Wagner, M., Gleyzes, D., Massier, T., Hamacher, T., Lienkamp, M., 2014. Life cycle greenhouse gas analysis for automotive applications - a case study for taxis in Singapore. International Journal of Smart Grid and Clean Energy.

ReVelle, C. S., Swain, R. W., 1970. Central facilities location. Geographical Analysis 2 (1), 30–42.
URL http://dx.doi.org/10.1111/j.1538-4632.1970.tb00142.x

Riemann, R., Wang, D., Busch, F., 2015. Optimal location of wireless charging facilities for electric vehicles: Flow-capturing location model with stochastic user equilibrium. Transportation Research Part C: Emerging Technologies 58, 1–12.

Ross, J. N., 2013. Nissan Leaf all-electric start pilot program in NYC. Retrieved on 3.8.2017.
URL https://www.autoblog.com/2013/04/23/nissan-leaf-all-electric-taxis-start-pilot-program-in-nyc-w-vid/

Schroeder, A., Traber, T., 2012. The economics of fast charging infrastructure for electric vehicles. Energy Policy 43 (Supplement C), 136 – 144.
URL http://www.sciencedirect.com/science/article/pii/S0301421511010470

Sellmair, R., Hamacher, T., 2014. Optimization of charging infrastructure for electric taxis. Transportation Research Records 2416.
URL https://doi.org/10.3141/2416-10

Sellmair, R., Schelo, T., 2018. Analysis of the effect of charging infrastructure design on electric taxi driving profiles: A case study approach on the example of Singapore. International Journal of Sustainable Transportation.
URL https://doi.org/10.1080/15568318.2018.1485792

Shahraki, N., Cai, H., Turkay, M., Xu, M., 2015. Optimal locations of electric public charging stations using real world vehicle travel patterns. Transportation Research Part D: Transport and Environment 41, 165 – 176.
URL http://www.sciencedirect.com/science/article/pii/S1361920915001352

Shampine, L. F., Reichelt, M. W., Jan. 1997. The MATLAB ODE suite. SIAM J. Sci. Comput. 18 (1), 1–22.
URL http://dx.doi.org/10.1137/S1064827594276424

Sherman, D., 2014. Drag queens. Car and Driver magazine 6.
URL https://www.tesla.com/sites/default/files/blog_attachments/the-slipperiest-car-on-the-road.pdf

Simpson, A., 2005. Parametric modelling of energy consumption in road vehicles. Ph.D. thesis, University of Queensland.

Singapore Customs, 2017. Duties & dutiable goods. Retrieved on 17.10.2017.
URL https://www.customs.gov.sg/businesses/valuation-duties-taxes--fees/duties-and-dutiable-goods

SMRT, 2015. Fares. Website, retrieved on 11.11.2015.
URL http://www.smrt.com.sg/Journey-with-Us/Fares-Claims

SMRT, 2017. SMRT Corporation. Retrieved on 23.10.2017.
URL https://www.smrt.com.sg/

Sundstrom, O., Binding, C., March 2012. Flexible charging optimization for electric vehicles considering distribution grid constraints. IEEE Transactions on Smart Grid 3 (1), 26–37.

Sustrans, 2014. Key London statistics data sheet. Tech. rep.
URL http://www.sustrans.org.uk/sites/default/files/images/files/policy/Key%20statistics/Key-London-Statistics-Data-Sheet-V1-13-06-2014.pdf

Tesla, 2017a. Model 3. Retrieved on 5.10.2017.
URL https://www.tesla.com/model3

Tesla, 2017b. Model S. Retrieved on 3.8.2017.
URL https://www.tesla.com/sites/default/files/tesla-model-s.pdf

The Economist, 2017. Worldwide cost of living 2017. Tech. rep.
URL https://kjarninn.overcastcdn.com/documents/EconomistListi.pdf

The Online Citizen, 2017. Groupe PSA and nuTonomy from stratigic partnership to test fully autonomous vehicles in Singapore. Retrived on 3.10.2017.
URL https://www.theonlinecitizen.com/2017/05/03/groupe-psa-and-nutonomy-form-strategic-partnership-to-test-fully-autonomous-vehicles-in-singapore/

The Straits Times, 2017. Letting Jurong evolve into a hip CBD. Retrieved on 3.10.2017.
URL http://www.straitstimes.com/opinion/st-editorial/letting-jurong-evolve-into-a-hip-cbd

Thoma, Y., 2014. Technological and economic matching of electric vehicles' charging concpets to different use ccase in the context of Singapore. Master's thesis, Technical University of Munich.

Thomas, C. S., 2009. Transportation options in a carbon-constrained world: Hybrids, plug-in hybrids, biofuels, fuel cell electric vehicles, and battery electric vehicles. International Journal of Hydrogen Energy 34 (23), 9279 – 9296.
URL http://dx.doi.org/10.1016/j.ijhydene.2009.09.058

Toyota, 2015. Prius 2015. Brochure, retrieved on 17.11.2015.
URL http://www.toyota.com/content/ebrochure/2015/prius_ebrochure.pdf

Tran, T. N., Drab, K., Daszykowski, M., 2013. Revised DBSCAN algorithm to cluster data with dense adjacent clusters. Chemometrics and Intelligent Laboratory Systems 120, 92 – 96.
URL http://dx.doi.org/10.1016/j.chemolab.2012.11.006

Trippe, A. E., Arunachala, R., Massier, T., Jossen, A., Hamacher, T., Oct 2014. Charging optimization of battery electric vehicles including cycle battery aging. In: IEEE PES Innovative Smart Grid Technologies, Europe. pp. 1–6.

Tu, W., Li, Q., Fang, Z., lung Shaw, S., Zhou, B., Chang, X., 2016. Optimizing the locations of electric taxi charging stations: A spatial-temporal demand coverage approach. Transportation Research Part C: Emerging Technologies 65, 172 – 189.
URL http://www.sciencedirect.com/science/article/pii/S0968090X15003538

TUM CREATE, 2013. EVA by TUM CREATE.
URL https://www.tum.de/uploads/media/EVA_Brochure_EN_web_01.pdf

Ungureanu, I., 2014. Now you can ask for a Tesla Model S taxi in Vienna. Retrieved on 3.8.2017.
URL https://www.autoevolution.com/news/now-you-can-ask-for-a-tesla-model-s-taxi-in-vienna-87153.html

United Nations, 9 2014. Transport joint action statement.
URL http://www.un.org/climatechange/summit/wp-content/uploads/sites/2/2014/07/TRANSPORT-joint-Action-Statement.pdf

United Nations, 10 2015. Resolution adopted by the general assembly on 25 September 2015.
URL http://www.un.org/ga/search/view_doc.asp?symbol=A/RES/70/1&Lang=E

Verheijen, E., Jabben, J., 2010. Effect of electric cars on traffic noise and safety. Tech. rep., National Institute for Public Health and the Environment.
URL http://www.rivm.nl/bibliotheek/rapporten/680300009.pdf

Vetter, M., 2016. Development and evaluation of business model for the implementation of a smart electric taxi system for Singapore. Master's thesis, Technical University of Munich.

Wolfram, C., 2015. Energy tourism: The Tesla taxi in Oslo. Retrieved on 3.8.2017.
URL https://energyathaas.wordpress.com/2015/04/13/energy-tourism-the-tesla-taxi-in-oslo/

Wu, F., Sioshansi, R., 2017. A stochastic flow-capturing model to optimize the location of fast-charging stations with uncertain electric vehicle flows. Transportation Research Part D: Transport and Environment 53, 354 – 376.
URL http://www.sciencedirect.com/science/article/pii/S136192091630102X

Wu, G., Inderbitzin, A., Bening, C., 2015. Total cost of ownership of electric vehicles compared to conventional vehicles: A probabilistic analysis and projection across market segments. Energy Policy 80, 196 – 214.
URL http://www.sciencedirect.com/science/article/pii/S0301421515000671

Wu, H. H., Gilchrist, A., Sealy, K. D., Bronson, D., Aug 2012. A high efficiency 5 kW inductive charger for EVs using dual side control. IEEE Transactions on Industrial Informatics 8 (3), 585–595.

Yang, J., Dong, J., Hu, L., 2017. A data-driven optimization-based approach for siting and sizing of electric taxi charging stations. Transportation Research Part C: Emerging Technologies 77, 462 – 477.
URL http://www.sciencedirect.com/science/article/pii/S0968090X17300542

Ying, F. J., 2017. HDT Singapore Taxi launches first fleet of 50 e-taxis. Retrieved on 2.8.2017.
URL http://www.tnp.sg/news/singapore/hdt-singapore-taxi-launches-first-fleet-50-e-taxis

Glossary

acceleration profile	derivative of *speed profile* with respect to time
acceleration share	share of *speed profile* when vehicle accelerated
action	event of the driving profile simulation which is executed by an agent
active action	*action* during which the agent searches for the next customer and transports her or him to the requested destination
additional registration fee (ARF)	fee to register a vehicle which is calculated with respect to the vehicle's OMV
agent handler	module of driving profile simulation model which manages all agents
agent memory	feature of each agent which records values derived from previously executed *actions* of this particular agent
battery swapping	concept which enables the exchanging of a vehicle's discharged battery by a fully charged battery
break	short *standstill periods* during a *shift* when the driver has a rest
break location	location where a *break* event took place
break set	set of all *breaks* which occurred during one *shift*
candidate charging location	location were charging stations can be installed
certificate of entitlement (COE)	certificate of entitlement to register a vehicle in Singapore, obtained by a bidding system
change action	transition *action* where the agent's behaviour models decide which *action* shall be executed next
charging behaviour model	model which decides when, where, and how much energy the agent has to recharge

charging break	additional stop agents have to make to recharge the battery
charging break action	*action* when agent executes a *charging break*
charging demand	required use duration of charging stations to sufficiently supply electric vehicles with energy
charging location	location where charging stations are installed
charging schedule	schedule containing *energy targets* amount of rechargeable energy of each *scheduled break* and *charging break*
charging station	equipment to recharge the battery of an electric vehicle, each charging station can only recharge one vehicle at a time
charging station cost factor	TCO of one charging station per day
cluster centre node	*street network node* which is closest to the cluster's centroid
common standstill cluster	cluster of *standstill* events which were derived from all taxis
constant power (CP) *charging*	charging the battery with constant power
constant voltage (CV) *charging*	charging the battery with constant voltage
controller	unit which manages the driving profile simulation including initialisation, execution, termination, and logging of results
cruise share	share of *speed profile* when vehicle drove with constant speed
deceleration share	share of *speed profile* when vehicle decelerated
detour cost factor	factor to quantify loss of revenue due to driving detours to *charging locations*
driving share	share of a driving status (e.g. idle) during a *pass-through* of a *street network section*
dynamic inductive charging	contactless charging of the vehicle's battery while driving
energy target	amount of energy which must be stored in the battery after a *scheduled* or *charging break*
engaged trip	trip while the taxi is serving a customer
execution layer	layer of the driving profile simulation in which *actions* are executed by updating the *physical layer*

fast charging limit	amount of energy when CP charging ends and the charging power has to be reduced
high frequency data (HFD)	data set build on *logger*, *status*, and *revenue data set*
home charging	use of a private charging station during *shift change*
idle share	share of *speed profile* when vehicle was stationary
individual standstill cluster	cluster of *standstill period locations* which were derived from one taxi
instant pickup trip	*engaged trip* which immediately followed after another *engaged trip* without a *search trip* or *standstill period* in between
logger data set	data set containing location and speed extracted from GPS loggers which were installed in the taxis
low frequency data (LFD)	data set based on the *status data set*
mental layer	layer of the driving profile simulation in which agents decide what to do next
open circuit voltage	voltage of a battery which is not connected with any electric circuit
open market value (OMV)	value of a vehicle assessed by Singapore customs before taxation
out of charge action	*action* which reproduces the event when the agent cannot reach any *charging location* due to insufficient SOE
pass-through speed	average speed of consecutive data points when the taxi drove through one *street network section*
physical layer	layer of the driving profile simulation which describes the current situation, e.g. location of agents, topology of street network, utilisation of charging stations
private charging	use of a a charging station which is accessible by only one taxi
public charging	use of a charging station which is accessible by any taxi
regenerative braking	conversion of kinetic energy to electric energy while braking to supply vehicle internal consumers or recharge the battery
revenue data set	data set containing the start time of *engaged trips* and the fare which was charged at the end of the trip
route	set of all *street network sections* of one trip
scheduled break	*break* included in *shift schedule* which agents make to emulate the taxi driver's rests, recharging during these *breaks* is possible

scheduled break action	*action* when the agent executes a *scheduled break*
search trip	trip while the taxi was searching for the next customer
shift	period when taxi driver is working (including *breaks* in between)
shift change	long *standstill period* between two *shifts*
shift change action	*action* when agent executes a *shift change*
shift change location	location where *shift change* took place
shift schedule	data set describing the drivers activity during one *shift* including start time, end time, and *break set*
shift schedule set	set of all *shift schedules* which were derived from the driving profiles of the same taxi
shift schedule pool	module of driving profile simulation which assigns *shift schedules* to agents
simulation time	time within a simulated scenario (each agent has a different *simulation time*)
speed cluster	set of time windows during which the taxis' average speed was similar
speed profile	set of consecutive speed values equally distributed with respect to time
standstill action	all *actions* which execute *standstill periods* (*scheduled break, charging break,* and *shift change action*)
standstill behaviour model	model which decides when, where, and how long agents have to make scheduled breaks or *shift changes*
standstill location	location where a *standstill period* took place
standstill period	time period when the taxi stopped for at least five minutes
state of charge (SOC)	charging level of the battery
state of energy (SOE)	energy level of the battery
static inductive charging	contactless charging of the vehicle's battery while the vehicle is stationary
status data set	data set containing the taxi's status and location
street network node	intersection connecting at least two different streets

street network section	street segments directly connecting two *street network nodes*
street network way	set of *street network sections* which belong to the same street
terminal voltage	voltage applied by the charger to recharge the battery
total cost of ownership (TCO)	total costs of a product including acquisition costs, installation costs (if applicable), operating costs, and end of life costs
trip generator	module of driving profile simulation which either samples trips or synthesises trips
waiting time cost factor	factor to quantify loss of revenue due to waiting for an available charging station

Acronyms

AC	Alternating Current
ARF	Additional Registration Fee
CBD	Central Business District
CEP	Circular Error Distribution
CEVS	Carbon Emission-based Vehicle Scheme
CFRP	Carbon Fibre Reinforced Polymer
CL	Charging Location
CO_2	Carbon dioxide
COE	Certificate Of Entitlement
CP	Constant Power
CREATE	Campus for Research Excellence And Technological Enterprise
CS	Charging Station
CV	Constant Voltage
DBSCAN	Density-Based Spatial Clustering of Applications with Noise
DC	Direct Current
ED	Excise Duty
EoL	End of Life
ERP	Electronic Road Pricing
EUR	Euro
FK	Foreign Key
GPS	Global Positioning System
GST	Goods and Service Tax
HFD	High Frequency Data
HWFET	HighWay Fuel Economy Test driving schedule

LFD	Low Frequency Data
Li	Lithium
LTA	Land Transport Authority
MDT	Mobile Data Terminal
MRT	Mass Rapid Transit
OCV	Open Circuit Voltage
OMV	Open Market Value
OSM	Open Street Map
PK	Primary Key
RMSE	Root Mean Square Error
SGD	Singapore Dollar
SOC	State Of Charge
SOE	State Of Energy
ST	Spatial-Temporal
STC	Soon To Clear
STD	Standard Deviation
TCO	Total Cost of Ownership
TUM	Technical University of Munich
UDDS	Urban Dynamometer Driving Schedule
USD	United States Dollar

List of Figures

1.1 Approach of thesis . . . 3

2.1 Map of Singapore (Open Street Map, 2017a) . . . 6
2.2 Trajectory sample . . . 12
2.3 Street network definitions . . . 14
2.4 Street network of Singapore . . . 15

3.1 Distribution of *break* (a) and *shift change* (b) duration . . . 21
3.2 Activity of taxi fleet with respect to time . . . 22
3.3 Map with *common standstill clusters* . . . 23
3.4 Share of status with respect to driving distance (a) and duration (b) . . . 25
3.5 Origin-destination map of *engaged trips* for different times of the day . . . 27
3.6 Driving distance estimation . . . 28
3.7 Distribution of average daily mileage (a) and revenue (b) per taxi . . . 29
3.8 Map matching graph with candidate *section* and transition probabilities (Lou et al., 2009) . . . 30
3.9 Usage share of street types with respect to driving distance (a) and driving duration (b) . . . 31
3.10 Average speed profile with respect to time of the day . . . 32
3.11 Inverse cumulative frequency distribution of *pass-through speeds* for *sections* of type *primary* and all *speed clusters* . . . 33
3.12 Fit of acceleration with respect to *pass-through speed* of all *primary sections* 34
3.13 *Driving shares* of *sections* of street type *primary* with respect to *pass-through speed* . . . 36

4.1 Power flow diagram of electric vehicle . . . 39
4.2 Example of battery pack charging curve . . . 46
4.3 Simplified battery pack model . . . 47
4.4 Charging energy with respect to time . . . 50

5.1 Model design (Sellmair and Schelo, 2018) . . . 54
5.2 *Actions* agents can execute . . . 55
5.3 Connected *shift schedule set* . . . 58
5.4 *Shift* connectivity matrix . . . 59
5.5 Distribution of recorded and simulated average speed per trip . . . 62
5.6 Generation of trips within *active action* . . . 63
5.7 Number and percentage of unique *engaged trips* for k^{th} trip of *shift* . . . 65
5.8 Number of charging events per agent at one *charging location* . . . 67

5.9 Recorded and simulated driving distance to clustered (a) and non-clustered (b) *break locations* . . . 70
5.10 *Charging schedule* generation . . . 72
5.11 Distribution of recorded and simulated daily mileage (a) and revenue (b) . 75
5.12 Average revenue per day and taxi and waiting time of conventional and EVA vehicles with respect to the number of simulated taxis . . . 77
5.13 Revenue per day and taxi (a), waiting time and charging station utilisation (b) for charging infrastructures with one and four *charging locations* (CL) . 78
5.14 Waiting times (a) at and driving distances (b) to each *charging location* with respect to the number of taxis . . . 79

6.1 TCO by cost category for all vehicle types . . . 84
6.2 TCO with respect to daily mileage . . . 85

7.1 Optimisation approach . . . 98
7.2 Fit of waiting time with respect to the charging station utilisation and the number of charging stations with linear condition (a) and quadratic condition (b) . . . 101
7.3 Clustered *street network nodes* . . . 104
7.4 Algorithm to reallocate *charging demand* among *charging locations* (CL) . 108

8.1 Optimised number of charging stations and locations for different vehicle types without *home charging* (a) and with *home charging* (b) . . . 112
8.2 Number of charging stations (a) and *charging locations* (b) with respect to the taxi fleet size without *home charging* . . . 113
8.3 Number of charging stations with respect to battery capacity and charging power . . . 113
8.4 Charging station map for 2,949 EVA taxis and 160 kW charging power without *home charging* . . . 114
8.5 Optimised and simulated waiting time per charging event for EVA with scaled and unscaled *charging demand* without *home charging* . . . 115
8.6 Charging station utilisation (a) and waiting time per day (b) with respect to the number of taxis without *home charging* . . . 116
8.7 Charging and use duration of charging stations per taxi and day . . . 117
8.8 Charging load per region with respect to time for 2,949 EVA taxis without *home charging* . . . 118
8.9 Mileage (a) and revenue (b) per day with respect to the number of taxis without *home charging* . . . 119
8.10 Infrastructure costs (a) and profit (b) per taxi and day without *home charging* 120
8.11 Difference in economic key values per taxi and day between charging infrastructures without and with *home charging* for 2,949 taxis . . . 121
8.12 Vehicle costs (a), infrastructure costs (b), revenue (c), profit (d) per taxi and day with respect to battery capacity and charging power . . . 122

D.1 Design of HFD database . . . 174
D.2 Design of LFD database . . . 175
D.3 Design of simulation database . . . 176

E.1 *Controller* related classes . . . 178

E.2 *Scenario* related classes 179
E.3 *ActionHandler* related classes 180

F.1 Classes 182
F.2 Flow diagram of *change action* 184
F.3 Flow diagram of *active action* 185
F.4 Flow diagram of *scheduled break action* 186
F.5 Flow diagram of *charging break action* 187
F.6 Flow diagram of *shift change action* 188
F.7 Flow diagram of *out of charge action* 188

List of Tables

2.1 Cities with electric taxis . . . 8
2.2 Technical parameter of electric vehicles . . . 9
2.3 Logger data excerpt . . . 11
2.4 Taxi status description . . . 13
2.5 Status data excerpt . . . 13
2.6 Revenue data excerpt . . . 14
2.7 Key figures of street network . . . 15

3.1 Key figures of data sets . . . 18
3.2 Statistics of *search* and *engaged trips* of the HFD . . . 26
3.3 Revenue estimation parameter . . . 28

4.1 Nomenclature of energy consumption model . . . 37
4.2 Dynamometer coefficients (EPA, 2016) . . . 40
4.3 Efficiencies of components . . . 41
4.4 Energy consumption of driving cycles: simulated (measured) . . . 42
4.5 Simulated energy consumption on Singapore driving profiles . . . 43
4.6 Route-base energy consumption correction factors . . . 44
4.7 Nomenclature of charging model . . . 45
4.8 Open circuit voltage parameter (Chen and Rincon-Mora, 2006) . . . 47

5.1 Averages and standard deviation of features over all *shift schedule sets* . . . 60
5.2 Difference of average and standard deviation (STD) between selected *shift schedule sets* and all *shift schedule sets* . . . 60
5.3 Nomenclature of behaviour models . . . 69
5.4 Comparison of recorded and simulated daily averages and (standard deviations) 75

6.1 OMV of vehicle types in Singapore (Kochhan et al., 2014; Kochhan, 2017) 82
6.2 Costs of charging stations (Thoma, 2014; Schroeder and Traber, 2012; ERI@N, 2016; Nationale Platform Elektromobilitaet, 2015) . . . 86
6.3 Fitted parameter for charging station equipment and installation costs . . . 87
6.4 TCO of charging stations in SGD . . . 87
6.5 Waiting time and detour costs factors of all vehicle types . . . 89

7.1 Matching of optimisation criteria of each approach . . . 96
7.2 Nomenclature of waiting time estimation . . . 99
7.3 Waiting time fit parameter values . . . 102
7.4 Nomenclature of optimisation problem . . . 103

8.1 Scenario definition 111

A.1 OSM street type description (Open Street Map, 2017b) 156

B.1 Time windows of *speed clusters* 158

C.1 Fit parameter of speed distribution 159
C.2 Fit parameter of average acceleration 162
C.3 Fit parameter of average deceleration 164
C.4 Units of driving share fit parameter 166
C.5 Fit parameter of *idle share* 166
C.6 Fit parameter of *acceleration share* 169
C.7 Fit parameter of *deceleration share* 171

G.1 Infrastructure optimisation approaches I 190
G.2 Infrastructure optimisation approaches II 191

Appendix A

OSM street type description

Table A.1 contains all street type descriptions from (Open Street Map, 2017b) (street types are denoted as "highway" by OSM).

Table A.1: OSM street type description (Open Street Map, 2017b)

Street type	Description
motorway	A restricted access major divided highway, normally with 2 or more running lanes plus emergency hard shoulder. Equivalent to the Freeway, Autobahn, etc..
trunk	The most important roads in a country's system that aren't motorways. (Need not necessarily be a divided highway.)
primary	The next most important roads in a country's system. (Often link larger towns.)
secondary	The next most important roads in a country's system. (Often link towns.)
tertiary	The next most important roads in a country's system. (Often link smaller towns and villages)
unclassified	The least most important through roads in a country's system – i.e. minor roads of a lower classification than tertiary, but which serve a purpose other than access to properties. Often link villages and hamlets. (The word 'unclassified' is a historical artefact of the UK road system and does not mean that the classification is unknown; you can use highway=road for that.)
residential	Roads which serve as an access to housing, without function of connecting settlements. Often lined with housing.
service	For access roads to, or within an industrial estate, camp site, business park, car park etc. Can be used in conjunction with service=* to indicate the type of usage and with access=* to indicate who can use it and in what circumstances.

Street type	Description
motorway link	The link roads (sliproads/ramps) leading to/from a motorway from/to a motorway or lower class highway. Normally with the same motorway restrictions.
trunk link	The link roads (sliproads/ramps) leading to/from a trunk road from/to a trunk road or lower class highway.
primary link	The link roads (sliproads/ramps) leading to/from a primary road from/to a primary road or lower class highway.
secondary link	The link roads (sliproads/ramps) leading to/from a secondary road from/to a secondary road or lower class highway.
tertiary link	The link roads (sliproads/ramps) leading to/from a tertiary road from/to a tertiary road or lower class highway.

Appendix B

Speed clusters

Table B.1 contains the time windows of the *speed clusters* derived in Chapter 3.4.2.

Table B.1: Time windows of *speed clusters*

Cluster	Start time	End time
Low Speed	11:07:30	12:22:30
	13:37:30	14:52:30
	17:37:30	19:52:30
Medium Speed	10:07:30	11:07:30
	12:22:30	13:37:30
	14:52:30	16:07:30
	16:37:30	17:37:30
	19:52:30	20:22:30
High Speed	2:22:30	3:22:30
	7:37:30	10:07:30
	16:07:30	16:37:30
	20:22:30	22:07:30
Very High Speed	3:22:30	7:37:30
	22:07:30	0:00:00
	0:00:00	2:22:30

Appendix C

Fit parameter

This appendix contains all fit parameter values which were fitted to the recorded driving profiles in order to describe the traffic statistics in Singapore (Chapter 3.4). These fits were made for all street types (Chapter 2.5) and *speed clusters* (Chapter 3.4.2) individually. Each *speed cluster* defines a set of time windows (Appendix B) when the vehicles' average speed was about equal. In total four clusters were defined:

- *Low Speed*
- *Medium Speed*
- *High Speed*
- *Very High Speed*

With respect to these clusters, time dependent traffic conditions were taken into account. Furthermore, there is one general category (*All*) which is time independent and contains all recorded data points.

The first set of parameters was fitted to describe the taxis' speed distribution while passing through a *street network section*, these speeds $\overline{v}$ are denoted as *pass through speeds:*

$$\overline{v}\,(p) = a \cdot p - b \cdot (\exp\,(-c \cdot p) - 1) + d \cdot (\exp\,(e \cdot p) - 1) \tag{C.1}$$

This function returns the *pass-through speed* with respect to a given quantile *p,* e.g. if *p* is 0.7 then in 70% of all passes through a *section* of this street type the average speed was lower than $\overline{v}\,(0.7)$. The parameters *a*, *b*, and *d* have the unit km/h while *c* and *e* have no unit, the root mean square error (RMSE) of each fit is given in the unit of km/h. All fitted parameter values are listed in Table C.1.

Table C.1: Fit parameter of speed distribution

Street type	Speed cluster	RMSE	a	b	c	d	e
LIVING STREET	All	3.820	3.820	50.191	0.258	0.863	0.060
LIVING STREET	Low Speed	2.157	2.157	5.819	0.031	0.105	7.731
LIVING STREET	Medium Speed	2.901	2.901	14.502	0.017	0.346	8.016
LIVING STREET	High Speed	3.306	3.306	17.159	0.023	0.007	13.158

Street type	Speed cluster	RMSE	a	b	c	d	e
LIVING STREET	Very High Speed	4.610	4.610	47.369	2.285	0.138	0.303
MOTORWAY	All	1.468	1.468	31.224	58.532	12.759	0.000
MOTORWAY	Low Speed	1.384	1.384	31.252	54.470	11.347	0.000
MOTORWAY	Medium Speed	1.497	1.497	28.858	57.746	13.510	0.000
MOTORWAY	High Speed	1.195	1.195	30.563	57.653	12.485	0.000
MOTORWAY	Very High Speed	1.987	1.987	28.456	66.714	14.290	0.000
MOTORWAY LINK	All	0.798	0.798	35.467	33.084	7.189	0.000
MOTORWAY LINK	Low Speed	0.670	0.670	36.192	29.493	6.771	0.000
MOTORWAY LINK	Medium Speed	0.663	0.663	33.993	32.255	7.626	0.000
MOTORWAY LINK	High Speed	0.668	0.668	36.396	31.438	7.279	0.000
MOTORWAY LINK	Very High Speed	1.118	1.118	32.603	39.826	7.492	0.000
PRIMARY	All	1.068	1.068	36.279	8.223	13.644	0.000
PRIMARY	Low Speed	1.062	1.062	32.866	7.020	13.271	0.000
PRIMARY	Medium Speed	1.034	1.034	33.369	8.177	12.986	0.000
PRIMARY	High Speed	1.015	1.015	34.557	9.012	14.441	0.000
PRIMARY	Very High Speed	1.094	1.094	38.647	12.214	10.857	0.000
PRIMARY LINK	All	0.721	0.721	0.002	55.976	1.633	0.002
PRIMARY LINK	Low Speed	0.503	0.503	0.000	57.816	1.404	0.002
PRIMARY LINK	Medium Speed	0.420	0.420	0.002	55.681	1.543	0.002
PRIMARY LINK	High Speed	0.531	0.531	0.002	55.614	1.625	0.002
PRIMARY LINK	Very High Speed	0.793	0.793	0.302	45.290	2.867	0.019
RESIDENTIAL	All	1.131	1.131	25.639	3.951	2.161	0.000
RESIDENTIAL	Low Speed	1.169	1.169	24.352	3.504	1.758	0.000
RESIDENTIAL	Medium Speed	1.117	1.117	24.850	3.642	1.880	0.000
RESIDENTIAL	High Speed	1.021	1.021	25.791	3.933	2.462	0.000
RESIDENTIAL	Very High Speed	1.184	1.184	27.406	4.549	2.908	0.000
SECONDARY	All	0.994	0.994	33.716	5.598	9.769	0.000
SECONDARY	Low Speed	0.896	0.896	31.779	4.342	10.881	0.000
SECONDARY	Medium Speed	0.917	0.917	32.941	4.805	11.312	0.000
SECONDARY	High Speed	0.909	0.909	34.045	5.347	13.459	0.000
SECONDARY	Very High Speed	1.454	1.454	35.653	7.032	9.495	0.000
SECONDARY LINK	All	1.185	1.185	48.554	3.759	1.044	0.001
SECONDARY LINK	Low Speed	1.194	1.194	44.259	0.167	0.005	0.006
SECONDARY LINK	Medium Speed	1.222	1.222	43.576	11.219	0.435	0.005
SECONDARY LINK	High Speed	1.016	1.016	44.034	16.469	0.490	0.001
SECONDARY LINK	Very High Speed	4.437	4.437	40.746	11.060	1.658	0.002
SERVICE	All	1.177	1.177	19.344	0.000	0.007	0.001
SERVICE	Low Speed	1.133	1.133	17.852	0.000	0.006	0.000
SERVICE	Medium Speed	1.169	1.169	18.516	0.000	0.006	0.001

Street type	Speed cluster	RMSE	a	b	c	d	e
SERVICE	High Speed	1.229	1.229	19.346	0.000	0.007	0.001
SERVICE	Very High Speed	1.298	1.298	21.776	0.018	0.005	0.001
TERTIARY	All	0.545	0.545	36.983	4.303	7.490	0.001
TERTIARY	Low Speed	0.457	0.457	32.954	4.437	5.676	0.001
TERTIARY	Medium Speed	0.491	0.491	33.312	5.173	6.083	0.002
TERTIARY	High Speed	0.633	0.633	35.864	4.603	8.727	0.001
TERTIARY	Very High Speed	0.545	0.545	38.057	7.462	5.287	0.000
TERTIARY LINK	All	0.969	0.969	42.840	0.013	0.001	0.000
TERTIARY LINK	Low Speed	1.412	1.412	37.312	0.011	0.000	0.000
TERTIARY LINK	Medium Speed	0.919	0.919	41.329	0.012	0.001	0.000
TERTIARY LINK	High Speed	1.158	1.158	41.964	0.012	0.000	0.000
TERTIARY LINK	Very High Speed	1.781	1.781	49.438	2.886	0.425	0.000
TRACK	All	2.925	2.925	23.337	1.652	5.895	0.784
TRACK	Low Speed	3.456	3.456	2.384	0.000	0.763	6.515
TRACK	Medium Speed	2.117	2.117	0.000	0.106	4.300	3.832
TRACK	High Speed	2.855	2.855	22.515	0.000	0.008	0.484
TRACK	Very High Speed	3.406	3.406	37.327	0.035	0.482	1.066
TRUNK	All	0.689	0.689	33.333	40.000	4.564	0.000
TRUNK	Low Speed	0.557	0.557	31.723	39.225	3.613	0.000
TRUNK	Medium Speed	0.503	0.503	32.869	37.281	4.843	0.000
TRUNK	High Speed	0.567	0.567	35.263	37.851	4.388	0.000
TRUNK	Very High Speed	1.145	1.145	34.014	43.942	6.711	0.000
TRUNK LINK	All	0.729	0.729	59.923	12.352	10.974	0.000
TRUNK LINK	Low Speed	0.756	0.756	56.522	10.271	10.091	0.000
TRUNK LINK	Medium Speed	0.914	0.914	57.314	11.676	11.227	0.000
TRUNK LINK	High Speed	0.574	0.574	62.436	10.626	11.205	0.000
TRUNK LINK	Very High Speed	1.668	1.668	55.699	19.634	10.004	0.000
UNCLASSIFIED	All	1.054	1.054	24.241	7.895	1.166	0.104
UNCLASSIFIED	Low Speed	0.875	0.875	29.700	0.499	0.013	0.079
UNCLASSIFIED	Medium Speed	0.808	0.808	32.195	0.748	0.013	0.075
UNCLASSIFIED	High Speed	0.817	0.817	33.746	4.253	0.028	0.041
UNCLASSIFIED	Very High Speed	1.445	1.445	8.790	74.647	0.351	0.174

The average acceleration and deceleration $\dot{v}$ was estimated with respect to the *pass-through speed* $\bar{v}$ (Chapter 3.4.3):

$$\dot{v}(\bar{v}) = a\left(\exp\left(-b \cdot \bar{v}\right) - \exp\left(-c \cdot \bar{v}\right)\right) \tag{C.2}$$

Thereby, the acceleration fit was made for all recorded values of $\dot{v} \geq 0.2\,\mathrm{m/s^2}$ while decelerations were defined as $\dot{v} \leq -0.2\,\mathrm{m/s^2}$. Parameter *a* has the unit $\mathrm{m/s^2}$ while

b and c are in h/km. The parameter values of the average accelerations are listed in Table C.2 while the results of the deceleration fit are given in Table C.3.

Table C.2: Fit parameter of average acceleration

Street type	Speed cluster	RMSE	a	b	c
LIVING STREET	All	0.383	0.383	0.639	-0.002
LIVING STREET	Low Speed	0.350	0.350	0.579	-0.005
LIVING STREET	Medium Speed	0.357	0.357	0.597	-0.002
LIVING STREET	High Speed	0.383	0.383	0.670	-0.001
LIVING STREET	Very High Speed	0.415	0.415	0.701	0.000
MOTORWAY	All	0.260	0.260	0.627	0.006
MOTORWAY	Low Speed	0.259	0.259	0.624	0.006
MOTORWAY	Medium Speed	0.263	0.263	0.650	0.007
MOTORWAY	High Speed	0.275	0.275	0.662	0.007
MOTORWAY	Very High Speed	0.276	0.276	0.657	0.007
MOTORWAY LINK	All	0.382	0.382	0.904	0.010
MOTORWAY LINK	Low Speed	0.369	0.369	0.892	0.010
MOTORWAY LINK	Medium Speed	0.379	0.379	0.959	0.011
MOTORWAY LINK	High Speed	0.385	0.385	0.944	0.011
MOTORWAY LINK	Very High Speed	0.393	0.393	1.028	0.012
PRIMARY	All	0.447	0.447	1.230	0.015
PRIMARY	Low Speed	0.434	0.434	1.140	0.014
PRIMARY	Medium Speed	0.443	0.443	1.229	0.016
PRIMARY	High Speed	0.444	0.444	1.242	0.016
PRIMARY	Very High Speed	0.446	0.446	1.408	0.017
PRIMARY LINK	All	0.487	0.487	1.104	0.010
PRIMARY LINK	Low Speed	0.466	0.466	1.051	0.009
PRIMARY LINK	Medium Speed	0.473	0.473	1.084	0.010
PRIMARY LINK	High Speed	0.470	0.470	1.087	0.010
PRIMARY LINK	Very High Speed	0.482	0.482	1.185	0.011
RESIDENTIAL	All	0.444	0.444	0.851	0.006
RESIDENTIAL	Low Speed	0.433	0.433	0.806	0.005
RESIDENTIAL	Medium Speed	0.438	0.438	0.822	0.005
RESIDENTIAL	High Speed	0.442	0.442	0.841	0.006
RESIDENTIAL	Very High Speed	0.442	0.442	0.847	0.006
SECONDARY	All	0.470	0.470	1.144	0.013
SECONDARY	Low Speed	0.457	0.457	1.038	0.012
SECONDARY	Medium Speed	0.467	0.467	1.103	0.013
SECONDARY	High Speed	0.470	0.470	1.154	0.014
SECONDARY	Very High Speed	0.466	0.466	1.196	0.014

Street type	Speed cluster	RMSE	a	b	c
SECONDARY LINK	All	0.465	0.465	0.932	0.005
SECONDARY LINK	Low Speed	0.451	0.451	0.889	0.004
SECONDARY LINK	Medium Speed	0.463	0.463	0.920	0.004
SECONDARY LINK	High Speed	0.467	0.467	0.937	0.005
SECONDARY LINK	Very High Speed	0.482	0.482	1.021	0.007
SERVICE	All	0.412	0.412	0.718	0.003
SERVICE	Low Speed	0.400	0.400	0.687	0.002
SERVICE	Medium Speed	0.435	0.435	0.736	0.003
SERVICE	High Speed	0.419	0.419	0.744	0.004
SERVICE	Very High Speed	0.396	0.396	0.701	0.003
TERTIARY	All	0.466	0.466	1.121	0.013
TERTIARY	Low Speed	0.463	0.463	1.063	0.012
TERTIARY	Medium Speed	0.470	0.470	1.077	0.012
TERTIARY	High Speed	0.470	0.470	1.107	0.012
TERTIARY	Very High Speed	0.468	0.468	1.139	0.013
TERTIARY LINK	All	0.461	0.461	0.895	0.005
TERTIARY LINK	Low Speed	0.452	0.452	0.890	0.006
TERTIARY LINK	Medium Speed	0.454	0.454	0.869	0.005
TERTIARY LINK	High Speed	0.459	0.459	0.912	0.006
TERTIARY LINK	Very High Speed	0.480	0.480	0.934	0.006
TRACK	All	0.441	0.441	0.811	0.005
TRACK	Low Speed	0.441	0.441	0.815	0.005
TRACK	Medium Speed	0.413	0.413	0.777	0.006
TRACK	High Speed	0.437	0.437	0.775	0.004
TRACK	Very High Speed	0.471	0.471	1.010	0.008
TRUNK	All	0.355	0.355	1.132	0.015
TRUNK	Low Speed	0.358	0.358	1.064	0.014
TRUNK	Medium Speed	0.364	0.364	1.270	0.017
TRUNK	High Speed	0.362	0.362	1.043	0.013
TRUNK	Very High Speed	0.370	0.370	1.454	0.018
TRUNK LINK	All	0.438	0.438	1.137	0.013
TRUNK LINK	Low Speed	0.429	0.429	1.009	0.011
TRUNK LINK	Medium Speed	0.430	0.430	1.159	0.014
TRUNK LINK	High Speed	0.433	0.433	1.113	0.012
TRUNK LINK	Very High Speed	0.453	0.453	1.420	0.016
UNCLASSIFIED	All	0.411	0.411	0.833	0.008
UNCLASSIFIED	Low Speed	0.405	0.405	0.800	0.007
UNCLASSIFIED	Medium Speed	0.405	0.405	0.823	0.008
UNCLASSIFIED	High Speed	0.418	0.418	0.861	0.008

Street type	Speed cluster	RMSE	a	b	c
UNCLASSIFIED	Very High Speed	0.430	0.430	0.849	0.008

Table C.3: Fit parameter of average deceleration

Street type	Speed cluster	RMSE	a	b	c
LIVING STREET	All	0.453	0.453	0.568	1.638
LIVING STREET	Low Speed	0.391	0.391	0.531	1.954
LIVING STREET	Medium Speed	0.360	0.360	0.504	2.709
LIVING STREET	High Speed	0.388	0.388	0.583	1.687
LIVING STREET	Very High Speed	0.556	0.556	0.646	1.008
MOTORWAY	All	0.272	0.272	0.698	1.084
MOTORWAY	Low Speed	0.278	0.278	0.687	1.042
MOTORWAY	Medium Speed	0.282	0.282	0.727	0.662
MOTORWAY	High Speed	0.284	0.284	0.712	1.053
MOTORWAY	Very High Speed	0.264	0.264	0.705	0.633
MOTORWAY LINK	All	0.424	0.424	1.060	0.313
MOTORWAY LINK	Low Speed	0.422	0.422	1.020	0.294
MOTORWAY LINK	Medium Speed	0.429	0.429	1.113	0.293
MOTORWAY LINK	High Speed	0.429	0.429	1.041	0.317
MOTORWAY LINK	Very High Speed	0.437	0.437	1.155	0.242
PRIMARY	All	0.481	0.481	1.236	0.256
PRIMARY	Low Speed	0.465	0.465	1.125	0.316
PRIMARY	Medium Speed	0.473	0.473	1.208	0.280
PRIMARY	High Speed	0.486	0.486	1.261	0.258
PRIMARY	Very High Speed	0.513	0.513	1.462	0.212
PRIMARY LINK	All	0.502	0.502	1.021	0.453
PRIMARY LINK	Low Speed	0.481	0.481	0.974	0.494
PRIMARY LINK	Medium Speed	0.485	0.485	1.007	0.473
PRIMARY LINK	High Speed	0.502	0.502	1.038	0.456
PRIMARY LINK	Very High Speed	0.543	0.543	1.158	0.385
RESIDENTIAL	All	0.461	0.461	0.807	0.750
RESIDENTIAL	Low Speed	0.439	0.439	0.767	0.865
RESIDENTIAL	Medium Speed	0.452	0.452	0.786	0.790
RESIDENTIAL	High Speed	0.461	0.461	0.810	0.748
RESIDENTIAL	Very High Speed	0.476	0.476	0.814	0.739
SECONDARY	All	0.489	0.489	1.047	0.351
SECONDARY	Low Speed	0.469	0.469	0.950	0.476
SECONDARY	Medium Speed	0.480	0.480	1.036	0.368
SECONDARY	High Speed	0.492	0.492	1.094	0.347

Street type	Speed cluster	RMSE	a	b	c
SECONDARY	Very High Speed	0.520	0.520	1.155	0.309
SECONDARY LINK	All	0.483	0.483	0.898	0.547
SECONDARY LINK	Low Speed	0.472	0.472	0.868	0.589
SECONDARY LINK	Medium Speed	0.473	0.473	0.897	0.556
SECONDARY LINK	High Speed	0.479	0.479	0.909	0.507
SECONDARY LINK	Very High Speed	0.513	0.513	0.950	0.546
SERVICE	All	0.400	0.400	0.624	0.958
SERVICE	Low Speed	0.380	0.380	0.602	0.925
SERVICE	Medium Speed	0.412	0.412	0.657	0.975
SERVICE	High Speed	0.413	0.413	0.650	0.985
SERVICE	Very High Speed	0.395	0.395	0.596	1.063
TERTIARY	All	0.489	0.489	1.096	0.337
TERTIARY	Low Speed	0.475	0.475	1.038	0.386
TERTIARY	Medium Speed	0.485	0.485	1.052	0.388
TERTIARY	High Speed	0.492	0.492	1.086	0.366
TERTIARY	Very High Speed	0.515	0.515	1.116	0.338
TERTIARY LINK	All	0.474	0.474	0.872	0.586
TERTIARY LINK	Low Speed	0.452	0.452	0.830	0.675
TERTIARY LINK	Medium Speed	0.459	0.459	0.897	0.544
TERTIARY LINK	High Speed	0.474	0.474	0.881	0.560
TERTIARY LINK	Very High Speed	0.513	0.513	0.916	0.536
TRACK	All	0.457	0.457	0.772	0.723
TRACK	Low Speed	0.460	0.460	0.728	0.801
TRACK	Medium Speed	0.456	0.456	0.769	0.883
TRACK	High Speed	0.445	0.445	0.766	0.690
TRACK	Very High Speed	0.479	0.479	0.841	0.615
TRUNK	All	0.425	0.425	1.398	0.211
TRUNK	Low Speed	0.411	0.411	1.190	0.268
TRUNK	Medium Speed	0.408	0.408	1.451	0.225
TRUNK	High Speed	0.415	0.415	1.156	0.289
TRUNK	Very High Speed	0.439	0.439	1.888	0.153
TRUNK LINK	All	0.478	0.478	1.169	0.295
TRUNK LINK	Low Speed	0.461	0.461	1.049	0.316
TRUNK LINK	Medium Speed	0.471	0.471	1.164	0.378
TRUNK LINK	High Speed	0.476	0.476	1.141	0.322
TRUNK LINK	Very High Speed	0.500	0.500	1.488	0.197
UNCLASSIFIED	All	0.436	0.436	0.805	0.710
UNCLASSIFIED	Low Speed	0.426	0.426	0.778	0.768
UNCLASSIFIED	Medium Speed	0.429	0.429	0.799	0.719

Street type	Speed cluster	RMSE	a	b	c
UNCLASSIFIED	High Speed	0.440	0.440	0.825	0.704
UNCLASSIFIED	Very High Speed	0.471	0.471	0.828	0.713

Driving shares describe the probability of a driving status with respect to the *pass-through speed* $\bar{v}$ (Chapter 3.4.4):

Idle: $v = 0$

Acceleration: $v > 0 \ \wedge \ \dot{v} > 0.2\frac{\mathrm{m}}{\mathrm{s}^2}$

Deceleration: $v > 0 \ \wedge \ \dot{v} < -0.2\frac{\mathrm{m}}{\mathrm{s}^2}$

Cruise: $v > 0 \ \wedge \ -0.2\frac{\mathrm{m}}{\mathrm{s}^2} \leq \dot{\mathrm{v}} \leq 0.2\frac{\mathrm{m}}{\mathrm{s}^2}$

Following fit functions were used to describe these shares:

$$f_{idle}(\bar{v}) = \exp\left(-\left(a_{idle} \cdot \sqrt{\bar{v}} + b_{idle} \cdot \bar{v}^2\right)\right) \tag{C.3}$$

$$f_{acc}(\bar{v}) = a_{acc}\left(\exp\left(-b_{acc} \cdot \bar{v}\right) - \exp\left(-c_{acc} \cdot \bar{v}\right)\right) \tag{C.4}$$

$$f_{dec}(\bar{v}) = a_{dec}\left(\exp\left(-b_{dec} \cdot \bar{v}\right) - \exp\left(-c_{dec} \cdot \bar{v}\right)\right) \tag{C.5}$$

$$f_{cruise}(\bar{v}) = 1 - \left(f_{idle}(\bar{v}) + f_{acc}(\bar{v}) + f_{dec}(\bar{v})\right) \tag{C.6}$$

Table C.4 lists the units of all fit parameter.

Table C.4: Units of driving share fit parameter

Parameter	Unit
a_{idle}	$\sqrt{\frac{h}{km}}$
b_{idle}	$\left(\frac{h}{km}\right)^2$
a_{acc}	-
b_{acc}	$\frac{h}{km}$
c_{acc}	$\frac{h}{km}$
a_{dec}	-
b_{dec}	$\frac{h}{km}$
c_{dec}	$\frac{h}{km}$

The fitted *idle share* parameter values are given in Table C.5, *acceleration share* parameter in Table C.6 and *deceleration share* parameter in Table C.7. There were no parameter fitted for the *cruise share* as this share is calculated with respect to the other shares.

Table C.5: Fit parameter of *idle share*

Street type	Speed cluster	RMSE	a_{idle}	b_{idle}
LIVING STREET	All	0.220	0.220	0.513

Street type	Speed cluster	RMSE	a_{idle}	b_{idle}
LIVING STREET	Low Speed	0.215	0.215	0.507
LIVING STREET	Medium Speed	0.201	0.201	0.509
LIVING STREET	High Speed	0.206	0.206	0.500
LIVING STREET	Very High Speed	0.235	0.235	0.513
MOTORWAY	All	0.109	0.109	0.427
MOTORWAY	Low Speed	0.108	0.108	0.439
MOTORWAY	Medium Speed	0.108	0.108	0.452
MOTORWAY	High Speed	0.108	0.108	0.435
MOTORWAY	Very High Speed	0.110	0.110	0.367
MOTORWAY LINK	All	0.130	0.130	0.265
MOTORWAY LINK	Low Speed	0.129	0.129	0.265
MOTORWAY LINK	Medium Speed	0.129	0.129	0.265
MOTORWAY LINK	High Speed	0.131	0.131	0.265
MOTORWAY LINK	Very High Speed	0.131	0.131	0.265
PRIMARY	All	0.118	0.118	0.240
PRIMARY	Low Speed	0.119	0.119	0.247
PRIMARY	Medium Speed	0.117	0.117	0.242
PRIMARY	High Speed	0.116	0.116	0.235
PRIMARY	Very High Speed	0.119	0.119	0.229
PRIMARY LINK	All	0.231	0.231	0.302
PRIMARY LINK	Low Speed	0.230	0.230	0.302
PRIMARY LINK	Medium Speed	0.229	0.229	0.302
PRIMARY LINK	High Speed	0.231	0.231	0.302
PRIMARY LINK	Very High Speed	0.232	0.232	0.302
RESIDENTIAL	All	0.147	0.147	0.287
RESIDENTIAL	Low Speed	0.145	0.145	0.287
RESIDENTIAL	Medium Speed	0.147	0.147	0.287
RESIDENTIAL	High Speed	0.147	0.147	0.287
RESIDENTIAL	Very High Speed	0.149	0.149	0.287
SECONDARY	All	0.140	0.140	0.267
SECONDARY	Low Speed	0.139	0.139	0.267
SECONDARY	Medium Speed	0.139	0.139	0.267
SECONDARY	High Speed	0.140	0.140	0.267
SECONDARY	Very High Speed	0.140	0.140	0.267
SECONDARY LINK	All	0.240	0.240	0.330
SECONDARY LINK	Low Speed	0.237	0.237	0.330
SECONDARY LINK	Medium Speed	0.238	0.238	0.330
SECONDARY LINK	High Speed	0.243	0.243	0.330
SECONDARY LINK	Very High Speed	0.243	0.243	0.330

Street type	Speed cluster	RMSE	a_{idle}	b_{idle}
SERVICE	All	0.177	0.177	0.333
SERVICE	Low Speed	0.175	0.175	0.336
SERVICE	Medium Speed	0.175	0.175	0.335
SERVICE	High Speed	0.180	0.180	0.332
SERVICE	Very High Speed	0.177	0.177	0.317
TERTIARY	All	0.177	0.177	0.287
TERTIARY	Low Speed	0.173	0.173	0.287
TERTIARY	Medium Speed	0.177	0.177	0.287
TERTIARY	High Speed	0.178	0.178	0.287
TERTIARY	Very High Speed	0.178	0.178	0.287
TERTIARY LINK	All	0.216	0.216	0.319
TERTIARY LINK	Low Speed	0.214	0.214	0.319
TERTIARY LINK	Medium Speed	0.212	0.212	0.319
TERTIARY LINK	High Speed	0.220	0.220	0.319
TERTIARY LINK	Very High Speed	0.216	0.216	0.319
TRACK	All	0.234	0.234	0.555
TRACK	Low Speed	0.233	0.233	0.565
TRACK	Medium Speed	0.233	0.233	0.568
TRACK	High Speed	0.217	0.217	0.505
TRACK	Very High Speed	0.249	0.249	0.701
TRUNK	All	0.171	0.171	0.329
TRUNK	Low Speed	0.172	0.172	0.343
TRUNK	Medium Speed	0.169	0.169	0.331
TRUNK	High Speed	0.171	0.171	0.329
TRUNK	Very High Speed	0.170	0.170	0.298
TRUNK LINK	All	0.191	0.191	0.297
TRUNK LINK	Low Speed	0.189	0.189	0.297
TRUNK LINK	Medium Speed	0.189	0.189	0.297
TRUNK LINK	High Speed	0.191	0.191	0.297
TRUNK LINK	Very High Speed	0.196	0.196	0.297
UNCLASSIFIED	All	0.188	0.188	0.308
UNCLASSIFIED	Low Speed	0.184	0.184	0.308
UNCLASSIFIED	Medium Speed	0.185	0.185	0.308
UNCLASSIFIED	High Speed	0.191	0.191	0.308
UNCLASSIFIED	Very High Speed	0.193	0.193	0.308

Table C.6: Fit parameter of *acceleration share*

Street type	Speed cluster	RMSE	a_{acc}	b_{acc}	c_{acc}
LIVING STREET	All	0.220	0.220	0.193	0.015
LIVING STREET	Low Speed	0.215	0.215	0.227	0.017
LIVING STREET	Medium Speed	0.201	0.201	0.245	0.021
LIVING STREET	High Speed	0.206	0.206	0.268	0.025
LIVING STREET	Very High Speed	0.235	0.235	0.196	0.011
MOTORWAY	All	0.109	0.109	0.392	0.008
MOTORWAY	Low Speed	0.108	0.108	0.392	0.008
MOTORWAY	Medium Speed	0.108	0.108	0.373	0.007
MOTORWAY	High Speed	0.108	0.108	0.397	0.008
MOTORWAY	Very High Speed	0.110	0.110	0.325	0.007
MOTORWAY LINK	All	0.130	0.130	0.422	0.005
MOTORWAY LINK	Low Speed	0.129	0.129	0.423	0.005
MOTORWAY LINK	Medium Speed	0.129	0.129	0.423	0.005
MOTORWAY LINK	High Speed	0.131	0.131	0.423	0.005
MOTORWAY LINK	Very High Speed	0.131	0.131	0.423	0.004
PRIMARY	All	0.118	0.118	0.492	0.009
PRIMARY	Low Speed	0.119	0.119	0.458	0.008
PRIMARY	Medium Speed	0.117	0.117	0.497	0.010
PRIMARY	High Speed	0.116	0.116	0.520	0.010
PRIMARY	Very High Speed	0.119	0.119	0.553	0.010
PRIMARY LINK	All	0.231	0.231	41.756	0.026
PRIMARY LINK	Low Speed	0.230	0.230	103.006	0.026
PRIMARY LINK	Medium Speed	0.229	0.229	86.756	0.026
PRIMARY LINK	High Speed	0.231	0.231	118.631	0.026
PRIMARY LINK	Very High Speed	0.232	0.232	127.909	0.026
RESIDENTIAL	All	0.147	0.147	20.361	0.028
RESIDENTIAL	Low Speed	0.145	0.145	40.517	0.028
RESIDENTIAL	Medium Speed	0.147	0.147	62.549	0.029
RESIDENTIAL	High Speed	0.147	0.147	62.861	0.028
RESIDENTIAL	Very High Speed	0.149	0.149	64.424	0.028
SECONDARY	All	0.140	0.140	18.187	0.026
SECONDARY	Low Speed	0.139	0.139	51.000	0.026
SECONDARY	Medium Speed	0.139	0.139	53.812	0.026
SECONDARY	High Speed	0.140	0.140	52.718	0.026
SECONDARY	Very High Speed	0.140	0.140	33.968	0.026
SECONDARY LINK	All	0.240	0.240	20.726	0.039
SECONDARY LINK	Low Speed	0.237	0.237	37.288	0.040

Street type	Speed cluster	RMSE	a_{acc}	b_{acc}	c_{acc}
SECONDARY LINK	Medium Speed	0.238	0.238	51.976	0.040
SECONDARY LINK	High Speed	0.243	0.243	29.320	0.040
SECONDARY LINK	Very High Speed	0.243	0.243	84.788	0.040
SERVICE	All	0.177	0.177	1.688	0.026
SERVICE	Low Speed	0.175	0.175	5.468	0.033
SERVICE	Medium Speed	0.175	0.175	5.111	0.032
SERVICE	High Speed	0.180	0.180	2.384	0.029
SERVICE	Very High Speed	0.177	0.177	0.793	0.016
TERTIARY	All	0.177	0.177	49.834	0.031
TERTIARY	Low Speed	0.173	0.173	139.850	0.031
TERTIARY	Medium Speed	0.177	0.177	185.347	0.031
TERTIARY	High Speed	0.178	0.178	87.334	0.031
TERTIARY	Very High Speed	0.178	0.178	156.084	0.031
TERTIARY LINK	All	0.216	0.216	70.638	0.031
TERTIARY LINK	Low Speed	0.214	0.214	204.295	0.031
TERTIARY LINK	Medium Speed	0.212	0.212	91.263	0.031
TERTIARY LINK	High Speed	0.220	0.220	135.638	0.031
TERTIARY LINK	Very High Speed	0.216	0.216	93.763	0.031
TRACK	All	0.234	0.234	0.822	0.016
TRACK	Low Speed	0.233	0.233	1.737	0.018
TRACK	Medium Speed	0.233	0.233	11.466	0.030
TRACK	High Speed	0.217	0.217	12.328	0.032
TRACK	Very High Speed	0.249	0.249	0.396	0.008
TRUNK	All	0.171	0.171	0.476	0.009
TRUNK	Low Speed	0.172	0.172	0.588	0.013
TRUNK	Medium Speed	0.169	0.169	0.449	0.008
TRUNK	High Speed	0.171	0.171	0.430	0.008
TRUNK	Very High Speed	0.170	0.170	0.520	0.011
TRUNK LINK	All	0.191	0.191	18.866	0.025
TRUNK LINK	Low Speed	0.189	0.189	78.554	0.026
TRUNK LINK	Medium Speed	0.189	0.189	28.397	0.026
TRUNK LINK	High Speed	0.191	0.191	25.897	0.026
TRUNK LINK	Very High Speed	0.196	0.196	49.491	0.026
UNCLASSIFIED	All	0.188	0.188	40.721	0.038
UNCLASSIFIED	Low Speed	0.184	0.184	101.346	0.038
UNCLASSIFIED	Medium Speed	0.185	0.185	93.221	0.038
UNCLASSIFIED	High Speed	0.191	0.191	66.971	0.038
UNCLASSIFIED	Very High Speed	0.193	0.193	45.096	0.038

Table C.7: Fit parameter of *deceleration share*

Street type	Speed cluster	STD	a_{dec}	b_{dec}	c_{dec}
LIVING STREET	All	0.220	0.220	0.593	0.029
LIVING STREET	Low Speed	0.215	0.215	0.802	0.035
LIVING STREET	Medium Speed	0.201	0.201	68.056	0.068
LIVING STREET	High Speed	0.206	0.206	0.844	0.038
LIVING STREET	Very High Speed	0.235	0.235	0.597	0.026
MOTORWAY	All	0.109	0.109	0.300	0.005
MOTORWAY	Low Speed	0.108	0.108	0.294	0.005
MOTORWAY	Medium Speed	0.108	0.108	0.282	0.004
MOTORWAY	High Speed	0.108	0.108	0.308	0.005
MOTORWAY	Very High Speed	0.110	0.110	0.266	0.004
MOTORWAY LINK	All	0.130	0.130	10.385	0.024
MOTORWAY LINK	Low Speed	0.129	0.129	61.948	0.024
MOTORWAY LINK	Medium Speed	0.129	0.129	31.010	0.024
MOTORWAY LINK	High Speed	0.131	0.131	30.385	0.024
MOTORWAY LINK	Very High Speed	0.131	0.131	50.073	0.024
PRIMARY	All	0.118	0.118	0.483	0.010
PRIMARY	Low Speed	0.119	0.119	0.508	0.012
PRIMARY	Medium Speed	0.117	0.117	0.487	0.011
PRIMARY	High Speed	0.116	0.116	0.497	0.011
PRIMARY	Very High Speed	0.119	0.119	0.607	0.013
PRIMARY LINK	All	0.231	0.231	0.412	0.011
PRIMARY LINK	Low Speed	0.230	0.230	0.412	0.011
PRIMARY LINK	Medium Speed	0.229	0.229	0.412	0.011
PRIMARY LINK	High Speed	0.231	0.231	0.412	0.011
PRIMARY LINK	Very High Speed	0.232	0.232	0.412	0.011
RESIDENTIAL	All	0.147	0.147	0.565	0.013
RESIDENTIAL	Low Speed	0.145	0.145	0.565	0.013
RESIDENTIAL	Medium Speed	0.147	0.147	0.565	0.013
RESIDENTIAL	High Speed	0.147	0.147	0.565	0.013
RESIDENTIAL	Very High Speed	0.149	0.149	0.565	0.013
SECONDARY	All	0.140	0.140	0.572	0.013
SECONDARY	Low Speed	0.139	0.139	0.572	0.013
SECONDARY	Medium Speed	0.139	0.139	0.572	0.013
SECONDARY	High Speed	0.140	0.140	0.572	0.013
SECONDARY	Very High Speed	0.140	0.140	0.572	0.013
SECONDARY LINK	All	0.240	0.240	0.602	0.017
SECONDARY LINK	Low Speed	0.237	0.237	0.602	0.018

Street type	Speed cluster	STD	a_{dec}	b_{dec}	c_{dec}
SECONDARY LINK	Medium Speed	0.238	0.238	0.602	0.018
SECONDARY LINK	High Speed	0.243	0.243	0.602	0.018
SECONDARY LINK	Very High Speed	0.243	0.243	0.603	0.017
SERVICE	All	0.177	0.177	0.634	0.019
SERVICE	Low Speed	0.175	0.175	0.690	0.022
SERVICE	Medium Speed	0.175	0.175	0.620	0.019
SERVICE	High Speed	0.180	0.180	0.646	0.020
SERVICE	Very High Speed	0.177	0.177	1.108	0.025
TERTIARY	All	0.177	0.177	0.547	0.016
TERTIARY	Low Speed	0.173	0.173	0.547	0.016
TERTIARY	Medium Speed	0.177	0.177	0.547	0.016
TERTIARY	High Speed	0.178	0.178	0.547	0.016
TERTIARY	Very High Speed	0.178	0.178	0.547	0.016
TERTIARY LINK	All	0.216	0.216	0.822	0.018
TERTIARY LINK	Low Speed	0.214	0.214	0.822	0.018
TERTIARY LINK	Medium Speed	0.212	0.212	0.822	0.018
TERTIARY LINK	High Speed	0.220	0.220	0.822	0.018
TERTIARY LINK	Very High Speed	0.216	0.216	0.822	0.018
TRACK	All	0.234	0.234	0.373	0.010
TRACK	Low Speed	0.233	0.233	0.406	0.014
TRACK	Medium Speed	0.233	0.233	0.287	0.004
TRACK	High Speed	0.217	0.217	0.466	0.014
TRACK	Very High Speed	0.249	0.249	0.495	0.015
TRUNK	All	0.171	0.171	0.387	0.009
TRUNK	Low Speed	0.172	0.172	0.415	0.010
TRUNK	Medium Speed	0.169	0.169	0.439	0.011
TRUNK	High Speed	0.171	0.171	0.376	0.008
TRUNK	Very High Speed	0.170	0.170	0.350	0.007
TRUNK LINK	All	0.191	0.191	0.626	0.013
TRUNK LINK	Low Speed	0.189	0.189	0.626	0.013
TRUNK LINK	Medium Speed	0.189	0.189	0.627	0.013
TRUNK LINK	High Speed	0.191	0.191	0.626	0.013
TRUNK LINK	Very High Speed	0.196	0.196	0.627	0.013
UNCLASSIFIED	All	0.188	0.188	0.747	0.020
UNCLASSIFIED	Low Speed	0.184	0.184	0.747	0.020
UNCLASSIFIED	Medium Speed	0.185	0.185	0.747	0.020
UNCLASSIFIED	High Speed	0.191	0.191	0.747	0.020
UNCLASSIFIED	Very High Speed	0.193	0.193	0.747	0.020

Appendix D

Database design

In order to create one consistent data source and to make the data handling more convenient, all recorded data as well as the data output of the driving profile simulation model (Chapter 5) was stored in custom designed databases. This appendix presents the design of these databases.

Each database consists of several tables which are related via primary keys (PK) and foreign keys (FK). The Figures D.1, D.2, and D.3 show the design of the developed databases. Every block of these diagrams represents one table. Thereby, the top row contains the table name, the following row the name of the table's PK while below the names of the table's columns are listed. To link tables with each other these columns contain FKs which refer to PKs of other tables. As en example, in Figure D.1 the *DataPoint* table is linked with the *Trip* table via the key *idTrip*, hence all entries of the *DataPoint* table with the same *idTrip* value belong to one trip while the *Trip* table contains additional information of the trip. The arrows of the diagram illustrate which tables are linked to each other.

The design of the database containing the High Frequency Data set (HFD), introduced in Chapter 3.1, is presented by Figure D.1. This database contains all recorded data points which were aggregated to trips, *shifts*, and vehicles. The database also contains the OSM street network (Chapter 2.5) and links each data point to the *section* it was map-matched to. The fit parameters (Chapter 3.4) derived from these statistics are included as well. Moreover, data points are also matched to spatial areas denoted as *SubZone*, *PlanningArea*, and *Region*.

This database contains all *search* and *engaged trips* (Chapter 3.3.1) which were used by the simulation model and the energy consumption of each vehicle type simulated with the speed-based approach (Chapter 4.1.2). The results of a survey conducted by (Kochhan, 2017) are included as well.

The design of the database for the Low Frequency Data set (LFD) is depicted by Figure D.2. As well as the HFD database, its recorded data points are aggregated to trips, *shifts*, and vehicles. Furthermore, this database contains an assignment of all *standstill periods* to *common* and *individual standstill clusters* (Chapter 3.2.3). In order to avoid redundant data, some tables of this database are related to tables of the HFD database. The respective HFD tables are represented by blocks with grey background.

The results of the driving profile simulation are stored in another database. The design of this database is shown in Figure D.3. This database contains the definition of the simulated scenarios - namely the used vehicle type of each agent and the placement

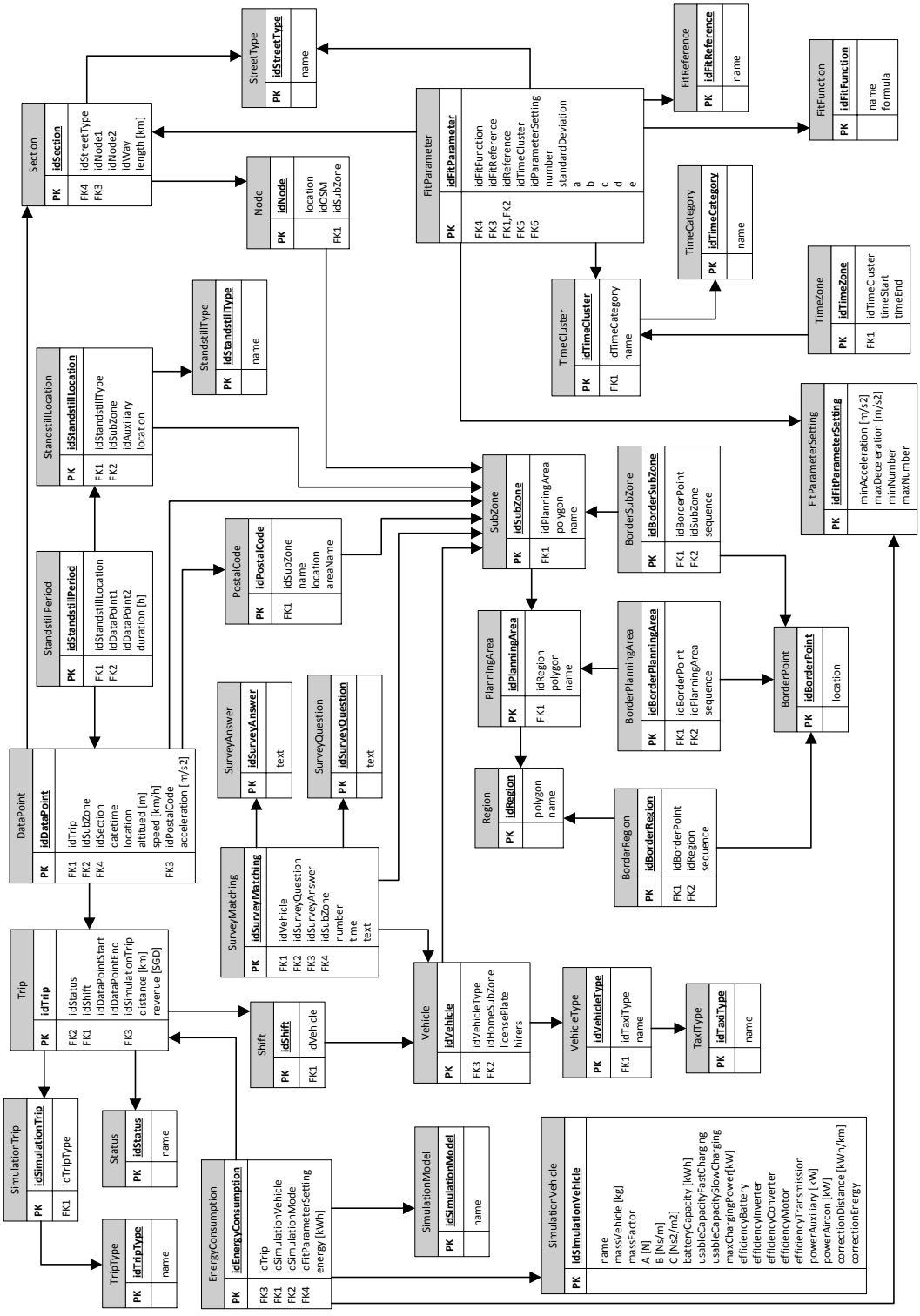

Figure D.1: Design of HFD database

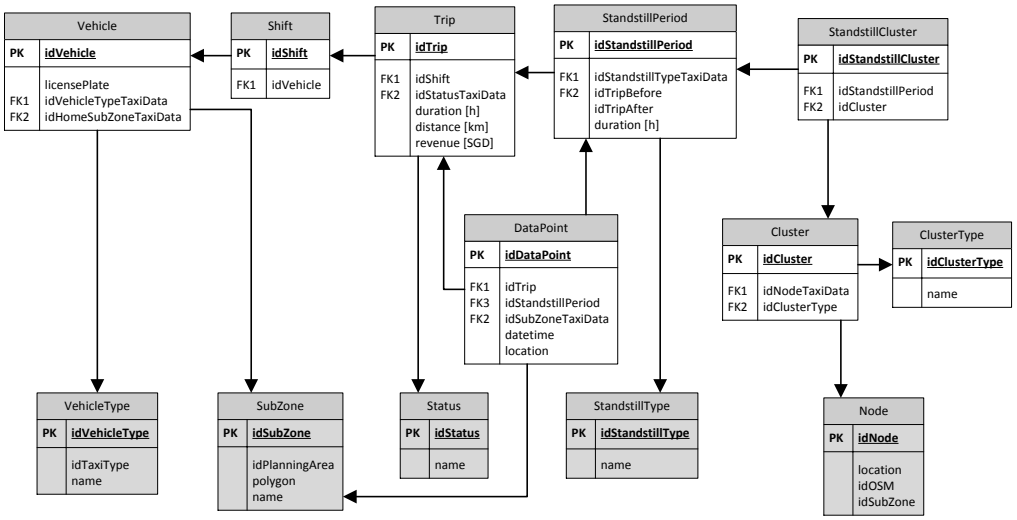

Figure D.2: Design of LFD database

and power of charging stations. In order to be able to reproduce the simulated results, the database contains the revision numbers of each code and data file which was used to run the simulation. The code and data files are organised in a repository which allows to trace back changes with respect to the revision number. The random seed of the simulation run and all parameter values are stored as well.

In contrast to the other databases, the simulation database does not contain data points but has *sections* of the agents' *route* choices as lowest level of information. These *sections* are aggregated to trips, *shifts*, and vehicles. Furthermore, the vehicle's State of Energy (SOE) is recorded at the start and the end of each trip. Every simulated charging process is recorded and linked to the agent's *standstill period* and the *charging location* where it took place.

Again, in order to avoid redundant data, tables of this database are related to tables of the HFD and LFD database.

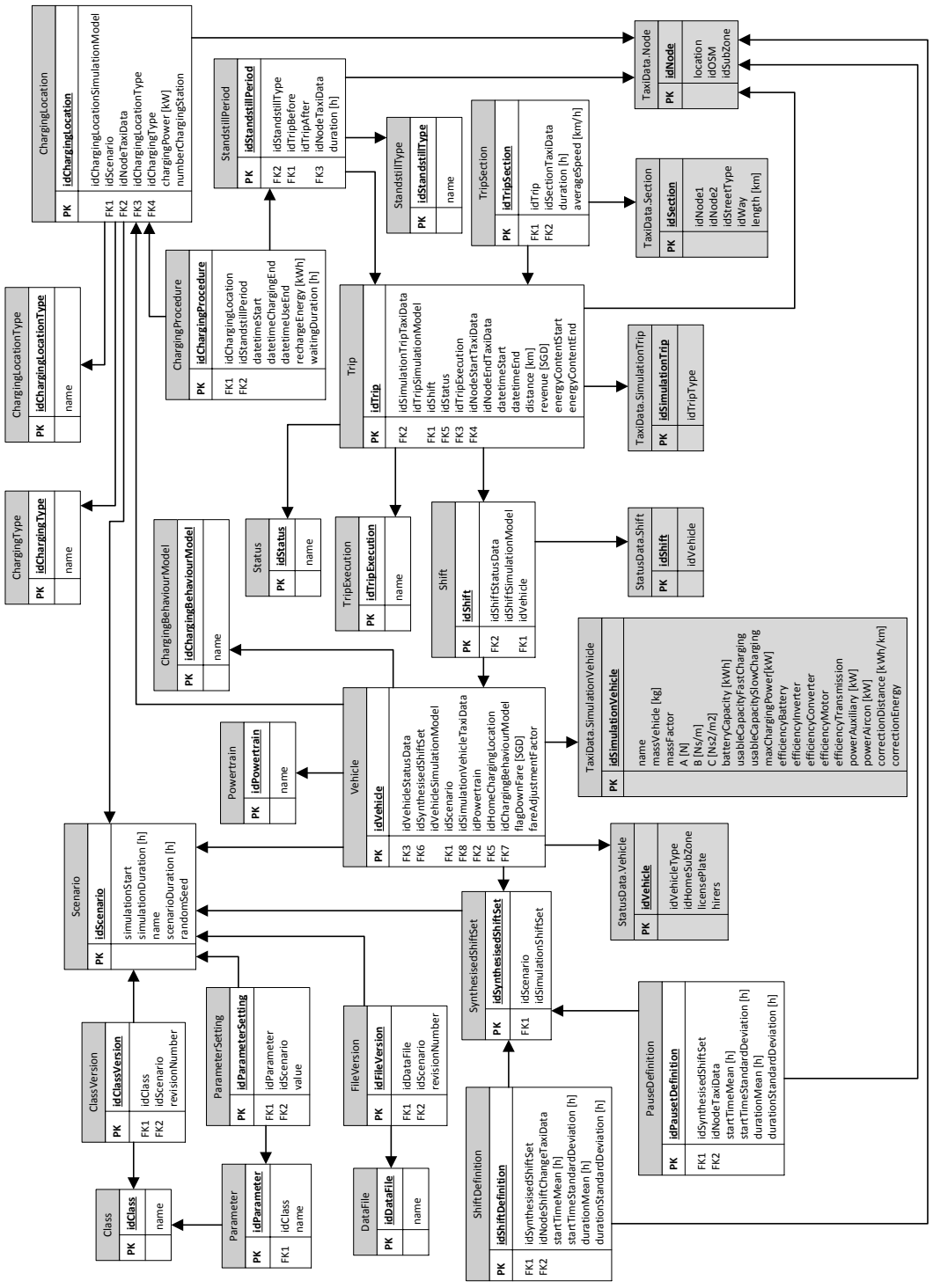

Figure D.3: Design of simulation database

Appendix E

Simulation model classes

This appendix introduces the class structure of the object-oriented driving profile simulation model (Chapter 5).

Each class is represented by one block which is further separated into three boxes. The top box contains the name of the class, the middle box lists all public properties of the class and the bottom box lists all public methods of the class. The solid lines show which object of one class constructs objects of other classes. Thereby, the diagram's upper object always constructs objects below, e.g. in Figure E.1 the *Controller* constructs the *SampleGenerator*. Dashed lines indicate which objects are an input to construct another object, e.g. in the same diagram, a *ControllerSettings* object is required to construct the *Controller*. Solid lines with an arrow at the end show relations of base and sub classes, e.g. in Figure E.2 the *VehicleBasicImpl* class is a subclass of the *VehicleAbstract* class. Base classes define properties and methods which must be defined in each of its sub classes.

The *Controller* is the top class of the simulation model which triggers the initialisation of all other classes. All classes which are closely linked to the *Controller* are depicted in Figure E.1.

First of all, in order to construct a *Controller* object, the *ControllerSettings* object must be constructed. This object contains all settings of the *Controller* like i.a. where the simulation results shall be saved or how much information shall be displayed during the simulation. After the initialisation of the *Controller* a *Scenario* object is created which handles all information of the physical world, i.a. the street network or the placement of charging stations. In order to execute the simulation, *MobSim* is constructed by giving the *Scenario* object as input. *MobSim* further constructs the *ActionHandler* and the *AgentHandler.* During the simulation, the *AgentHandler* selects the agent which is next to execute an *action* and hands it over to the *ActionHandler* which executes the next *action* for this agent.

Once each agent has exceeded the defined simulation duration, the *AgentHandler* terminates the simulation. Afterwards, the *Controller* creates and saves a *ScenarioResults* object which includes the main simulation results, the path to all log files and the definition of the scenario.

All objects which initialisation is triggered by the *Scenario* object are shown in Figure E.2.

The *ScenarioDefinition* object is required as input in order to construct the *Scenario* object. *ScenarioDefinition* contains all information about the scenario which was sim-

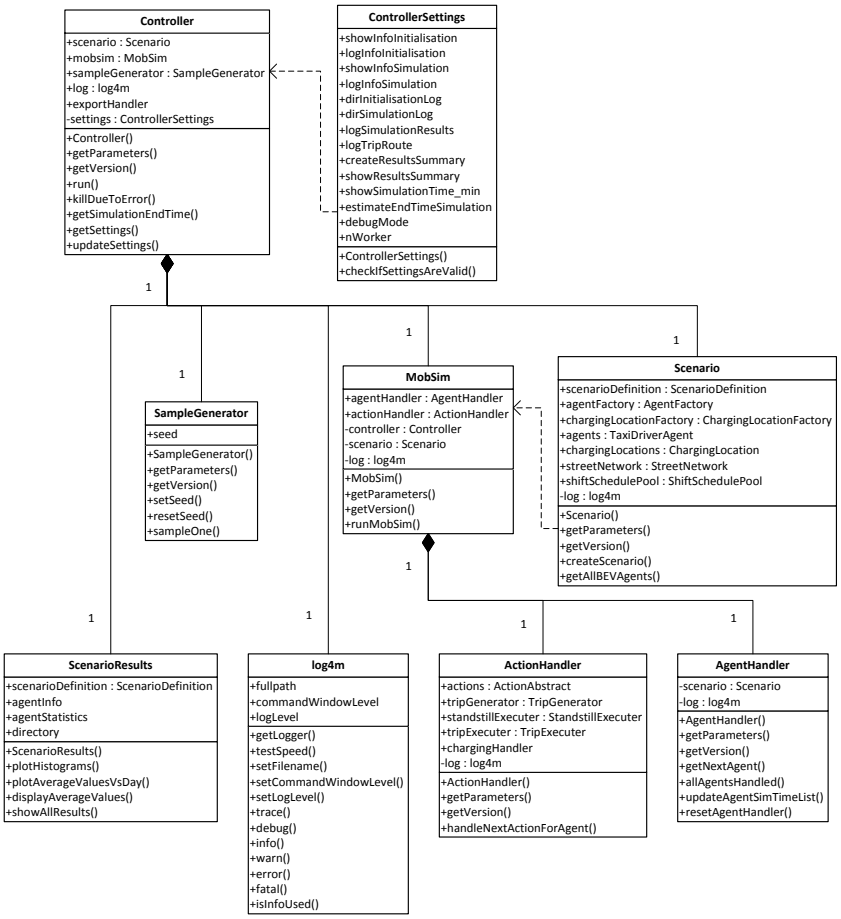

Figure E.1: *Controller* related classes

ulated, i.e. simulation duration, number of agents, or the agents' vehicle type. Based on this information, object factories construct all *ChargingLocation* and *Agent* objects. Each *Agent* gets a *Vehicle*, *ChargingBehaviourModel* (Chapter 5.7.2), *StandstillBehaviourModel* (Chapter 5.7.1), *EstimationModel*, and *TaxiAgentMemory* (Chapter 5.6) object assigned.

The objects which are constructed by the *ActionHandler* to execute the simulation are shown in Figure E.3.

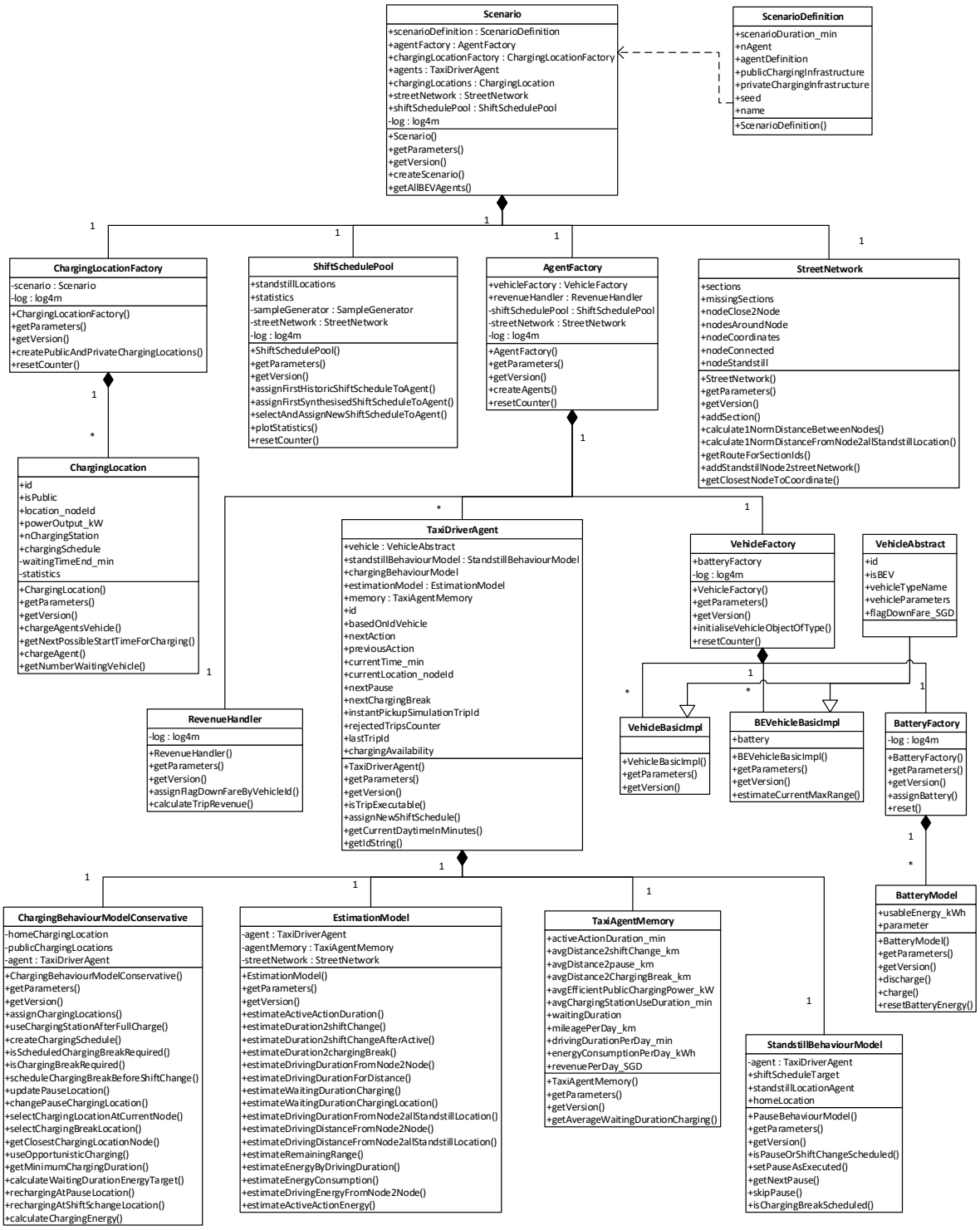

Figure E.2: *Scenario* related classes

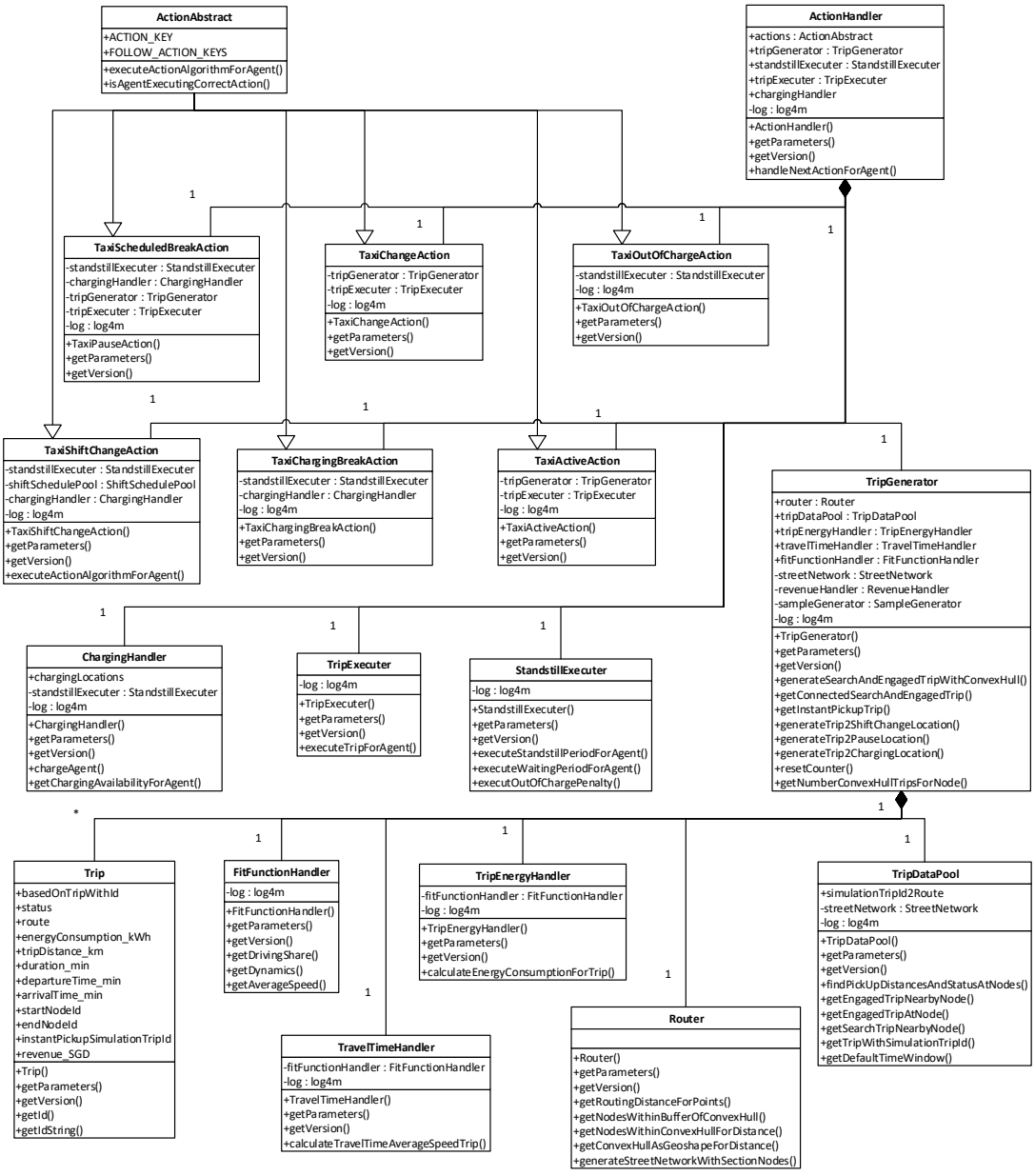

Figure E.3: *ActionHandler* related classes

First of all, one object for each *action* introduced in Chapter 5.2 is created. To execute the *actions*, *ChargingHandler*, *TripExecuter*, *StandstillExecuter*, and *TripGenerator* (Chapter 5.5) objects are constructed. Thereby, the *TripGenerator* creates *Trip* objects which are handed over to the *TripExecuter* which executes these trip for the selected agent.

To create *Trip* objects, the *TripGenerator* uses following objects:

TripDataPool sample recorded *engaged* or *search trips* (Chapter 5.5.2)

Router generate *route* to synthesise trip

FitFunctionHandler obtain traffic statistics of selected route (Chapter 3.4)

TravelTimeHandler assign *pass-through speed* to each *section* of the *route* (Chapter 5.5.1)

TripEnergyHandler assign energy consumption to sampled or synthesised trip (Chapter 4.1)

Appendix F

Functional design of actions

This appendix describes the functional design of all *actions* (Chapter 5.3) of the driving profile simulation model.

Therefore, flow diagrams for each *action* are presented. Each flow diagram starts with a block naming the respective *action* and ends with the name of the *action* which has to be executed next. All other blocks describe steps and decisions which have to be made in between. The blocks' colours refer to the class which has to execute the respective step or decision. Figure F.1 shows the chosen colour code.

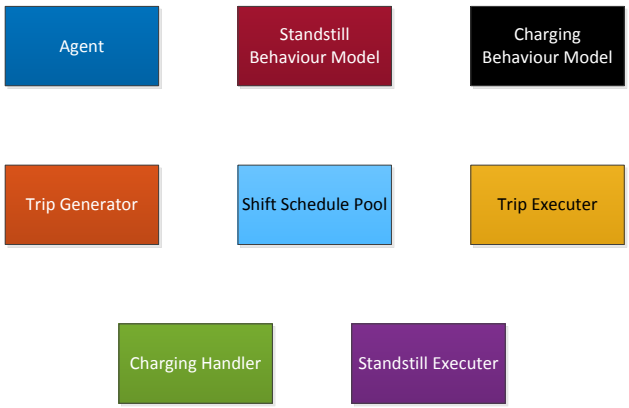

Figure F.1: Classes

Following classes are required to execute the *actions*:

Agent makes estimations based on its memory values (Chapter 5.6) and makes decisions with respect to the vehicles status, i.a. the battery's State of Energy (SOE)

Standstill behaviour model decides when and where the agent has to make *breaks* or *shift changes* (Chapter 5.7.1)

Charging behaviour model decides when and where the agent has to recharge how much energy (Chapter 5.7.2)

Trip generator assigns recorded or synthesised trips to the agents (Chapter 5.5)

Shift schedule pool assigns *shift schedules* to agents (Chapter 5.4)

Trip executer executes trips which were assigned to the agents by updating the agents' time, location, and SOE

Charging handler assigns agents to charging stations and triggers the charging process

Standstill executer simulates standstill periods of agents' by updating their time

The integration of these classes into the simulation model is described by Appendix E. The flow diagrams of following *actions*, are depicted:

Change action: Figure F.2

Active action: Figure F.3

Scheduled break action: Figure F.4

Charging break action: Figure F.5

Shift change action: Figure F.6

Out of charge action: Figure F.7

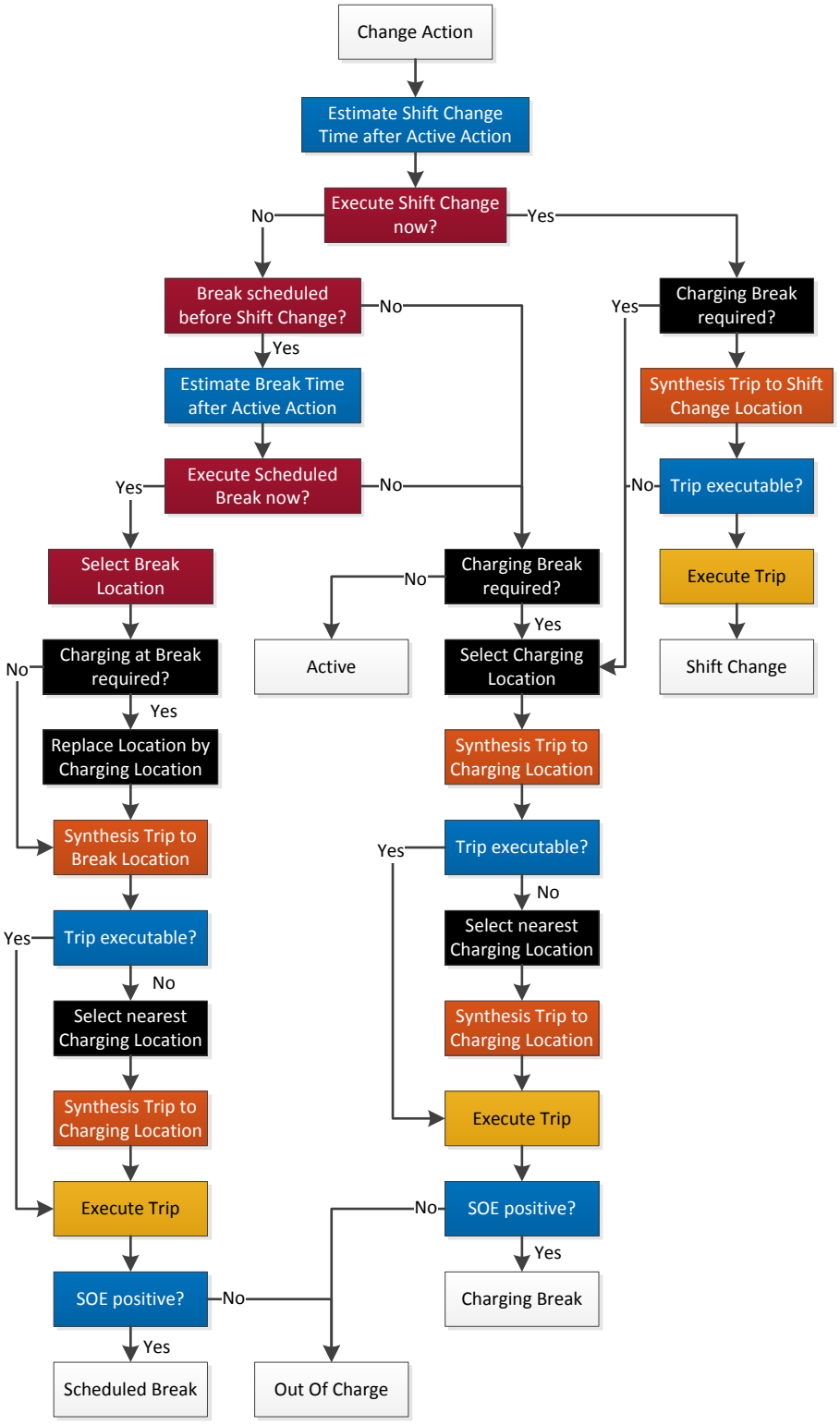

Figure F.2: Flow diagram of *change action*

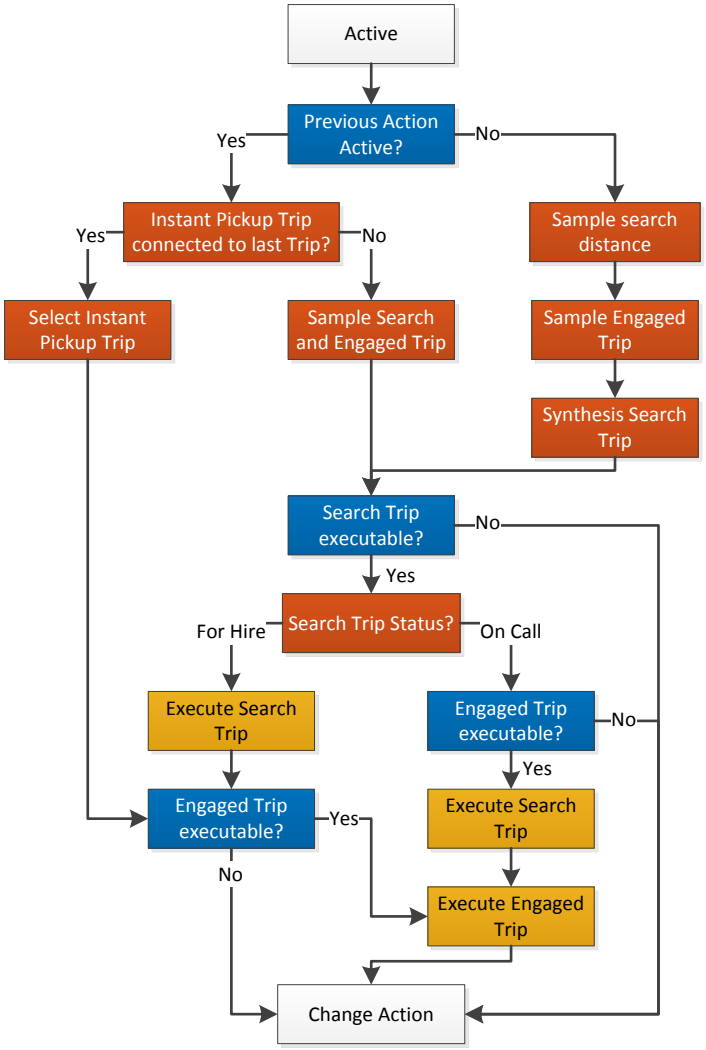

Figure F.3: Flow diagram of *active action*

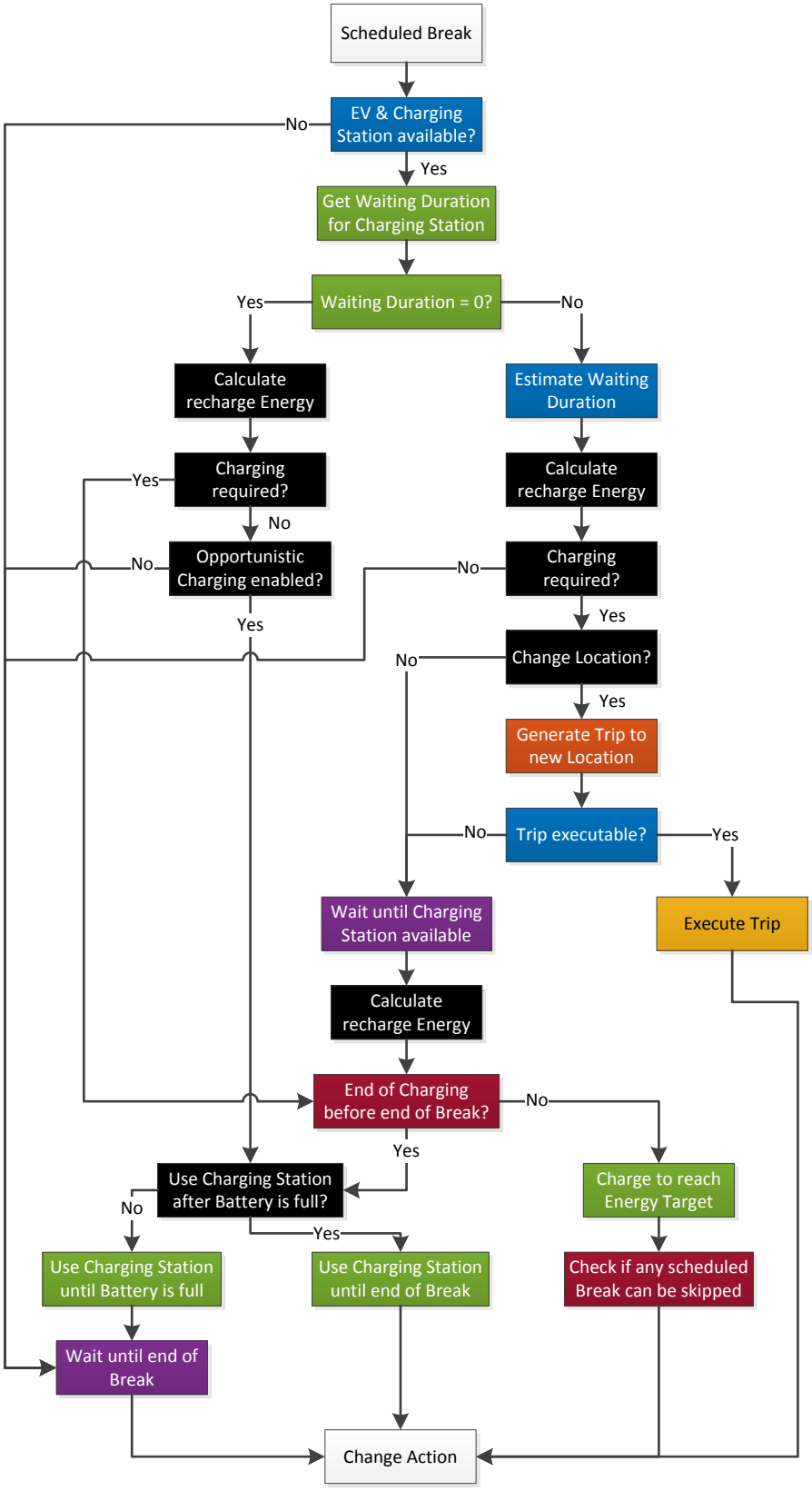

Figure F.4: Flow diagram of *scheduled break action*

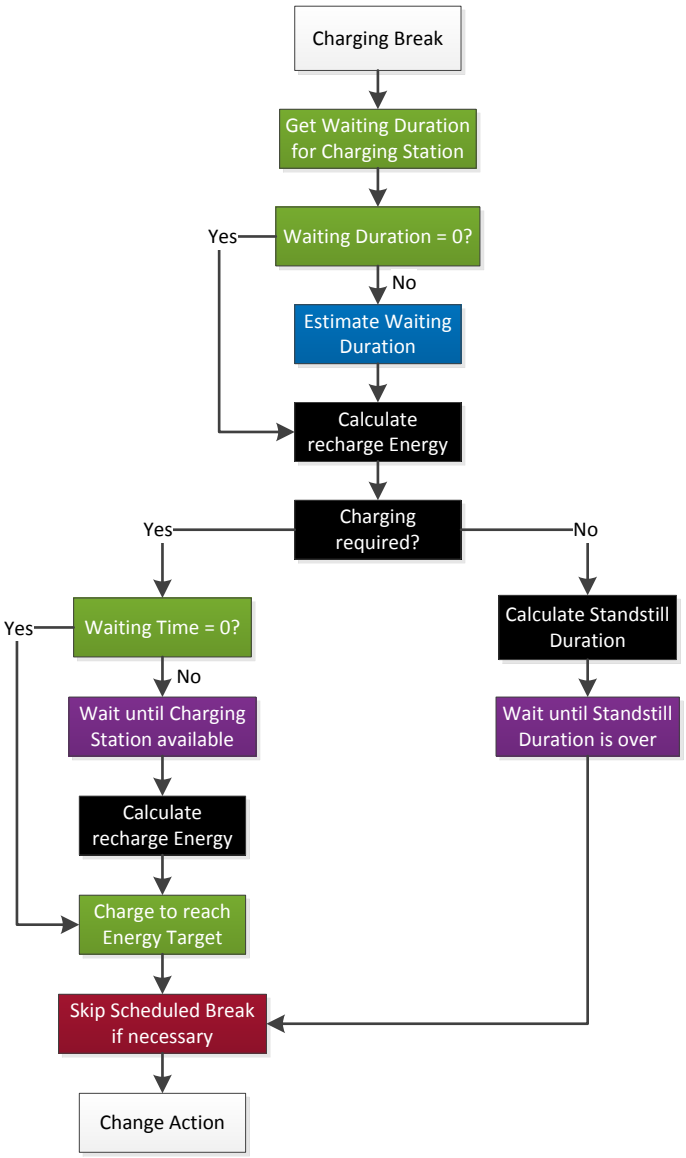

Figure F.5: Flow diagram of *charging break action*

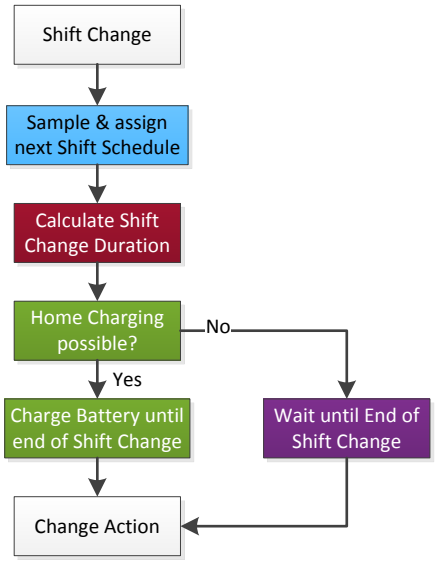

Figure F.6: Flow diagram of *shift change action*

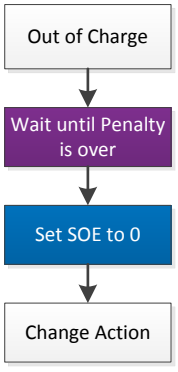

Figure F.7: Flow diagram of *out of charge action*

Appendix G

Infrastructure optimisation approaches

This appendix is an extension of the literature review on charging infrastructure optimisation methods presented in Chapter 7.3. Table G.1 summarises the classification of the approaches. Furthermore, it lists the data background, the optimisation problem type, the applied method to solve the problem and the used street network for which the charging infrastructure was optimised. Moreover, Table G.2 contains the input, objective, constraint, and output of each optimisation approach.

Table G.1: Infrastructure optimisation approaches I

Citation	Classification	Data background	Problem type	Solving method	Street network
Shahraki et al., 2015	flow capturing	11,880 taxis, 3 weeks	mixed-integer linear	CPLEX	none
Li et al., 2015	p-median	490 electric taxis	mixed-integer linear & mixed-integer non-linear	greedy algorithm	Shenzhen
Gacias and Meunier 2015	maximum covering	synthesised	mixed-integer linear	CPLEX	synthesised
Asamer et al., 2016	maximum covering	800 taxis	mixed-integer linear	CPLEX	none
Ko et al., 2017	maximum covering	20,295 taxis	mixed-integer linear	greedy algorithm	Soul 7,500 nodes
Ahn and Yeo, 2015	analytical	955 taxis	analytical	root of derivative	none
Tu et al., 2016	simulation based	15,000 taxis	mixed-integer non-linear	greedy algorithm	none
Han et al., 2016	simulation based	1,000 taxis	mixed-integer linear	evolution algorithm	none
Sellmair and Hamacher, 2014	simulation based	5 taxis	mixed-integer non-linear	greedy algorithm	none
Yang et al., 2017	multiple server location	7,910 taxis, 1 week	mixed-integer linear	Gurobi	none
Jung et al., 2014	multiple server location	600 taxis	mixed-integer non-linear	greedy algorithm	Soul

Table G.2: Infrastructure optimisation approaches II

Citation	Input	Objective	Constraints	Output
Shahraki et al., 2015	trajectory of vehicles	minimise non-executable driving distance	number of charging stations (CS), recharging only when trip destination near charging station	selection of charging locations (CL)
Li et al., 2015	origins of trips to CS	minimise total driving distance to CS, minimise CS utilisation	number of CS, number of CL	number CS per location
Gacias and Meunier 2015	charging demand points	maximise coverage of demand	max. number of CS, cover whole demand	number CS per location
Asamer et al., 2016	origin and destination of engaged trips	maximise served demand	number of CS, no CS in area with existing CS	selection areas with CS
Ko et al., 2017	charging demand points	maximise served demand	number of CS, max. distance of demand point to CL	selection of CL
Ahn and Yeo, 2015	number of taxis per cell	minimise waiting time, detour, and infrastructure costs	number of CS per location	CL density per area
Tu et al., 2016	origin, destination, and time of engaged trips	maximise driving distance, minimise waiting time	number of CL, number of CS per location	selection of CL
Han et al., 2016	charging demand points	minimise CL, CS, detour, and waiting costs	max. number CS, max. driving distance to CL, max. waiting time	number CS per location
Sellmair and Hamacher, 2014	distribution of waiting times and trips per taxi stand	maximise economic profit	only charging at taxi stands, max. number of CS per taxi stand	number CS per taxi stand
Yang et al., 2017	dwell locations and times, arrival rates	minimise investment costs	max. charging rejection rate	number CS per location
Jung et al., 2014	charging demand points	minimise driving duration to CS and waiting times	max. number of CS, max. number CS per location	number CS per location